Mathematical methods for analysis swimming at low Reynolds number

Laëtitia Giraldi

Centre de Mathématiques Appliquées

École doctorale de l'Ecole polytechnique

Doctorat de l'Ecole polytechnique

(spécialité mathématiques appliquées)

présentée par

Laetitia GIRALDI

pour l'obtention du diplôme de

Docteur de l'Ecole polytechnique

Sujet de la thèse :

Méthodes mathématiques pour l'analyse de la natation à l'échelle microscopique

Soutenue publiquement le 25 septembre 2013

après avis des rapporteurs :

Emmanuel Trélat
Marius Tucsnak

devant le jury composé de :

François Alouges	Directeur de thèse
Karine Beauchard	Examinateur
Vincent Calvez	Examinateur
Olivier Glass	Examinateur
Bertrand Maury	Examinateur
Emmanuel Trélat	Rapporteur
Marius Tucsnak	Rapporteur

Centre de Mathématiques Appliquées — UMR 7641

Mis en page avec la classe thloria.

À la mémoire de mes chers grands-parents Jeanne Weber et Robert Ruelle,

Remerciements

Que mon directeur de thèse, François Alouges, veuille trouver ici l'expression de ma vive gratitude pour sa bienveillance, ses précieux conseils et sa confiance jamais altérée pendant ces trois années. Je le remercie de m'avoir confié le sujet passionnant qui a motivé ces recherches. Si travailler avec lui a toujours été extrêmement enrichissant, la grande liberté qu'il m'a offerte a été essentielle dans ce travail.

Je voudrais remercier Emmanuel Trélat, d'avoir accepté de rapporter cette thèse. En plus d'être touchée par l'intérêt qu'il a porté à mon travail, je suis honorée par sa présence dans mon jury. Je dois avouer que son livre occupe une place de choix dans ma bibliothèque lorsqu'il n'est pas sur ma table de chevet. Je remercie également Marius Tucsnak, dont le nom est cité de nombreuses fois dans ce manuscrit, de m'avoir fait l'honneur de rapporter ce travail. Je lui témoigne toute ma gratitude pour les discussions très instructives et conviviales que nous avons eu lors de mon séjour à l'institut Élie Cartan de Nancy.

Je remercie aussi Karine Beauchard, Olivier Glass et Bertrand Maury de me faire l'honneur d'être membre de mon jury. De même, j'exprime ma sincère gratitude à Vincent Calvez pour sa participation au jury de la thèse et pour m'avoir offert le Post-doc "de mes rêves".

Je tiens à remercier tous mes co-auteurs, sans qui rien n'aurait été possible.

J'ai eu la chance de collaborer avec Thomas Chambrion qui m'a fait découvrir la géométrie sous-riemannienne. Je le remercie pour les séances de travail passionnées dans son bureau pendant lesquelles la sélection de références allait du célèbre livre d'Andrei Agrachev au fameux passage du film Matrix lorsque l'armurerie vient à "Néo" évoqué comme un parallèle à l'utilisation de résultats mathématiques sophistiqués.

J'adresse toute ma gratitude à Antonio DeSimone pour son hospitalité, pour le temps qu'il m'a consacré, pour ses précieux conseils et enfin pour sa gentillesse. Ce fut pour moi un grand honneur de travailler avec lui et notre collaboration a été une expérience très formatrice. J'espère que l'occasion de revenir à la SISSA se présentera à nouveau.

J'ai eu le grand plaisir de travailler avec David Gérard-Varet. Je lui sais gré d'avoir accepté d'étudier avec moi "la contrôlabilité du Three-sphere avec un bord rugueux". Outre la grande fierté que j'ai eu à travailler avec un mathématicien de cette réputation, j'ai été très touchée par sa simplicité. J'avoue que cette fabuleuse aventure pleine de péripéties a été très formatrice.

Je remercie Pierre Martinon pour le temps qu'il m'a consacré. J'ai beaucoup apprécié le dynamisme qui a animé notre petit groupe ces six derniers mois. Je me souviens de ses recommandations avisées, qui résonnaient pour moi comme des formules magiques pour prévenir les mauvaises critiques.

J'exprime également ma sincère gratitude à Alexandre Munnier. Un grand merci pour son hospitalité. Je lui suis également très reconnaissante pour ses corrections qui ont beaucoup profité à la dernière partie de cette thèse.

Enfin, je remercie très chaleureusement ma plus jeune collaboratrice, Marta Zoppello. C'est un grand plaisir de travailler avec Marta.

Je souhaite adresser mes sincères remerciements à Benoît Perthame, à l'époque il était responsable de mon Master 2. Je n'oublie pas le temps précieux qu'il m'a consacré pour m'aider à choisir mon sujet de thèse.

Cette thèse a été effectué au Centre de mathématiques appliquées de l'École polytechnique (CMAP), où j'ai pu bénéficier de conditions de travail exceptionnelles. Les chercheurs ont toujours été très accessibles et sympathiques. Plus particulièrement, j'adresse mes sincères remerciements à Antonin Chambolle, pour sa bienveillance et parce qu'il a soutenu ma parti-

cipation à de nombreuses conférences, et à Sylvie Méléard, pour sa gentillesse et ses conseils toujours très enrichissants. Je témoigne également ma sincère gratitude à Ugo Boscain pour m'avoir consacré un temps précieux, à Grégoire Allaire pour sa sollicitude, à Emmanuel Gobet pour nos conversations agréables, à Frederic Bonnans pour sa convivialité, à Carl Graham pour nos discussions lors des pots de thèse du laboratoire et à Anne De Bouard pour sa courtoisie. Je souhaite aussi remercier Benoit Merlet pour sa franchise et Stefano De Marco pour sa sympathie.

Pendant la thèse, j'ai eu la chance d'enseigner à l'École polytechnique les mathématiques appliquées aux élèves du parcours EV2. Je voudrais remercier Olivier Pantz et Aline Lefebvre qui m'ont accompagné dans cette mission. Je remercie également très chaleureusement Pascale Harinck, chargée de recherche et responsable du parcours EV2. Elle a été une confidente pour moi, je lui sais gré de nos discussions sur les mathématiques, sur l'enseignement ou bien sur la vie en général.

Je souhaite profiter de l'occasion pour saluer le travail de l'équipe administrative du CMAP. Un grand merci à Nasséra Naar et Alexandra Noiret sans qui bien des choses auraient été plus compliquées. Je n'oublie pas non plus Christian Feeley qui a rejoint le sud de la France. Je remercie également Sylvain Ferrand pour avoir été toujours à l'écoute de mes problèmes informatiques.

J'adresse mes sincères remerciements à la principauté de Monaco qui m'a permis de bénéficier d'un logement au sein de la Fondation de Monaco à la Cité internationale universitaire de Paris pendant ces trois années de thèse.

Je remercie tous mes camarades doctorants et post-docs avec qui j'ai partagé d'agréables moments, un repas, une pause café, un trajet RER et bien plus encore. En particulier, je pense à Pascal Benchimol, Camille Coron, Davide Barilari, Xavier Dupuis, Gwenael Mercier, Gorgios Michailidis, Sepideh Mirrahimi, Laurent Pfeiffer et Dario Prandi. En cette occasion spéciale, je tiens également à saluer la fidélité de mes amis, Audrey Abbattista, Khanh Daoduc, Marie-Hélène Djivas, Michaël Goldman, Mathieu Pedro, Marine Tort, Magali Tournus et Romain Yvinec.

J'exprime aussi ma gratitude à mes oncles et mes tantes, à Bernard Ruelle pour m'avoir fait découvrir les mathématiques, à Jean-Marc Giraldi pour son aide, à Martine Ruelle pour son affection. Je remercie également mes grands-parents Jean-Albert et Ida Giraldi. À leurs côtés j'ai compris ce que voulait dire le mot travail.

J'ai une pensée très affectueuse pour mes parents, Philippe Giraldi et Brigitte Ruelle-Weber. Je les remercie de l'amour qu'ils me manifestent. J'exprime ma profonde gratitude à ma sœur Caroline Giraldi, que je tiens en haute estime, pour le grand réconfort qu'elle m'apporte lorsque je suis égarée. Je remercie également ma petite sœur, Juliette Giraldi, pour tout l'amour qu'elle me témoigne. Enfin, je remercie le "petit" Jean-Baptiste Ricard l'attachement qu'il me porte.

Mes derniers remerciements sont adressés à Areski Cousin. Merci d'avoir partagé avec moi toutes ces épreuves, d'avoir été fort lorsque j'étais faible, d'avoir été enthousiaste lorsque j'étais triste, d'avoir eu foi en moi lorsque j'échouais, d'avoir été valide lorsque j'étais malade, d'avoir été bavard lorsque j'étais silencieuse, d'avoir ennobli mon âme. L'amour que tu me donnes est à nul autre pareil.

"It is very difficult to find a black cat in a dark room, warns an old proverb.
Especially when there is no cat."
Stuart Firestein, in **Ignorances : how it drives sciences**

Table des matières

Introduction

Le but de cette thèse est d'étudier les mécanismes permettant la nage à l'échelle microscopique. Les domaines d'applications de ce travail concernent la biologie, à travers la compréhension du déplacement des bactéries, des spermatozoïdes, du plancton et d'autres micro-organismes, et l'ingénierie puisque les résultats de cette thèse pourraient être exploités pour la conception de micro-robots "nageurs".

Les stratégies de déplacement des micro-organismes immergés dans un fluide diffèrent de celles qui sont utilisées à l'échelle humaine. En effet, l'écoulement du fluide a lieu à faible nombre de Reynolds. De plus, l'inertie d'un micro-nageur est négligeable et sa dynamique est gouvernée principalement par l'effet des forces de viscosité. L'étude de la nage à échelle microscopique se développe à partir des années 50 avec le travail de G. Taylor [84] qui propose un modèle d'auto-propulsion basé sur le mouvement sinusoïdal d'un flagelle. Il montre qu'un fil infini immergé dans un fluide de Stokes qui suit des oscillations sinusoïdales se déplace à une vitesse non nulle.

Contrairement à ce que l'intuition pourrait laisser supposer, le théorème de la coquille Saint-Jacques, prouvé par E. M. Purcell en 1977 dans [70], mentionne que pour effectuer un déplacement effectif dans un fluide de Stokes, il faut adopter un cycle de déformation non réciproque. Le nom de ce résultat évoque le fait qu'une coquille Saint-Jacques effectue exactement un mouvement réciproque au cours d'une brassée, i.e., un mouvement périodique et symétrique en temps (cf Fig 1). E. M. Purcell propose alors deux types de stratégies qui permettent le déplacement à cette échelle.

FIGURE 1 – Le mouvement d'une coquille Saint-Jacques.

La première stratégie consiste à imposer un mouvement de rotation à certaines extrémités du nageur dans le but de créer des forces de friction sur le fluide puis de produire une propulsion (voir par exemple la Fig. 2 du nageur proposé par E. M. Purcell dans [70]). La seconde stratégie est basée sur un cycle non réciproque de déformations du corps du nageur. Le "Three links swimmer", proposé par E. M. Purcell, constitue le premier exemple d'un tel modèle de nageur. La preuve formelle du déplacement du Three links swimmer sera donnée bien des années plus tard (voir par exemple [5], [15], [44]). Dans la suite de la thèse, nous nous concentrerons sur des nageurs qui utilisent des déformations non réciproques pour se mouvoir. Pour des exemples d'études de nageurs qui utilisent la première stratégie pour se

déplacer, nous renvoyons le lecteur aux travaux de Y. Or et M. Murray [68], [98] et ceux de J. San Martin, T. Takahashi et M. Tucsnak [61].

FIGURE 2 – Nageur capable de se déplacer sans se déformer (voir [70]).

D'autres développements importants sur le sujet proviennent de connexions récentes entre la théorie du contrôle et la nage à faible nombre de Reynolds. A échelle microscopique, la dynamique d'un nageur est donnée par une équation différentielle ordinaire qui est linéaire en la vitesse de ses déformations et sans dérive. En considérant que les vitesses de déformations sont des paramètres maîtrisables, on peut alors s'intéresser à la contrôlabilité d'un tel système, i.e., la possibilité pour le nageur d'atteindre un point donné connaissant sa position initiale et le cycle de déformation qu'il effectue. Parmi les contributions qui considèrent la nage comme un problème de contrôle, nous citons, par exemple, les travaux de A. Shapere et F. Wilczek [79], J. San Martin, T. Takahashi et M. Tucsnak [61], J. Loheac et J. F. Scheid [60], J. Loheac et A. Munnier [59], ainsi que F. Alouges, A. DeSimone et A. Lefevbre [8], F. Alouges, A. DeSimone et L. Heltai [6], E. Lauga et S. Michelin [62].

La suite de cette introduction s'organise en quatre parties. La première partie est consacrée au rappel des principes du couplage fluide-solide qui permettent de déduire la dynamique du nageur. La deuxième partie introduit les principaux résultats de la théorie du contrôle qui seront utilisés dans la thèse. La troisième partie décrit le contenu de cette thèse et présente les principaux résultats obtenus. Enfin, une section de conclusion évoque les perspectives qui émanent de ce travail.

1 Du couplage fluide-solide vers la dynamique du nageur

Dans cette partie, nous rappelons comment le mouvement d'un micro-nageur dans un fluide peut-être gouverné par une équation différentielle ordinaire qui est linéaire en la vitesse de déformation du nageur et sans dérive (voir par exemple [7], [8], [32], [59], [64]).

1.1 Description générique des nageurs

Le nageur est représenté par un domaine solide noté $\mathcal{N}$. Il est décrit par le couple $(\boldsymbol{\xi}, \mathbf{p})$,

- où la variable notée $\boldsymbol{\xi}$ décrit la forme du nageur. Généralement, elle est représentée par un k-uplet. Une brassée consiste en un changement de forme périodique (i.e., les coordonnées de $\boldsymbol{\xi}$ sont des fonctions périodiques) ;

- la variable $\mathbf{p} \in \mathbb{R}^3_+ \times SO(3)$ représente la position du nageur. Elle donne à la fois les coordonnées d'un point fixé $\mathbf{x}_c$ du nageur et son orientation dans l'espace.

Remarquons que toutes ces variables dépendent implicitement du temps à travers le transport et la déformation du nageur.

Enfin, nous appellons $\mathcal{S} \subset \mathbb{R}^M$ (pour un entier $M \in \mathbb{N}$ convenable) l'ensemble des états admissibles $(\boldsymbol{\xi}, \mathbf{p})$. Généralement, l'ensemble des états admissibles contient des contraintes géométriques, comme par exemple le non contact entre le nageur et les bords du domaine fluide, où d'autres contraintes spécifiques au modèle du nageur. Dans tous les exemples qui suivront, $\mathcal{S}$ sera supposé être une sous-variété lisse de $\mathbb{R}^M$.

1.2 Modélisation du fluide

Nous considérons que le nageur est totalement immergé. Il évolue dans le domaine fluide, noté par $\mathcal{O}$. La vitesse du fluide en chaque point du domaine $\mathcal{F} := \mathcal{O} \setminus \mathcal{N}$ est notée $\mathbf{u}$, et la pression est notée p. Nous supposons que le fluide est gouverné par les équations de Stokes, i.e., $(\mathbf{u}, p)$ est solution de l'équation,

$$-\mu \Delta \mathbf{u} + \nabla p = 0\,, \quad \text{div } \mathbf{u} = 0 \quad \text{dans } \mathcal{F}, \tag{1}$$

où μ est la viscosité du fluide. Nous ajoutons les conditions standards de non glissement sur les bords,

$$\begin{cases} \mathbf{u} = \Omega \times (\mathbf{x} - \mathbf{x}_c) + \mathbf{v} + \mathbf{u}_d & \text{sur } \partial\mathcal{N}, \\ \mathbf{u} = 0 & \text{sur } \partial\mathcal{O}. \end{cases} \tag{2}$$

En d'autres termes, nous imposons la continuité des vitesses à la fois sur le bord fixe du domaine fluide et sur le bord déformable du nageur. Remarquons que le champ de vitesses est composé de deux parties.

- Tout d'abord, la première partie correspond à un mouvement rigide inconnu, ayant une vitesse angulaire Ω et une vitesse de translation $\mathbf{v}$. On peut identifier le vecteur $\mathbf{v}$ à la vitesse du point $\mathbf{x}_c$.
- Ensuite, la seconde partie associée à la vitesse $\mathbf{u}_d$ est due à la déformation connue du nageur.

En introduisant l'espace de Hilbert

$$\mathcal{V} = \left\{ \mathbf{u} \in \mathcal{D}'(\mathcal{F}, \mathbf{R}^3) \,|\, \nabla \mathbf{u} \in L^2(\mathcal{F}),\ \frac{\mathbf{u}(\mathbf{r})}{\sqrt{1+|\mathbf{r}|^2}} \in L^2(\mathcal{F}) \right\}, \tag{3}$$

nous obtenons, pour toutes configurations du nageur $\mathcal{N}$ et vitesses $(\Omega, \mathbf{v}, \mathbf{u}^d) \in H^{1/2}(\partial\mathcal{N})$, l'existence d'une unique solution $(\mathbf{u}, p)$ de l'équation (1) -(2) dans $\mathcal{V} \times L^2(\mathcal{F})$.

1.3 Equation du mouvement du nageur

Les précédentes relations décrivent les équilibres du fluide à chaque instant t. Pour obtenir une équation qui décrit le modèle (c'est-à-dire qui gouverne le couplage "fluide-nageur" au cours du temps), nous allons appliquer les lois de Newton sur le système. En négligeant l'inertie, celles-ci s'expriment de la manière suivante :

$$\begin{cases} \displaystyle\int_{\partial\mathcal{N}} \boldsymbol{\sigma}(\mathbf{u}, p) \cdot \mathbf{n}\, \mathrm{d}s = 0\,, \\ \displaystyle\int_{\partial\mathcal{N}} \boldsymbol{\sigma}(\mathbf{u}, p) \cdot \mathbf{n} \times (\mathbf{x} - \mathbf{x}_c)\, \mathrm{d}s = 0\,, \end{cases} \tag{4}$$

où $\boldsymbol{\sigma}(\mathbf{u}, p) = \mu(\nabla \mathbf{u} + \nabla^t \mathbf{u}) - p\mathbf{Id}$ est le tenseur de Cauchy.

De plus, si nous introduisons une base orthonormale $(\mathbf{e}_1, \mathbf{e}_2, \mathbf{e}_3)$ et en utilisant la linéarité de l'équation de Stokes, $\mathbf{u}$ se décompose en plusieurs termes,

$$\mathbf{u} = \sum_{i=1}^{3} \Omega_i \mathbf{u}_i + \sum_{i=4}^{6} v_{i-3} \mathbf{u}_i \ + \mathbf{u}^d.$$

On a noté $\mathbf{u}_i$ et $\mathbf{u}^d$ les solutions de l'équation de Stokes, avec une condition de Dirichlet nulle au bord du fluide $\partial\mathcal{O}$, et une condition de Dirichlet inhomogène aux extrémités du nageur. Les données de Dirichlet sont $\mathbf{e}_i \times (\mathbf{x} - \mathbf{x}_c)$ pour $i = 1, 2, 3$, $\mathbf{e}_{i-3}$ for $i = 4, 5, 6$, $\mathbf{u}_d$ pour la vitesse de déformation maitrisée par le nageur $\mathbf{u}^d$. Remarquons que la vitesse $\mathbf{u}^d$ peut s'exprimer comme une combinaison linéaire des vitesses de déformation du corps du nageur $(\dot{\xi}_i)_{i=1}^k$,

$$\mathbf{u}^d = \sum_{i=1}^{k} \mathbf{u}_i^d \dot{\xi}_i. \tag{5}$$

En identifiant $(\Omega, \mathbf{v})^t$ avec $\dot{\mathbf{p}}$, le système (4) se réduit à une équation différentielle ordinaire que l'on peut écrire sous la forme :

$$\mathbf{M}(\boldsymbol{\xi}, \mathbf{p})\, \dot{\mathbf{p}} + \mathbf{N}(\boldsymbol{\xi}, \mathbf{p}) = 0 \tag{6}$$

où la matrice $\mathbf{M}(\boldsymbol{\xi}, \mathbf{p})$ est définie par,

$$\mathbf{M}_{i,j}(\boldsymbol{\xi}, \mathbf{p}) := \begin{cases} \displaystyle\sum_{l=i}^{N} \int_{\partial B_l} ((\mathbf{x} - \mathbf{x}_c) \times \mathbf{e}_i) \cdot \boldsymbol{\sigma}(\mathbf{u}_j, p_j)\, \mathbf{n}_t \, \mathrm{d}s \quad (1 \le i \le 3, 1 \le j \le 6)\ , \\ \displaystyle\sum_{i=i}^{N} \int_{\partial B_l} \mathbf{e}_{i-3} \cdot \boldsymbol{\sigma}(\mathbf{u}_j, p_j)\, \mathbf{n}_t \, \mathrm{d}s \quad (4 \le i \le 6, 1 \le j \le 6)\ , \end{cases}$$

et $\mathbf{N}(\boldsymbol{\xi}, \mathbf{p})$ est le vecteur de $\mathbb{R}^6$ dont les composantes sont définies par

$$\mathbf{N}_i(\boldsymbol{\xi}, \mathbf{p}) := \begin{cases} \displaystyle\sum_{l=1}^{N} \int_{\partial B_l} ((\mathbf{x} - \mathbf{x}_c) \times \mathbf{e}_i) \cdot \boldsymbol{\sigma}(\mathbf{u}^d, p^d)\, \mathbf{n}_t \, \mathrm{d}s \quad (1 \le i \le 3)\ , \\ \displaystyle\sum_{l=1}^{N} \int_{\partial B_l} \mathbf{e}_{i-3} \cdot \boldsymbol{\sigma}(\mathbf{u}^d, p^d)\, \mathbf{n}_t \, \mathrm{d}s \quad (4 \le i \le 6)\ . \end{cases}$$

La matrice $\mathbf{M}(\boldsymbol{\xi}, \mathbf{p})$ est symétrique définie positive. En l'inversant, l'équation (6) se réécrit comme l'équation qui gouverne l'état du nageur,

$$\dot{\mathbf{p}} = -\mathbf{M}^{-1}(\boldsymbol{\xi}, \mathbf{p}) \mathbf{N}(\boldsymbol{\xi}, \mathbf{p})\,. \tag{7}$$

En utilisant (5), nous déduisons qu'il existe k champs de vecteurs $\mathbf{F}_i$, $i = 1, \ldots, k$, définis sur $\mathcal{S}$, tels que l'équation (4.8) s'exprime

$$\dot{\mathbf{p}} = \sum_{i=1}^{k} \mathbf{F}_i(\boldsymbol{\xi}, \mathbf{p}) \dot{\xi}_i\,. \tag{8}$$

2 Quelques résultats classiques de la théorie du contrôle géométrique

Dans cette section, nous rappelons les principaux résultats de contrôlabilité utilisés dans cette thèse.

Soient $\mathbf{F}$ et $\mathbf{G}$ deux champs définis sur une variété lisse de dimension finie $\mathcal{M}$. Le crochet de Lie de $\mathbf{F}$ et $\mathbf{G}$ est le champ de vecteurs défini par $[\mathbf{F},\mathbf{G}](\mathbf{X}) := (\mathbf{F}\cdot\nabla)\,\mathbf{G}(\mathbf{X}) - (\mathbf{G}\cdot\nabla)\,\mathbf{F}(\mathbf{X})$, pour tout point $\mathbf{X}\in\mathcal{M}$. Pour une famille de champs de vecteurs $\mathcal{F}$ sur $\mathcal{M}$, Lie$(\mathcal{F})$ représente l'algèbre de Lie générée par $\mathcal{F}$. En d'autres termes, elle est définie comme la plus petite algèbre qui contient l'ensembles des crochets de Lie et leurs itérés de la famille de champs de vecteurs $\mathcal{F}$. Finalement, pour tout point $\mathbf{X}\in\mathcal{M}$, Lie$_{\mathbf{X}}(\mathcal{F})$ représente l'espace de tous les vecteurs tangents $\mathbf{V}(\mathbf{X})$ avec $\mathbf{V}$ dans Lie$(\mathcal{F})$. Il s'en suit que Lie$_{\mathbf{X}}(\mathcal{F})$ est un sous espace linéaire de $T_{\mathbf{X}}\mathcal{M}$ et donc il est de dimension finie.

Les crochets de Lie et l'algèbre de Lie jouent un rôle important en théorie du contrôle de dimension finie. En effet, nous rappelons le théorème de Chow (voir [29] pour plus de détails) :

Théorème 1 (Chow) *Soit $\mathcal{M}$ une variété connexe non vide. Supposons que $\mathcal{F}=(\mathbf{F}_i)_{i=1}^m$ soit une famille de champs de vecteurs sur $\mathcal{M}$ telle que $\mathbf{F}_i\in C^\infty(\mathcal{M},T\mathcal{M})$, $\forall i\in\{1,\dots,m\}$. Si l'algèbre de Lie vérifie*

$$Lie_{\mathbf{X}}(\mathcal{F}) = T_{\mathbf{X}}(\mathcal{M})\,,\ \forall \mathbf{X}\in\mathcal{M}\,,$$

alors,pour tout $(\mathbf{X}^0,\mathbf{X}^1)\in\mathcal{M}\times\mathcal{M}$, et pour tout $T>0$, il existe $\mathbf{u}\in L^\infty([0,T];\mathbb{R}^m)$ tel que la solution du problème de Cauchy,

$$\begin{cases} \dot{\mathbf{X}} = \displaystyle\sum_{i=1}^m u_i\mathbf{F}_i(\mathbf{X})\,, \\ \mathbf{X}(0) = \mathbf{X}^0\,, \end{cases} \tag{9}$$

soit définie sur $[0,T]$ et satisfasse $\mathbf{X}(T)=\mathbf{X}^1$.

Le théorème 1 est un résultat de contrôlabilité global. Nous rappelons aussi celui qui donne la contrôlabilité locale pour des temps petits (voir [29], p. 135).

Théorème 2 *Soient Ω un sous espace non vide de $\mathbb{R}^n$ et $\mathcal{F}=(\mathbf{F}_i)_{i=1}^m$, une famille de champs de vecteurs, tel que $\mathbf{F}_i\in C^\infty(\Omega,\mathbb{R}^n)$, $\forall i\in\{1,\dots,m\}$.*
Soit $\mathbf{X}_e\in\mathcal{M}$ tel que

$$Lie_{\mathbf{X}_e}(\mathcal{F}) = \mathbb{R}^n\,.$$

Alors, pour tout $\epsilon>0$, il existe a nombre réel $\eta>0$ tel que, pour tout $(\mathbf{X}^0,\mathbf{X}^1)\in\{\mathbf{X}$ tel que $\|\mathbf{X}-\mathbf{X}_e\|<\eta\}^2$, il existe une fonction bornée et mesurable $\mathbf{u}:[0,\epsilon]\to\mathbb{R}^n$ tel que la solution du problème de Cauchy

$$\begin{cases} \dot{\mathbf{X}} = \displaystyle\sum_{i=1}^m u_i\mathbf{F}_i(\mathbf{X})\,, \\ \mathbf{X}(0) = \mathbf{X}^0\,, \end{cases} \tag{10}$$

est définie sur $[0,\epsilon]$ et satisfait $\mathbf{X}(\epsilon)=\mathbf{X}^1$.

Lorsque les champs de vecteurs sont analytiques et la variété $\mathcal{M}$ est analytique, le théorème de Hermann-Nagano donne des résultats plus fins (voir par exemple [51]).

Théorème 3 (Hermann-Nagano) *Soit $\mathcal{M}$ un variété lisse, et $\mathcal{F}$ une famille de champs de vecteurs analytique sur $\mathcal{M}$. Alors,*

1. *chaque orbite de $\mathcal{F}$ est une sous-variété analytique de $\mathcal{M}$, et*

2. *si $\mathcal{N}$ est une orbite de $\mathcal{F}$, alors l'espace tangent de $\mathcal{N}$ au point $\mathbf{X}$ est donné par $Lie_{\mathbf{X}}(\mathcal{F})$. En particulier, la dimension de $Lie_{\mathbf{X}}(\mathcal{F})$ est constante lorsque $\mathbf{X}$ varie sur l'orbite $\mathcal{N}$.*

Dans notre contexte, la famille de champs de vecteurs est donnée par les fonctions $\mathcal{F} = (\mathbf{F}_i)_{1\leq i\leq k}$ qui apparaissent dans la dynamique du nageur (8) et qui sont définies sur la variété $\mathcal{S}$. Enfin, les contrôles u_i sont représentés par les vitesses de déformation du nageur $\dot{\xi}_i$.

3 Synthèse des principales contributions de la thèse

La thèse est composée de trois parties découpées en cinq chapitres indépendants avec chacun leur propre notation.

La première partie de cette thèse présente un modèle de nageur appelé le "N-link swimmer". Cette partie est composée de deux chapitres. Le premier chapitre présente le "N-link swimmer". Ce modèle a l'intérêt d'avoir une dynamique simple, permettant ainsi à notre prototype d'être un outil facile à utiliser pour le design et l'optimisation de micro-machine inspirée de la biologie. Le second chapitre étudie la contrôlabilité du "N-link swimmer". Il en résulte une analyse numérique des brassées associées à un déplacement optimal en temps. La seconde partie traite de l'effet de la présence d'un bord sur la contrôlabilité de micro-nageurs. Cette étude sera développée pour des nageurs particuliers constitués de plusieurs boules reliés les unes aux autres par des bras. Tout d'abord, nous consacrons le chapitre 3 à l'analyse des effets d'un bord lisse sur la contrôlabilité de ces nageurs. Ensuite, le chapitre 4 étend les résultats du chapitre précédent au cas d'un bord rugueux. Enfin, la partie 5 s'intéresse aux propriétés mathématiques qui caractérisent un déplacement optimal d'un nageur ayant une dynamique sans dérive.

Nous développons maintenant une synthèse des principaux résultats obtenus pour chaque chapitre de la thèse.

3.1 Partie 1 : Le N-link swimmer

Cette partie est consacrée à l'étude d'un modèle de nageur simplifié, appelé le "N-link swimmer". Il est une généralisation à N tiges du "Three-link swimmer", nageur introduit par Purcell dans [70]. Nous proposons une étude approfondie de ses caractéristiques en terme de mobilité dans le plan et de stratégie optimale de déplacement. Le chapitre 1 introduit le modèle. Le chapitre 2 est consacré au problème de la contrôlabilité du nageur et de ses déplacements optimaux.

Chapitre 1 : Self-propulsion of slender micro-swimmers by curvature control : N-link swimmers

Les résultats de ce chapitre ont fait l'objet d'une publication écrite en collaboration avec François Alouges, Antonio DeSimone et Marta Zoppello, à paraître dans la revue *International Journal of Non-Linear Mechanics*.

Le N-link swimmer est un modèle de nageur constitué de N tiges rigides liées les unes aux autres. Il est supposé évoluer dans un plan. L'état du nageur est décrit par les coordonnées de l'extrémité de la première tige, notée $\mathbf{x}_1$ et par son orientation, notée θ_1. La forme du nageur est représentée par le $(N-1)$–uplet $(\alpha_2, \cdots, \alpha_N)$ qui décrit l'orientation relative des tiges (voir figure 1.1).

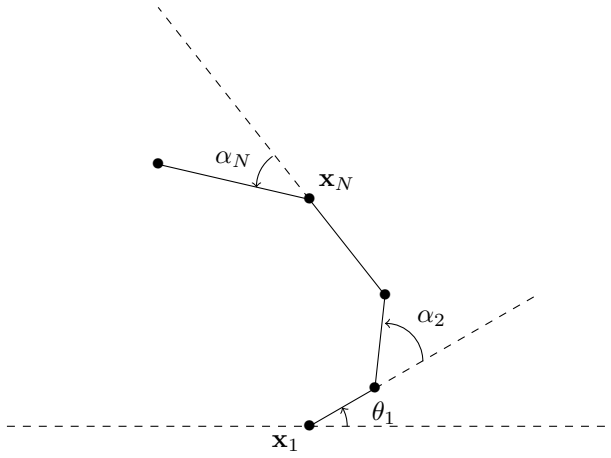

FIGURE 3 – Système de coordonnées du "N-link swimmer".

Dans ce chapitre, nous utilisons l'approximation de la "Resisitive Force Theory" pour obtenir les forces que le fluide exerce sur le nageur. Cette approximation de couplage hydrodynamique entre le fluide et le solide est introduite par J. Gray and J. Hancook en 1955 dans [49] pour approcher la dynamique d'un flagelle. La dynamique prédite en utilisant ce couplage dépend beaucoup du ratio des coefficients de friction η et ξ. Leur valeur est un paramètre clef qui a été le sujet de nombreuses études (voir [23], [26], [31], [50], [55], [78]). Il a été observé ([26], [49], [52], [73], [96]) que cette approche simple et concise permet une bonne approximation de la dynamique d'un flagelle lorsque celui-ci est confiné entre deux surfaces solides.

En notant $\mathbf{e}_i$ (respectivement $\mathbf{e}_i^\perp$) le vecteur unitaire directeur d'une tige de longueur L (respectivement le vecteur directeur perpendiculaire à la tige), la "Resistive Force Theory" définie la densité des forces exercées par le fluide sur la tige par l'expression,

$$\mathbf{f}_i(s) := -\xi \left(\mathbf{v}_i(s) \cdot \mathbf{e}_i\right) \mathbf{e}_i - \eta \left(\mathbf{v}_i(s) \cdot \mathbf{e}_i^\perp\right) \mathbf{e}_i^\perp, \tag{11}$$

où $s \in [0, L]$, η et ξ sont respectivement des coefficients de friction.

En négligeant la force que les tiges exercent les unes sur les autres, nous obtenons une expression de la dynamique du N-link swimmer de la forme,

$$\begin{pmatrix} \dot{\mathbf{x}}_1 \\ \dot{\theta}_1 \end{pmatrix} = \sum_{i=2}^{N} \mathbf{g}_i \left(\theta_1, \alpha_2, \cdots, \alpha_N\right) \dot{\alpha}_i \,, \tag{12}$$

où les $N-1$ champs de vecteurs $\{\mathbf{g}_i\}_{i=2}^N$ sur $[0, 2\pi]^{N-1}$ sont explicites (voir chapitre 1). Les angles entre les tiges permettent une représentation discrète de la courbure du nageur, concentrée en chaque point de lien entre les tiges. Ainsi, l'équation du mouvement (12) donne une unique trajectoire en réponse à une déformation donnée du nageur.

La simplicité des équations qui gouvernent la dynamique (12) permet de faire de notre modèle un outil intéressant pour le design de micro-robots nageurs et l'optimisation de leur performance. Le chapitre 1 contient une étude numérique qui teste les propriétés de précisions et de robustesse de ce modèle à travers trois exemples représentatifs de la micro-nage :

le Purcell's swimmer, la récente étude quantitative du mouvement circulaire d'un spermatozoïde contenu dans le papier de Fredrich [37] et le nageur de Taylor introduit dans [84]. Enfin, nous obtenons aussi une formule explicite du déplacement du Purcell's swimmer introduit par Purcell (voir [70]) pour des déformations de petites amplitudes.

Chapitre 2 : Controllability and Optimal Strokes for N-link Microswimmer

Les résultats de ce chapitre ont fait l'objet d'un proceeding écrit en collaboration avec Pierre Martinon et Marta Zoppello, soumis à la conférence *Decision and Control 2013 (IEEE)*.

Le chapitre 2 étudie la mobilité du "N-link swimmer". En particulier, les questions traitées sont les suivantes :

1. Le "N-link swimmer" est-il capable d'atteindre tous les points de l'espace dans lequel il évolue (i.e., le plan) ?
2. Quelle est la meilleure stratégie pour atteindre le plus rapidement possible une position donnée ?

La contrôlabilité du "N-link swimmer" est caractérisée par le résultat suivant :

Théorème 4 *En considérant le "N-link swimmer" décrit plus haut avec $N \geq 3$. Pour presque toutes longueurs de tiges $(L_i)_{i=1,\dots,N}$, pour toutes configurations initiales $(\mathbf{x}_1^i, \theta_1^i, \alpha_2^i, \cdots, \alpha_N^i) \in \mathbb{R}^2 \times [0, 2\pi]^N$, pour toutes configurations finales $(\mathbf{x}_1^f, \theta_1^f, \alpha_2^f, \cdots, \alpha_N^f)$ et pour tout temps $T > 0$, il existe une déformation de forme du nageur $(\alpha_2, \cdots, \alpha_N) \in \mathcal{W}^{1,\infty}([0,T])$ qui verifie $(\alpha_2, \cdots, \alpha_N)(0) = (\alpha_2^i, \cdots, \alpha_N^i)$ et $(\alpha_2, \cdots, \alpha_N)(T) = (\alpha_2^f, \cdots, \alpha_N^f)$ et telle que si le nageur démarre au point $(\mathbf{x}_1^i, \theta_1^i)$ avec la forme $(\alpha_2^i, \cdots, \alpha_N^i)$, il atteint la position $(\mathbf{x}_1^f, \theta_1^f)$ avec la forme $(\alpha_2^f, \cdots, \alpha_N^f)$ au temps T en utilisant la déformation $t \mapsto (\alpha_2, \cdots, \alpha_N)(t)$.*

En d'autres termes, pour tout nageur composé de plus de trois tiges, il existe un cycle de déformation qui lui permet d'atteindre la position désirée. La preuve de ce résultat repose sur l'utilisation d'outils développés par la théorie du contrôle géométrique (théorème de Chow 1 et théorème de Nagano 3). Intuitivement, un nageur constitué de nombreux degrés de liberté devrait être contrôlable. La résultat précédent permet de montrer que le "N-link swimmer" est contrôlable dès lors que $N \geq 3$.

Par conséquent, le problème de contrôle optimal qui consiste à trouver un cycle de déformation de forme qui minimise le temps d'atteinte de la configurations désirée en partant d'un point fixé est bien posé. L'existence de solutions est un corollaire du résultat de contrôlabilité 4 et s'appuie sur le theorème de Filippov-Cesary (voir [85]).

Enfin, plusieurs stratégies optimales obtenues numériquement dans le cas $N = 3$ sont comparées à la brassée introduite par Purcell. Ces développements numériques indiquent que, pour certaines positions initiales et finales, les solutions au problème de contrôle optimal sont périodiques et peuvent donc être assimilées à des brassées.

3.2 Partie 2 : Effets des bords sur la contrôlabilité d'un nageur

Dans cette partie, nous examinerons les effets de la présence d'un bord sur la mobilité de micro-nageurs. En effet, le bord modifie la distribution de vitesse du fluide à l'intérieure du domaine (voir par exemple [24], [20]). De nombreuses expériences biologiques ont montré que la mobilité de micro-organismes est affectée dans un espace confiné (voir par exemple

[74], [91], [92]). Ces observations conduisent à des investigations plus théoriques qui mettent en évidence les conséquences de la présence du bord sur le déplacement de micro-nageurs. Ainsi, les travaux de J. R. Blake et al. [38], [81], [82] modélisent les effets attractifs de la présence de bord sur la dynamique de nageurs ayant un flagelle. D'autres approches plus théorique, comme celle de A. P. Berke et P. Allison dans [17] (ils mettent en évidence des effets attractifs lorsque le nageur est modélisé par un dipôle), et celle de Y. Or et M. Murray dans [68], ils analysent la dynamique de nageurs près d'un mur plat, cependant les modèles considérés se déplacent sans changer de forme i.e., qu'ils imposent un mouvement de rotation sur leur extrémités. Dans cette partie, nous analysons l'influence du mur plat ou rugueux sur la mobilité de micro-nageurs, en faisant usage de la théorie du contrôle pour développer notre analyse. L'objectif est de comprendre si la présence d'un bord change la capacité de déplacement d'un micro nageur. Nous commençons par étudier, dans le chapitre 3, les effets de la présence d'un mur "lisse" (i.e., plat) sur la contrôlabilité de micro-nageurs. Puis, le chapitre 4 propose d'élargir l'analyse précédente au cas où le bord est rugueux.

Chapitre 3 : Enhanced controllability of low Reynolds number swimmers in the presence of a wall

Les résultats de ce chapitre ont fait l'objet d'une publication écrite en collaboration avec François Alouges, publiée dans la revue *Acta Applicandae Mathematicae* (voir [11]).

Dans ce chapitre, le domaine fluide $\mathcal{O}$ est défini par le demi-espace $\{(x, y, z) \in \mathbf{R}^3 \text{ s.t. } z \geq 0\}$. De plus, nous considérons deux nageurs particuliers constitués de plusieurs boules liées par des bras très fins. Plus particulièrement, nous concentrons notre attention sur le "3-sphere" et le "4-sphere swimmer" représentés (resp.) par la figure 4.2 et la figure 4. Le "3-sphere swimmer" a été introduit par Najafi and Golestanian dans [66], Ce modèle de nageur a ensuite été le sujet de nombreuses études, citons par exemples les travaux Golestanian et Adjari [47], [48], et ceux de F. Alouges et A. DeSimone et al. [7], [8].

Soit un tétraèdre régulier $(\mathbf{S}_1, \mathbf{S}_2, \mathbf{S}_3, \mathbf{S}_4)$ ayant pour centre $\mathbf{O} \in \mathbf{R}^3_+$. Le "4-sphere swimmer" est constitué de quatre sphères reliées par des bras qui sont capables de se rétrécir ou bien de se rallonger selon la direction $\overrightarrow{\mathbf{OS}}_i$ (voir Fig. 4). Le nageur est décrit par la liste de paramètres $(\xi_1, \ldots, \xi_4, \mathbf{c}, \boldsymbol{\mathcal{R}}) \in \mathcal{S}$ où $\mathcal{S} = (\sqrt{\frac{3}{2}}a, \infty)^4 \times \mathbb{R}^3_+ \times SO(3)$. La variable ξ_i denote la longueur du bras i $(i = 1, \ldots, 4)$, $\mathbf{c}$ est la coordonnée du centre du nageur et $\boldsymbol{\mathcal{R}}$ décrit l'orientation du nageur.

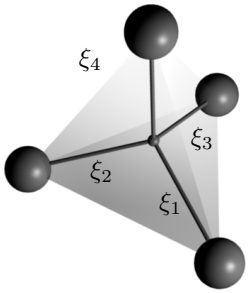

FIGURE 4 – The Four-sphere swimmer.

Le "3-sphere swimmer" est constitué de trois boules alignées (voir Fig 4.2). Il est représenté par le vecteur $(\xi_1, \xi_2, \theta, \phi, \mathbf{x}_c) \in \mathbb{R}^3 \times [0, 2\pi]^2$ où θ est l'angle entre le nageur et l'axe z, ϕ est l'angle entre l'axe y et la projection de la direction du nageur dans le plan Oxy et $\mathbf{x}_c$ est la coordonnée du centre de la sphère milieu.

L'objectif est de comparer les résultats obtenus pour ces nageurs dans l'espace $\mathbb{R}^3$ tout entier avec leur généralisation dans le cas où ils évoluent dans le demi-espace $\mathcal{F}$. Dans le cas de l'espace $\mathbb{R}^3$, il a été montré dans [7] que le "4-sphere swimmer" est contrôlable, tandis que le "3-sphere swimmer" peut se déplacer dans une unique direction (celle qui définie son orientation).

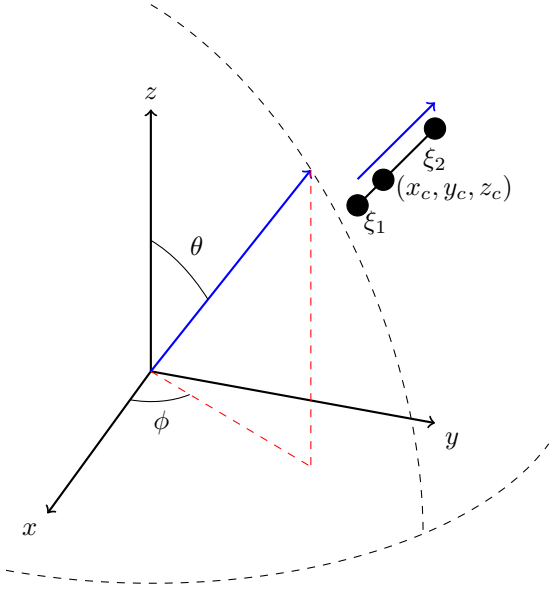

FIGURE 5 – Coordinates of the 3-sphere swimmer

On considère que le nageur est constitué de N sphères de rayon a que l'on note B_l, $l = 1, \ldots, N$ ($N = 3$ pour le "3-sphere swimmer" et $N = 4$ pour le "4-sphere swimmer"). Par ailleurs, on note $H^{1/2}$ (resp. $H^{-1/2}$) l'espace fractionnaire de Sobolev classique (resp. l'espace fonctionnel définie comme l'espace image par l'opérateur Trace de H^1), pour une définition plus détaillée de ces espaces voir [25].

Une étape préliminaire est de considérer l'opérateur Dirichlet-to-Neumann associé au problème de Stokes.

$$DN : \prod_{l=1}^{N} H^{1/2}(\partial B_l) \mapsto \prod_{l=1}^{N} H^{-1/2}(\partial B_l), \quad (\mathbf{u}_l) \mapsto (\mathbf{f}_l := \sigma(\mathbf{u}, p)n|_{\partial B_l}),$$

où $(\mathbf{u}, p)$ est solution du problème de Stokes

$$-\Delta \mathbf{u} + \nabla p = 0, \quad \text{div } \mathbf{u} = 0 \quad \text{in } \mathcal{F}, \quad \mathbf{u}|_{\partial \mathcal{O}} = 0, \quad \mathbf{u}|_{\partial B_l} = \mathbf{u}_l.$$

Plus précisément, les champs de vecteurs utilisent l'opérateur DN restreint aux N-uplet de champ vitesses rigides définis sur la frontière entre les boules et le fluide, i.e., ∂B_l,

$l = 1, \dots, N$. Nous appelons R l'espace de dimension fini de tel N-uplets. Nous pouvons remarquer que pour tout $(\mathbf{u}_l)_{l=1}^N \in R$

$$DN\left((\mathbf{u}_l)\right) \;=\; \mathcal{T}^{-1}\left((\mathbf{u}_l)\right)$$

où

$$\mathcal{T} : \prod_{l=1}^{N} H^{-1/2}(\partial B_l) \mapsto \prod_{l=1}^{N} H^{1/2}(\partial B_l), \quad (\mathbf{f}_l) \mapsto (\mathbf{u}_l \;:=\; \mathbf{u}|_{\partial B_l})$$

et $\mathbf{u}$ est la solution du problème de Stokes suivant dans $\mathcal{O}$:

$$-\Delta \mathbf{u} + \nabla p \;=\; \sum_{l=1}^{N} 1_{\partial B_l} \mathbf{f}_l, \quad \text{div } \mathbf{u} = 0 \quad \text{dans} \quad \mathcal{O}, \quad \mathbf{u}|_{\partial \mathcal{O}} = 0.$$

Dans le cas d'un mur plat, l'opérateur $\mathcal{T}$ est explicite et s'exprime à l'aide de la formulation intégrale suivante,

$$\forall \mathbf{r} \in \partial B, \qquad (\mathcal{T}(\mathbf{f}_1, \dots, \mathbf{f}_N))_i(\mathbf{r}) = \sum_{j=1}^{N} \int_{\partial B} \mathbf{K}(\mathbf{x}_i + a\mathbf{r}, \mathbf{x}_j + a\mathbf{s}) \mathbf{f}_j(\mathbf{s}) d\mathbf{s}. \tag{13}$$

La fonction de Green $\mathbf{K}$ est exprimée comme une perturbation de la fonction de Green $\mathbf{G}$ associée à l'espace $\mathbb{R}^3$. En d'autres termes, la fonction $\mathbf{K}$ s'écrit comme suit

$$\mathbf{K}(\mathbf{r}, \mathbf{r}_0) = \mathbf{G}(\mathbf{r} - \mathbf{r}_0) + \tilde{\mathbf{K}}_1(\mathbf{r}, \mathbf{r}_0)\,. \tag{14}$$

où $\tilde{\mathbf{K}}_1$ est donnée explicitement dans le chapitre 3. Notons que la fonction $\tilde{\mathbf{K}}_1$ a été introduite par Blake dans les années 70 (voir [20]).

Une première conséquence de ces derniers developpements est l'obtention du résultat de persistance de la contrôlabilité du "4-sphere swimmer" presque partout dans le demi-espace. Le résultat s'énonce comme suit,

Théorème 5 *Soit le "4-sphere swimmer". Nous supposerons qu'il est auto-propulsé, qu'il est immergé dans un fluide de Stokes, et qu'il évolue dans un demi-espace. Pour presque toute configuration initiale $(\boldsymbol{\xi}^i, \mathbf{p}^i) \in \mathcal{S}$, pour presque toute configuration finale $(\boldsymbol{\xi}^f, \mathbf{p}^f)$ dans un voisinage de $(\boldsymbol{\xi}^i, \mathbf{p}^i) \in \mathcal{S}$ et pour tout temps $T > 0$, il existe une brassée $\boldsymbol{\xi} \in \mathcal{W}^{1,\infty}([0,T])$ qui vérifie $\boldsymbol{\xi}(0) = \boldsymbol{\xi}^i$ et $\boldsymbol{\xi}(T) = \boldsymbol{\xi}^f$ et telle que le nageur démarre en position $\mathbf{p}^i$ avec la forme $\boldsymbol{\xi}^i$ au temps intial et atteint la position $\mathbf{p}^f$ avec la forme $\boldsymbol{\xi}^f$ au temps T par la déformation $t \mapsto \boldsymbol{\xi}(t)$.*

Notons que la preuve de ce théorème utilise des arguments généraux qui peuvent probablement être utilisés pour d'autre modèle de micro-nageurs.

La seconde partie de ce chapitre traite de la contrôlabilité du "3-sphere swimmer". Remarquons que, due à la symétrie du système "fluide-nageur", celui-ci ne peut pas quitter le plan dans lequel il démarre au temps $t = 0$. En d'autres termes, l'angle ϕ reste constant égal à $\phi(0)$ pour tout $t > 0$.

Dans le cas du "3-sphere swimmer", nous montrons que la présence d'un bord augmente le nombre de directions dans lesquelles le nageur peut se déplacer. Plus précisément, nous montrons que ce nageur peut atteindre localement toutes les directions du plan. Le théorème que nous obtenons s'énonce comme suit,

Théorème 6 *Soit le "3-sphere swimmer". Nous supposerons qu'il est auto-propulsé, qu'il est immergé dans un fluide de Stokes et qu'il évolue dans un demi-espace. Pour presque toute configuration initiale* $(\boldsymbol{\xi}^i, \mathbf{p}^i) \in \mathcal{S}$*, pour presque toute configuration finale* $(\boldsymbol{\xi}^f, \mathbf{p}^f)$ *dans un voisinage de* $(\boldsymbol{\xi}^i, \mathbf{p}^i) \in \mathcal{S}$ *et pour tout temps* $T > 0$*, il existe une brassée* $\boldsymbol{\xi} \in \mathcal{W}^{1,\infty}([0,T])$ *qui vérifie* $\boldsymbol{\xi}(0) = \boldsymbol{\xi}^i$ *et* $\boldsymbol{\xi}(T) = \boldsymbol{\xi}^f$ *et telle que le nageur démarre en position* $\mathbf{p}^i$ *avec la forme* $\boldsymbol{\xi}^i$ *au temps initial et atteint la position* $\mathbf{p}^f$ *et la forme* $\boldsymbol{\xi}^f$ *au temps* T *par la déformation* $t \mapsto \boldsymbol{\xi}(t)$*.*

La preuve de ce théorème est basée sur une analyse très précise de l'algèbre de Lie engendrée par les champs de vecteurs de la dynamique du nageur. Cette étude est basée sur un développement asymptotique des champs de vecteurs qui génèrent l'algèbre de Lie considérée. Finalement, le résultat de contrôlabilité est basé sur le théorème de Chow 1. Notons que la régularité des champs de vecteurs est fondamentale dans la preuve de ce résultat.

Chapitre 4 : Rough wall effect on micro-swimmers

Les résultats de ce chapitre ont été écrits en collaboration avec David Gérard-Varet.

Ce chapitre est une généralisation du précèdent. Il concerne l'extension des Théorèmes 5 et 6 dans le cas où le mur présente une rugosité, représenté par la surface $(x, y) \mapsto \varepsilon h(x, y)$. Nous supposons que $\|h\|_\infty = 1$. Ainsi, la variable ε représente l'amplitude de la rugosité du bord.

Le principe, qui guide cette étude, est de considérer le nouveau système "fluide-nageur" comme une perturbation du système précèdent. Le système fluide-solide est représenté par le problème de Stokes (1) où le domaine du fluide est donné par

$$\mathcal{O} := \{(x, y, z) \text{ tel que } z > h(x, y)\} .$$

La difficulté intervient, principalement, dans le fait que l'opérateur Dirichlet-to-Neumann associé à ce problème n'est pas explicite, contrairement au cas du bord lisse traité précédemment. Ainsi, la régularité des champs de vecteurs constitue dans ce chapitre un résultat délicat. Il s'énonce comme suit.

Théorème 7 *Soit l'ensemble*

$$\mathcal{A} := \{(\varepsilon, a, \boldsymbol{\xi}, \mathbf{p}) \in \mathbb{R} \times \mathbb{R}_+^* \times (\mathbb{R}_+^*)^k \times (\mathbb{R}^3 \times SO(3)) \text{ tel que } B_i \cap B_j = \emptyset \, \forall i \neq j, \text{ and } B_i \cap \partial\mathcal{O} = \emptyset \, \forall i\},$$

pour tout $i = 1, \dots, k$*, le champ* $\mathbf{F}^i(\xi, p)$ *associé à la dynamique (8) du nageur pour le domaine fluide* $\mathcal{F}$ *est une fonction analytique de* (ε, a, ξ, p) *sur* $\mathcal{A}$*.*

La preuve nécessite plusieurs étapes. Tout d'abord, un habile changement de variables permet de se ramener à un problème elliptique à bord fixe ayant les paramètres qui interviennent analytiquement en tant que coefficient. Ensuite, la régularité découle du théorème des fonctions implicites ainsi que de la proposition suivant qui garantie l'existence de solutions au problème de Stokes "généralisé".

Proposition 8 *Soit*

$$\overline{\mathcal{V}}_0 := \left\{ \mathbf{U} \in \mathcal{D}'(\overline{\mathcal{F}}, \mathbf{R}^3) \,|\, \nabla \mathbf{U} \in L^2(\overline{\mathcal{F}}), \, \frac{\mathbf{U}(\mathbf{r})}{\sqrt{1 + |\mathbf{r}|^2}} \in L^2(\overline{\mathcal{F}}), \quad \mathbf{U}|_{\partial\bar{\mathcal{O}}} = 0. \right\} .$$

Soit $(F, G, V_1, ..., V_N)$ *donné dans* $(\mathcal{V}_0)' \times L^2(\mathcal{F}) \times \prod_l H^{1/2}(B_l)$. *Il existe une unique solution* (V, Q) *in* $\mathcal{V}_0 \times L^2(\mathcal{F})$ *de*

$$\begin{aligned} -\Delta V + \nabla Q &= F \quad in\, \mathcal{F}, \\ div\, V &= G \quad in\, \mathcal{F}, \\ V = 0 \quad at\, \partial\mathcal{O}, \quad V = V_l \quad at\, \partial B_l, \quad l &= 1...N. \end{aligned}$$

Cette proposition est l'extension du résultat de Bogovskii (voir [39]). Le théorème 5 dans le cas d'un mur rugueux découle de la régularité des champs de vecteurs.

Ensuite, nous montrons que la présence de rugosité permet au "3-sphere swimmer" d'être localement contrôlable. Il est important de remarquer que l'angle qui définit la rotation du nageur autour de son axe n'est pas utile pour décrire la position du nageur. Il sera prouvé dans ce chapitre qu'il n'intervient pas dans les termes principaux du développement asymptotique considéré par la suite pour prouver le théorème suivant énonçant la contrôlabilité du "3-sphere swimmer".

Théorème 9 *Il existe une surface* $h(x, y)$ *telle que le 3-sphere swimmer est localement controlable presque partout (à rotation autour de son axe près).*

Notons d'abord que la dynamique considérée pour obtenir ce résultat est celle du sous-système qui gouvernent l'évolution des variables ξ_1, ξ_2, θ, ϕ et $\mathbf{x}_c$.

La preuves de ce résultat est basée sur le développement asymptotique des champs de vecteurs $\mathbf{F}_i$ $i = 1, .., k$ lorsque la rugosité ε et le rayon des boules a sont petits. Il s'agit ensuite de calculer les premiers crochets de Lie de ces champs de vecteurs et d'expliciter le développement asymptotique du déterminant de cinq d'entres eux. La contrôlabilité du nageur en découle en utilisant le théorème de Chow 1.

3.3 Partie 3 : Problème de contrôle optimal

Les résultats de ce chapitre ont été écrit en collaboration avec Thomas Chambrion et Alexandre Munnier.

L'objectif de ce travail est de fournir un cadre à l'étude de problèmes de contrôle optimal associés aux déplacements de micro-nageurs. L'étude propose de développer la connexion, déjà souligné dans le livre de R. Montgomery [63], entre la géométrie sous-Riemannienne et les problèmes de contrôle optimal liés à la nage de micro-organismes. Plus précisément, nous utilisons les structures géométriques, Riemannienne et sous-Riemannienne, sous-jacentes afin de caractériser les stratégies optimales de déplacement pour les nageurs ayant une dynamique sans dérive. Plus particulièrement, nos résultats s'appliquent à tous les nageurs qui sont gouvernés par une dynamique linéaire en les vitesses de déformations de leur corps et sans dérive. Ce type d'équation du mouvement est aussi obtenu lorsque le fluide est gouvernée par l'équation d'Euler sans vorticité. Ce régime est utilisé pour modéliser le déplacement de poisson ayant un corps très allongé (comme par exemple une anguille). Nous citons les travaux de T. Chambrion et A. Munnier sur ce sujet [27], [28], [64], [65]. Nous signalons que dans le cas d'un fluide parfait ayant une vorticité non nulle, la dynamique du nageur n'a plus la forme considéré plus haut (linéaire en les vitesse de déformation de l'objet). Nous referons au travaux de O. Glass et T. Horsin qui prouvent des résultats de contrôlabilité un ensemble de particules (représenté par une courbe de Jordan) immergée dans un fluide parfait en dimension deux et trois ([45], [46]).

Afin de mieux comprendre les problèmes de contrôle optimal qui sont considérés dans ce chapitre, nous présentons le contexte mathématique sous-jacent. Dans la suite, nous nous intéressons à l'étude de brassée optimale i.e., le problème optimal a pour contrainte que le nageur ait la même forme au début et à la fin de son mouvement. Nous allons associé au nageur le 5-uplet $\mathfrak{S} = (\mathcal{S}, \mathbf{g}, \mathbf{Q}^{\mathcal{S}}, \mathbf{s}^{\dagger}, \mathcal{L})$, où :

- $(\mathcal{S}, \mathbf{g})$ est une variété connectée de dimension N ($N \geq 1$) muni d'une structure Riemannienne $\mathbf{g}$. Chaque élément $\mathbf{s}$ de $\mathcal{S}$ correspond à une forme du nageur possible. La déformation du nageur est représentée par une fonction à valeur dans $[0, T]$, l'intervalle de temps considéré, $\mathbf{s} : [0, T] \mapsto \mathbf{s}(t) \in \mathcal{S}$.

- La métrique $\mathbf{g}$ est utilisée pour quantifier le cout nécessaire à la déformation du nageur. Le cout du changement de forme $\mathbf{s} : [0, T] \mapsto \mathbf{s}(t) \in \mathcal{S}$ est, par exemple, donné par la longueur de la courbe paramétrée par la fonction $\mathbf{s}$, i.e.

$$\int_0^T \sqrt{\mathbf{g}_{\mathbf{s}(t)}(\dot{\mathbf{s}}(t), \dot{\mathbf{s}}(t))} \mathrm{d}t, \tag{15a}$$

  ou représenté par un cout "énergétique",

$$\frac{1}{2} \int_0^T \mathbf{g}_{\mathbf{s}(t)}(\dot{\mathbf{s}}(t), \dot{\mathbf{s}}(t)) \mathrm{d}t. \tag{15b}$$

- L'application $\mathbf{Q}^{\mathcal{S}} : T\mathcal{S} \to \mathbb{R}^n$ est une forme linéaire analytique. Elle représente les contraintes physiques imposées sur la déformation du nageur (comme, par exemple, conservation du volume au cours de la déformation, ou bien, empêcher les mouvement de translation du centre de masse). Pour être plus explicite,

  Définition 10 *Une déformation admissible est représentée par toute courbe absolument continue* $\mathbf{s} : [0, T] \to \mathcal{S}$*, ayant une dérivée bornée et qui vérifie pour presque tout temps,*

$$\mathbf{Q}^{\mathcal{S}}_{\mathbf{s}(t)} \dot{\mathbf{s}}(t) = 0. \tag{16}$$

- La forme de référence $\mathbf{s}^{\dagger}$ est un point de $\mathcal{S}$ qui peut être la forme avec laquelle le nageur commence sa brassée.

- Pour simplifier, nous supposons que la déformation du corps du nageur est axisymétrique. Par conséquent, elle provoque un déplacement du centre de masse du nageur dans une unique direction. On dénote par le réel r la position du centre de masse du nageur. Le mouvement dans cette direction est mesuré pare à la forme linéaire $\mathcal{L}$ sur $\mathcal{S}$. Plus précisément, pour toute courbe admissible $\mathbf{s} : [0, T] \to \mathcal{S}$, le déplacement du nageur, qui résulte de cette déformation, est donné par la formule :

$$\int_0^T \mathcal{L}_{\mathbf{s}(t)}(\dot{\mathbf{s}}(t)) \mathrm{d}t. \tag{17}$$

Dans ce chapitre, l'équation du mouvement du nageur (8) est modifiée, on prend aussi en compte la dynamique de ses variables de formes. En notant par $\boldsymbol{\xi}$ le vecteur $(\mathbf{s}, r)$, on obtient l'existence d'une famille de champs de vecteurs, noté par $\mathcal{X}$, et représentée par des fonctions $\mathbf{Z}_j$ ($j = 1, \ldots, p$ pour un certain $p \in \mathbb{N}$) de $\mathcal{M} := \mathcal{S} \times \mathbb{R}$, tel que la dynamique de la position du nageur et de sa forme soit gouvernée par :

$$\dot{\boldsymbol{\xi}}(t) = \sum_{j=1}^{p} u_j(t)\mathbf{Z}_j(\boldsymbol{\xi}(t)) \quad (t>0), \tag{18a}$$

$$\boldsymbol{\xi}(0) = \boldsymbol{\xi}^\dagger, \tag{18b}$$

où $\boldsymbol{\xi}^\dagger = (\mathbf{s}^\dagger, 0)$ est la configuration initiale du nageur où $\mathbf{s}^\dagger$ représente sa forme initiale et 0 est sa position initiale. Ensuite, nous introduisons les projections $\pi_{\mathcal{S}}$ et $\pi_{\mathbb{R}}$ par :

$$\pi_{\mathcal{S}} : \begin{array}{ccc} \mathcal{M} & \to & \mathcal{S} \\ (\mathbf{s}, r) & \mapsto & \pi_{\mathcal{S}}(\boldsymbol{\xi}) = \mathbf{s} \end{array} \quad \text{et} \quad \pi_{\mathbb{R}} : \begin{array}{ccc} \mathcal{M} & \to & \mathbb{R} \\ (\mathbf{s}, r) & \mapsto & \pi_{\mathbb{R}}(\boldsymbol{\xi}) = r. \end{array}$$

De plus, nous définissons l'ensemble des contrôles 'admissibles" par :

Définition 11 *Soient $T>0$ et $\mathfrak{S} = (\mathcal{S}, \mathbf{g}, \mathbf{Q}^{\mathcal{S}}, \mathbf{s}^\dagger, \mathcal{L})$ un 5-uplet associé au nageur considéré et soit une famille de champs de vecteur analytique $\mathcal{X}$, nous appelons par $\mathcal{U}^{\mathcal{X}}_{\mathfrak{S}}(T)$ l'ensemble de tous les contôles $\mathbf{u} = (u_j)_{1\le j\le p} \in L^\infty([0,T], \mathbb{R}^p)$ pour lesquels la solution de (18) est définie sur $[0,T]$.*

Pour chaque contrôle $\mathbf{u} \in \mathcal{U}^{\mathcal{X}}_{\mathfrak{S}}(T)$, on appelle

$$t \in [0,T] \mapsto \boldsymbol{\xi}^{\mathcal{X}}_{\mathfrak{S}}(t, \mathbf{u}) \in \mathcal{M},$$

la solution de (18) avec le contrôle $\mathbf{u}$. Soit $\mathfrak{S} = (\mathcal{S}, \mathbf{g}, \mathbf{Q}^{\mathcal{S}}, \mathbf{s}^\dagger, \mathcal{L})$ un nageur contrôlable, soit $\mathcal{K}$ un compact de $\mathcal{S}$ contenant $\mathbf{s}^\dagger$ et soit $\mathcal{X}$ une famille de champs de vecteurs telle que leur projection sur $\mathcal{S}$ est base orthonormale de $\ker \mathbf{Q}^{\mathcal{S}}$. Soient $\boldsymbol{\xi}^\ddagger \in \mathcal{M}$ et $T \ge 0$, nous allons définir les sous-espaces de $\mathcal{U}^{\mathcal{X}}_{\mathfrak{S}}(T)$ suivants :

$$\begin{aligned}
\mathcal{U}^{\mathcal{X}}_{\mathfrak{S}}(\boldsymbol{\xi}^\ddagger, T) &:= \left\{ \mathbf{u} \in \mathcal{U}^{\mathcal{X}}_{\mathfrak{S}}(T) \,:\, \boldsymbol{\xi}^{\mathcal{X}}_{\mathfrak{S}}(T, \mathbf{u}) = \boldsymbol{\xi}^\ddagger \right\}; \\
\widehat{\mathcal{U}}^{\mathcal{X}}_{\mathfrak{S}}(\boldsymbol{\xi}^\ddagger, T) &:= \left\{ \mathbf{u} \in \mathcal{U}^{\mathcal{X}}_{\mathfrak{S}}(\boldsymbol{\xi}^\ddagger, T) \,:\, \|\mathbf{u}(t)\|_{\mathbb{R}^p} = 1 \ \forall\, t \in [0,T] \right\}; \\
\mathcal{U}^{\mathcal{X}}_{\mathfrak{S},\mathcal{K}}(T) &:= \left\{ \mathbf{u} \in \mathcal{U}^{\mathcal{X}}_{\mathfrak{S}}(T) \,:\, \pi_{\mathcal{S}}\boldsymbol{\xi}^{\mathcal{X}}_{\mathfrak{S}}(t, \mathbf{u}) \in \mathcal{K} \quad \forall t \in [0,T] \right\}; \\
\mathcal{U}^{\mathcal{X}}_{\mathfrak{S},\mathcal{K}}(\boldsymbol{\xi}^\ddagger, T) &:= \left\{ \mathbf{u} \in \mathcal{U}^{\mathcal{X}}_{\mathfrak{S}}(\boldsymbol{\xi}^\ddagger, T) \,:\, \pi_{\mathcal{S}}\boldsymbol{\xi}^{\mathcal{X}}_{\mathfrak{S}}(t, \mathbf{u}) \in \mathcal{K} \quad \forall t \in [0,T] \right\}; \\
\widehat{\mathcal{U}}^{\mathcal{X}}_{\mathfrak{S},\mathcal{K}}(\boldsymbol{\xi}^\ddagger, T) &:= \left\{ \mathbf{u} \in \mathcal{U}^{\mathcal{X}}_{\mathfrak{S},\mathcal{K}}(\boldsymbol{\xi}^\ddagger, T) \,:\, \|\mathbf{u}(t)\|_{\mathbb{R}^p} = 1 \ \forall\, t \in [0,T] \right\}.
\end{aligned}$$

Les problèmes de contrôle optimal auxquels on s'intéresse sont formulés par les énoncés suivants.

Problème 12 (Minimiser la longueur Riemannienne) *Soient $\delta^\dagger \in \mathbb{R}$ et $T>0$, posons $\boldsymbol{\xi}^\ddagger = (\mathbf{s}^\dagger, \delta^\dagger)$ la position initiale du nageur et déterminons :*

$$\Phi^{\mathcal{X}}_{\mathfrak{S},\mathcal{K}}(\delta^\dagger, T) = \inf \left\{ \int_0^T \|\mathbf{u}(t)\|_{\mathbb{R}^p} \mathrm{d}t \,:\, \mathbf{u} \in \mathcal{U}^{\mathcal{X}}_{\mathfrak{S},\mathcal{K}}(\boldsymbol{\xi}^\ddagger, T) \right\}. \tag{19}$$

En modifiant le cout, nous nous considérons le problème lié au déplacement qui minimise l'action (l'énergie).

Problème 13 (Minimiser l'action) *Pour tout $\delta^\dagger \in \mathbb{R}$ et $T>0$, posons $\boldsymbol{\xi}^\ddagger = (\mathbf{s}^\dagger, \delta^\dagger)$ et déterminons :*

$$\Theta^{\mathcal{X}}_{\mathfrak{S},\mathcal{K}}(\delta^\dagger, T) = \inf \left\{ \frac{1}{2} \int_0^T \|\mathbf{u}(t)\|^2_{\mathbb{R}^p} \mathrm{d}t \,:\, \mathbf{u} \in \mathcal{U}^{\mathcal{X}}_{\mathfrak{S},\mathcal{K}}(\boldsymbol{\xi}^\ddagger, T) \right\}. \tag{20}$$

Nous énonçons maintenant le problème de temps optimal, étudié par exemple dans ce contexte dans [60].

Problème 14 (Optimiser le temps) *Pour tout $\delta^\dagger \in \mathbb{R}$, on appelle $\boldsymbol{\xi}^\ddagger = (\mathbf{s}^\dagger, \delta^\dagger)$ et déterminons :*

$$T^{\mathcal{X}}_{\mathfrak{S},\mathcal{K}}(\delta^\dagger) = \inf\{T \,:\, \widehat{\mathcal{U}}^{\mathcal{X}}_{\mathfrak{S},\mathcal{K}}(\boldsymbol{\xi}^\ddagger, T) \neq \emptyset\}.$$

Enfin, les problèmes suivants se concentrent sur les stratégies qui permettent au nageur de se déplacer le plus loin possible avec une contrainte sur sa brassée.

Problème 15 (Nager le plus loin possible avec une longueur Riemannienne bornée) *Pour tout $l \geq 0$ and $T \geq 0$, determine :*

$$\Psi^{\mathcal{X}}_{\mathfrak{S},\mathcal{K}}(l,T) = \sup\Big\{\pi_{\mathbb{R}}\boldsymbol{\xi}^{\mathcal{X}}_{\mathfrak{S}}(T,\mathbf{u}) \,:\, \mathbf{u} \in \mathcal{U}^{\mathcal{X}}_{\mathfrak{S},\mathcal{K}}(T),\, \pi_{\mathcal{S}}\xi^{\mathcal{X}}_{\mathfrak{S}}(T,\mathbf{u}) = \mathbf{s}^\dagger, \\ \text{and } \int_0^T \|\mathbf{u}(t)\|_{\mathbb{R}^p}\mathrm{d}t \leq l\Big\}. \quad (21)$$

Problème 16 (Nager le plus loin possible avec une action bornée) *Pour tout $l \geq 0$ et $T \geq 0$, déterminons :*

$$\Lambda^{\mathcal{X}}_{\mathfrak{S},\mathcal{K}}(l,T) = \sup\Big\{\pi_{\mathbb{R}}\boldsymbol{\xi}^{\mathcal{X}}_{\mathfrak{S}}(T,\mathbf{u}) \,:\, \mathbf{u} \in \mathcal{U}^{\mathcal{X}}_{\mathfrak{S},\mathcal{K}}(T),\, \pi_{\mathcal{S}}\xi^{\mathcal{X}}_{\mathfrak{S}}(T,\mathbf{u}) = \mathbf{s}^\dagger, \\ \text{and } \frac{1}{2}\int_0^T \|\mathbf{u}(t)\|^2_{\mathbb{R}^p}\mathrm{d}t \leq l\Big\}. \quad (22)$$

L'objectif de ce chapitre est d'analyser les aspects mathématiques de ces problèmes. Plus particulièrement, nous démontrons :

1. l'existence de solutions à ces problèmes.

2. Nous montrons comment ces problèmes de contrôle optimal pour différents couts fonctionnelles peuvent se déduire les uns des autres.

3. Nous nous intéressons aux propriétés quantitatives des solutions. En particulier, certaines preuves de ces propriétés résultent de la structure de variété sous-Riemannienne que l'on peut définir sur $\mathcal{M}$ muni de la distance, dite de *Carnot-Caratheodory* défini par :

$$\mathrm{d}(\boldsymbol{\xi}^\dagger, \boldsymbol{\xi}^\ddagger) = \inf\left\{\int_0^T \|\mathbf{u}(s)\|_{\mathbb{R}^p}\mathrm{d}s,\, \mathbf{u} \in \mathcal{U}^{\mathcal{X}}_{\mathfrak{S}}(T, \boldsymbol{\xi}^\ddagger)\right\},$$

   où $(\boldsymbol{\xi}^\dagger, \boldsymbol{\xi}^\ddagger)$ sont deux points de $\mathcal{M}$.

4. Nous observons que dans le cas où il y a deux degrés de liberté, la variété $\mathcal{M}$ possède une structures géométrique particulière (elle est dite de *contact*). Ainsi, en utilisant les résultats de l'étude de A. A. Agrachev [1], nous en déduisons des propriétés géométriques supplémentaires pour les solutions des problèmes de contrôle optimal.

5. Enfin, toutes les propriétés seront discutées numériquement en utilisant un modèle de nageur immergé dans un fluide parfait ayant une dynamique explicite (introduit par T. Chambrion et A. Munnier dans [27]).

4 Conclusions et perspectives

Cette section traite des conclusions et des perceptives de la thèse. Elle est divisée en quatre parties. Les trois première sections traitent de la conclusion de la partie considérée et la dernière partie donne des perspectives générales qui émanent de ce travail.

Partie 1 : N-link swimmer

Le N-link swimmer est un modèle de nageur simplifié. Son intérêt principal est qu'il possède une dynamique explicite tout en ayant un comportement proche d'observations empiriques. Les simulations numériques présentées dans le chapitre 2 suggèrent que les solutions du problème de contrôle optimal en temps sont des brassées, c'est à dire des solutions périodiques, sans que cette contrainte soit imposée. Une étude en cours a pour but de montrer théoriquement qu'il existe des stratégies optimales de déplacement qui sont effectivement des brassées.

Dans un second temps, pour élargir notre étude numérique,

- nous souhaitons, tout d'abord, réaliser des tests pour des "N-link swimmer" constitués de plus de trois tiges. Observera-t-on des comportements limites pour N grand ? L'obtention de tel résultat permettrait une comparaison avec la nage de micro-organismes constitués de filaments.
- Ensuite, nous voudrions aussi changer le coût fonctionnel à minimiser. En d'autres termes, plutôt que de travailler sur les stratégies qui minimisent le temps d'atteinte d'un point cible, nous souhaiterions obtenir des stratégies optimales de nage qui minimisent une énergie pour le système (à définir).
- Enfin, l'optimisation des longueurs des tiges du nageur est aussi une direction que nous étudions. Quel profil de nageurs va-t-on obtenir ? Des nageurs ayant des longueurs de tiges égales, toutes différentes, rangées par ordre croissant, etc... ?

Enfin, une dernière perspective de ce travail est de considérer que les tiges du nageur possèdent une charge magnétique et que la déformation du corps du nageur est due à un champ magnétique qui se propage dans le fluide. Que se passe-t-il pour la contrôlabilité d'un tel système de nageur ? Quel champ magnétique permettrait le déplacement désiré ? A ce jour, des physiciens du laboratoire le Spintec à Grenoble, T. Dietsch et H. Joisten, travaillent en collaboration avec F. Alouges, A. DeSimone et moi-même pour tenter de réaliser un micro robot de ce type. Une étude théorique est en cours et plusieurs tests de tels micro-robots ont déjà vu le jour.

Partie 2 : Effets du bord sur la contrôlabilité des micro-nageurs

Dans cette partie, nous étudions l'impact du bord sur la mobilité de nageurs constitués de sphères reliées entres elles. Nous montrons que la présence du bord ne change pas la capacité d'un nageur à se déplacer. Cependant, nous prouvons l'introduction d'un bord permet à un nageur d'augmenter ses directions de déplacement. Intuitivement, la présence du bord a pour effet de briser les symétries du système fluide-solide. La conclusion de cette étude peut s'énoncer simplement : dans la nature, tous les micro-nageurs, aussi symétriques qu'ils soient, sont contrôlables.

Nous souhaiterions poursuivre ces travaux dans deux voies distinctes.

- La première direction est de généraliser cette étude de contrôlabilité à des domaines fluides bornés.

- La seconde direction est de comparer les stratégies de nage optimales dans différents cas : $\mathbb{R}^3$ tout entier, bord lisse et bord rugueux. Cette étude à la fois numérique et théorique permettrait d'expliquer les observations des biologistes si elle montre qu'il est "plus difficile" de s'éloigner du bord plutôt que de s'en rapprocher.

Partie 3 : Problèmes de contrôle optimal

Dans ce chapitre nous proposons un cadre d'étude au problème de contrôle optimal associé au déplacement de nageur ayant une dynamique sans dérive. L'étude est appliquée à un modèle de nageur ayant une dynamique explicite. Une des directions de recherche est d'appliquer notre analyse à un nageur dont la dynamique est non explicite. C'est le cas par exemple du "3-sphere swimmer". En particulier, serait-il possible d'utiliser ici les développements asymptotiques de la partie II pour obtenir les caractérisations géométriques présentées dans la partie III ?

Enfin, un terme de dérive apparait dans la dynamique du nageur lorsque des forces extérieures sont considérées (par exemple dans le cas d'un champ magnétique exogène qui agit sur le corps du nageur). Comment est-il possible d'étendre cette étude dans le cas où le nageur est gouverné par une dynamique avec dérive ?

Perspectives générales

Les perspectives générales de cette thèse sont développées ci-dessous.

- Une piste de recherche est de modéliser le déplacement de nageurs encore plus petits (de la taille d'un nanomètre). A cette échelle, l'agitation des molécules d'eau a un effet notable sur le déplacement du nageur. L'action "aléatoire" des molécules d'eau sur le corps du nageur peut-être formalisée par l'ajout d'un terme stochastique dans sa dynamique. Comment obtenir l'équation du mouvement du nageur ? Comment est-il possible d'étendre les résultats de contrôlabilité à ce cas ?

- Par ailleurs, de nombreux groupes de recherche travaillent sur la modélisation de la nage lorsque le fluide n'est plus gouverné par les équation de Stokes mais par celles d'Euler ou plus généralement celles de Navier-Stokes (qui ne sont plus linéaires). Nous référons aux récentes études de S. Court [30] et de J. San Martìn, J. F. Scheid, T. Takahashi, et M. Tucsnak [75] qui montrent l'existence de solutions fortes globales en temps pour le problème du couplage fluide-solide en utilisant les équation de Navier-Stokes ainsi qu'aux travaux de G. P. Galdi et al. (voir par exemple [40] et [41]). Nous mentionnons aussi les résultats de O. Glass et T. Horsin qui traitent de la contrôlabilité d'un ensemble de particules immergé dans un fluide parfait (voir [45],[46]). Plus généralement, l'extension de résultats de contrôlabilité de solides immergés dans un fluide qui est régi par une équation non linéaire (par exemple lorsque le fluide est parfait ou bien lorsqu'il est gouverné par les équations de Navier-Stokes) est l'enjeu de nombreuses études en cours (voir par exemple la section conclusion de la thèse de J. Lohéac [58]).

- Enfin, une autre voie de recherche concerne la modélisation du déplacement de population de micro-organismes. Nous référons aux travaux P. Degond et al. [33], L. V. Berlyand et al. [18] et [19] qui traitent de ce sujet en utilisant les outils de la théorie cinétique. Une nouvelle approche, en cours d'étude avec F. Alouges, S. De Marco et moi-même, est d'étudier l'évolution d'une densité de nageurs mais en faisant usage de résultats empruntés au calcul de Malliavin. Dans notre travail, nous nous intéressons

au cas d'une population de "3-sphere swimmer" qui nagent tous indépendamment les uns des autres et dont les déformations sont gouvernées par une lois de probabilité (voir par exemple [48] qui étudie l'évolution d'un "3-sphere swimmer"et d'un "2-sphere swimmer" dans ce cas).

Première partie

N-link swimmer

Chapitre 1

Self-propulsion of slender micro-swimmers by curvature control : N-link swimmers

---

This work is done in collaboration with F. Alouges, A. DeSimone and M. Zoppello. It will appear in International Journal of Non-linear Mechanics. We discuss a reduced model to compute the motion of slender swimmers which propel themselves by propagating a bending wave along their body. Our approach is based on the use of Resistive Force Theory for the evaluation of the viscous forces and torques exerted by the surrounding fluid, and on discretizing the kinematics of the swimmer by representing its body through an articulated chain of N rigid links capable of planar deformations. The resulting system of ODEs governing the motion of the swimmer is easy to assemble and to solve, making our reduced model a valuable tool in the design and optimization of bio-inspired engineered microdevices. We test the accuracy and robustness of our approach on three benchmark examples: Purcell's 3-link swimmer, Taylor's swimming sheet and some recent quantitative observations of circular motion of a sperm cell. An explicit formula for the displacement of Purcell's 3-link swimmer generated by a square stroke of small amplitude is also discussed.

1.1 Introduction

The study of the swimming strategies of micro-organisms is attracting increasing attention in the recent literature. This is both because of the intrinsic biological interest, and for the possible implications these studies may have on the design of bio-inspired artificial replicas reproducing the functionalities of biological systems. The reader is referred to the recent reviews [38, 53] for an extensive list of references.

One of the pioneering works in the field is the one by Taylor [84], who established the mathematical setting for the problem of biological self-propulsion powered by thin undulating filaments. He called attention on the paradoxical nature of swimmers of microscopic size: they move by exploiting (viscous) resistance to motion, since at small scales viscous forces dominate over inertial ones. This is apparent by recalling the definition of Reynolds number $\mathrm{Re} = \frac{LV}{\nu}$, a dimensionless measure of the relative importance of inertial versus viscous forces, where L is the body size, V is the swimming speed, and ν is the kinematic viscosity to the surrounding fluid ($10^{-6}(\mathrm{m}^2\mathrm{s}^{-1})^{-1}$ for water at room temperature). Since for biological swimmers V is typically of the order of one body length per second, $\mathrm{Re} \sim 1$ for organisms of 1-mm size, and $\mathrm{Re} \sim 10^{-6} << 1$ when the size drops to 1 μm. It follows that for micron-sized swimmers inertial effects are negligible: Taylor's analysis focussed on a model swimmer consisting of an infinite sheet propelling itself by propagating a sinusoidal traveling wave of deformation, while surrounded by a fluid governed by Stokes equations (the zero-Re-limit of Navier-Stokes equations).

Later, Purcell showed that, at low Reynolds numbers, reciprocal strokes inevitably produce zero net displacements (a statement commonly referred to as the 'scallop theorem' [70]). Moreover, he proposed a minimal device (the 3-link swimmer) able to 'beat' the scallop theorem, namely, to exhibit net displacements by executing periodic, non-reciprocal strokes.

Another crucial development for our analysis is the recent emergence of the connection between swimming and Control Theory, see, e.g., [63]. In fact, low Reynolds number swimming can be considered as a control problem which is linear in the control, and without drift [8]. Many recent works share this point of view, see for example [7, 11, 13, 28, 60]. One of the main difficulties in exploiting Control Theory in order to solve effectively motion planning or optimal control problems is the complexity of the hydrodynamic forces exerted by the fluid on the swimmer as a reaction to its shape changes. Resistive Force Theory [49] provides a simple and concise way to compute a local approximation of such forces, and it has been successfully used in several recent studies, see for example [15, 37]. In this paper, we use this approach as well, in order to obtain the forces acting on the swimmer.

In addition, we simplify the kinematics of the swimmer by discretizing its body. This is represented by a chain of N rigid links moving in a plane (N-link swimmer). Thus, its motion is described by a system of ODEs that can be easily assembled and solved, hence providing a valuable tool for the quantitative description of the motion of biological micro-swimmers. The simplicity of the governing equations makes our model particularly appealing as a tool for the design of engineered devices and for the optimization of their performance as some design parameters are varied. We prove the accuracy and robustness of our approach by checking it against three benchmark examples: Purcell's 3-link swimmer, some recent quantitative observations of circular motion of a sperm cell contained in [37], and Taylor's swimming sheet.

Thanks to the application of well known tools from Geometric Control Theory, we also obtain an explicit formula for the displacement of Purcell's 3-link swimmer generated by a square stroke of small amplitude.

1.2 Mathematical setting of the problem

In this section we describe the kinematics of the N-link swimmer, a generalization of Purcell's 3-link swimmer. The angles between successive links provide a discrete representation of the swimmer's curvature, concentrated at the joints between successive links. We think of them as freely prescribed shape parameters. We then write the equations of motion (balance of total viscous force and torque) and solve for the time evolution of position and orientation of the swimmer in response to a prescribed history of (concentrated) curvatures along the swimmer's body.

1.2.1 Kinematics of the N-link swimmer

We focus here on essentially one–dimensional swimmers moving in a plane. This two-dimensional setting is suitable for the study of slender, essentially one-dimensional swimmers exploring planar trajectories. While the general case is slightly more involved because of the non-additivity of three–dimensional rotations, see e.g. [7], it can be handled with similar techniques.

Our swimmer consists of N rigid links with joints at their ends (see Fig. 1.1), moving in a plane (2d lab-frame) which is defined by the vectors $(\mathbf{e}_x, \mathbf{e}_y)$. We set $\mathbf{e}_z := \mathbf{e}_x \times \mathbf{e}_y$. The i-th link is the segment with end points $\mathbf{x}_i$ and $\mathbf{x}_{i+1}$. It has length $L_i > 0$ and makes an angle θ_i with the horizontal x-axis. The size of the sticks is chosen such that the length of the swimmer is of order of μm. We define by $\mathbf{x}_i := (x_i, y_i)$ $(i = 1, \cdots, N)$ the coordinates of the first end of each link. Note that, for $i \in \{2 \cdots N\}$, the coordinates $\mathbf{x}_i$ can be expressed as a function of $\mathbf{x}_1$, θ_k and L_k, with $k \in \{1 \cdots i-1\}$:

$$\mathbf{x}_i := \mathbf{x}_1 + \sum_{k=1}^{i-1} L_k \begin{pmatrix} \cos(\theta_k) \\ \sin(\theta_k) \end{pmatrix} . \tag{1.1}$$

The swimmer is described by two sets of variables:

- the state variables which specify the position and the orientation of one selected link, labeled as the $i*$-th one;
- the shape variables which describe the relative orientations between successive links. For each link with $i > i*$, this is the angle relative to the preceding one, denoted by $\alpha_i = \theta_i - \theta_{i-1}$, for $i* < i \leq N$. For $i < i*$ this is the the angle relative to the following one, denoted by $\alpha_i = \theta_{i+1} - \theta_i$, for $1 \leq i < i*$.

For example, if the triplet $(\mathbf{x}_1, \theta_1)$ describes the state of the swimmer then the vector $(\alpha_2 = \theta_2 - \theta_1, \cdots, \alpha_N = \theta_N - \theta_{N-1})$ represents the shape of the swimmer. This will be the default choice in the rest of the paper, with the only exception of subsection 1.3.1, where the central link is selected as the $i*$-th one, in order to exploit the symmetries of the 3-link swimmer.

1.2.2 Equations of motion

The equations which govern the dynamics of the swimmer form a system of three ODEs, which is linear with respect to the rate of deformation, and without drift.

The dynamics of the swimmer follows from Newton laws, in which inertia is neglected. These read

$$\begin{cases} \mathbf{F} = 0 \,, \\ \mathbf{e}_z \cdot \mathbf{T}_{\mathbf{x}_1} = 0 \,, \end{cases} \tag{1.2}$$

where $\mathbf{F}$ is the total force exerted on the swimmer by the fluid and $\mathbf{T}_{\mathbf{x}_1}$ is the corresponding total torque computed with respect to the point $\mathbf{x}_1$.

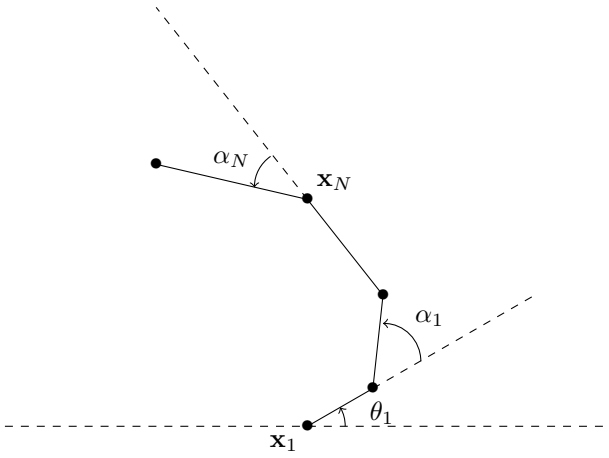

Figure 1.1: Coordinates for the N-link swimmer.

To couple the fluid and the swimmer, we use the local drag approximation of Resistive Force Theory. We denote by s the arc length coordinate on the i-th link ($0 \leq s \leq L_i$) and by $\mathbf{v}_i(s)$ the velocity of the corresponding point. We also introduce the unit vectors $\mathbf{e}_i = \begin{pmatrix} \cos(\theta_i) \\ \sin(\theta_i) \end{pmatrix}$ and $\mathbf{e}_i^\perp = \begin{pmatrix} -\sin(\theta_i) \\ \cos(\theta_i) \end{pmatrix}$ in the directions parallel and perpendicular to the i-th link and write $\mathbf{x}_i(s) = \mathbf{x}_i + s\mathbf{e}_i$. By differentiation, we obtain,

$$\mathbf{v}_i(s) = \dot{\mathbf{x}}_i + s\dot{\theta}_i \mathbf{e}_i^\perp \,. \tag{1.3}$$

The density of the force $\mathbf{f}_i$ acting on the i-th segment is assumed to depend linearly on the velocity. It is defined by

$$\mathbf{f}_i(s) := -\xi \left(\mathbf{v}_i(s) \cdot \mathbf{e}_i\right) \mathbf{e}_i - \eta \left(\mathbf{v}_i(s) \cdot \mathbf{e}_i^\perp\right) \mathbf{e}_i^\perp, \tag{1.4}$$

where ξ and η are respectively the drag coefficients in the directions of $\mathbf{e}_i$ and $\mathbf{e}_i^\perp$ measured in $\mathrm{N\,s\,m^{-2}}$. We thus obtain

$$\begin{cases} \mathbf{F} = \displaystyle\sum_{i=1}^{N} \int_0^{L_i} \mathbf{f}_i(s)\, ds \,, \\ \mathbf{e}_z \cdot \mathbf{T}_{\mathbf{x}_1} = \mathbf{e}_z \cdot \displaystyle\sum_{i=1}^{N} \int_0^{L_i} \left(\mathbf{x}_i(s) - \mathbf{x}_1\right) \times \mathbf{f}_i(s)\, ds \,. \end{cases} \tag{1.5}$$

Using (2.3) and (2.4) into (2.5), the total force and torque can be expressed as

$$\mathbf{F} = -\sum_{i=1}^{N} L_i \xi (\dot{\mathbf{x}}_i \cdot \mathbf{e}_i)\, \mathbf{e}_i + \left(L_i \eta (\dot{\mathbf{x}}_i \cdot \mathbf{e}_i^\perp) + \frac{L_i^2}{2} \eta \dot{\theta}_i \right) \mathbf{e}_i^\perp \,, \tag{1.6}$$

and

$$\begin{aligned} \mathbf{e}_z \cdot \mathbf{T}_{\mathbf{x}_1} &= -\sum_{i=1}^{N} \frac{L_i^2}{2} \eta \left(\dot{\mathbf{x}}_i \cdot \mathbf{e}_i^\perp\right) + \frac{L_i^3}{3} \eta \dot{\theta}_i \\ &+ (\mathbf{x}_i - \mathbf{x}_1) \times \left(L_i \xi (\dot{\mathbf{x}}_i \cdot \mathbf{e}_i)\, \mathbf{e}_i + \left(L_i \eta (\dot{\mathbf{x}}_i \cdot \mathbf{e}_i^\perp) + \frac{L_i^2}{2} \eta \dot{\theta}_i \right) \mathbf{e}_i^\perp \right) \cdot \mathbf{e}_z \,. \end{aligned} \tag{1.7}$$

Moreover, differentiating (2.1) gives

$$\dot{\mathbf{x}}_i = \dot{\mathbf{x}}_1 + \sum_{k=1}^{i-1} L_k \dot{\theta}_k \mathbf{e}_k^{\perp}, \tag{1.8}$$

an expression linear in $\dot{\mathbf{x}}_1$ and $(\dot{\theta}_k)_{1\leq k\leq N}$. This entails that (2.6) and (2.7) are linear in $\dot{\mathbf{x}}_1$ and $\dot{\theta_i}$ for $i \in [1 \cdots N]$, and therefore system (2.2) reads

$$\begin{pmatrix} \mathbf{F} \\ \mathbf{e}_z \cdot \mathbf{T}_{\mathbf{x}_1} \end{pmatrix} = \mathbf{M}\left(\theta_1, \cdots, \theta_N\right) \begin{pmatrix} \dot{\mathbf{x}}_1 \\ \dot{\theta}_1 \\ \dot{\theta}_2 \\ \vdots \\ \dot{\theta}_N \end{pmatrix} = \begin{pmatrix} 0 \\ 0 \\ 0 \end{pmatrix} . \tag{1.9}$$

Observing that for all $i \in \{2, \cdots, N\}$, $\alpha_i = \theta_i - \theta_{i-1}$, equations (2.6) and (2.7) can be expressed using the angles $(\alpha_i)_{i=2,\cdots,N}$ instead of the variables $(\theta_i)_{2\leq i\leq N}$. To this end, we introduce the matrix $\mathbf{C}$ defined by

$$\mathbf{C} = \begin{pmatrix} 1 & 0 & \cdots & \cdots & \cdots & \cdots & 0 \\ 0 & 1 & \ddots & \ddots & \ddots & \ddots & \vdots \\ 0 & 0 & 1 & \ddots & \ddots & & \vdots \\ 0 & 0 & -1 & \ddots & \ddots & & \vdots \\ \vdots & \vdots & 0 & \ddots & \ddots & & 0 \\ \vdots & \vdots & \vdots & \ddots & \ddots & \ddots & 0 \\ 0 & 0 & 0 & \cdots & 0 & -1 & 1 \end{pmatrix} \tag{1.10}$$

and obtain

$$\mathbf{C} \begin{pmatrix} \dot{\mathbf{x}}_1 \\ \dot{\theta}_1 \\ \dot{\theta}_2 \\ \vdots \\ \dot{\theta}_N \end{pmatrix} = \begin{pmatrix} \dot{\mathbf{x}}_1 \\ \dot{\theta}_1 \\ \dot{\alpha}_2 \\ \vdots \\ \dot{\alpha}_N \end{pmatrix} . \tag{1.11}$$

Therefore, by setting

$$\mathbf{N}(\theta_1, \alpha_2, \cdots, \alpha_N) := \mathbf{M}\left(\theta_1, \theta_2(\theta_1, \alpha_2, \cdots, \alpha_N), \cdots, \theta_N(\theta_1, \alpha_2, \cdots, \alpha_N)\right) \mathbf{C}^{-1}, \tag{1.12}$$

system (1.9) can be rewritten in the equivalent form

$$\mathbf{N}\left(\theta_1, \alpha_2, \cdots, \alpha_N\right) \begin{pmatrix} \dot{\mathbf{x}}_1 \\ \dot{\theta}_1 \\ \dot{\alpha}_2 \\ \vdots \\ \dot{\alpha}_N \end{pmatrix} = \begin{pmatrix} 0 \\ 0 \\ 0 \end{pmatrix} . \tag{1.13}$$

We observe that the $3 \times (N+2)$ matrix $\mathbf{N}\left(\theta_1, \alpha_2, \cdots, \alpha_N\right)$ can be block-decomposed into a 3×3 sub-matrix $\mathbf{A}\left(\theta_1, \alpha_2, \cdots, \alpha_N\right)$ and a $3 \times (N-1)$ sub-matrix $\mathbf{B}\left(\theta_1, \alpha_2, \cdots, \alpha_N\right)$, according to

$$\mathbf{N} = \left(\mathbf{A} \,|\, \mathbf{B}\right) . \tag{1.14}$$

The matrix $\mathbf{A}$ is the 'grand-resistance-matrix' of a rigid system evolving at frozen shape, i.e., with $\dot{\alpha}_i \equiv 0$, $i = 2, \ldots, N$, see [24]. It is symmetric and negative definite [24], as it can be easily verified, hence it is invertible. We can then recast the equations of motion of the swimmer as an affine system without drift. Indeed, solving (1.13) for $(\dot{\mathbf{x}}_1, \dot{\theta}_1)$ leads to

$$\begin{pmatrix} \dot{\mathbf{x}_1} \\ \dot{\theta_1} \end{pmatrix} = -\mathbf{A}^{-1}\left(\theta_1, \alpha_2, \cdots, \alpha_N\right) \mathbf{B}\left(\theta_1, \alpha_2, \cdots, \alpha_N\right) \begin{pmatrix} \dot{\alpha}_2 \\ \vdots \\ \dot{\alpha}_N \end{pmatrix}$$

that we rewrite in the form

$$\begin{pmatrix} \dot{\mathbf{x}_1} \\ \dot{\theta_1} \end{pmatrix} = \sum_{i=2}^{N} \mathbf{g}_i\left(\theta_1, \alpha_2, \cdots, \alpha_N\right) \dot{\alpha}_i \,, \tag{1.15}$$

where the $N-1$ vector fields $\{\mathbf{g}_i\}_{i=2}^N$, are the columns of the $3 \times (N-1)$ matrix $-\mathbf{A}^{-1}\mathbf{B}$.

The equation above links the displacement (both translation and rotation) of the swimmer to its deformation. In other words, for a given history of shapes, prescribed through functions $t \mapsto (\alpha_2, \cdots, \alpha_N)(t)$, the motion of the swimmer is obtained by solving the system (1.15). Typically, in what follows a stroke is given by a time-periodic shape change, i.e., the functions $t \mapsto \alpha_i(t)$, $i = 2, \cdots, N$ are all periodic, with the same period.

In order to solve (1.15) numerically, we need to construct the vector fields $\mathbf{g}_i$ explicitly. To this end, we observe that $\mathbf{F}$ and $\mathbf{T}_{\mathbf{x}_1}$ depend linearly on $(\dot{\mathbf{x}}_i)_{1\le i\le N}$ and $(\dot{\theta}_i)_{1\le i\le N}$ and that these quantities depend in turn linearly on $(\dot{\mathbf{x}}_1, \dot{\theta}_1, \cdots, \dot{\theta}_N)$ in view of (2.8). Therefore, we can rewrite (2.6) and (2.7) as

$$\mathbf{F} = \mathbf{P}_1 \begin{pmatrix} \dot{\mathbf{x}}_1 \\ \vdots \\ \dot{\mathbf{x}}_N \\ -- \\ \dot{\theta}_1 \\ \vdots \\ \dot{\theta}_N \end{pmatrix} = \mathbf{P}_1\mathbf{Q} \begin{pmatrix} \dot{\mathbf{x}}_1 \\ \dot{\theta}_1 \\ \vdots \\ \dot{\theta}_N \end{pmatrix}, \quad \mathbf{e}_z \cdot \mathbf{T}_{\mathbf{x}_1} = \mathbf{P}_2 \begin{pmatrix} \dot{\mathbf{x}}_1 \\ \vdots \\ \dot{\mathbf{x}}_N \\ -- \\ \dot{\theta}_1 \\ \vdots \\ \dot{\theta}_N \end{pmatrix} = \mathbf{P}_2\mathbf{Q} \begin{pmatrix} \dot{\mathbf{x}}_1 \\ \dot{\theta}_1 \\ \vdots \\ \dot{\theta}_N \end{pmatrix}, \tag{1.16}$$

where

$$\mathbf{P}_1 := \begin{pmatrix} -\mathbf{m}_1 & \cdots & -\mathbf{m}_N & | & \frac{\eta}{2} L_1^2 \mathbf{e}_1^\perp & \cdots & \frac{\eta}{2} L_N^2 \mathbf{e}_N^\perp \end{pmatrix}$$

with $\mathbf{m}_i := L_i(\xi \mathbf{e}_i \otimes \mathbf{e}_i + \eta \mathbf{e}_i^\perp \otimes \mathbf{e}_i^\perp)$ for $i = 1 \cdots N$,

$$\mathbf{P}_2 := \begin{pmatrix} \cdots & -(L_i^2 \eta \mathbf{e}_i^\perp + (\mathbf{x}_i - \mathbf{x}_1) \times \mathbf{m}_i)^T & \cdots & | & \cdots & \eta L_i^2 (\frac{L_i}{3} + \frac{(\mathbf{x}_i - \mathbf{x}_1) \times \mathbf{e}_i^\perp \cdot \mathbf{e}_z}{2}) & \cdots \end{pmatrix},$$

and, finally,

$$\mathbf{Q} = \begin{pmatrix} 1 & 0 & 0 & 0 & \cdots & 0 \\ 1 & L_1\mathbf{e}_1^\perp & 0 & 0 & \cdots & 0 \\ 1 & L_1\mathbf{e}_1^\perp & L_2\mathbf{e}_2^\perp & 0 & \cdots & 0 \\ \vdots & \vdots & \vdots & \ddots & \cdots & 0 \\ 1 & L_1\mathbf{e}_1^\perp & L_2\mathbf{e}_2^\perp & \cdots & L_{N-1}\mathbf{e}_{N-1}^\perp & 0 \\ 0 & & & & & \\ \vdots & & & \mathbf{Id} & & \\ 0 & & & & & \end{pmatrix}.$$

We thus have

$$\mathbf{M} = \begin{pmatrix} \mathbf{P}_1\mathbf{Q} \\ \mathbf{P}_2\mathbf{q} \end{pmatrix}$$

and can compute $\mathbf{N} = \mathbf{C}^{-1}\mathbf{M}$, where $\mathbf{C}^{-1}$ is explicitly given as

$$\mathbf{C}^{-1} = \begin{pmatrix} 1 & 0 & \cdots & \cdots & \cdots & \cdots & 0 \\ 0 & 1 & \ddots & \ddots & \ddots & \ddots & \vdots \\ 0 & 0 & 1 & \ddots & \ddots & & \vdots \\ 0 & 0 & 1 & \ddots & \ddots & & \vdots \\ \vdots & \vdots & 1 & \ddots & \ddots & & 0 \\ \vdots & \vdots & \vdots & \ddots & \ddots & \ddots & 0 \\ 0 & 0 & 1 & \cdots & 1 & 1 & 1 \end{pmatrix}. \tag{1.17}$$

Matrices $\mathbf{A}$ and $\mathbf{B}$ are obtained from the columns of $\mathbf{N}$ as in (1.14) and, finally, the vectors $\mathbf{g}_i$ are simply the columns of $-\mathbf{A}^{-1}\mathbf{B}$.

1.3 Applications

1.3.1 Purcell's 3−link swimmer

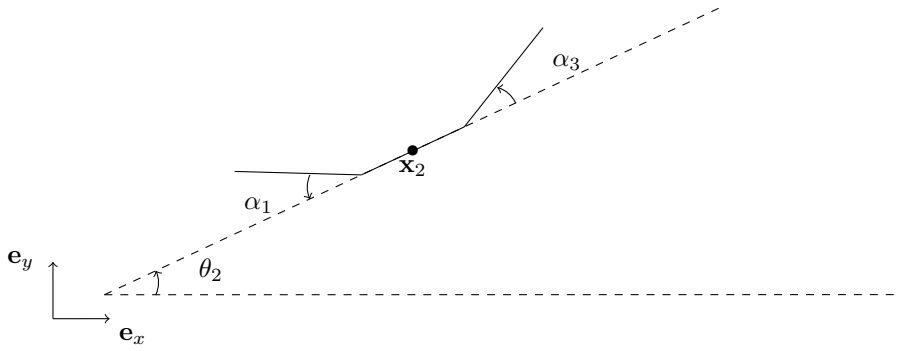

Figure 1.2: Purcell's 3-link swimmer.

We now focus on the case $N = 3$ (Purcell's 3−link swimmer). To benefit from the symmetry of the system, we use as state variables the coordinate $\mathbf{x}_2 := (x_2, y_2)$ of the middle point of the second segment, and the angle θ_2 that it forms with the x-axis. With the notation of the preceding sections, we call $\alpha_1 = \theta_2 - \theta_1$ and $\alpha_3 = \theta_3 - \theta_2$ the relative angles to the central link of the left and right arms respectively, see Figure 2.2.

Purcell introduced this system in [70], where he predicted that it would exhibit net motion as a consequence of a suitable non-reciprocal stroke (a square loop in the (α_1, α_3) plane). He also argued by symmetry that, for a swimmer with first and third links of equal length, this symmetric stroke would produce a net displacement along the direction of the central link, but did not provide a formula to predict either the sign or the magnitude of this displacement. In the following, we show the connection between Purcell's proposed stroke and Lie brackets, a classical tool of Geometric Control Theory. This enables us to obtain a formula for the displacement induced by a Purcell-type stroke of infinitesimal amplitude. We also compute numerically the motion resulting from a Purcell-type stroke of finite amplitude and check it against the theoretical prediction.

Setting $\mathbf{X} := (\alpha_1, \alpha_3, x_2, y_2, \theta_2)^{\mathbf{T}}$, and using (1.15), the equations of motion become

$$\dot{\mathbf{X}} = \mathbf{g}_1(\theta_2, \alpha_1, \alpha_3)\dot{\alpha_1} + \mathbf{g}_2(\theta_2, \alpha_1, \alpha_3)\dot{\alpha_3}\,. \tag{1.18}$$

We refer the reader to Appendix A for the explicit calculation of the coefficients appearing in (1.18). We remark that none of them depends on (x_2, y_2) as a consequence of the translational invariance of the problem.

Displacement for square strokes of small amplitude

Proposition 1.3.1 *Let $\epsilon > 0$, and consider the square stroke defined by*

$$\begin{array}{l}(\dot{\alpha_1}(t), \dot{\alpha_3}(t)) = (1, 0) \text{ for } t \in (0, \epsilon),\\ (\dot{\alpha_1}(t), \dot{\alpha_3}(t)) = (0, 1) \text{ for } t \in (\epsilon, 2\epsilon),\\ (\dot{\alpha_1}(t), \dot{\alpha_3}(t)) = (-1, 0) \text{ for } t \in (2\epsilon, 3\epsilon),\\ (\dot{\alpha_1}(t), \dot{\alpha_3}(t)) = (0, -1) \text{ for } t \in (3\epsilon, 4\epsilon).\end{array} \tag{1.19}$$

Then, for small ϵ, the solution of (1.18) *with initial condition $\mathbf{X}(0)$ is given by*

$$\mathbf{X}\,(4\epsilon) - \mathbf{X}\,(0) = \begin{pmatrix} 0 \\ 0 \\ \epsilon^2\delta + O(\epsilon^3) \\ O(\epsilon^3) \\ O(\epsilon^3) \end{pmatrix}, \tag{1.20}$$

where

$$\delta = \frac{L_1L_2L_3\left(L_1^2 + L_1(L_2+L_3) + L_3(L_2+L_3)\right)(\eta - \xi)}{(L_1+L_2+L_3)^4\xi} \tag{1.21}$$

Proof: The first two components in (1.20) vanish, as it is obvious from direct integration of (1.19). Moreover, it is well known (see,e.g., [29]) and easy to check that the solution of (1.18) for the square stroke given by (1.19) satisfies the expansion

$$X(4\epsilon) - X(0) = \epsilon^2[\mathbf{g}_1, \mathbf{g}_2] + O(\epsilon^3)$$

where the *Lie bracket* $[\mathbf{g}_1, \mathbf{g}_2]$ is defined by

$$[\mathbf{g}_1, \mathbf{g}_2](\mathbf{y}) := (\mathbf{g}_1 \cdot \nabla)\,\mathbf{g}_2(\mathbf{y}) - (\mathbf{g}_1 \cdot \nabla)\,\mathbf{g}_2(\mathbf{y})\,. \tag{1.22}$$

The direct calculation of this Lie bracket[1] shows that

$$[\mathbf{g}_1, \mathbf{g}_2](\mathbf{y})|_{\mathbf{y}=(0,0,0)} = \begin{pmatrix} 0 \\ 0 \\ \delta \\ 0 \\ 0 \end{pmatrix}, \tag{1.23}$$

□

The proposition above provides us with an explicit formula for the net displacement which, in the symmetric case $L_1 = L_3 = L$, reads

$$\Delta\mathbf{x}_2 = \epsilon^2 \frac{L^3L_2(3L+2L_2)}{(2L+L_2)^4}\left(\frac{\eta - \xi}{\xi}\right)\mathbf{e}_2 + O(\epsilon^3)\,. \tag{1.24}$$

[1] We have used for this step the symbolic computation software MAPLE and the formulas given in Appendix A.

Formula (1.24) above shows that the net displacement at leading order is along the axis of the central link and vanishes when $\eta = \xi$. As already stated by Purcell, it can also be shown that a square stroke (1.19) on such a symmetric swimmer does not produce any global rotation or vertical displacement.

By integrating numerically the equations of motion for small angle excursion ϵ and small times 4ϵ, we have obtained the state of the swimmer, $t \mapsto (x_2(t), y_2(t), \theta_2(t))$. We have verified that after the square stroke $y_2(4\epsilon)$ and $\theta_2(4\epsilon)$ vanish, in accordance with the previous remark, and that the net displacement along the $x-$axis is given by formula (1.24) (see Figure 1.3).

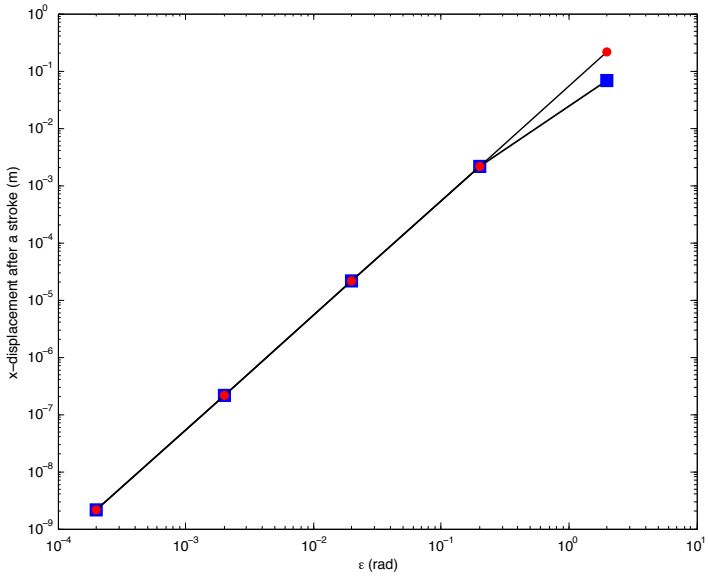

Figure 1.3: Graphs of the displacement of the 3-link-swimmer in meters after one square stroke, as a function of the angle amplitude ϵ in radians. Here $L_1 = L_3 = 1\mu\,\mathrm{m}$, $L_2 = 2\,\mu\,\mathrm{m}$, and $\eta = 2\xi\,\mathrm{N\,s\,m^{-2}}$. The blue squares are obtained by numerical integration of the equations of motion, while the red circles are obtained from the Lie bracket formula (1.24).

Displacement for square strokes of large amplitude

The preceding results only apply to infinitesimal strokes. For strokes of large amplitude, we can integrate the equations of motion numerically and compare our results to known results from the literature. To this aim, we use the same data as in [15], namely $L_1 = L_3 = L = 1$, $L_2 = 2$, $\xi = 1$ and $\eta = 2$, $\Delta\theta = \frac{\pi}{3}$ and the control angles given by

$$\alpha_1(t) = \begin{cases} -(\dfrac{\Delta\theta}{2} - t) & \text{if } 0 \le t \le \Delta\theta \\ \dfrac{\Delta\theta}{2} & \text{if } \Delta\theta \le t \le 2\Delta\theta \\ -(t - \dfrac{5\Delta\theta}{2}) & \text{if } 2\Delta\theta \le t \le 3\Delta\theta \\ -\dfrac{\Delta\theta}{2} & \text{if } 3\Delta\theta \le t \le 4\Delta\theta \end{cases}, \quad \alpha_3(t) = \begin{cases} \dfrac{\Delta\theta}{2} & \text{if } 0 \le t \le \Delta\theta \\ (\dfrac{3\Delta\theta}{2} - t) & \text{if } \Delta\theta \le t \le 2\Delta\theta \\ -\dfrac{\Delta\theta}{2} & \text{if } 2\Delta\theta \le t \le 3\Delta\theta \\ (t - \dfrac{7\Delta\theta}{2}) & \text{if } 3\Delta\theta \le t \le 4\Delta\theta \end{cases}.$$

This leads to a square stroke of amplitude $\frac{\pi}{3}$, as shown in Figure 1.4. Such a stroke produces the displacement of the swimmer given in Figure 1.5, which matches exactly Figure 6 in [15].

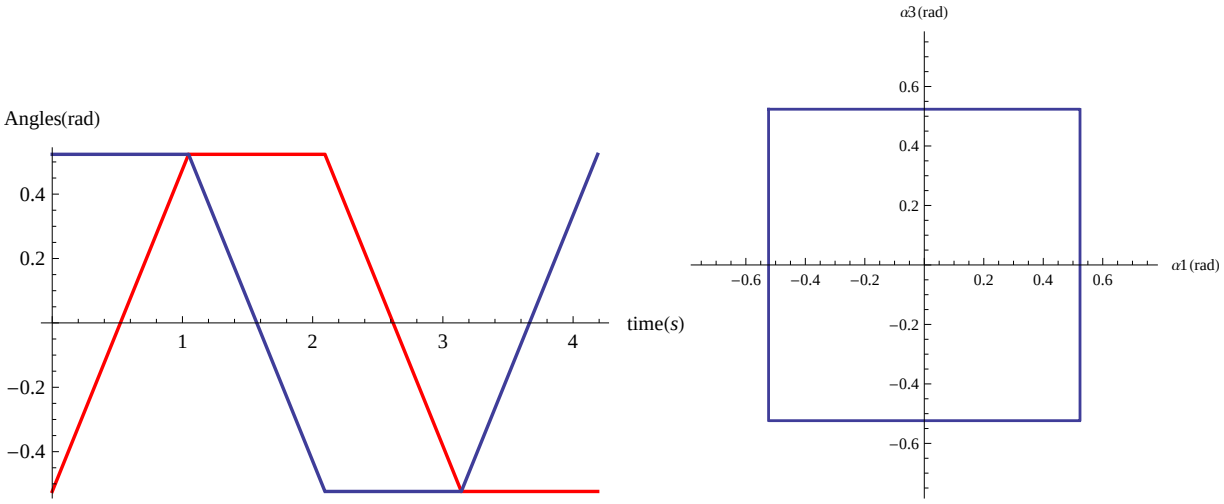

Figure 1.4: Control functions α_1 (red) and α_3 (blue) as functions of time (left), and their phase portrait (right). The square loop on the right is traced clockwise.

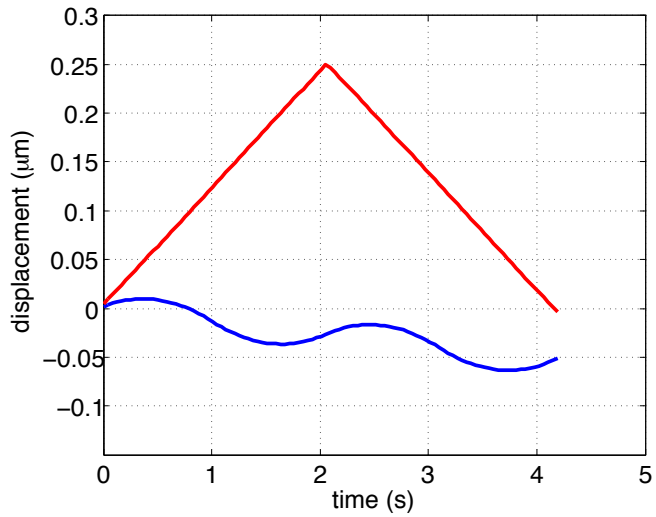

Figure 1.5: Graphs of $x_2(t)$ (blue), and $y_2(t)$ (red) as a function of time during the stroke of Figure 1.4. A net horizontal backward displacement is observed when the square stroke is traced clockwise, matching the results of [15].

1.3.2 $N-$link swimmers

The full $N-$link swimmer can be used as a discrete model of a flexible tail whose shape is controlled by curvature. We show how curvature control can be implemented in our model in some concrete cases reproducing the motion of Taylor's sheet [84] and the motion of a sperm cell analyzed in [37].

Curvature approximation

Here, we show how to approximate the curvature of a beating tail with a discrete N link swimmer. Let $L > 0$ be the total length of the flexible tail and let us denote by $\mathbf{r}(s,t)$ the position at time $t > 0$ of the point of arc-length coordinate $s \in [0, L]$ along the tail, in the body frame of the swimmer (see Figure 1.6). We also define $\Psi(s,t)$ as the angle between the tangent vector to the tail at the point $\mathbf{r}(s,t)$ and the $x-$axis in the lab-frame. We recall that the derivative of $\Psi(s,t)$ with respect to s is the local curvature of the curve.

We divide the swimmer into N equal parts of size $L_i = L/N$, and define the angles $(\theta_i)_{1\leq i\leq N}$ by averaging $\Psi(s,t)$ on the interval $[iL/N, (i+1)L/N]$

$$\theta_i(t) = \frac{N}{L}\int_{\frac{(i-1)L}{N}}^{\frac{iL}{N}} \Psi(s,t)\,ds\,, \quad i = 1\dots N\,. \tag{1.25}$$

Finally, we differentiate (1.25) with respect to time to get $\dot\theta_i$, $i = 1, \cdots, N$,

$$\dot\theta_i(t) = \frac{N}{L}\int_{\frac{(i-1)L}{N}}^{\frac{iL}{N}} \frac{\partial\Psi(s,t)}{\partial t}\,ds\,, \quad i = 1\dots N\,. \tag{1.26}$$

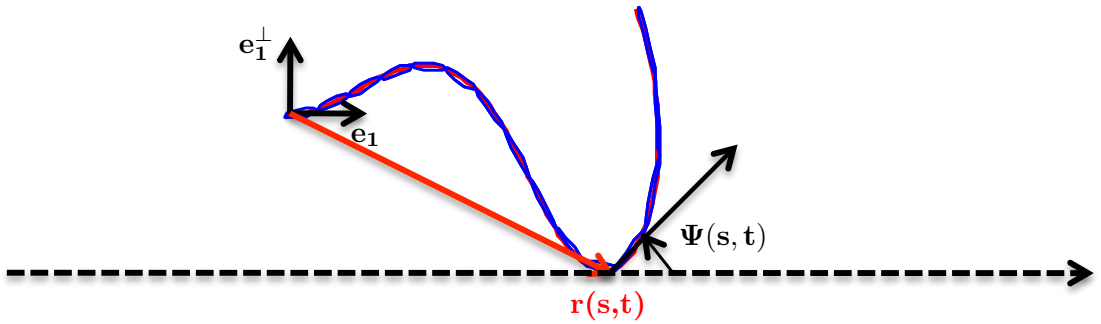

Figure 1.6: A prescribed continuous wave (red curve) and its discrete approximation by the N-link swimmer (blue curve), $N = 15$.

N-link approximation of Taylor's swimming sheet

We now use our discretization method to compute the displacement and velocity of the so-called Taylor sheet [84]. To that aim, we describe a sinusoidal wave propagating along the tail in its frame by

$$\mathbf{r}(s(x,t),t) = b\sin(kx - \sigma t) + b\sin(\sigma t) \tag{1.27}$$

where the arclength s and x are linked by

$$s(x,t) = \int_0^x \sqrt{1 + b^2k^2(\cos(ku - \sigma t))^2}\,du\,. \tag{1.28}$$

(Notice that $\mathbf{r}(0,t) = 0$, which keeps the origin fixed in the swimmer's frame.)

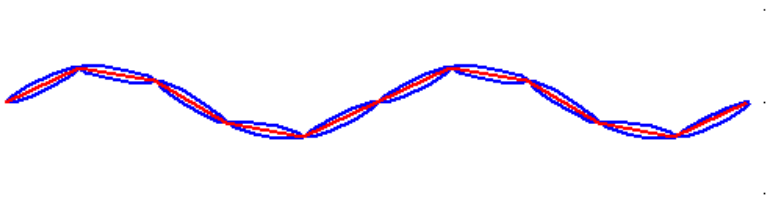

Figure 1.7: A sinusoidal wave (red) and its $N-$link approximation (blue) with $N = 10$

Using Resistive Force Theory, Gray and Hancock give in [49] the following formula for the velocity of the sheet in the horizontal direction:

$$V_x = \sigma k b^2 \left(\frac{\xi - \eta}{\eta} \right) , \tag{1.29}$$

from which one can recover Taylor's formula

$$V_x = -\frac{1}{2} k \sigma b^2 \tag{1.30}$$

by setting $\xi = 1$ and $\eta = 2$. The net displacement of the swimmer after a period $T = \frac{2\pi}{\sigma}$ is therefore

$$\Delta x = V_x T = \sigma k b^2 \left(\frac{\xi - \eta}{\eta} \right) T \, . \tag{1.31}$$

We have solved numerically the equations of motion choosing as parameters $\sigma = 1\,\mathrm{rad\,s^{-1}}$, $k = 4\,\mathrm{rad\,\mu m^{-1}}$, and $N = 50$ links to describe the swimmer, and drag coefficients $\xi = 1\mathrm{N\,s\,\mu m^{-2}}$ and $\eta = 2\,\mathrm{N\,s\,\mu m^{-2}}$. The displacement in the parallel direction after one period is plotted in Figure 1.8, together with the the one predicted by (1.31), for a wave amplitude $b = 0.001\,\mu\mathrm{m}$.

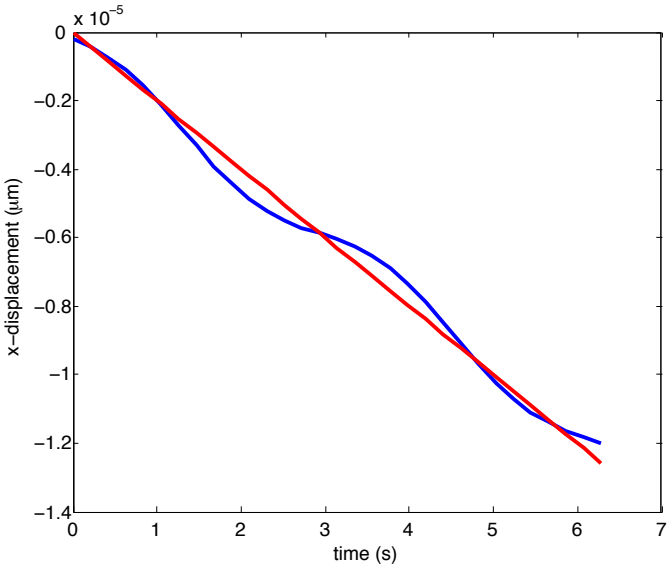

Figure 1.8: Graphs of the displacement of Taylor's sheet for $b = 1 \cdot 10^{-3}\,\mu$m. The blue curve is the one obtained by numerical integration of the equations of motion while the red one is the one predicted by (1.31)

.

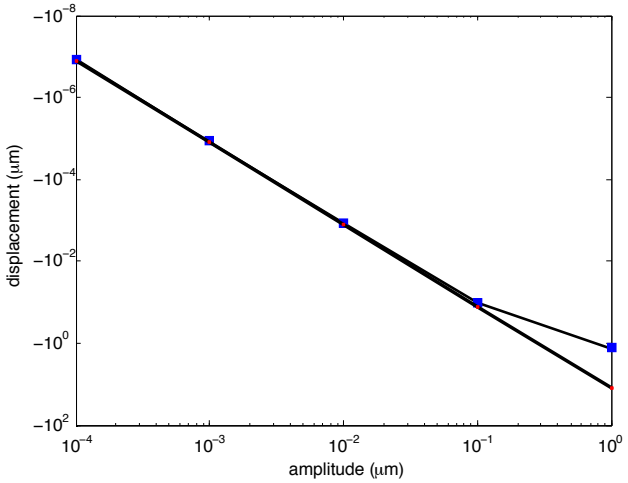

Figure 1.9: Logarithmic plot of the x-displacement as a function of the amplitude b (blue squares) compared with the one obtained from (1.31) (red dots).

The dependence of the displacements on the amplitude b is shown in Figure 1.9. The

graph shows that formula (1.31) gives an accurate prediction for an amplitude of the wave b smaller than $1 \cdot 10^{-1}$.

N-link approximation of sperm cell swimmer

We now turn to the simulation of the motion of a sperm cell and compare to the one reported in [37]. To that aim, we modify the first segment of the $N-$link swimmer to take into account the presence of the head of the sperm cell, which possesses its own translational and rotational viscous drag. Indeed, we call $\mathbf{x}_1$ the position of the center of the head and θ_1 the angle that the direction $\mathbf{e}_1$ of first segment (attached to the head) makes with the horizontal axis. We assume that the viscous force and torque generated by a movement of the head are given by

$$\mathbf{F}_{\text{head}} = -\xi_{\text{head}}(\dot{\mathbf{x}}_1 \cdot \mathbf{e}_1)\mathbf{e}_1 - \eta_{\text{head}}(\dot{\mathbf{x}}_1 \cdot \mathbf{e}_1^{\perp})\mathbf{e}_1^{\perp}\,, \tag{1.32}$$

and

$$\mathbf{T}_{\text{head}} \cdot \mathbf{e}_z = -\zeta_{\text{head}}\dot{\theta_1}\,. \tag{1.33}$$

We also assume that the head length is $L_{\text{head}} = 10\,\mu$m and we call again L the length of the tail which is fixed to one of the extremities of the head segment. The wave profile along the tail of the sperm cell was obtained from experimental data, keeping only the two first Fourier modes as suggested in [72] and we use the method described in section 1.3.2 to approximate the motion of the tail.

More precisely, we describe the wave shape shown in Fig. 1.10 by

$$\mathbf{r}(s,t) = \frac{L_{\text{head}}}{2}\,\mathbf{e}_1(t) + \int_0^s \cos(\Psi(u,t))\mathbf{e}_1(t) + \sin(\Psi(u,t)\mathbf{e}_1^{\perp}(t)du\,. \tag{1.34}$$

where

$$\Psi(s,t) = K_0 s + 2A_0 s\cos(\omega t - \frac{2\pi s}{\lambda})\,. \tag{1.35}$$

In the preceding equations, K_0 is the mean flagellar curvature while ω, λ and A_0 are respectively the frequency, the wave-length and the amplitude of the wave. Following [37], in the numerical simulations below we use the following values for the wave parameters: $A_0 = 15.2 \cdot 10^3\,\text{rad}\,\text{m}^{-1}$, $K_0 = 19.1 \cdot 10^3\,\text{rad}\,\text{m}^{-1}$, $\omega = 200\,\text{rad}\,\text{s}^{-1}$ and $\lambda = 71.6 \cdot 10^{-6}\,\text{m}$.

Apart from the first segment, the rest of the tail is discretized with $N-1$ segments of extremities $(\mathbf{x}_i, \mathbf{x}_{i+1})$ for $i = 2, \cdots, N$. We discretize the beating wave using the method described in section 1.3.2, and obtain the shapes shown in Figure 1.11 for one period ($0 \leq t \leq \frac{2\pi}{\omega}$).

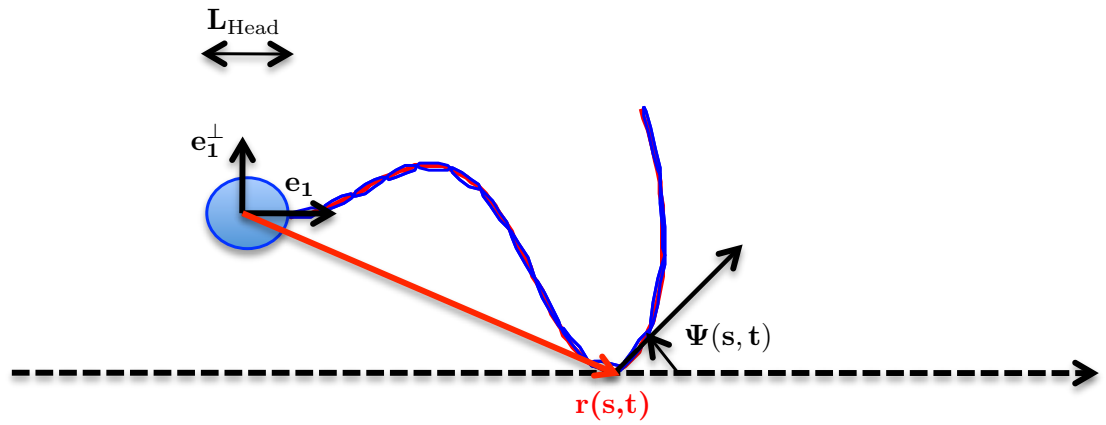

Figure 1.10: The prescribed continuous wave (red curve) and its discrete approximation by the N-link swimmer (blue curve), $N = 15$.

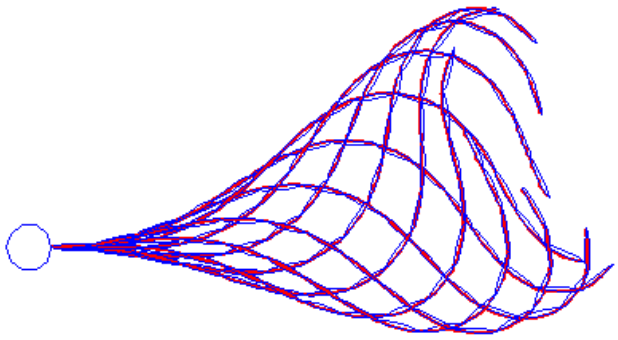

Figure 1.11: Flagellar beating during one period. The red curve represents the tail as described by formula (1.34) while the blue links describe the tail according to our discrete approximation.

With the notation above, the equations of motion become

$$\begin{cases} \mathbf{F} = \mathbf{F}_{\text{head}} + \displaystyle\sum_{i=1}^{N} \int_0^{L_i} \mathbf{f}_i(s)\, ds\,, \\ \mathbf{T}_{\mathbf{x}_1} = \mathbf{T}_{\text{head}} + \displaystyle\sum_{i=1}^{N} \int_0^{L_i} \mathbf{f}_i(s) \times (\mathbf{x}_i(s) - \mathbf{x}_1)\, ds\,. \end{cases} \tag{1.36}$$

where $L_i = L/N$ is the length of each segment $(\mathbf{x}_i, \mathbf{x}_{i+1})$ for $i = 2, \cdots, N$, while the first segment, also of size $L_1 = L/N$ is given by $(\mathbf{x}_1 + \frac{L_{\text{head}}}{2}\mathbf{e}_1, \mathbf{x}_2)$.

Thanks to the fact that the two previous formulas (1.36) are linear in $\dot\theta_1$ and $\dot{\mathbf{x}}_1$, we get the same compact expression of the equations of motion as in (1.15). More in detail, the matrix $\mathbf{P}_1$ and $\mathbf{P}_2$ defined the system (1.16) are replaced by

$$\mathbf{P}_1^{\text{head}} := \big(-\xi_{\text{head}}\mathbf{e}_1 \otimes \mathbf{e}_1 + \eta_{\text{head}}\mathbf{e}_1^{\perp} \otimes \mathbf{e}_1^{\perp} \quad -\mathbf{m}_1 \quad \cdots \quad -\mathbf{m}_N \quad | \quad \tfrac{\eta}{2}L_1^2\mathbf{e}_1^{\perp} \quad \cdots \quad \tfrac{\eta}{2}L_N^2\mathbf{e}_N^{\perp}\big)$$

and

$$\mathbf{P}_2^{\text{head}} := \begin{pmatrix} -p_1 & \cdots & -p_N & | & -\zeta_{\text{head}} + q_1 & q_2 & \cdots & q_N \end{pmatrix},$$

with $\mathbf{m}_i := L_i(\xi \mathbf{e}_i \otimes \mathbf{e}_i + \eta \mathbf{e}_i^\perp \otimes \mathbf{e}_i^\perp)$ for $i = 1 \cdots N$, and $p_i := (L_i^2 \eta \mathbf{e}_i^\perp + (\mathbf{x}_i - \mathbf{x}_1) \times \mathbf{m}_i)^T$, $q_i := \eta L_i^2 (\frac{L_i}{3} + \frac{(\mathbf{x}_i - \mathbf{x}_1) \times \mathbf{e}_i^\perp \cdot \mathbf{e}_z}{2})$, for $i = 1 \cdots N$.
We use the following values for the drag coefficients

- for the head, $\xi_{\text{head}} = 40.3 \cdot 10^3 \,\text{pN s m}^{-1}$, $\eta_{\text{head}} = 46.1 \cdot 10^3 \,\text{pN s m}^{-1}$, and $\zeta_{\text{head}} = 0.84 \cdot 10^{-6} \,\text{pN s m}$
- for the links representing the tail, $\xi = 0.38 \cdot 10^9 \,\text{pN s m}^{-2}$, $\frac{\eta}{\xi} = 1.89$.

Our results, summarized by the graphs in Figures 1.12 and 1.13 below, are in perfect agreement with those of [37] (see Figure 3 for the trajectory and Figure 4 for the various speeds).

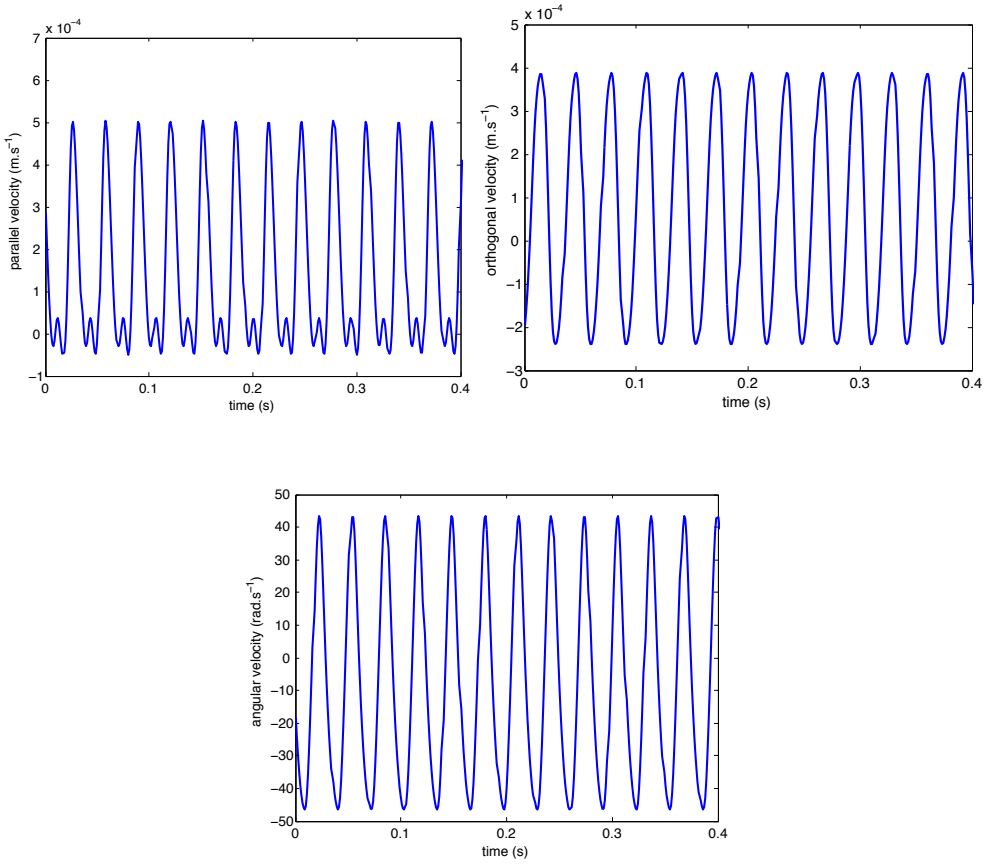

Figure 1.12: Above translational speed of the swimmer head in the tangent and perpendicular directions, and below rotational speed.

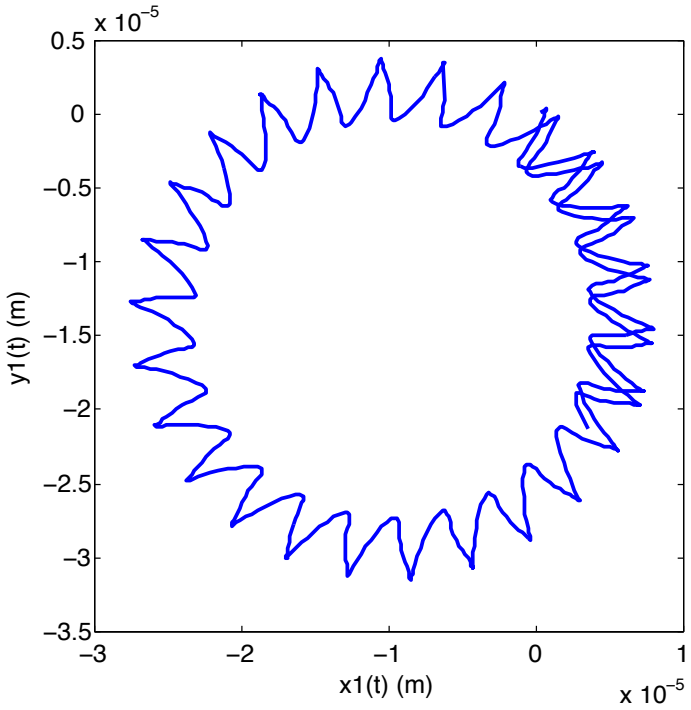

Figure 1.13: Trajectory of the head of the sperm-cell during one period.

1.4 Conclusions and perspectives

In this paper, we have presented a discrete model of a slender swimmer which swims by propagating bending waves along its body, and in which hydrodynamic interactions are treated with the local drag approximation of Resistive Force Theory. The model is easy to assemble and to solve, and surprisingly accurate, as shown by the comparison with some benchmark examples such as the measured trajectories of sperm cells reported in [37]. The ease of use of our model will be very valuable in the study of optimal design and stroke optimization questions, which will be the subject of future work.

The approach described in this paper can be extended in a number of natural ways. To begin with, we have restricted our attention to slender swimmers exploring planar trajectories. The general three–dimensional case, while computationally more demanding, is conceptually straightforward, see [7, 32]. Furthermore, in several realistic situations, curvature is not entirely controlled. For example, it may happen that the curvature actuation mechanism is present or activated only in a portion of the filament (active part of the filament, say, the part closer to the 'head'), while the curvature of the remainder (passive part of the filament, say at the tail end) is a-priori unknown and emerges from the balance of viscous forces from the fluid against elastic restoring forces due its bending stiffness. Interesting examples of this type are the octopus tentacles [95], or artificial systems such as the one discussed in [69]. The extension of our model to scenarios of this kind is immediate, by representing the bending stiffness of the passive part of the filament through angular springs reacting elastically to angle differences between two successive links. Future work will also explore the possibilities offered by active materials capable of large deformations, such as Liquid Crystal

Elastomers actuated in bending [16, 35, 77], and of more classical concepts such as flexible filaments made of magnetic particles and driven by oscillating magnetic fields [34, 36].

Acknowledgments. Part of this work was done while LG and MZ were visiting SISSA, whose hospitality and financial support are gratefully acknowledged. We thank also Direction Générale de l'Armement (DGA) for a financial support to LG.

1.5 Appendix A

The forces $\mathbf{F}_i$, $i = 1, 2, 3$ acting on each segment of Purcell's 3-link swimmer, introduced in subsection 1.3.1 are given by

$$\begin{aligned}
\mathbf{F}_1 = \quad & -\xi L_1(\dot{x}_2\cos(\theta_2+\alpha_1) + \dot{y}_2\sin(\theta_2+\alpha_1) - \tfrac{L_2}{2}\sin\alpha_1\dot{\theta}_2)\mathbf{e}_1 \\
& -\eta(-L_1\dot{x}_2\sin(\theta_2+\alpha_1) + L_1\dot{y}_2\cos(\theta_2+\alpha_1) - \tfrac{L_1L_2}{2}\cos\alpha_1\dot{\theta}_2 - \tfrac{L_1^2}{2}(\dot{\theta}_2+\dot{\alpha}_1))\mathbf{e}_1^\perp\,, \\
\mathbf{F}_2 = \quad & -\xi L_2(\dot{x}_2\cos\theta_2 + \dot{y}_2\sin\theta_2)\mathbf{e}_2 - \eta L_2(-\dot{x}_2\sin\theta_2 + \dot{y}_2\cos\theta_2)\mathbf{e}_2^\perp\,, \\
\mathbf{F}_3 = \quad & -\xi L_3(\dot{x}_2\cos(\theta_2+\alpha_3) + \dot{y}_2\sin(\theta_2+\alpha_3) + \tfrac{L_2}{2}\sin\alpha_3\dot{\theta}_2)\mathbf{e}_3 \\
& \eta(-L_3\dot{x}_2\sin(\theta_2+\alpha_3) + L_3\dot{y}_2\cos(\theta_2+\alpha_3) + \tfrac{L_3L_2}{2}\cos\alpha_3\dot{\theta}_2 + \tfrac{L_3^2}{2}(\dot{\theta}_2+\dot{\alpha}_3))\mathbf{e}_3^\perp\,,
\end{aligned} \tag{1.37}$$

while the total torque, obtained by using formula (2.5), is given by

$$\begin{aligned}
\mathbf{T}_{\mathbf{x}_2}\cdot\mathbf{e}_z = & \dot{x}_2(\xi\frac{L_1L_2}{2}\sin\alpha_1\cos(\theta_2+\alpha_1) - \eta\frac{L_1L_2}{2}\cos\alpha_1\sin(\theta_2+\alpha_1) - \eta\frac{L_1^2}{2}\sin(\theta_2+\alpha_1) \\
& - \xi\frac{L_3L_2}{2}\sin\alpha_3\cos(\theta_2+\alpha_3) + \eta\frac{L_3L_2}{2}\cos\alpha_3\sin(\theta_2+\alpha_3) + \eta\frac{L_3^2}{2}\sin(\theta_2+\alpha_3)) \\
& \dot{y}_2(\xi\frac{L_1L_2}{2}\sin\alpha_1\sin(\theta_2+\alpha_1) + \eta\frac{L_1L_2}{2}\cos\alpha_1\cos(\theta_2+\alpha_1) + \eta\frac{L_1^2}{2}\cos(\theta_2+\alpha_1) \\
& - \xi\frac{L_3L_2}{2}\sin\alpha_3\sin(\theta_2+\alpha_3) - \eta\frac{L_3L_2}{2}\cos\alpha_3\cos(\theta_2+\alpha_3) - \eta\frac{L_3^2}{2}\cos(\theta_2+\alpha_3)) \\
& \dot{\theta}_2(-\xi\frac{L_1L_2^2}{4}\sin^2\alpha_1 - \eta L_1(\frac{L_1}{2}+\frac{L_2}{2}\cos\alpha_1)^2 + \eta\frac{L_1^3}{12} - \xi\frac{L_3L_2^2}{4}\sin^2\alpha_3 \\
& - \eta L_1(\frac{L_3}{2}+\frac{L_2}{2}\cos\alpha_3)^2 + \eta\frac{L_3^3}{12}) \\
& + \dot{\alpha}_1(-\eta(\frac{L_1^3}{3}+\frac{L_1^2L_2}{4}\cos\alpha_1)) + \dot{\alpha}_3(-\eta(\frac{L_3^3}{3}+\frac{L_3^2L_2}{4}\cos\alpha_3))\,.
\end{aligned} \tag{1.38}$$

We now write the equations of motion of the system. Since we are neglecting inertia these reduce to $F = 0$ and $M = 0$. These scalar equations can be seen as ODEs in the unknown functions $x_2(t)$, $y_2(t)$ and $\theta_2(t)$. Explicitly, they read as

$$\begin{aligned}
F_x = & \dot{x}_2(-\xi L_1(\cos(\theta_2+\alpha_1))^2 - \eta L_1(\sin(\theta_2+\alpha_1))^2 - \xi L_2(\cos(\theta_2))^2 - \eta L_2(\sin(\theta_2))^2 - \\
& - \xi L_3(\cos(\theta_2+\alpha_3))^2 - \eta L_3(\sin(\theta_2+\alpha_3))^2) \\
& + \dot{y}_2(-\xi L_1\cos(\theta_2+\alpha_1)\sin(\theta_2+\alpha_1) + \eta L_1\cos(\theta_2+\alpha_1)\sin(\theta_2+\alpha_1) - \xi L_2\sin(\theta_2)\cos(\theta_2) + \\
& + \eta L_2\cos(\theta_2)\sin(\theta_2) - \xi L_3\sin(\theta_2+\alpha_3)\cos(\theta_2+\alpha_3) + \eta L_3\sin(\theta_2+\alpha_3)\cos(\theta_2+\alpha_3)) + \\
& + \dot{\theta}_2(\xi L_1\frac{L_2}{2}\sin(\alpha_1)\cos(\theta_2+\alpha_1) - \eta L_1\frac{L_2}{2}\cos(\alpha_1)\sin(\theta_2+\alpha_1) - \eta L_1(\frac{L_1}{2})\sin(\theta_2+\alpha_1) \\
& - \xi L_3\frac{L_2}{2}\sin(\alpha_3)\cos(\theta_2+\alpha_3) + \eta L_3\frac{L_2}{2}\cos(\alpha_3)\sin(\theta_2+\alpha_3) + \eta L_3(\frac{L_3}{2})\sin(\theta_2+\alpha_3) \\
& + \dot{\alpha}_1(-\eta\frac{L_1^2}{2}\sin(\theta_2+\alpha_1)) + \dot{\alpha}_3(\eta\frac{L_3^2}{2}\sin(\theta_2+\alpha_3)) = 0\,.
\end{aligned} \tag{1.39}$$

$$
\begin{aligned}
F_y = {} & \dot{x}_2(-\xi L_1 \cos(\theta_2+\alpha_1)\sin(\theta_2+\alpha_1) + \eta L_1 \cos(\theta_2+\alpha_1)\sin(\theta_2+\alpha_1) - \xi L_2 \sin(\theta_2)\cos(\theta_2) + \\
& + \eta L_2 \cos(\theta_2)\sin(\theta_2) - \xi L_3 \sin(\theta_2+\alpha_3)\cos(\theta_2+\alpha_3) + \eta L_3 \sin(\theta_2+\alpha_3)\cos(\theta_2+\alpha_3)) + \\
& + \dot{y}_2(-\xi L_1(\sin(\theta_2+\alpha_1))^2 - \eta L_1(\cos(\theta_2+\alpha_1))^2 - \xi L_2(\sin(\theta_2))^2 - \eta L_2(\cos(\theta_2))^2 - \\
& - \xi L_3(\sin(\theta_2+\alpha_3))^2 - \eta L_3(\cos(\theta_2+\alpha_3))^2) + \\
& + \dot{\theta}_2(\xi L_1 \frac{L_2}{2}\sin(\alpha_1)\sin(\theta_2+\alpha_1) + \eta L_1 \frac{L_2}{2}\cos(\alpha_1)\cos(\theta_2+\alpha_1) + \eta L_1(\frac{L_1}{2})\cos(\theta_2+\alpha_1) \\
& - \xi L_3 \frac{L_2}{2}\sin(\alpha_3)\sin(\theta_2+\alpha_3) - \eta L_3 \frac{L_2}{2}\cos(\alpha_3)\cos(\theta_2+\alpha_3) - \eta L_3(\frac{L_3}{2})\cos(\theta_2+\alpha_3)) \\
& + \dot{\alpha}_1(\eta \frac{L_1^2}{2}\cos(\theta_2+\alpha_1)) + \dot{\alpha}_3(-\eta \frac{L_3^2}{2}\cos(\theta_2+\alpha_3)) = 0\,.
\end{aligned}
\tag{1.40}
$$

$$
\begin{aligned}
T_{\mathbf{x}_2} = {} & \dot{x}_2(\xi L_1 \frac{L_2}{2}\sin(\alpha_1)\cos(\theta_2+\alpha_1) - \eta L_1 \frac{L_2}{2}\cos(\alpha_1)\sin(\theta_2+\alpha_1) - \eta L_1(\frac{L_1}{2})\sin(\theta_2+\alpha_1) \\
& - \xi L_3 \frac{L_2}{2}\sin(\alpha_3)\cos(\theta_2+\alpha_3) + \eta L_3 \frac{L_2}{2}\cos(\alpha_3)\sin(\theta_2+\alpha_3) + \eta L_3(\frac{L_3}{2})\sin(\theta_2+\alpha_3)) \\
& \dot{y}_2(\xi L_1 \frac{L_2}{2}\sin(\alpha_1)\sin(\theta_2+\alpha_1) + \eta L_1 \frac{L_2}{2}\cos(\alpha_1)\cos(\theta_2+\alpha_1) + \eta L_1(\frac{L_1}{2})\cos(\theta_2+\alpha_1) \\
& - \xi L_3 \frac{L_2}{2}\sin(\alpha_3)\sin(\theta_2+\alpha_3) - \eta L_3 \frac{L_2}{2}\cos(\alpha_3)\cos(\theta_2+\alpha_3) - \eta L_3(\frac{L_3}{2})\cos(\theta_2+\alpha_3) \\
& \dot{\theta}_2(-\xi L_1 \frac{(L_2)^2}{4}(\sin(\alpha_1))^2 + \frac{\eta}{3}((\frac{L_2}{2}\cos(\alpha_1))^3 - (\frac{L_2}{2}\cos(\alpha_1) + L_1)^3) \\
& - \eta(\frac{L_2^3}{12}) - \xi L_3 \frac{(L_2)^2}{4}(\sin(\alpha_3))^2 - \frac{\eta}{3}((\frac{L_2}{2}\cos(\alpha_3) + L_3)^3 - (\frac{L_2}{2}\cos(\alpha_3))^3)) \\
& + \dot{\alpha}_1(-\eta(\frac{L_1^3}{3} + \frac{L_1^2 L_2}{4}\cos\alpha_1)) + \dot{\alpha}_3(-\eta(\frac{L_3^3}{3} + \frac{L_3^2 L_2}{4}\cos\alpha_3)) = 0\,.
\end{aligned}
\tag{1.41}
$$

These equations lead to the system

$$
A(\theta_2,\alpha_1,\alpha_3)\begin{pmatrix}\dot{x}_2\\ \dot{y}_2\\ \dot{\theta}_2\end{pmatrix} + \mathbf{b}_1(\theta_2,\alpha_1,\alpha_3)\dot{\alpha}_1 + \mathbf{b}_2(\theta_2,\alpha_1,\alpha_3)\dot{\alpha}_3 = 0\,, \tag{1.42}
$$

where

$$
A = \begin{pmatrix} a_{1\,1} & a_{1\,2} & a_{1\,3} \\ a_{1\,2} & a_{2\,2} & a_{2\,3} \\ a_{1\,3} & a_{2\,3} & a_{3\,3}\end{pmatrix} \tag{1.43}
$$

is a symmetric matrix with

$$
\begin{aligned}
a_{1\,1} &= -\xi L_1 \cos(\theta_2+\alpha_1)\sin(\theta_2+\alpha_1) + \eta L_1 \cos(\theta_2+\alpha_1)\sin(\theta_2+\alpha_1) - \xi L_2 \sin(\theta_2)\cos(\theta_2) + \\
&\quad + \eta L_2 \cos(\theta_2)\sin(\theta_2) - \xi L_3 \sin(\theta_2+\alpha_3)\cos(\theta_2+\alpha_3) + \eta L_3 \sin(\theta_2+\alpha_3)\cos(\theta_2+\alpha_3)\,, \\
a_{1\,2} &= -\xi L_1 \cos(\theta_2+\alpha_1)\sin(\theta_2+\alpha_1) + \eta L_1 \cos(\theta_2+\alpha_1)\sin(\theta_2+\alpha_1) - \xi L_2 \sin(\theta_2)\cos(\theta_2) + \\
&\quad + \eta L_2 \cos(\theta_2)\sin(\theta_2) - \xi L_3 \sin(\theta_2+\alpha_3)\cos(\theta_2+\alpha_3) + \eta L_3 \sin(\theta_2+\alpha_3)\cos(\theta_2+\alpha_3)\,, \\
a_{1\,3} &= (\xi L_1 \frac{L_2}{2}\sin(\alpha_1)\cos(\theta_2+\alpha_1) - \eta L_1 \frac{L_2}{2}\cos(\alpha_1)\sin(\theta_2+\alpha_1) - \eta L_1(\frac{L_1}{2})\sin(\theta_2+\alpha_1) \\
&\quad - \xi L_3 \frac{L_2}{2}\sin(\alpha_3)\cos(\theta_2+\alpha_3) + \eta L_3 \frac{L_2}{2}\cos(\alpha_3)\sin(\theta_2+\alpha_3) + \eta L_3(\frac{L_3}{2})\sin(\theta_2+\alpha_3)\,, \\
a_{2\,2} &= -\xi L_1(\sin(\theta_2+\alpha_1))^2 - \eta L_1(\cos(\theta_2+\alpha_1))^2 - \xi L_2(\sin(\theta_2))^2 - \eta L_2(\cos(\theta_2))^2 - \\
&\quad - \xi L_3(\sin(\theta_2+\alpha_3))^2 - \eta L_3(\cos(\theta_2+\alpha_3))^2\,, \\
a_{2\,3} &= (\xi L_1 \frac{L_2}{2}\sin(\alpha_1)\sin(\theta_2+\alpha_1) + \eta L_1 \frac{L_2}{2}\cos(\alpha_1)\cos(\theta_2+\alpha_1) + \eta L_1(\frac{L_1}{2})\cos(\theta_2+\alpha_1) \\
&\quad - \xi L_3 \frac{L_2}{2}\sin(\alpha_3)\sin(\theta_2+\alpha_3) - \eta L_3 \frac{L_2}{2}\cos(\alpha_3)\cos(\theta_2+\alpha_3) - \eta L_3(\frac{L_3}{2})\cos(\theta_2+\alpha_3))\,, \\
a_{3\,3} &= (-\xi L_1 \frac{(L_2)^2}{4}(\sin(\alpha_1))^2 + \frac{\eta}{3}((\frac{L_2}{2}\cos(\alpha_1))^3 - (\frac{L_2}{2}\cos(\alpha_1)+L_1)^3) \\
&\quad - \eta(\frac{L_2^3}{12}) - \xi L_3 \frac{(L_2)^2}{4}(\sin(\alpha_3))^2 - \frac{\eta}{3}((\frac{L_2}{2}\cos(\alpha_3)+L_3)^3 - (\frac{L_2}{2}\cos(\alpha_3))^3))\,.
\end{aligned}
$$

The vector $\mathbf{b}_1$ (resp. $\mathbf{b}_2$) is the vector of total force and torque due to a rotation of the left (resp. right) arm $\dot{\alpha}_1 = 1$ (resp. $\dot{\alpha}_3 = 1$) while the other coordinates are kept constant. These vectors are given by

$$
\mathbf{b}_1 = \begin{pmatrix} -\eta\frac{L_1^2}{2}\sin(\theta_2+\alpha_1) \\ \\ \eta\frac{L_1^2}{2}\cos(\theta_2+\alpha_1) \\ \\ -\eta(L_1(\frac{L_1^2}{3} + \frac{L_2 L1}{4}\cos\alpha_1) \end{pmatrix}, \qquad \mathbf{b}_2 = \begin{pmatrix} \eta\frac{L_3^2}{2}\sin(\theta_2+\alpha_3) \\ \\ -\eta\frac{L_3^2}{2}\cos(\theta_2+\alpha_3) \\ \\ -\eta L_3(\frac{L_3^2}{3} + \frac{L_2 L_3}{4}\cos\alpha_3) \end{pmatrix}. \tag{1.44}
$$

Thanks to the invertibility of the matrix A we obtain the system (1.18), with

$$
\mathbf{g}_1(\theta_2,\alpha_1,\alpha_3) = \begin{pmatrix} 1 \\ 0 \\ -\mathbf{A}^{-1}(\theta_2,\alpha_1,\alpha_3)\mathbf{b}_1(\theta_2,\alpha_1,\alpha_3) \end{pmatrix} \tag{1.45}
$$

and

$$
\mathbf{g}_2(\theta_2,\alpha_1,\alpha_3) = \begin{pmatrix} 0 \\ 1 \\ -\mathbf{A}^{-1}(\theta_2,\alpha_1,\alpha_3)\mathbf{b}_2(\theta_2,\alpha_1,\alpha_3) \end{pmatrix}. \tag{1.46}
$$

Chapitre 2

Controllability and Optimal Strokes for N-link Microswimmer

In this paper we focus on the N-link swimmer, a generalization of the classical Purcell swimmer [70] that was introduced in [5]. We use the simplification of the Resistive Force Theory to derive the equation of motion for the swimmer in a fluid with a low Reynolds number, see for instance [49]. We prove that the swimmer is controllable in the whole plane when it is composed by more than 3 sticks and for almost every set of stick lengths. As a direct result, we show that there exists an optimal swimming strategy which leads to minimize the time to reach a desired configuration. Numerical experiments on the case of $N = 3$ (Purcell swimmer) suggest that the optimal strategy is periodic, i.e. composed of a sequence of identical strokes. Our results indicate that this candidate for an optimal stroke indeed gives abetter speed than the classical Purcell stroke.

2.1 Introduction

2.1.1 Locomotion at low Reynolds Number

Swimming at a micro scale is a subject of growing interest. A better understanding of the swimmer motion can lead to many useful applications in several fields such as medicine or micro and nano technology. The world of low Reynolds Number is inhabited by the majority of the micro organisms, for this reason the study of their swimming strategy is attracting increasing attention in the recent literature (see for instance [53] for an extensive list of references). One of the pioneering works is probably the one by Taylor in 1951 (see [84]) who introduces a model of swimmer as an infinite sheet in the form of a sinusoidal traveling wave. In this paper, Taylor presents a mathematical setting for the problem of self-propulsion of this thin undulating filament. Later in 1977, Purcell proved in [70] that the swimming strategies must change the shape of the swimmer in a non-reciprocal way, in order to permit a displacement through the fluid. In the same paper, he introduced a 3-link swimmer model, known as the "Purcell swimmer", along with a stroke that allows it to move. More recently, several works have studied in more detail the physical characteristic of the Purcell swimmer as a toy model, see for instance [83], [15], [5], [69]. Another crucial development for our analysis is the recent emergence of the connection between swimming and Control Theory (see for instance [63], [8], [11], [28], [60], [**?**]). One of the difficulties is the study of the swimmer-fluid coupling which leads to derive the dynamics of the swimmer. At a micro scale, the non local hydrodynamic forces exerted by the fluid on the swimmer can be approximated with local drag forces depending linearly on the velocity of each point (see [49], [37]). This technique called Resistive Force Theory provides a simplified dynamics of the micro swimmer, that gives results in good agreement with those obtained by the full hydrodynamic, see [5], [37]. We use here the same approach than [5] to derive the dynamics of the N-link swimmer.

2.1.2 Contribution

In this paper, we present a controllability result for the N-link swimmer, and a new optimal stroke for displacement in minimum time. First, we prove by geometric control techniques that for $N \geq 3$ sticks, the N-link swimmer is capable to reach any configuration in the plane. More precisely, we show that for almost any swimmer (i.e. for almost every set of stick lengths) and for any initial configuration, the swimmer can reach any shape and position. The global controllability result proved here shows the existence of a suitable shape deformation which steers the swimmer to the desired final state. As a direct consequence, we show that the optimal swimming problem, that is to minimize the time to reach a given configuration, is well posed. Therefore, there exists an optimal strategy which leads to the final position and configuration in minimum time. Finally, we perform some numerical simulations for the Purcell swimmer ($N = 3$), without any assumptions on the structure of the optimal strategy. Our results suggest that the optimal swimming motion is indeed periodic, and we show that the stroke we obtain gives a better speed than the Purcell one.

2.2 Setting of the problem

In this section, we recall the N-link swimmer introduced in [5], and present its dynamics as a system of three ODEs. The system is linear with respect to the rate of deformation, and has no drift.

2.2.1 The N-link swimmer

The swimmer consists of $N \in \mathbf{N}$ rigid links with joints at their ends, see Fig. 2.1. Movement is expressed in the laboratory-frame, defined by the vectors $(\mathbf{e}_x, \mathbf{e}_y)$. We set $\mathbf{e}_z := \mathbf{e}_x \times \mathbf{e}_y$. The i-th link is the segment with end points $\mathbf{x}_i$ and $\mathbf{x}_{i+1}$. We note its length $L_i > 0$ and θ_i its angle with the horizontal x-axis. We define by $\mathbf{x}_i := (x_i, y_i)$ $(i = 1, \cdots, N)$ the coordinates of the first end of each link. Note that, for $i \in \{2 \cdots N\}$, the coordinates $\mathbf{x}_i$ can be expressed as a function of $\mathbf{x}_1$, θ_k and L_k, with $k \in \{1 \cdots i-1\}$:

$$\mathbf{x}_i := \mathbf{x}_1 + \sum_{k=1}^{i-1} L_k \begin{pmatrix} \cos(\theta_k) \\ \sin(\theta_k) \end{pmatrix} . \tag{2.1}$$

The swimmer is described by two sets of variables:

- the state variables which specify the position and the orientation of the first link, associated with the triplet $(\mathbf{x}_1 = (x_1, y_1), \theta_1)$.
- the shape variables which describe the relative orientations between successive links. For each link with $i \in [2, \cdots, N]$, we note $\alpha_i = \theta_i - \theta_{i-1}$ the angle relative to the preceding one. In the following, the vector $(\alpha_2, \ldots, \alpha_N)$ represents the shape of the swimmer.

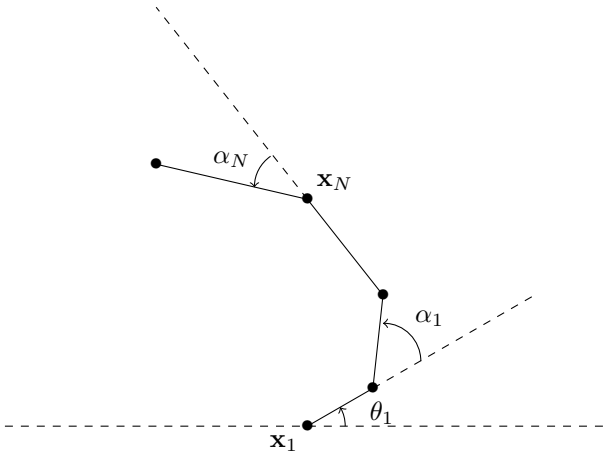

Figure 2.1: Coordinates for the N-link swimmer.

2.2.2 Dynamics

The dynamics for this swimmer was already described in [5]. We recall in this section the main steps to obtain the equations of motion.

The dynamics of the swimmer stems from Newton laws, in which inertia is neglected. These read

$$\begin{cases} \mathbf{F} = 0 \,, \\ \mathbf{e}_z \cdot \mathbf{T}_{\mathbf{x}_1} = 0 \,, \end{cases} \tag{2.2}$$

where $\mathbf{F}$ is the total force exerted on the swimmer by the fluid and $\mathbf{T}_{\mathbf{x}_1}$ is the corresponding total torque computed with respect to the point $\mathbf{x}_1$.

To couple the fluid and the swimmer, we use the local drag approximation of Resistive Force Theory. We denote by s the arc length coordinate on the i-th link ($0 \leq s \leq L_i$) and by $\mathbf{v}_i(s)$ the velocity of the corresponding point. We also introduce the unit vectors in the directions parallel and perpendicular to the i-th link
$\mathbf{e}_i = \begin{pmatrix} \cos(\theta_i) \\ \sin(\theta_i) \end{pmatrix}$ and $\mathbf{e}_i^\perp = \begin{pmatrix} -\sin(\theta_i) \\ \cos(\theta_i) \end{pmatrix}$
and write $\mathbf{x}_i(s) = \mathbf{x}_i + s\mathbf{e}_i$. By differentiation, we obtain,

$$\mathbf{v}_i(s) = \dot{\mathbf{x}}_i + s\dot{\theta}_i \mathbf{e}_i^\perp . \tag{2.3}$$

The density of the force $\mathbf{f}_i$ acting on the i-th segment is assumed to depend linearly on the velocity. It is defined by

$$\mathbf{f}_i(s) := -\xi \left(\mathbf{v}_i(s) \cdot \mathbf{e}_i\right) \mathbf{e}_i - \eta \left(\mathbf{v}_i(s) \cdot \mathbf{e}_i^\perp\right) \mathbf{e}_i^\perp, \tag{2.4}$$

where ξ and η are respectively the drag coefficients in the directions of $\mathbf{e}_i$ and $\mathbf{e}_i^\perp$. We thus obtain

$$\begin{cases} \mathbf{F} = \displaystyle\sum_{i=1}^{N} \int_0^{L_i} \mathbf{f}_i(s)\, ds\,, \\ \mathbf{e}_z \cdot \mathbf{T}_{\mathbf{x}_1} = \mathbf{e}_z \cdot \displaystyle\sum_{i=1}^{N} \int_0^{L_i} \left(\mathbf{x}_i(s) - \mathbf{x}_1\right) \times \mathbf{f}_i(s)\, ds\,. \end{cases} \tag{2.5}$$

Using (2.3) and (2.4) into (2.5), the total force $\mathbf{F}$ can be expressed as

$$-\sum_{i=1}^{N} L_i \xi (\dot{\mathbf{x}}_i \cdot \mathbf{e}_i)\, \mathbf{e}_i + \left(L_i \eta (\dot{\mathbf{x}}_i \cdot \mathbf{e}_i^\perp) + \frac{L_i^2}{2} \eta \dot{\theta}_i \right) \mathbf{e}_i^\perp\,, \tag{2.6}$$

and and torque $\mathbf{e}_z \cdot \mathbf{T}_{\mathbf{x}_1}$ as

$$\begin{array}{rl} -\displaystyle\sum_{i=1}^{N} & L_i \eta \left(\dot{\mathbf{x}}_i \cdot \mathbf{e}_i^\perp\right)\ \left(\mathbf{x}_i - \mathbf{x}_1\right)\ \times\ \mathbf{e}_i^\perp + \\ & L_i \xi\ \left(\dot{\mathbf{x}}_i \cdot \mathbf{e}_i\right)\ \left(\mathbf{x}_i - \mathbf{x}_1\right)\ \times\ \mathbf{e}_i\ + \\ & \frac{L_i^2}{2} \eta \dot{\theta}_i\quad \left(\mathbf{x}_i - \mathbf{x}_1\right)\ \times\ \mathbf{e}_i^\perp\quad + \\ & \frac{L_i^2}{2}\ \eta\ \left(\dot{\mathbf{x}}_i \cdot \mathbf{e}_i^\perp\right)\ +\ \frac{L_i^3}{3}\, \eta\, \dot{\theta}_i\,. \end{array} \tag{2.7}$$

Moreover, differentiating (2.1) gives

$$\dot{\mathbf{x}}_i = \dot{\mathbf{x}}_1 + \sum_{k=1}^{i-1} L_k \dot{\theta}_k \mathbf{e}_k^\perp, \tag{2.8}$$

which is linear in $\dot{\mathbf{x}}_1$ and $(\dot{\theta}_k)_{1 \leq k \leq N}$.

The angles $(\dot{\alpha}_k)_{2 \leq k \leq N}$ are a linear combinaison of $(\dot{\theta}_k)_{2 \leq k \leq N}$, thus formulas (2.6) and (2.7) are linear in $\dot{\mathbf{x}}_1$, $\dot{\theta}_1$ and $(\dot{\alpha}_k)_{2 \leq k \leq N}$.
Writing the system 2.5 in a matricial form we obtain

$$\mathbf{A}\left(\theta_1, \alpha_2, \cdots, \alpha_N\right) \cdot \begin{pmatrix} x_1 \\ y_1 \\ \theta_1 \end{pmatrix} - \mathbf{B}\left(\theta_1, \alpha_2, \cdots, \alpha_N\right) \cdot \begin{pmatrix} \alpha_2 \\ \vdots \\ \alpha_N \end{pmatrix} = 0 \tag{2.9}$$

where the matrix $\mathbf{A}(\theta_1, \alpha_2, \cdots, \alpha_N)$ is known as "Grand Resistance Matrix", and $\mathbf{B}(\theta_1, \alpha_2, \cdots, \alpha_N)$ is the linear map associated to the coefficients describing the shape of the swimmer [5].

By inverting $\mathbf{A}$, we get the existence of the family of vector fields $\{\tilde{\mathbf{g}}_i(\theta_1, \alpha_2, \cdots, \alpha_N)\}_{i=1,\cdots,N-1}$ defined on $[0, 2\pi]^N$ by $\tilde{\mathbf{g}}_i := \mathbf{A}^{-1}\mathbf{B}$. Then the dynamics of the swimmer reads

$$\begin{pmatrix} \dot{\alpha}_2 \\ \vdots \\ \dot{\alpha}_N \\ \dot{\mathbf{x}}_1 \\ \dot{\theta}_1 \end{pmatrix} = \sum_{i=1}^{N-1} \begin{pmatrix} \mathbf{b}_i \\ \tilde{\mathbf{g}}_i(\theta_1, \alpha_2, \cdots, \alpha_N) \end{pmatrix} \dot{\alpha}_{i+1}\,. \tag{2.10}$$

where $\mathbf{b}_i$ is the $i-$th vector of the canonical basis of $\mathbf{R}^{N-1}$.

2.3 Controllability

This Section is devoted to the controllability result of the N-link swimmer. Namely, we prove that there exist control functions which allow the swimmer to move everywhere in the plane.

Theorem 2.3.1 *Consider the N-link swimmer described in Section 2.2 evolving in the space $\mathbf{R}^2$. Then for almost every lengths of the sticks $(L_i)_{i=1,\cdots,N}$ and for any initial configuration $(\mathbf{x}_1^i, \theta_1^i, \alpha_2^i, \cdots, \alpha_N^i) \in \mathbf{R}^2 \times [0, 2\pi]^N$, any final configuration $(\mathbf{x}_1^f, \theta_1^f, \alpha_2^f, \cdots, \alpha_N^f)$ and any final time $T > 0$, there exists a shape function $(\alpha_2, \cdots, \alpha_N) \in \mathcal{W}^{1,\infty}([0, T])$, satisfying $(\alpha_2, \cdots, \alpha_N)(0) = (\alpha_2^i, \cdots, \alpha_N^i)$ and $(\alpha_2, \cdots, \alpha_N)(T) = (\alpha_2^f, \cdots, \alpha_N^f)$ and such that if the self-propelled swimmer starts in position $(\mathbf{x}_1^i, \theta_1^i)$ with the shape $(\alpha_2^i, \cdots, \alpha_N^i)$ at time $t = 0$, it ends at position $(\mathbf{x}_1^f, \theta_1^f)$ and shape $(\alpha_2^f, \cdots, \alpha_N^f)$ at time $t = T$ by changing its shape along $(\alpha_2, \cdots, \alpha_N)(t)$.*

Proof: The proof of the theorem is divided into three steps. First, we deal with the analyticity of the dynamics vector fields. Then, we prove the controllability of the Purcell 3-link swimmer, exploiting the Chow theorem and the Orbit theorem. Finally, we generalize the result to the N-link swimmer. We start by recalling some classical results used in the proof.

2.3.1 Classical results in geometric control

Theorem 2.3.2 *(Chow (see [29])) Let m,$n \in \mathbf{N}$ and let $(f_i)_{i=1,n}$ be $\mathcal{C}^\infty$ vector fields on $\mathbf{R}^n$. Consider the control system, of state trajectory $\mathbf{q}$,*

$$\dot{q} = \sum_{i=1}^{m} u_i f_i(\mathbf{q}), \tag{2.11}$$

with input function $\mathbf{u} = (u_i)_{i=1,m} \in L^\infty([0, +\infty[, \mathbf{B}_{\mathbf{R}^n}(0, r))$ for some $r > 0$.
Let $\mathcal{O}$ an open and connected set of $\mathbf{R}^n$ and assume that

$$\mathbf{L}ie_{\mathbf{q}}(f_1, ...f_m) = \mathbf{R}^n \quad \mathbf{q} \in \mathcal{O}\,.$$

Then the system (2.11) is controllable, i.e., for every $\mathbf{q}_0$, $\mathbf{q}_1$ in $\mathcal{O}$ and for every $T > 0$ exists $\mathbf{u} \in L^\infty((0, T), \mathbf{B}_{\mathbf{R}^n}(0, r))$ such that $\mathbf{q}(0) = \mathbf{q}_0$ and $\mathbf{q}(T) = \mathbf{q}_1$ and $\mathbf{q}(t) \in \mathcal{O}$ for every $t \in [0, T]$.

If the vector fields are analytic, we can apply the Orbit Theorem to extend the dimension property of the Lie algebra defined by the dynamics vector fields on the whole orbit.

Theorem 2.3.3 *(Orbit (see [51]) Let $\mathcal{M}$ be an analytic manifold, and $\mathcal{F}$ a family of analytic vector fields on $\mathcal{M}$. Then*

a) each orbit of $\mathcal{F}$ is an analytic submanifold of $\mathcal{M}$, and

b) if N is an orbit of $\mathcal{F}$, then the tangent space of $\mathcal{N}$ at x is given by $Lie_x(\mathcal{F})$. In particular the dimension of $Lie_x(\mathcal{F})$ is constant as x varies on $\mathcal{N}$.

In our case, the manifold in which the state and the shape of the swimmer evolve is defined by $\mathcal{M} := [0, 2\pi]^{N-1} \times \mathbf{R}^2 \times [0, 2\pi]$ The vector fields of the dynamics are denoted by

$$\mathbf{g}_i\left(\theta_1, \alpha_2, \cdots, \alpha_N\right) := \begin{pmatrix} \mathbf{b}_i \\ \tilde{\mathbf{g}}_i\left(\theta_1, \alpha_2, \cdots, \alpha_N\right) \end{pmatrix}.$$

We say that the Lie algebra of the family of vector fields $\{\mathbf{g}_i\}_{i=1,\cdots,N-1}$ is fully generated at the point $\mathbf{q} = (\alpha_2, \cdots, \alpha_N, x_1, y_1, \theta_1) \in \mathcal{M}$ if the tangent space of the manifold, $T_{\mathbf{q}}\mathcal{M}$, is equal to the Lie algebra $\mathrm{Lie}((\mathbf{g}_i))_{i=1,\cdots,N-1})(\mathbf{q})$.

2.3.2 Regularity

The first step is to prove that the vector fields of the motion equation of the swimmer are analytic on $\mathcal{M}$.

As a direct consequence of (2.6) and (2.7), the linear maps $\mathbf{A}$ and $\mathbf{B}$ belong to the set of matrices whose entries are analytic functions on $[0, 2\pi]^N$. The family of vector $(\tilde{\mathbf{g}}_i(\theta_1, \alpha_2, \cdots, \alpha_N))_{i=1,\cdots,N-1}$ is obtained by the multiplication of $\mathbf{A}^{-1}$ by $\mathbf{B}$. Since the coefficients of $\mathbf{A}^{-1}$ are obtained by multiplication and division of those of $\mathbf{A}$, and because the determinant of $\mathbf{A}$ is never null, the entries of inverse matrix $\mathbf{A}^{-1}$ remain analytic functions on $[0, 2\pi]^N$. Thus, the family of vector fields $(\tilde{\mathbf{g}}_i)_{i=1,\cdots,N}$ are analytic on $[0, 2\pi]^N$.

2.3.3 Controllability of the Purcell Swimmer (N=3)

Now we prove the controllability of the Purcell's swimmer. By replacing $N = 3$ in (5.10), the Purcell's dynamics reads

$$\begin{pmatrix} \dot{\alpha}_2 \\ \dot{\alpha}_3 \\ \dot{x}_1 \\ \dot{y}_1 \\ \dot{\theta}_1 \end{pmatrix} = \mathbf{g}_1(\theta_1, \alpha_2, \alpha_3)\dot{\alpha}_2 + \mathbf{g}_2(\theta_1, \alpha_2, \alpha_3)\dot{\alpha}_3\,. \tag{2.12}$$

We now express the Lie algebra of the vector fields $\mathbf{g}_1$ and $\mathbf{g}_2$ for any $\theta_1 \in [0, 2\pi]$ at the point $(\alpha_2, \alpha_3) = (0, 0)$, for a swimmer whose sticks have the length $L_1 = L_3 = L$ and $L_2 = 2L$ where $L > 0$.

The two vectors $\mathbf{g}_1(\theta_1,0,0)$ and $\mathbf{g}_2(\theta_1,0,0)$ are

$$\mathbf{g}_1(\theta_1,0,0)=\begin{pmatrix}1\\0\\\frac{9L\sin(\theta_1)}{64}\\-\frac{9L\cos(\theta_1)}{64}\\\frac{27}{32}\end{pmatrix},\qquad \mathbf{g}_2(\theta_1,0,0)=\begin{pmatrix}0\\1\\-\frac{7L\sin(\theta_1)}{64}\\\frac{7L\cos(\theta_1)}{64}\\-\frac{5}{32}\end{pmatrix}.$$

Then, the iterated Lie brackets are equals to

$$[\mathbf{g}_1,\mathbf{g}_2](\theta_1,0,0)=\begin{pmatrix}0\\0\\\frac{7L(\eta-\xi)\cos(\theta_1)}{128\xi}\\\frac{7L(\eta-\xi)\sin(\theta_1)}{128\xi}\\0\end{pmatrix},$$

$$[\mathbf{g}_1,[\mathbf{g}_1,\mathbf{g}_2]](\theta_1,0,0)=\begin{pmatrix}0\\0\\-\frac{L\left(126\eta^2+31\xi\eta-76\xi^2\right)\sin(\theta_1)}{4096\eta\xi}\\\frac{L\left(126\eta^2+31\xi\eta-76\xi^2\right)\cos(\theta_1)}{4096\eta\xi}\\-\frac{3\left(9\eta^2-4\xi\eta+4\xi^2\right)}{2048\eta\xi}\end{pmatrix},$$

$$[\mathbf{g}_2,[\mathbf{g}_1,\mathbf{g}_2]](\theta_1,0,0)=\begin{pmatrix}0\\0\\\frac{L\left(36\eta^2-103\xi\eta+148\xi^2\right)\sin(\theta_1)}{4096\eta\xi}\\-\frac{L\left(36\eta^2-103\xi\eta+148\xi^2\right)\cos(\theta_1)}{4096\eta\xi}\\\frac{3\left(9\eta^2-4\xi\eta+4\xi^2\right)}{2048\eta\xi}\end{pmatrix}.$$

The determinant of the matrix whose columns are the previous vector fields is equal to

$$\begin{aligned}&\Big|\Big(\mathbf{g}_1\ \mathbf{g}_2\ [\mathbf{g}_1,\mathbf{g}_2]\ [\mathbf{g}_1,[\mathbf{g}_1,\mathbf{g}_2]]\ [\mathbf{g}_2,[\mathbf{g}_1,\mathbf{g}_2]]\Big)(\theta_1,0,0)\Big|\\&\quad=\frac{21L^2(\eta-\xi)^2(45\eta+112\xi)\left(9\eta^2-4\eta\xi+4\xi^2\right)}{536870912\eta^2\xi^3}.\end{aligned}\tag{2.13}$$

Since the two drag coefficients ξ and η, are supposed positive, this determinant is never null exept for isotropic coefficients ($\xi=\eta$). If we assume the drag coefficients to be equal, physically means that the sticks are subjected to the same drag force in both paralel and orthogonal dirctions, so they would not be sticks but spheres. Thus tthis case is not physically acceptable.

Thus for any $\theta_1\in[0,2\pi]$, the Lie algebra of the vector fields $\mathbf{g}_1$ and $\mathbf{g}_2$ is fully generated at the point $(\theta_1,\alpha_2,\alpha_3)=(\theta_1,0,0)$. Remark that any point $(\alpha_2,\alpha_3,\mathbf{x}_1,\theta_1)\in$

$[0, 2\pi]^2 \times \mathbf{R}^2 \times [0, 2\pi]$ belongs to the orbit of the point $(0, 0, \mathbf{x}_1, \theta_1)$. Since the vector fields are analytic, Orbit Theorem 2.3.3 guarantees that the Lie algebra of $\mathbf{g}_1$ and $\mathbf{g}_2$ is fully generated everywhere in the manifold $[0, 2\pi]^2 \times \mathbf{R}^2 \times [0, 2\pi]$.

To conclude, by Chow Theorem 2.3.2 we get the controllability of the Purcell's swimmer whose sticks have same length.

2.3.4 Controllability of the N-link swimmer

The third step is to generalize the previous controllability result to the N-link swimmer.

The dynamics of this swimmer is described by the ODE (5.10). By construction, the family of vector fields $\mathbf{g}_i$ generates the tangent space of the manifolds $[0, 2\pi]^{N-1}$,

$$\mathrm{Span}(\mathbf{g}_1, \cdots, \mathbf{g}_{N-1}) = \mathbf{R}^{N-1}. \tag{2.14}$$

The two vector fields $\mathbf{g}_1$ and $\mathbf{g}_2$ are related to the Purcell's one defined in (2.12): we add $N-2$ rows of zeroes, take sticks of null length $L_i = 0$ for $4 \leq i \leq N-1$, while keeping the three sticks $L_1 = L_3 = L$ and $L_2 = 2L$ unchanged.

In this case, for any $(\mathbf{x}_1, \theta_1) \in \mathbf{R}^2 \times [0, 2\pi]$ Subsection 2.3.3 shows that the vectors $\mathbf{g}_1(\theta_1, 0, \cdots 0)$, $\mathbf{g}_2(\theta_1, 0, \cdots 0)$ and their iterated Lie brackets $[\mathbf{g}_1, \mathbf{g}_2](\theta_1, 0, \cdots 0)$, $[\mathbf{g}_1, [\mathbf{g}_1, \mathbf{g}_2]](\theta_1, 0, \cdots 0)$, and $[\mathbf{g}_2, [\mathbf{g}_1, \mathbf{g}_2]](\theta_1, 0, \cdots 0)$ are linearly independent.

Therefore, the Lie algebra of the family $(\mathbf{g}_i)_{i=1,\cdots,N-1}$ at the point $(\theta_1, 0, \cdots, 0)$ is equal to the tangent space $T_{(0,\cdots,0,\mathbf{x}_1,\theta_1)}\mathcal{M}$.

Then, by analyticity of the vector fields $\mathbf{g}_i$, Orbit Theorem 2.3.3 states that the Lie algebra is fully generated everywhere for a swimmer whose the length of sticks verify $L_1 = L_3 = L$, $L_2 = 2L$ and $L_i = 0$, for $4 \leq i \leq N-1$.

Notice that the vector fields of the motion equation depend analytically also on the sticks length L_i, $i = 1, \cdots, N$. We define by $D^{(0,\cdots,0)}$, the function which associates to the $N-$uplet of the stick lengths the determinant of the vectors $\mathbf{g}_1(0, \cdots, 0), \cdots, \mathbf{g}_{N-1}(0, \cdots, 0)$ and their iterated Lie brakets at $(0, \cdots, 0)$.

Since the dependance on L_i of vector fields $\mathbf{g}_i$ is analytic, we get the analyticity of the function $D^{(0,\cdots,0)}$. Thus for any $L > 0$, the value of $D^{(0,\cdots,0)}$ at the point $(L, 2L, L, 0 \cdots 0)$ is not null. Then, by analyticity it remains non null almost everywhere in $\mathbf{R}^N$. Therefore, we obtain that the Lie algebra of a full rank for almost every swimmer.

Finally, by using Chow Theorem 2.3.2, we get the controllability stated in the Theorem 2.3.1.

2.4 Minimum time optimal problem for the N-link swimmer

This Section describes the minimum time optimal control problem for the N-link swimmer. The problem is defined in 2.4.1, and is well defined, from the controllability result proven in 2.3. Then in 2.4.2 we present the optimization strategy we used to find a solution to this optimal control problem.

2.4.1 Optimal Time Control Problem Statement

For any time $t > 0$, let us denote the state of the swimmer by $\mathbf{z}(t) := (\alpha_2, \cdots, \alpha_N, \mathbf{x}_1, \theta_1)(t)^T$, the control function by $\mathbf{u}(t) := (\dot{\alpha}_2, \cdots, \dot{\alpha}_N)(t)$ and the dynamics by $\mathbf{f}(\mathbf{z}(t), \mathbf{u}(t)) = \sum_{i=1}^{N-1} \mathbf{g}_i(\mathbf{z}(t))\, \dot{\alpha}_{i+1}(t)$. In the following we assume that the swimmer starts at the initial configuration $\mathbf{z}^i$ and we set a final state $\mathbf{z}^f$. We want to find an optimal swimming strategy which minimizes the time to reach the final configuration, i.e.,

$$(OCP) \begin{cases} \inf\ T\,, \\ \dot{\mathbf{z}}(t) = f(\mathbf{z}(t), \mathbf{u}(t))\ ,\ \forall t \in [0, T]\,, \\ \mathbf{u}(t) \in \mathbf{U} := [-1, 1]^N\ ,\ \forall t \in [0, T]\,, \\ \mathbf{z}(0) = \mathbf{z}^i\,, \\ \mathbf{z}(T) = \mathbf{z}^f\,. \end{cases}$$

By applying Filippov-Cesary Theorem (as stated in [85]), there exist a minimal time such that the constraints are satisfied, and the optimal problem reads

$$(OCP) \begin{cases} \min\ T\,, \\ \dot{\mathbf{z}}(t) = f(\mathbf{z}(t), \mathbf{u}(t))\ ,\ \forall t \in [0, T]\,, \\ \mathbf{u}(t) \in \mathbf{U} := [-1, 1]^N\ ,\ \forall t \in [0, T]\,, \\ \mathbf{z}(0) = \mathbf{z}^i\,, \\ \mathbf{z}(T) = \mathbf{z}^f\,. \end{cases} \tag{2.15}$$

2.4.2 Optimization Strategy

In order to solve this optimal control problem, we use a so-called direct approach. The direct approach transforms the infinite dimensional optimal control problem (OCP) into a finite dimensional optimization problem (NLP). This is done by a discretization in time applied to the state and control variables, as well as the dynamics equation. These methods are usually less precise than indirect methods based on Pontryagin's Maximum Principle, but more robust with respect to the initialization. Also, they are more straightforward to apply, hence they are widely used in industrial applications.

Summary of the time discretization:

$t \in [0, T]$	$\rightarrow$	$\{t_0 = 0, \ldots, t_N = T\}$
$z(\,\cdot\,), u(\,\cdot\,)$	$\rightarrow$	$X = \{z_0, \ldots, z_N, u_0, \ldots, u_{N-1}, T\}$
Criterion	$\rightarrow$	$\min\ T$
Dynamics	$\rightarrow$	$(ex : Euler)\ z_{i+i} = z_i + hf(z_i, u_i)$
Adm. Cont.	$\rightarrow$	$-1 \leq u_i \leq 1$
Bnd. Cond.	$\rightarrow$	$\Phi(z_0, z_N) = 0$

We therefore obtain a nonlinear programming problem on the discretized state and control variables

$$(NLP) \begin{cases} \min\ F(z) = T \\ LB \leq C(z) \leq UB \end{cases}$$

All tests were run using the software BOCOP[2] ([21]). The discretized nonlinear optimization problem is solved by the well-known solver IPOPT [86] with MUMPS [12], while the derivatives are computed by sparse automatic differentiation with ADOL-C [87] and COLPACK [42]. In the numerical experiments, we used a Midpoint (implicit 2nd order) discretization with 1000 time steps. Execution times on a Xeon 3.2GHz CPU were a few minutes.

[2] http://bocop.org

2.5 Numerical simulation for the Purcell's swimmer (N= 3)

In this Section, we present the numerical simulations associated with the problem (2.15) in the case of $N = 3$ sticks (Purcell's swimmer). We observe that while we did not make any assumptions on the structure of the optimal trajectory, the solution given by the direct solver Bocop shows a periodic structure. We extract a stroke from these solutions, and check that we obtain a better displacement better than the one of Purcell ([70], [15]).

In the rest of the paper, we reformulate the system in order to match the state variables used in the literature for the Purcell swimmer [15]. Following [15], we take the sticks lengths $L_1 = L_3 = 1$ and $L_2 = 2$. From now on, the state of the swimmer (see Fig 2.2) is described by

- the position (x_2, y_2) of the center of the second stick, and $\theta_2 := \theta_1 - \alpha_2$ the angle between the x-axis and the second stick
- the shape of the swimmer, defined by the two angles $\beta_1 := -\alpha_2$ and $\beta_3 := \alpha_3$.

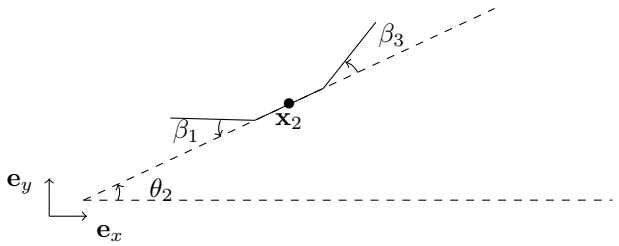

Figure 2.2: Purcell's 3-link swimmer.

The time derivative of the new variables which describe the swimmer are linear in the previous ones,

$$\begin{pmatrix} \dot{\beta}_1 \\ \dot{\beta}_3 \\ \dot{\mathbf{x}}_2 \\ \dot{\theta}_2 \end{pmatrix} = \mathbf{M}\left(\theta_2, \beta_1\right) \begin{pmatrix} \dot{\alpha}_2 \\ \dot{\alpha}_3 \\ \dot{\mathbf{x}}_1 \\ \dot{\theta}_1 \end{pmatrix},$$

where the matrix $\mathbf{M}\left(\theta_2, \beta_1\right)$ is defined by,

$$\mathbf{M}\left(\theta_2, \beta_1\right) = \begin{pmatrix} -1 & 0 & 0 & 0 & 0 \\ 0 & 1 & 0 & 0 & 0 \\ \sin(\theta_2) + \cos(\beta_1) & 0 & 1 & 0 & -\sin(\theta_2) \\ -\cos(\beta_1) - \cos(\theta_2) & 0 & 0 & 1 & \cos(\theta_2) \\ -1 & 0 & 0 & 0 & 1 \end{pmatrix}.$$

As a result, the dynamics (5.10) reads in this case

$$\begin{pmatrix} \dot{\beta}_1 \\ \dot{\beta}_3 \\ \dot{\mathbf{x}}_2 \\ \dot{\theta}_2 \end{pmatrix} = \tilde{\mathbf{f}}_1\left(\theta_2, \beta_2, \beta_3\right)\, \dot{\beta}_1 + \tilde{\mathbf{f}}_2\left(\theta_2, \beta_2, \beta_3\right)\, \dot{\beta}_3 \tag{2.16}$$

where for $i = 1, 2$

$$\tilde{\mathbf{f}}_i\left(\theta_2, \beta_1, \beta_3\right) = \mathbf{M}\left(\theta_2, \beta_1, \right) \tilde{\mathbf{g}}_i\left(\theta_1, \alpha_2, \alpha_3\right) . \tag{2.17}$$

Since the variables which describe the swimmer are the image of the previous one by a one-to-one mapping, it is clear that the controllability result proved in Section 2.3.3 holds for the ODE (2.16).

2.5.1 The classical Purcell stroke

The stroke presented by Purcell in [70] is used in the rest to compare the optimal strategy given by our numerical results. Let us denote by $\Delta\theta$, the angular excursion of β_1 and β_3. It means that during the stroke β_1 and β_3 belong to the interval $[-\frac{\Delta\theta}{2}, \frac{\Delta\theta}{2}]$. Calling T the interval of time in which the swimmer performs the stroke, the Purcell stroke is defined by the following periodic cycle of deformation,

$$\beta_1(t) = \begin{cases} \dfrac{4\Delta\theta}{T}t - \dfrac{\Delta\theta}{2} & \text{if } 0 \le t \le \frac{T}{4} \\ \dfrac{\Delta\theta}{2} & \text{if } \frac{T}{4} \le t \le \frac{T}{2} \\ -\dfrac{4\Delta\theta}{T}t + \dfrac{5\Delta\theta}{2} & \text{if } \frac{T}{2} \le t \le \frac{3T}{4} \\ -\dfrac{\Delta\theta}{2} & \text{if } \frac{3T}{4} \le t \le T \end{cases} ,$$

and

$$\beta_3(t) = \begin{cases} \dfrac{\Delta\theta}{2} & \text{if } 0 \le t \le \frac{T}{4} \\ -\dfrac{4\Delta\theta}{T}t + \dfrac{3\Delta\theta}{2} & \text{if } \frac{T}{4} \le t \le \frac{T}{2} \\ -\dfrac{\Delta\theta}{2} & \text{if } \frac{T}{2} \le t \le \frac{3T}{4} \\ \dfrac{4\Delta\theta}{T}t - \dfrac{7\Delta\theta}{2} & \text{if } \frac{3T}{4} \le t \le T \end{cases} .$$

In the following, we call the "classical" Purcell stroke the one corresponding to $\Delta\theta = \frac{\pi}{3}$ and $T = 4\Delta\theta$. The time period T is chosen for satisfying the constraints on the speed of deformation fixed by the optimal problem (2.15) (i.e., $\dot{\beta}_i(t) \in [-1, 1]$, $i = 1, 3$, for all time $t \in [0, T]$).

2.5.2 Comparison of the optimal stroke with the classical Purcell stroke

For the comparison, we take the initial position $\mathbf{x}_2 = (0, 0)$ and $\theta_2 = 0$ and the final position $\mathbf{x}_2 = (-0.25, 0)$ and $\theta_2 = 0$. We also constrain the angles $\beta_1(t)$ and $\beta_3(t)$ to vary between $-\frac{\pi}{6}$ and $\frac{\pi}{6}$ for all time $t > 0$. Solving the minimum time problem with the direct method gives us a periodic solution from which we extract a candidate for the time optimal stroke. We describe this stroke in more details, and show its displacement versus the Purcell one.

Solving the optimal problem (2.15) we observe that the solution is periodic, as show the graphs on Fig. 2.3 for the angles functions β_1, β_3 and the x-displacement.

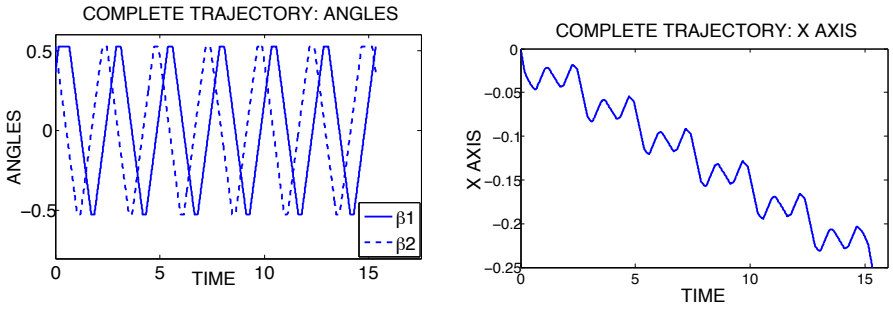

Figure 2.3: Angles and x-displacement for a whole periodic trajectory.

From the plots above it is evident that the optimal controls have a periodic structure and perform more than one period in the optimal interval of time. In order to compare the results for the displacement with the Purcell's ones, we need to select only one period (i.e. one stroke). We show on Fig. 2.4 the angles functions β_1 and β_3, as well as the phase portrait for both the classical Purcell stroke and our selected optimal stroke. Notice that for satisfying the constraints on the speed of deformation $\mathbf{u} \in [-1, 1]$, the time performed by the swimmer to do the Purcell Stroke is greater than the time to do the optimal one.

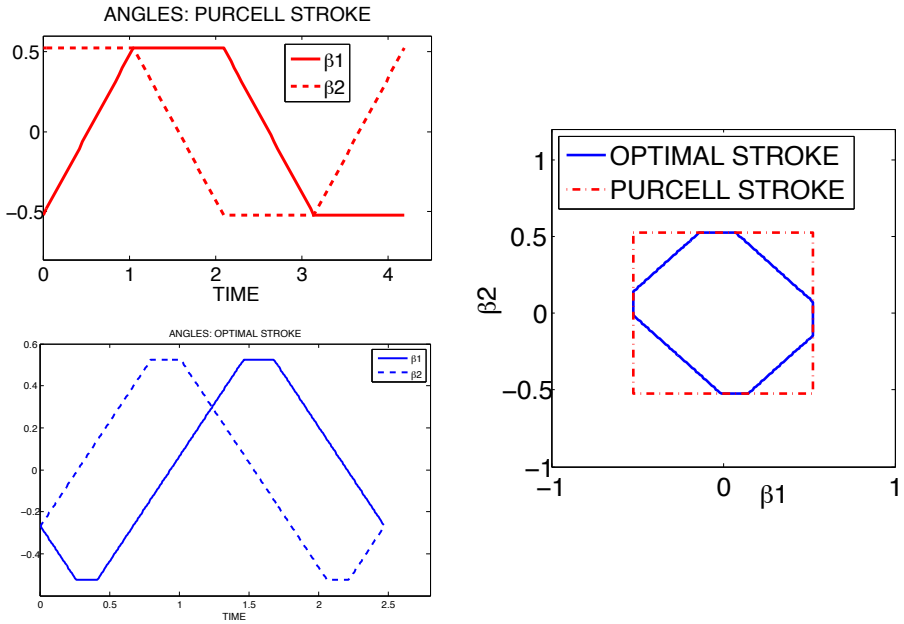

Figure 2.4: Angles and phase portrait - Purcell stroke and optimal stroke.

We show now the shape changes in the (X,Y) plane for the Purcell and optimal stroke. Figure 2.5 shows the Purcell swimmer in four different times during the classical Purcell stroke, and Fig. 2.6 shows the swimmer performing the selected optimal stroke.

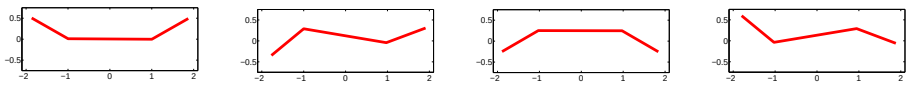

Figure 2.5: Shape changes for the Purcell's stroke.

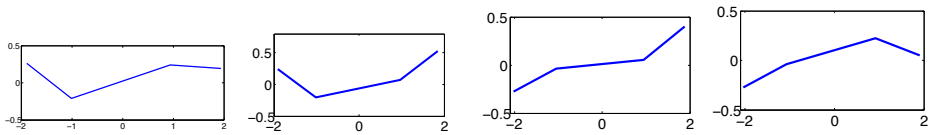

Figure 2.6: Shape changes for the optimal stroke.

We draw on Fig. 2.7 the $x-$displacement of the swimmer when it uses the classical Purcell stroke represented by the red curve and the optimal stroke depicted by the bleu curve. The interval of time $[0, 15.3252]$ is the one given by the numeric simulation, it leads the swimmer to reach $\mathbf{x}_2 = (-0.25\,, 0)$ with the optimal strategy, instead by the Purcell strategy the swimmer reaches only $(\approx -0.18, 0)$. We observe that our optimal stroke allows the swimmer to move further in the x-direction. More precisely, the optimal stroke leads a $x-$displacement close to one given by the Purcell stroke. But, the cycle of deformation of the optimal stroke is performed in less time than the Purcell one. So, for a time fixed, the optimal stroke steers the swimmer to have a greater $x-$displacement. In Fig. 2.7, we discern that almost 3.5 Purcell strokes are performed during the time $[0, 15.3252]$, whereas there are six optimal strokes in the same time.

Remark 2.5.1 *We see that the gap between the two curves grows with time, which confirms that the optimal stroke is better, regardless of the small difference in the initial shape of the swimmer.*

Notice that the final displacement after one Purcell strokes matches the results of [15].

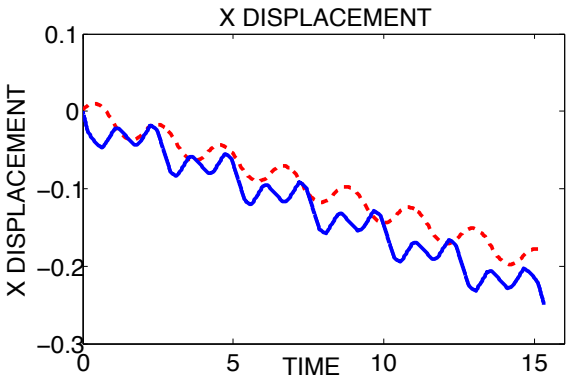

Figure 2.7: x and y displacement for one Purcell and one optimal stroke.

We study now for both strokes the x-displacement for a stroke with respect to the angular excursion, as shown on Fig. 2.8. In both cases, we see that a larger interval of angular excursion gives a greater displacement. Here again, it is obvious that the strokes given by our optimization strategy produce a greater speed (x-displacement over stroke period) than the Purcell one for any range of angular excursion.

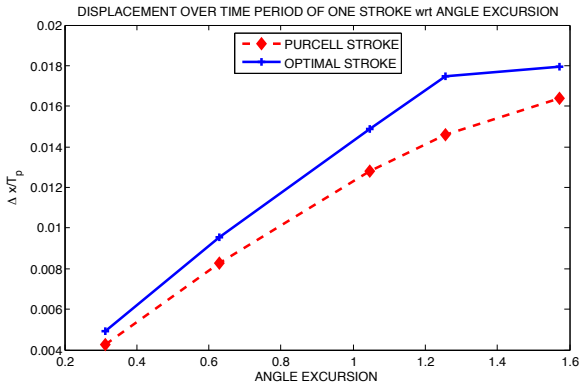

Figure 2.8: x displacement, noted Δx, over the time period to perform a stroke, denoted by T, wrt angular excursion, Purcell (in red) and optimal stroke (in bleu).

2.6 Conclusions

In this paper we study the N-link swimmer, and use the Resistive Force Theory to derive its dynamics, as was done in [5]. In this context, we prove that for N greater than 3 and for almost any N-uplet of sticks lengths, the swimmer is globally controllable in the whole plane. Then, we focus on finding a swimming strategy that leads the N-link swimmer from an fixed initial position to a given final position, in minimum time. As a consequence of the controllability result, we show that there exists a shape change function which allows to reach the final state in a minimal time. We formulate this optimal control problem and solve it with a direct approach (Bocop) for the case $N = 3$ (Purcell swimmer). Without any assumption on the structure of the trajectory, we obtain a periodic solution, from which we identify an optimal stroke. Comparing this optimal stroke with the Purcell one confirms that it is better, actually giving a greater displacement speed. More precisely, the difference is due to the fact that optimal stroke is executed in less time than the Purcell one.

Current and still ongoing works include solving the optimal control problem for more complex displacements (along the y axis, rotations) and/or for different cost functions (such as energy-type). Also, noticing that the N-link swimmer was introduced in [5] in the perspective of approximating the motion of several living micro-organisms, an interesting extension of this model is to generalize the simulations to greater values of N. Of course, comparing the candidate for the optimal motion strategy with the one used by real micro-organisms could be a more tricky issue. On the other hand, another interesting direction is to study formally the existence of the periodic solution for the optimal problem.

Deuxième partie

Les effets du bord sur la contrôlabilité de micro-nageurs

Chapitre 3

Enhanced controllability of low Reynolds number swimmers in the presence of a wall

---

This work is done in collaboration with F. Alouges. It was published in *Acta Applicandae Mathematicae* (see [11]). Swimming, i.e., being able to advance in the absence of external forces by performing cyclic shape changes, is particularly demanding at low Reynolds numbers which is the regime of interest for micro-organisms and micro-robots. We focus on self-propelled stokesian robots composed of assemblies of balls and we prove that the presence of a wall has an effect on their motility. To rest on what has been done in [7] for such systems swimming on $\mathbf{R}^3$, we demonstrate that a controllable swimmer remains controllable in a half space whereas the reachable set of a non fully controllable one is increased by the presence of a wall.

3.1 Introduction

Swimming at low Reynolds number is now a well established topic of research which probably dates back to the pioneering work of Taylor [84] who explains how a micro-organism can swim without inertia. Later on, Purcell [70] formalized the so-called "scallop theorem" which states that, due to the reversibility of the viscous flow, a reciprocal deformation of the body cannot lead to a displacement of the swimmer. However, this obstruction can be circumvented using many swimming strategies [70]. Swimmers can be distinguished with respect to their ability to change their shape or to impose rotational motions of some parts of their body in order to create viscous friction forces on the fluid, and produce by reaction, the propulsion.

Many applications are concerned by this problem as for example, the conception of medical micro devices. The book by J.P. Sauvage [76] presents a lot of engine models adapted for tiny devices while the design and fabrication of such engines have been recently investigated by e.g. B. Watson, J. Friend, and L. Yeo [88]. As an example, let us quote the toroidal swimmer, first introduced by Purcell [70] and which has been subsequently improved by A.M Leshansky and O. Kenneth [57], Y. Or and M. Murray [68], A. Najafi and R. Zargar [67] among others.

The strategy for swimming consists in a cyclic deformation of body with a non-reciprocal motion. The first swimmer prototype belonging to this class is the three link swimmer also designed by Purcell [70]. More recently, R. Golestanian and A. Ajdari [47] introduced the Three-sphere swimmer which is geometrically simpler and allows for exact calculations of motion and speed [8], or even explicit in some asymptotic regimes [47]. Numerical approaches may also be used as in [6].

In the continuation of [8], F. Alouges, A. DeSimone, L. Heltai, A. Lefebvre, and B. Merlet [7] showed that the trajectory of the Three-sphere swimmer is governed by a differential equation whose control functions correspond to the rate of changing shape. The swimming capability of the device now is recast in terms of a control problem to which classical results apply [10].

Of particular importance for applications is the issue of the influence of any boundary on the effective swimming capabilities of micro-devices or real micro-swimmers. Indeed, boundaries clearly affect the hydrodynamics (see [24]) and may have an influence on the swimmer's capabilities. In that direction, a biological study of Rothschild [74] claimed for instance that spermatozoids tend to accumulate on walls. More recently, H. Winet, G. S. Bernstein, and J. Head [91] proved this related boundary effect for the sperm of humans which evolves in a narrow channel. Swimming in a geometrically confined environment has then become a subject of major interest, in particular to model this attraction phenomenon (see [81], [38],[17]). D. J Smith, E. A. Gaffney and J. R. Blake [82] have described the motion of a stylized bacterium propelled by a single flagellum and they show that the attraction by the wall is effective. Later, H. Shum, E.A Gaffney, and J. Smith [80] investigated to which extent this attraction effect is impacted by a change in swimmer's morphology.

On a more theoretical side, other approaches provide results that show an attraction effect by the wall. A. P. Berke and P. Allison [17], modelling the swimmer with a simple dipole, put in evidence an attraction due to the presence of the wall. Y. Or and M. Murray [68] derived the swimmer dynamics near a wall for three various swimmers, but with unvarying shapes.

The case of a changing shape swimmer has been studied by R. Zargar and A. Najafi [97], where the dynamics of the Three-sphere swimmer in the presence of a wall is given. However, some fundamental symmetry are not satisfied in their swimmer's motion equation.

The aim of this paper is to attack the same problem, namely, the influence of a plane wall on the swimmer's capabilities of motion, by means of control theory. Several recent works present a controllability results for a self-propelled micro-swimmers in a space without

boundary, as example, let us quote the review paper [9] or the paper by J. Lohéac, J. F. Scheid and M. Tucsnak [60] and the study of J. Lohéac and A. Munnier [59] made of the spherical swimmer in the whole space (see also [28] for the same kind of results in a perfect fluid). Furthermore, F. Alouges, A. DeSimone, L. Heltai, A. Lefebvre, and B. Merlet [7] treated with the controllability on $\mathbf{R}^3$ for the Three-sphere swimmer and others specific swimmers. The question that we want to address now is whether the presence of the plane wall modifies the controllability results. We here prove two results in that direction. Namely, considering the fully controllable Four sphere swimmer proposed in [7], we show that in the half space, the swimmer remains fully controllable, while a Three-sphere swimmer enriches its reachable set, at least generically which seems at first sight contradictory with earlier results. Indeed, although previous works show an attraction from the boundary, the set of reachable points could be of higher dimension. In other words, if the dynamics is somehow more constrained due to the presence of the wall, the set of points that the swimmer may reach could be larger than what it was without the wall.

The paper is organized as follows. In Section 3.2, we describe the two model swimmers to which our analytical and numerical tools are later applied. Section 3.2.3 presents the main controllability results associated with the introduced swimmers. In Section 3.3, we show that swimming is indeed an affine control problem without drift by using a similar approach than [10, 7].

The controllability result is proved in Section 3.4 for the Four-sphere swimmer and in Section 3.5 for the Three-sphere swimmer. Concluding remarks are given in Section 3.6.

3.2 Notation and main results

We carry on the study of specific swimmers that were considered in [7] in $\mathbf{R}^3$. In order to fix notation, the wall is modeled by the plane $W = \{(x, y, z) \in \mathbb{R}^3 \text{ s. t. } y = 0\}$, and the swimmers, which consist of N spheres $(B_i)_{i=1..N}$ of radii a connected by thin jacks, are assumed to move in the half space $\mathbf{R}^3_+ = \{(x, y, z) \in \mathbf{R}^3 \text{ s. t. } y > 0\}$. As in [7] , the viscous resistance associated with the jacks is neglected and the fluid is thus assumed to fill the whole set $\mathbf{R}^3_+ \setminus \cup_{i=1}^N B_i$. The state of the swimmer is described by two sets of variables :

- the shape variables, denoted by $\boldsymbol{\xi}$ (here in $\mathbf{R}^{N-1}$ or $\mathbf{R}^N$), which define the lengths of the jacks. A stroke consists in changing the lengths of these jacks in a periodic manner;
- the position variables, denoted by $\mathbf{p} \in \mathbf{R}^3_+ \times SO(3)$, which define swimmer's position and orientation in the half-space.

In what follows, we call $\mathcal{S} \subset \mathbf{R}^M$ for a suitable $M \in \mathbf{N}$ the set of admissible states $(\boldsymbol{\xi}, \mathbf{p})$ that we assume to be a connected nonempty smooth submanifold of $\mathbf{R}^M$. We thereafter focus on two swimmers that have been considered in the literature, the Three-sphere swimmer (see [66], [8], [7]) and the Four sphere swimmer (see [7]). It turns out that this latter is easier to understand than the former, and we therefore start with it.

3.2.1 The Four-sphere swimmer

We consider a regular tetrahedron $(\mathbf{S}_1, \mathbf{S}_2, \mathbf{S}_3, \mathbf{S}_4)$ with center $\mathbf{O} \in \mathbf{R}^3_+$. The swimmer consists of four balls linked by four arms of fixed directions $\vec{\mathbf{OS}}_i$ which are able to elongate and shrink (in a referential associated to the swimmer). The four ball cluster is completely described by the list of parameters $(\boldsymbol{\xi}, \mathbf{p}) = (\xi_1, \ldots, \xi_4, \mathbf{c}, \boldsymbol{\mathcal{R}}) \in \mathcal{S} = (\sqrt{\frac{3}{2}}a, \infty)^4 \times \mathbf{R}^3_+ \times SO(3)$. It is known (see [7]) that the Four sphere swimmer is controllable in $\mathbf{R}^3$. This means that it is able to move to any point and with any orientation under the constraint of being self-propelled, and when the surrounding flow is dominated by the viscosity. This swimmer is depicted in Fig. 4.1.

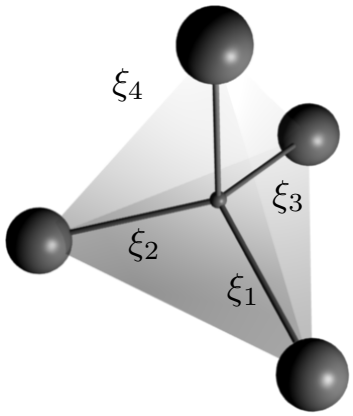

Figure 3.1: The Four-sphere swimmer.

3.2.2 The Three-sphere swimmer

This swimmer is composed of three aligned spheres as shown in Fig. 3.2. We assume that at $t = 0$ the swimmer starts in the vertical half-plane $H = \{(x, y, 0) \in \mathbf{R}^3 \text{ s.t. } y \geq 0\}$, it is clear from the symmetry of the problem that the swimmer stays in H for all time, for whatever deformation of its arms it may carry out. We characterize swimmer's position and orientation in H by the coordinates $(\mathbf{c}, \theta) \in \mathbf{R}^2 \times [0, 2\pi]$, where $\mathbf{c} \in H$ is the position of one of the three spheres, and θ is the angle between the swimmer and the $x-$axis. Therefore, in that case, the swimmer is completely described by the vector $(\boldsymbol{\xi}, \mathbf{p}) = (\xi_1, \xi_2, \mathbf{c}, \theta) \in \mathcal{S} = (2a, \infty)^2 \times H \times [0, 2\pi) \subset (2a, \infty)^2 \times \mathbf{R}^2 \times \mathbf{R}/2\pi\mathbf{Z}$. In the three dimensional space $\mathbf{R}^3$ (when there is no boundary), it is obvious by symmetry that the angle θ cannot change in time, and thus this swimmer is not fully controllable. One of the main contributions of this paper is to understand the modifications of this behavior due to the presence of the plane wall.

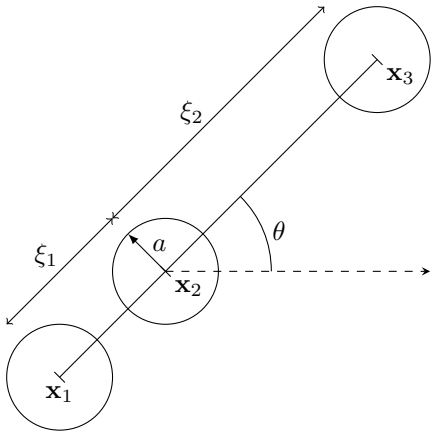

Figure 3.2: The Three-sphere swimmer.

3.2.3 Main results

Consider any of the swimmers described above, and assume it is self-propelled in a three dimensional half space viscous flow modeled by Stokes equations. In this paper, we establish that both swimmers are locally fully controllable almost everywhere in $\mathcal{S}$. By this we mean the precise following statements.

Theorem 3.2.1 *Consider the Four-sphere swimmer described in Section 3.2.2, and assume it is self-propelled in a three dimensional viscous flow modeled by Stokes equations in the half space $\mathbf{R}^3_+$. Then for almost any initial configuration $(\boldsymbol{\xi}^i, \mathbf{p}^i) \in \mathcal{S}$, any final configuration $(\boldsymbol{\xi}^f, \mathbf{p}^f)$ in a suitable neighborhood of $(\boldsymbol{\xi}^i, \mathbf{p}^i)$ and any final time $T > 0$, there exists a stroke $\boldsymbol{\xi} \in \mathcal{W}^{1,\infty}([0,T])$, satisfying $\boldsymbol{\xi}(0) = \boldsymbol{\xi}^i$ and $\boldsymbol{\xi}(T) = \boldsymbol{\xi}^f$ and such that if the self-propelled swimmer starts in position $\mathbf{p}^i$ with the shape $\boldsymbol{\xi}^i$ at time $t = 0$, it ends at position $\mathbf{p}^f$ and shape $\boldsymbol{\xi}^f$ at time $t = T$ by changing its shape along $\boldsymbol{\xi}(t)$.*

Theorem 3.2.2 *Consider the Three-sphere swimmer described in Section 3.2.1, and assume it is self-propelled in a three dimensional viscous flow modeled by Stokes equations in the half space $\mathbf{R}^3_+$. Then for almost any initial configuration $(\boldsymbol{\xi}^i, \mathbf{p}^i) \in \mathcal{S}$ such that $\mathbf{p}^i \in H$, any final configuration $(\boldsymbol{\xi}^f, \mathbf{p}^f)$ in a suitable neighborhood of $(\boldsymbol{\xi}^i, \mathbf{p}^i)$ with $\mathbf{p}^f \in H$ and any final time $T > 0$, there exists a stroke $\boldsymbol{\xi} \in \mathcal{W}^{1,\infty}([0,T])$, satisfying $\boldsymbol{\xi}(0) = \boldsymbol{\xi}^i$ and $\boldsymbol{\xi}(T) = \boldsymbol{\xi}^f$ and such that if the self-propelled swimmer starts in position $\mathbf{p}^i$ with the shape $\boldsymbol{\xi}^i$ at time $t = 0$, it ends at position $\mathbf{p}^f$ and shape $\boldsymbol{\xi}^f$ at time $t = T$ by changing its shape along $\boldsymbol{\xi}(t)$ and staying in H for all time $t \in [0,T]$.*

Remark 3.2.3 *The sense of "almost every initial configuration" can be further precised as everywhere outside a (possibly empty) analytic manifold of codimension 1.*

The proof of the controllability of the Four-sphere swimmer is given in Section 3.4 whereas Section 3.5 is devoted to demonstrate Theorem 3.2.2.

3.3 Mathematical setting of the problem

As for their 3D counterparts, the equation of motion of both swimmers take the form of an affine control problem without drift. In this section, we detail the derivation of this system.

3.3.1 Modelization of the fluid

The flow takes place at low Reynolds number and we assume that inertia of both the swimmer and the fluid is negligible. As a consequence, denoting by $\Omega = \cup_{i=1}^N B_i$ the space occupied by the swimmer, the flow in $\mathbf{R}^3_+ \setminus \Omega$ satisfies the (static) Stokes equation

$$\left\{\begin{array}{l} -\mu\Delta\mathbf{u} + \nabla p = 0 \text{ in } \mathbf{R}^3_+ \setminus \Omega, \\ \text{div } \mathbf{u} = 0 \text{ in } \mathbf{R}^3_+ \setminus \Omega, \\ -\boldsymbol{\sigma}\mathbf{n} = \mathbf{f} \text{ on } \partial\Omega, \\ \mathbf{u} = 0 \text{ on } \partial\mathbf{R}^3_+, \\ \mathbf{u} \to 0 \text{ at } \infty. \end{array}\right. \tag{3.1}$$

Here, we have denoted by $\boldsymbol{\sigma} = \mu(\nabla\mathbf{u} + \nabla^t\mathbf{u}) - p\mathbf{Id}$ the Cauchy stress tensor, $\mathbf{n}$ is the unit normal to $\partial\Omega$ pointing outward to the swimmer. We also set

$$\mathcal{V} = \left\{ \mathbf{u} \in \mathcal{D}'(\mathbf{R}^3_+ \setminus \Omega, \mathbf{R}^3) \,|\, \nabla\mathbf{u} \in L^2(\mathbf{R}^3_+ \setminus \Omega),\ \frac{\mathbf{u}(\mathbf{r})}{\sqrt{1+|\mathbf{r}|^2}} \in L^2(\mathbf{R}^3_+ \setminus \Omega) \right\}.$$

It is well known that $\mathcal{V}$ is a Hilbert space when endowed with the norm (and the associated scalar product)

$$\|\mathbf{u}\|_{\mathcal{V}}^2 := \int_{\mathbf{R}^3_+\setminus\Omega} |\nabla \mathbf{u}|^2 .$$

We also assume that $\mathbf{f} \in H^{-1/2}(\partial\Omega)$ in order to obtain a unique solution $(\mathbf{u}, p)$ to the problem (3.1) in $\mathcal{V} \times L^2(\mathbf{R}^3_+ \setminus \Omega)$ which can be expressed in terms of the associated Green's function (obtained by the method of "images", see [20]) as

$$\mathbf{u}(\mathbf{r}) = \int_{\partial\Omega} \mathbf{K}(\mathbf{r}, \mathbf{s})\mathbf{f}(\mathbf{s})d\mathbf{s}, \tag{3.2}$$

where the matricial Green function $\mathbf{K} = (K_{ij})_{i,j=1,2,3}$ is given by

$$\mathbf{K}(\mathbf{r}, \mathbf{r}_0) = \mathbf{G}(\mathbf{r} - \mathbf{r}_0) + \mathbf{K}_1(\mathbf{r}, \mathbf{r}_0) + \mathbf{K}_2(\mathbf{r}, \mathbf{r}_0) + \mathbf{K}_3(\mathbf{r}, \mathbf{r}_0) , \tag{3.3}$$

the four functions $\mathbf{G}$, $\mathbf{K}_1$, $\mathbf{K}_2$ and $\mathbf{K}_3$ being respectively the Stokeslet

$$\mathbf{G}(\mathbf{r}) = \frac{1}{8\pi\mu}\left(\frac{\mathbf{Id}}{|\mathbf{r}|} + \frac{\mathbf{r}\otimes\mathbf{r}}{|\mathbf{r}|^3}\right) \tag{3.4}$$

and the three "images"

$$\mathbf{K}_1(\mathbf{r}, \mathbf{r}_0) = -\frac{1}{8\pi\mu}\left(\frac{\mathbf{Id}}{|\mathbf{r}'|} + \frac{\mathbf{r}'\otimes\mathbf{r}'}{|\mathbf{r}'|^3}\right) , \tag{3.5}$$

$$K_{2,ij}(\mathbf{r}, \mathbf{r}_0) = \frac{1}{4\pi\mu} y_0^2 \,(1-\delta_{j2})\left(\frac{\delta_{ij}}{|\mathbf{r}'|^3} - \frac{3r'_i r'_j}{|\mathbf{r}'|^5}\right) , \tag{3.6}$$

$$K_{3,ij}(\mathbf{r}, \mathbf{r}_0) = -\frac{1}{4\pi\mu} y_0 \,(1-2\delta_{j2})\left(\frac{r'_2}{|\mathbf{r}'|^3}\delta_{ij} - \frac{r'_j}{|\mathbf{r}'|^3}\delta_{i2} + \frac{r'_i}{|\mathbf{r}'|^3}\delta_{j2} - \frac{3r'_i r'_j r'_2}{|\mathbf{r}'|^5}\right) . \tag{3.7}$$

Here $\mathbf{r}_0 = (x_0, y_0, z_0)$ and $\mathbf{r}' = \mathbf{r} - \tilde{\mathbf{r}}_0$, where $\tilde{\mathbf{r}}_0 = (x_0, -y_0, z_0)$ stands for the "image" of $\mathbf{r}_0$, that is to say, the point symmetric to $\mathbf{r}_0$ with respect to the wall.

Let B be the sphere of radius 1 centered at the origin. We identify the boundary of the domain occupied by the swimmer, $\partial\Omega$, with $(\partial B)^N$ and we represent by $\mathbf{f}_i \in H^{-1/2}(\partial B)$ the distribution of force on the sphere B_i. Correspondingly, $\mathbf{u}_i \in H^{1/2}(\partial B)$ stands for the velocity distribution on the sphere B_i (and of the fluid due to non-slip contact).

Following [7], we denote by $\mathcal{T}_{(\boldsymbol{\xi},\mathbf{p})}$ the Neumann-to-Dirichlet map

$$\begin{array}{rccc} \mathcal{T}_{(\boldsymbol{\xi},\mathbf{p})} : & \mathcal{H}^{-1/2} & \to & \mathcal{H}^{1/2} \\ & (\mathbf{f}_1, \ldots, \mathbf{f}_N) & \mapsto & (\mathbf{u}_1, \ldots, \mathbf{u}_N) \end{array} \tag{3.8}$$

where we have denoted by $\mathcal{H}^{\pm 1/2}$ the space $(H^{\pm 1/2}(\partial B))^N$. It is well known that the map $\mathcal{T}_{(\boldsymbol{\xi},\mathbf{p})}$ is a one to one mapping onto while its inverse is continuous.

Using (3.2), we can express $\mathbf{u}_i$ $(i = 1, \cdots, N)$ by

$$\begin{array}{rcl} \forall \mathbf{r} \in \partial B, \quad \mathbf{u}_i(\mathbf{r}) & = & \displaystyle\sum_{j=1}^{N} \int_{\partial B} \mathbf{K}(\mathbf{x}_i + a\mathbf{r}, \mathbf{x}_j + a\mathbf{s})\mathbf{f}_j(\mathbf{s})d\mathbf{s} \\ & := & \displaystyle\sum_{j=1}^{N} \langle \mathbf{f}_j, \mathbf{K}(\mathbf{x}_i + a\mathbf{r}, \mathbf{x}_j + a\,\cdot)\rangle_{\partial B} , \end{array} \tag{3.9}$$

where $\langle \cdot, \cdot \rangle_{\partial B}$ stands for the duality $\big(H^{-1/2}(\partial B), H^{1/2}(\partial B)\big)$.

Proposition 3.3.1 *The mapping $(\boldsymbol{\xi}, \mathbf{p}) \mapsto \mathcal{T}_{(\boldsymbol{\xi},\mathbf{p})}$ is analytic from $\mathcal{S}$ into $\mathcal{L}(\mathcal{H}^{-1/2}, \mathcal{H}^{1/2})$. Furthermore, $\mathcal{T}_{(\boldsymbol{\xi},\mathbf{p})}$ is an isomorphism for every $(\boldsymbol{\xi}, \mathbf{p}) \in \mathcal{S}$, and the mapping $(\boldsymbol{\xi}, \mathbf{p}) \mapsto \mathcal{T}^{-1}_{(\boldsymbol{\xi},\mathbf{p})}$ is also analytic.*

Proof. The proof is identical to the one given in [7], replacing the the Stokeslet by the Green kernel $\mathbf{K}$ which is also analytic outside its singularity.

Remark 3.3.2 *As the direct consequence, the mapping $\mathcal{T}_{(\boldsymbol{\xi},\mathbf{p})}$ and its inverse depend analytically on a.*

3.3.2 Equation of motion

In this section, we use the self-propulsion assumption in order to express the dynamics of the swimmer as an affine control system without drift.

This equation of motion is by now classical in this context (see [7], [8], [32], [59] or [64]). Let us recall the principle of its derivation.

We define the map Φ_i which give the position of the current point of the i-th sphere of the swimmer in the state $(\boldsymbol{\xi}, \mathbf{p}) \in \mathcal{S}$

$$\Phi_i : \quad \partial B_i \times \mathcal{S} \quad \to \quad \mathbf{R}^3 . \tag{3.10}$$

The non-slip boundary condition of the fluid on ∂B_i imposes that the velocity of the fluid is given by

$$\frac{d}{dt}\Phi_i(\mathbf{r}, \boldsymbol{\xi}, \mathbf{p}) = \left(\dot{\boldsymbol{\xi}} \cdot \nabla_{\boldsymbol{\xi}}\right) \Phi_i(\mathbf{r}, \boldsymbol{\xi}, \mathbf{p}) + \left(\dot{\mathbf{p}} \cdot \nabla_{\mathbf{p}}\right) \Phi_i(\mathbf{r}, \boldsymbol{\xi}, \mathbf{p}) . \tag{3.11}$$

When inertia is negligible, self-propulsion of the swimmer implies that the total viscous force and torque exerted by the surrounding fluid on the swimmer vanish i.e.,

$$\left\{ \begin{array}{ll} \displaystyle\sum_{i=1}^{N} \int_{\partial B} \mathcal{T}^{-1}_{(\mathbf{p},\boldsymbol{\xi})} \left(\frac{d}{dt}\Phi_1(\mathbf{r}, \boldsymbol{\xi}, \mathbf{p}), \cdots, \frac{d}{dt}\Phi_N(\mathbf{r}, \boldsymbol{\xi}, \mathbf{p}) \right) d\mathbf{x}_t & = 0 , \\ \displaystyle\sum_{i=1}^{N} \int_{\partial \Omega_t} \mathbf{x}_t \times \mathcal{T}^{-1}_{(\mathbf{p},\boldsymbol{\xi})} \left(\frac{d}{dt}\Phi_1(\mathbf{r}, \boldsymbol{\xi}, \mathbf{p}), \cdots, \frac{d}{dt}\Phi_N(\mathbf{r}, \boldsymbol{\xi}, \mathbf{p}) \right) d\mathbf{x}_t & = 0 . \end{array} \right. \tag{3.12}$$

By using (3.11) and the linearity of the Dirichlet-to-Neumann map, the system (3.12) is a set of linear equations which link $\dot{\mathbf{p}}$ and $\dot{\boldsymbol{\xi}}$. The coefficients corresponding to the swimmer's position $\dot{\mathbf{p}}$ consist in an invertible linear map, known as a *grand-resistance-matrice* (see [59] or [24]).

By inverting it, this permit us to solve $\dot{\mathbf{p}}$ uniquely and linearly in terms of $\dot{\boldsymbol{\xi}}$,

$$\dot{\mathbf{p}} = \sum_{i=1}^{N} \mathbf{W}_i(\boldsymbol{\xi}, \mathbf{p}) \dot{\xi}_i . \tag{3.13}$$

Finally, by considering the vector fields $\mathbf{F}_i(\boldsymbol{\xi}, \mathbf{p}) := \begin{pmatrix} \mathbf{e}_i \\ \mathbf{W}_i(\boldsymbol{\xi}, \mathbf{p}) \end{pmatrix}$ defined on the tangent bundle of $\mathcal{S}$, (here $\mathbf{e}_i$ is the i-th vector of the canonical basis of $\mathbf{R}^N$), we get the differential system which governs both state and shape of the swimmer,

$$\frac{d}{dt} \begin{pmatrix} \boldsymbol{\xi} \\ \mathbf{p} \end{pmatrix} = \sum_{i=1}^{N} \mathbf{F}_i(\boldsymbol{\xi}, \mathbf{p}) \dot{\xi}_i . \tag{3.14}$$

3.3.3 Classical results in geometric control

Let us recall some results which are used to study the controllability of such systems of ODE (see for instance [51]).

Let F and G be two vector fields defined on a smooth finite dimensional manifold $\mathcal{M}$. The Lie bracket of F and G is the vector field defined at any point $X \in \mathcal{M}$ by $[F,G](X) := (F\cdot\nabla)\,G(X) - (G\cdot\nabla)\,F(X)$. For a family of vector fields $\mathcal{F}$ on $\mathcal{M}$, $Lie(\mathcal{F})$ denotes the Lie algebra generated by $\mathcal{F}$. Namely, this is the smallest algebra - defined by the Lie bracket operation - which contains $\mathcal{F}$ (therefore $\mathcal{F} \subset Lie(\mathcal{F})$ and for any two vectorfields $F \in Lie(\mathcal{F})$ and $G \in Lie(\mathcal{F})$, the Lie bracket $[F,G] \in Lie(\mathcal{F})$). Eventually, for any point $X \in \mathcal{M}$, $Lie_X(\mathcal{F})$ denotes the set of all tangent vectors $V(X)$ with V in $Lie(\mathcal{F})$. It follows that $Lie_X(\mathcal{F})$ is a linear subspace of $T_X\mathcal{M}$ and is hence finite-dimensional.

Lie brackets and Lie algebras play a prominent role in finite dimensional control theory. Indeed, we recall Chow's theorem:

Theorem 3.3.3 (Chow [29]) *Let $\mathcal{M}$ be a connected nonempty manifold. Let us assume that $\mathcal{F} = (F_i)_{i=1}^m$, a family of vector fields on $\mathcal{M}$, is such that $F_i \in C^\infty(\mathcal{M}, T\mathcal{M}), \forall i \in \{1,\cdots,m\}$.*
Let us also assume that

$$Lie_X(\mathcal{F}) = T_X(\mathcal{M})\,,\ \forall X \in \mathcal{M}\,.$$

Then, for every $(X^0,X^1) \in \mathcal{M}\times\mathcal{M}$, and for every $T>0$, there exists $u \in L^\infty([0,T];\mathbf{R}^m)$ such that the solution of the Cauchy problem,

$$\left\{\begin{array}{l} \dot{X} = \displaystyle\sum_{i=1}^m u_i F_i(X)\,, \\ X(0) = X^0\,, \end{array}\right. \tag{3.15}$$

is defined on $[0,T]$ and satisfies $X(T) = X^1$.

The theorem 3.3.3 is a global controllability result, we also recall the one which gives a small-time local controllability.

Theorem 3.3.4 ([29], p. 135) *Let Ω be an nonempty open subset of $\mathbf{R}^n$, and let $\mathcal{F} = (F_i)_{i=1}^m$, a family of vectorfields, such that $F_i \in C^\infty(\Omega,\mathbf{R}^n), \forall i \in \{1,\cdots,m\}$.*
Let X_e such that

$$Lie_{X_e}(\mathcal{F}) = \mathbf{R}^n\,.$$

Then, for every $\epsilon>0$, there exists a real number $\eta>0$ such that, for every $(X^0,X^1) \in \{X\ s.\ t.\ \|X-X_e\|<\eta\}^2$, there exists a bounded measurable function $u:[0,\epsilon]\to\mathbf{R}^n$ such that the solution of the Cauchy problem

$$\left\{\begin{array}{l} \dot{X} = \displaystyle\sum_{i=1}^m u_i F_i(X)\,, \\ X(0) = X^0\,, \end{array}\right. \tag{3.16}$$

is defined on $[0,\epsilon]$ and satisfies $X(\epsilon) = X^1$.

When the vector fields are furthermore analytic (and the manifold $\mathcal{M}$ is also analytic) one also has the Hermann-Nagano Theorem of which we will make an important use in the theoretical study of the controllability for our model swimmers.

Theorem 3.3.5 (Hermann-Nagano [51]) *Let $\mathcal{M}$ be an analytic manifold, and $\mathcal{F}$ a family of analytic vectorfields on $\mathcal{M}$. Then*

1. *each orbit of $\mathcal{F}$ is an analytic submanifold of $\mathcal{M}$, and*

2. *if $\mathcal{N}$ is an orbit of $\mathcal{F}$, then the tangent space of $\mathcal{N}$ at X is given by $Lie_X(\mathcal{F})$. In particular, the dimension of $Lie_X(\mathcal{F})$ is constant as X varies over $\mathcal{N}$.*

In our context, the family of vector fields is given by $\mathcal{F} = (\mathbf{F}_i)_{1\leq i\leq k}$ which are defined on the manifold $\mathcal{M} = \mathcal{S}$, and the controls u_i are given by the rate of shape changes $\dot{\xi}_i$. In view of the preceding theorems, the controllability question of our model swimmers raised by Theorems 3.2.1 and 3.2.2 relies on the dimension of the Lie algebra generated by the vectorfields $(\mathbf{F}_i)_{1\leq i\leq k}$ which define the dynamics of the swimmer. In particular they are direct consequences of the following Lemma.

Lemma 3.3.6 *For almost every point (in the sense of remark 3.2.3) $(\boldsymbol{\xi}, \mathbf{p}) \in \mathcal{S}$, the Lie algebra generated by the vectorfields $(\mathbf{F}_i)_{1\leq i\leq k}$ at $(\boldsymbol{\xi}, \mathbf{p})$ is equal to $T_{(\boldsymbol{\xi},\mathbf{p})}\mathcal{S}$.*

The proof of this lemma is developed until the rest of the paper. Several tools are used in order to characterize this dimension among which we mainly use asymptotic behavior and symbolic computations. As we shall see, although the theory is clear, the explicit computation (or at least asymptotic expressions) is by no means obvious and requires a lot of care. In particular, before using symbolic calculations, a rigorous proof of the expansion, together with a careful control of the remainders in the expressions allowed us to go further.

3.4 The Four-sphere swimmer

In this section, we give the proof of the controllability result stated in Theorem 3.2.1.
Proof. The argument of the proof is based on the fact that $\mathbf{K}$ given by (4.13) satisfies

$$\mathbf{K}(\mathbf{r}, \mathbf{r}') = \mathbf{G}(\mathbf{r} - \mathbf{r}') + O\left(\frac{1}{y}\right), \tag{3.17}$$

where $\mathbf{r} = (x, y, z)$ and $\mathbf{r}' = (x', y', z')$ are two points of $\mathbf{R}^3_+$, and $\mathbf{G}$ is the Green function of the Stokes problem in the whole space $\mathbf{R}^3$, namely the Stokeslet, defined by (4.14).

As a consequence, we obtain that the Neumann to Dirichlet map given by (3.8) satisfies for a swimmer of shape $\boldsymbol{\xi}$ at position $\mathbf{p} = (p_x, p_y, p_z, \mathcal{R}) \in \mathbf{R}^3_+ \times SO_3$

$$\mathcal{T}_{(\boldsymbol{\xi},\mathbf{p})} = \mathcal{T}^0_{\boldsymbol{\xi}} + O\left(\frac{1}{p_y}\right), \tag{3.18}$$

where $\mathcal{T}^0_{\boldsymbol{\xi}}$ is the Neumann-to-Dirichlet map associated to the Green function $\mathbf{G}$.

The system (3.12) now reads

$$\begin{cases} \displaystyle\int_{\partial\Omega_t} \left(\left(\mathcal{T}^0_{\boldsymbol{\xi}}\right)^{-1} + O\left(\frac{1}{p_y}\right)\right)\left(\frac{d}{dt}\Phi_1(\mathbf{r}, \boldsymbol{\xi}, \mathbf{p}), \cdots, \frac{d}{dt}\Phi_N(\mathbf{r}, \boldsymbol{\xi}, \mathbf{p})\right) d\mathbf{x}_t & = 0\,, \\ \displaystyle\int_{\partial\Omega_t} \mathbf{x}_t \times \left(\left(\mathcal{T}^0_{\boldsymbol{\xi}}\right)^{-1} + O\left(\frac{1}{p_y}\right)\right)\left(\frac{d}{dt}\Phi_1(\mathbf{r}, \boldsymbol{\xi}, \mathbf{p}), \cdots, \frac{d}{dt}\Phi_N(\mathbf{r}, \boldsymbol{\xi}, \mathbf{p})\right) d\mathbf{x}_t & = 0\,. \end{cases}$$

Consequently, the ODE (3.14) becomes

$$\frac{d}{dt}\begin{pmatrix} \boldsymbol{\xi} \\ \mathbf{p} \end{pmatrix} = \sum_{i=1}^{4}\left(\mathbf{F}^0_i(\boldsymbol{\xi}) + O\left(\frac{1}{p_y}\right)\right)\dot{\xi}_i\,, \tag{3.19}$$

where $(\mathbf{F}^0_i)_{i=1,\cdots,4}$ are the vector fields obtained in the case of the whole space $\mathbf{R}^3$.

In other words, we obtain the convergence

$$\mathbf{F}(\boldsymbol{\xi}, \mathbf{p}) = \mathbf{F}^0(\boldsymbol{\xi}) + O\left(\frac{1}{p_y}\right) \text{ as } p_y \to +\infty \tag{3.20}$$

and also for all its derivatives to any order.

It has been proved in [7] that dim $Lie_{\boldsymbol{\xi}}(\mathbf{F}^0) = 10$ at all admissible shape $\boldsymbol{\xi}$, showing the global controllability in the whole space of the underlying swimmer. We thus obtain that for p_y sufficiently large

$$\dim\, Lie_{(\boldsymbol{\xi},\mathbf{p})}(\mathbf{F}) = 10\,, \tag{3.21}$$

and therefore due to the analyticity of the vector fields $(\mathbf{F}_i)_{i=1,\cdots,4}$, (3.21) holds in a dense subset of $\mathcal{S}$. This shows that the system satisfies the full rank condition almost everywhere in $\mathcal{S}$ and proves Lemma 3.3.6 in this context, and thus Theorem 3.2.1 by a simple application of Chow's theorem.

The preceding proof can be generalized to any swimmer for which the Lie algebra satisfies the full rank condition in $\mathbf{R}^3$. We now turn to an example for which this is not the case, namely the Three-sphere swimmer of Najafi Golestanian [66]. Indeed, when there is no boundary, this swimmer is constrained to move along its axis of symmetry. The purpose of the next section is to understand to which extent this is still the case when there is a flat boundary.

3.5 The Three-sphere swimmer

This section details the proof of Theorem 3.2.2 which is much more involved. It is organized in several subsections, and each of them focus on a particular step. In Section 3.5.1, we recall the expression of the equation of motion of the Three-sphere swimmer. Section 3.5.2 deals with the special symmetries which need to be verified by the vector fields of the motion equation. From this symmetry properties, we deduce the reachable set of the particular case where the swimmer is perpendicular to the wall. In Section 3.5.3, we give an expansion of the Neumann-To-Dirichlet map associated to the Three-sphere swimmer and its inverse, in the case where the radius of the sphere a is small enough and the lengths of the arms sufficiently large. In Section 4.5.2, we deduce from this previous approximation an expansion of the motion equation, for a small. Finally, the Section 3.5.5 presents some formal calculations of the vectorfields of the motion equation and their Lie brackets which lead to the dimension of its Lie algebra almost everywhere.

3.5.1 Equation of motion for the Three-sphere swimmer

From Section 3.2.2, we know that the swimmer's position is parameterized by the vector (x, y, θ) where (x, y) is the coordinate of the center of B_2 as depicted in Fig. 3.2 and θ is the angle between the swimmer and the $x-$axis. We recall that $\boldsymbol{\xi} := (\xi_1, \xi_2)$ stands for the lengths of both arms of the swimmer.

The motion equation (3.14) thus reads,

$$\frac{d}{dt}\begin{pmatrix} \xi_1 \\ \xi_2 \\ x \\ y \\ \theta \end{pmatrix} = \mathbf{F}_1(\boldsymbol{\xi}, x, y, \theta)\dot{\xi}_1 + \mathbf{F}_2(\boldsymbol{\xi}, x, y, \theta)\dot{\xi}_2\,. \tag{3.22}$$

Notice that, from translational invariance of the problem, both $\mathbf{F}_1$ and $\mathbf{F}_2$ actually do not depend on x.

In what follows, we denote by

$$d_{(\boldsymbol{\xi},y,\theta)} = \dim\, Lie_{(\boldsymbol{\xi},y,\theta)}(\mathbf{F}_1, \mathbf{F}_2)$$

the dimension of the Lie algebra $Lie_{(\boldsymbol{\xi},y,\theta)}(\mathbf{F}_1, \mathbf{F}_2) \subset \mathbb{R}^5$ at $(\boldsymbol{\xi}, y, \theta)$. It is clear, since $\mathbf{F}_1$ and $\mathbf{F}_2$ are independent one to another and never vanish, that

$$2 \leqslant d_{(\boldsymbol{\xi},y,\theta)} \leqslant 5\,. \tag{3.23}$$

3.5.2 Symmetry properties of the vector fields

Proposition 3.5.1 *Let* $\mathbf{S}$ *be the* 5×5 *matrix defined by*

$$\mathbf{S} = \begin{pmatrix} 0 & 1 & 0 & 0 & 0 \\ 1 & 0 & 0 & 0 & 0 \\ 0 & 0 & -1 & 0 & 0 \\ 0 & 0 & 0 & 1 & 0 \\ 0 & 0 & 0 & 0 & -1 \end{pmatrix}.$$

Then one has for all $\boldsymbol{\xi} = (\xi_1, \xi_2, x, y, \theta) \in \mathcal{S}$

$$\mathbf{F}_1(\xi_1, \xi_2, y, \theta) = \mathbf{S}\mathbf{F}_2(\xi_2, \xi_1, y, 2\pi - \theta) \tag{3.24}$$

and similarly for the Lie bracket

$$[\mathbf{F}_1, \mathbf{F}_2](\xi_1, \xi_2, y, \theta) = \mathbf{S}[\mathbf{F}_2, \mathbf{F}_1](\xi_2, \xi_1, y, 2\pi - \theta)\,. \tag{3.25}$$

Proof. Although the plane breaks the 3D axisymmetry along the swimmer's axis, we can still make use of the symmetry with respect to the vertical plane that passes through the center of the first sphere B_2. A swimmer with position (x, y, θ) and shape (ξ_1, ξ_2) is transformed by this symmetry to one at position $(x, y, 2\pi - \theta)$ and shape (ξ_2, ξ_1) (see Fig. 3.3). Making use of the fact that corresponding solutions to Stokes equations are symmetric one to another, we easily get the proposition.

Eventually, one deduces the Lie bracket symmetries by applying the former symmetries on the vectorfields themselves. An easy recurrence shows that the same identities hold for any Lie bracket of any order of the vectorfields $\mathbf{F}_1$ and $\mathbf{F}_2$. In particular one has for instance

$$[\mathbf{F}_1, [\mathbf{F}_1, \mathbf{F}_2]](\xi_1, \xi_2, y, \theta) = \mathbf{S}[\mathbf{F}_2, [\mathbf{F}_2, \mathbf{F}_1]](\xi_2, \xi_1, y, 2\pi - \theta)\,. \tag{3.26}$$

As a direct consequence of proposition 3.5.1, we deduce that the fourth coordinate of the Lie bracket $[\mathbf{F}_1, \mathbf{F}_2]$ vanishes at $(\xi, \xi, y, 0)$ and at (ξ, ξ, y, π).

Proposition 3.5.2 *Let* $\mathbf{T}$ *be the* 5×5 *matrix defined by*

$$\mathbf{T} = \begin{pmatrix} 1 & 0 & 0 & 0 & 0 \\ 0 & 1 & 0 & 0 & 0 \\ 0 & 0 & -1 & 0 & 0 \\ 0 & 0 & 0 & 1 & 0 \\ 0 & 0 & 0 & 0 & -1 \end{pmatrix}.$$

Then one has for all $\boldsymbol{\xi} = (\xi_1, \xi_2, x, y, \theta) \in \mathcal{S}$*, and* $i = 1, 2$

$$\mathbf{F}_i(\xi_1, \xi_2, y, \theta) = \mathbf{T}\mathbf{F}_i(\xi_1, \xi_2, y, \pi - \theta) \tag{3.27}$$

and similarly for the Lie bracket

$$[\mathbf{F}_1, \mathbf{F}_2](\xi_1, \xi_2, y, \theta) = \mathbf{T}[\mathbf{F}_1, \mathbf{F}_2](\xi_1, \xi_2, y, \pi - \theta)\,. \tag{3.28}$$

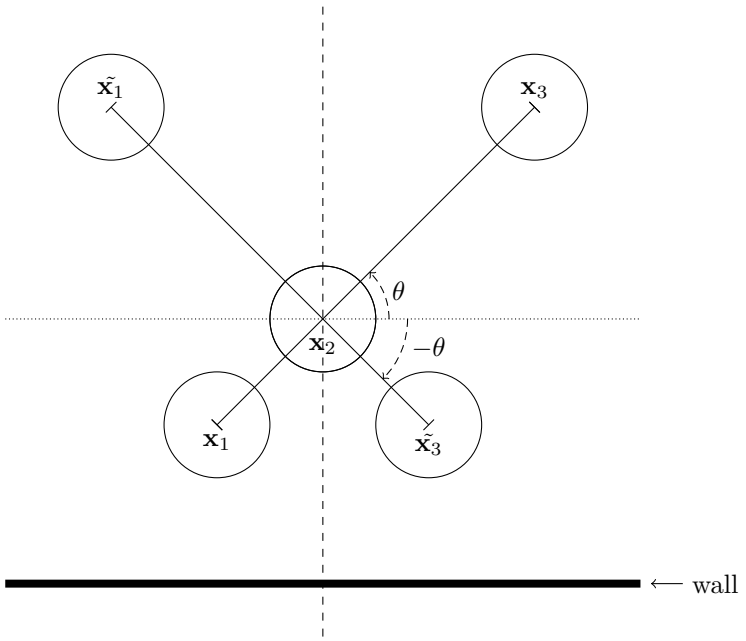

Figure 3.3: The plane symmetry which links the situation at $(\xi_1, \xi_2, x, y, \theta)$ with those at $(\xi_2, \xi_1, x, y, 2\pi - \theta)$. In both cases, solutions to Stokes flow are also symmetric one to another.

Proof. The two identities readily come from the symmetry which transforms a swimmer with position (x, y, θ) and a shape (ξ_1, ξ_2) to one at position $(x, y, \pi - \theta)$ with the same shape (see Fig. 3.4).

Eventually, one deduces the Lie bracket symmetries by applying the former symmetries on the vectorfields themselves. An easy recurrence shows that the same identities hold for any Lie bracket of any order of the vectorfields $\mathbf{F}_1$ and $\mathbf{F}_2$.

As a result, in the case where $\theta = \pm\frac{\pi}{2}$, we get the dimension of the Lie algebra of the vector field $\mathbf{F}_1$ and $\mathbf{F}_2$.

Corollary 3.5.3 *The dimension of the Lie algebra* $Lie_{(\xi_1,\xi_2,y,\pi/2)}(\mathbf{F}_1, \mathbf{F}_2)$ *is less than or equal to* 3.

Proof. We deduce from the preceding proposition that for $i = 1, 2$ and $j = 3, 5$, $\mathbf{F}_i^j(\xi_1, \xi_2, y, \pm\pi/2) = 0$. This simply means that a swimmer starting in the vertical position cannot change its angle θ and its abscissa x by changing the size of its arms. As a matter of fact, the same holds true for any Lie bracket of $\mathbf{F}_1$ and $\mathbf{F}_2$ at any order, and we can deduce from this that

$$d_{(\xi_1,\xi_2,y,\pi/2)} \leq 3\,,$$

since any vector of the Lie algebra $Lie_{(\xi_1,\xi_2,y,\pi/2)}(\mathbf{F}_1, \mathbf{F}_2)$ has a vanishing third and fifth component.

Moreover, by using the argument introduced in Section 3.4, we get, for almost every y, that the dimension of the Lie algebra is almost equal to the one without boundary (see [7]).

Remark 3.5.4 *By using Hermann-Nagano Theorem (see [51]), in the case where the swimmer is perpendicular to the wall, the set of states where the dimension of the Lie algebra*

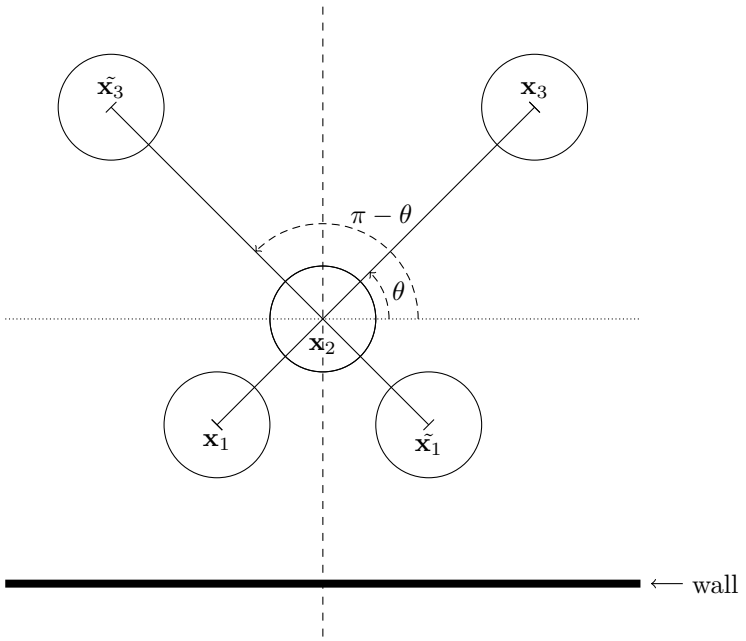

Figure 3.4: The plane symmetry which links the situation at $(\xi_1, \xi_2, x, y, \theta)$ with those at $(\xi_1, \xi_2, x, y, \pi - \theta)$. In both cases, solutions to Stokes flow are also symmetric one to another.

generated by $\mathbf{F}_1$ *and* $\mathbf{F}_2$ *is equal to two is an union of analytic submanifold of* $\mathcal{S}$ *of dimension two.*

Furthermore, the proof of the corollary 3.5.3 can be applied to all generic positions then, it implies that the dimension of the Lie algebra is at least equal to 3, almost everywhere, i.e.,

$$3 \leqslant d_{(\xi_1,\xi_2,y,\theta)} \leqslant 5\,.$$

3.5.3 Approximation for small spheres and large distances

For the general case ($\theta \neq \pi/2$), the preceding computation is not sufficient to conclude. In order to proceed, we make an expansion of the vectorfields and their Lie brackets with respect to a (the radius of the balls) near 0.

This part is devoted to the proof of the expansion of the Neumann to Dirichlet map (4.29) together with its inverse (4.30) at large arms' lengths. Let us first define for all $(i, j) \in \{1, 2, 3\}^2$, the linear map $\mathcal{T}_{i,j}$ as

$$\begin{aligned} \mathcal{T}_{i,j} : H^{-1/2}(\partial B) &\to H^{1/2}(\partial B) \\ \mathbf{f}_j &\mapsto \int_{\partial B} \mathbf{K}(\mathbf{x}_i + a\cdot, \mathbf{x}_j + a\mathbf{s})\, \mathbf{f}_j(\mathbf{s})\, \mathrm{d}\mathbf{s}\,. \end{aligned}$$

We recall that the Green kernel $\mathbf{K}$ writes (following (4.13)) as

$$\mathbf{K}(\mathbf{r}, \mathbf{r}') = \mathbf{G}(\mathbf{r} - \mathbf{r}') + \mathbf{K}_1(\mathbf{r}, \mathbf{r}') + \mathbf{K}_2(\mathbf{r}, \mathbf{r}') + \mathbf{K}_3(\mathbf{r}, \mathbf{r}')\,,$$

where $\mathbf{G}$ is the Stokeslet (see (4.14)) and each kernel is given by the corresponding counterpart in (4.13). Eventually, we call $\mathcal{T}^0$ the Neumann to Dirichlet map associated to $\mathbf{G}$

$$\begin{aligned}\mathcal{T}^0 : H^{-1/2}(\partial B) &\to H^{1/2}(\partial B)\\ \mathbf{f} &\mapsto \int_{\partial B} \mathbf{G}(a(\,\cdot - \mathbf{s}))\,\mathbf{f}(\mathbf{s})\,\mathrm{d}\mathbf{s}\,.\end{aligned}$$

Proposition 3.5.5 *Let $(i,j) \in \{1,2,3\}^2$. We have the following expansions, valid for $a \ll 1$:*

- *if $i \neq j$ then*
$$\mathcal{T}_{i,j} = \mathbf{K}(\mathbf{x}_i,\mathbf{x}_j)\langle \mathbf{f}_j, \mathbf{Id}\rangle_{\partial B} + \mathbf{R}_1 \tag{3.29}$$
where $||\mathbf{R}_1||_{\mathcal{L}(H^{-1/2},H^{1/2})} = O(a)$,
- *otherwise*
$$\mathcal{T}_{i,i} = \mathcal{T}^0 + \sum_{k=1}^{3} \mathbf{K}_k(\mathbf{x}_i,\mathbf{x}_i)\langle \mathbf{f}_i, \mathbf{Id}\rangle_{\partial B} + \mathbf{R}_2 \tag{3.30}$$
where $||\mathbf{R}_2||_{\mathcal{L}(H^{-1/2},H^{1/2})} = O(a)$.

Proof. Let $(i,j) \in \{1,2,3\}^2$ be such that $i \neq j$, and $\mathbf{f}_j \in H^{-1/2}(\partial B)$. We define

$$\forall \mathbf{r} \in \partial B\,,\ \mathbf{u}_i(\mathbf{r}) := (\mathcal{T}_{i,j}\mathbf{f}_j)(\mathbf{r}) = \int_{\partial B} \mathbf{K}(\mathbf{x}_i + a\mathbf{r}, \mathbf{x}_j + a\mathbf{s})\mathbf{f}_j(\mathbf{s})\mathrm{d}\mathbf{s}\,, \tag{3.31}$$

and

$$\mathbf{v}_i(\mathbf{r}) = \mathbf{u}_i(\mathbf{r}) - \mathbf{K}(\mathbf{x}_i,\mathbf{x}_j)\int_{\partial B} \mathbf{f}_j(\mathbf{s})\,d\mathbf{s} = \int_{\partial B} \left(\mathbf{K}(\mathbf{x}_i + a\mathbf{r}, \mathbf{x}_j + a\mathbf{s}) - \mathbf{K}(\mathbf{x}_i,\mathbf{x}_j)\right)\mathbf{f}_j(\mathbf{s})\mathrm{d}\mathbf{s}\,.$$

Our aim is to estimate the $H^{1/2}(\partial B)$ norm of $\mathbf{v}_i$. But[3]

$$\|\mathbf{v}_i\|_{H^{1/2}(\partial B)} \leq \|\mathbf{v}_i\|_{H^1(B)},$$

and since $\mathbf{K}(\mathbf{x},\mathbf{y})$ is a smooth function in the neighborhood of $\mathbf{x} = \mathbf{x}_i$ and $\mathbf{y} = \mathbf{x}_j$, one has $\forall \mathbf{r},\mathbf{s} \in B$

$$|\mathbf{K}(\mathbf{x}_i + a\mathbf{r}, \mathbf{x}_j + a\mathbf{s}) - \mathbf{K}(\mathbf{x}_i,\mathbf{x}_j)| = O(a)\,, \tag{3.32}$$

and for the gradients in both $\mathbf{r}$ and $\mathbf{s}$

$$\begin{aligned}&|\nabla_{\mathbf{r}}\mathbf{K}(\mathbf{x}_i + a\mathbf{r}, \mathbf{x}_j + a\mathbf{s})| = O(a)\,,\\ &|\nabla_{\mathbf{s}}\mathbf{K}(\mathbf{x}_i + a\mathbf{r}, \mathbf{x}_j + a\mathbf{s})| = O(a)\,,\\ &|\nabla_{\mathbf{r}}\nabla_{\mathbf{s}}\mathbf{K}(\mathbf{x}_i + a\mathbf{r}, \mathbf{x}_j + a\mathbf{s})| = O\left(a^2\right)\,.\end{aligned}$$

Therefore, we obtain $\forall \mathbf{r} \in B$

$$\begin{aligned}|\mathbf{v}_i(\mathbf{r})| &\leq \|\mathbf{K}(\mathbf{x}_i + a\mathbf{r}, \mathbf{x}_j + a\,\cdot) - \mathbf{K}(\mathbf{x}_i,\mathbf{x}_j)\|_{H^{\frac{1}{2}}} \|\mathbf{f}_j\|_{H^{-\frac{1}{2}}}\\ &\leq O(a)\,\|\mathbf{f}_j\|_{H^{-\frac{1}{2}}}\,,\end{aligned}$$

and similarly

$$\begin{aligned}|\nabla_{\mathbf{r}}\mathbf{v}_i(\mathbf{r})| &\leq \|\nabla_{\mathbf{r}}\left(\mathbf{K}(\mathbf{x}_i + a\mathbf{r}, \mathbf{x}_j + a\,\cdot)\right)\|_{H^{\frac{1}{2}}} \|\mathbf{f}_j\|_{H^{-\frac{1}{2}}}\\ &\leq O(a)\,\|\mathbf{f}_j\|_{H^{-\frac{1}{2}}}\,.\end{aligned}$$

[3]Here and in the sequel, we use the definition for the $H^{1/2}(\partial B)$ norm:

$$\|\mathbf{v}\|_{H^{1/2}(\partial B)} = \min_{\mathbf{w}\in H^1(B,\mathbb{R}^3),\,\mathbf{w}=\mathbf{v} \text{ on } \partial B} \|\mathbf{w}\|_{H^1(B)}\,.$$

This enables us to estimate the $H^{\frac{1}{2}}$ norm of $\mathbf{v}_i$ on ∂B

$$\begin{aligned}\|\mathbf{v}_i\|_{H^{\frac{1}{2}}(B)} &\leq \|\mathbf{v}_i\|_{H^1(B)} \\ &= \left(\|\mathbf{v}_i\|^2_{L^2(B)} + \|\nabla \mathbf{v}_i\|^2_{L^2(B)}\right)^{\frac{1}{2}} \\ &\leq O(a)\,\|\mathbf{f}_j\|_{H^{-\frac{1}{2}}},\end{aligned}$$

which proves (4.24).

In order to prove (4.25), we use the decomposition (4.13) where none of the kernels $(\mathbf{K}_i)_{i=1,2,3}$ is singular. Therefore $\forall \mathbf{r} \in \partial B$

$$\begin{aligned}\mathbf{u}_i(\mathbf{r}) := (\mathcal{T}_{i,i}\mathbf{f}_i)(\mathbf{r}) &= \int_{\partial B} \mathbf{K}(\mathbf{x}_i + a\mathbf{r}, \mathbf{x}_i + a\mathbf{s})\mathbf{f}_i(\mathbf{s})\mathrm{d}\mathbf{s} \\ &= \int_{\partial B} \mathbf{G}(a(\mathbf{r}-\mathbf{s}))\mathbf{f}_i(\mathbf{s})\mathrm{d}\mathbf{s} + \int_{\partial B} (\mathbf{K}_1 + \mathbf{K}_2 + \mathbf{K}_3)(\mathbf{x}_i + a\mathbf{r}, \mathbf{x}_i + a\mathbf{s})\mathbf{f}_i(\mathbf{s})\mathrm{d}\mathbf{s} \\ &= \mathcal{T}^0\mathbf{f}_i + \int_{\partial B} (\mathbf{K}_1 + \mathbf{K}_2 + \mathbf{K}_3)(\mathbf{x}_i + a\mathbf{r}, \mathbf{x}_i + a\mathbf{s})\mathbf{f}_i(\mathbf{s})\mathrm{d}\mathbf{s}\,.\end{aligned}$$

We finish as before, having remarked that for $l = 1, 2, 3$

$$\mathbf{K}_l(\mathbf{x}_i + a\mathbf{r}, \mathbf{x}_i + a\mathbf{s}) = \mathbf{K}_l(\mathbf{x}_i, \mathbf{x}_i) + O(a)\,. \tag{3.33}$$

Proposition 3.5.6 *For every $\mathbf{f} \in \mathcal{H}^{-1/2}$, and $\mathbf{x} = (\boldsymbol{\xi}, \mathbf{p}) \in \mathcal{S}$*

$$\left(\mathcal{T}_{\mathbf{x}}\mathbf{f}\right)_i(\mathbf{r}) = \mathcal{T}^0\mathbf{f}_i + \sum_{l=1}^{3} \mathbf{K}_l(\mathbf{x}_i, \mathbf{x}_i)\langle \mathbf{f}_i, \mathbf{Id}\rangle_{\partial B} + \sum_{j\neq i} \mathbf{K}(\mathbf{x}_i, \mathbf{x}_j)\langle \mathbf{f}_j, \mathbf{Id}\rangle_{\partial B} + \mathcal{R}_i(\mathbf{f}), \tag{3.34}$$

with $\|\mathcal{R}_i\|_{\mathcal{L}(\mathcal{H}^{-1/2}, \mathcal{H}^{1/2})} = O(a)$, and $i = 1, 2, 3$.

Proof.

For all $i \in \{1, 2, 3\}$, and all $\mathbf{r} \in \partial B$

$$\begin{aligned}\left(\mathcal{T}_{\mathbf{x}}\mathbf{f}\right)_i(\mathbf{r}) &:= \int_{\partial B} \mathbf{K}(\mathbf{x}_i + a\mathbf{r}, \mathbf{x}_i + a\mathbf{s})\,\mathbf{f}_i(\mathbf{s})\mathrm{d}\mathbf{s} + \sum_{i\neq j} \int_{\partial B} \mathbf{K}(\mathbf{x}_i + a\mathbf{r}, \mathbf{x}_j + a\mathbf{s})\,\mathbf{f}_j(\mathbf{s})\mathrm{d}\mathbf{s} \\ &= \mathcal{T}_{i,i}\mathbf{f}_i + \sum_{j\neq i} \mathcal{T}_{i,j}\mathbf{f}_j\end{aligned}$$

and the result follows from the application of (4.24) and (4.25) of Proposition 4.4.2.

Proposition 3.5.7 *In the regime $a \ll 1$, one has for every $\mathbf{u} \in \mathcal{H}^{1/2}$, and $\mathbf{x} = (\boldsymbol{\xi}, \mathbf{p}) \in \mathcal{S}$*

$$\begin{aligned}\left(\mathcal{T}_{\mathbf{x}}^{-1}\mathbf{u}\right)_i = {} & (\mathcal{T}^0)^{-1}\left(\mathbf{u}_i - \textstyle\sum_{k=1}^{3} \mathbf{K}_k(\mathbf{x}_i, \mathbf{x}_i)\langle (\mathcal{T}^0)^{-1}\mathbf{u}_i, \mathbf{Id}\rangle_{\partial B}\right) - \\ & (\mathcal{T}^0)^{-1}\left(\sum_{j\neq i} \mathbf{K}(\mathbf{x}_i, \mathbf{x}_j)\langle (\mathcal{T}^0)^{-1}\mathbf{u}_j, \mathbf{Id}\rangle_{\partial B}\right) + \tilde{\mathcal{R}}_i(\mathbf{u})\end{aligned} \tag{3.35}$$

with $\|\tilde{\mathcal{R}}_i\|_{\mathcal{L}(\mathcal{H}^{1/2}, \mathcal{H}^{-1/2})} = O\left(a^3\right)$, and $i = 1, 2, 3$.

Proof. We recall that

$$\begin{aligned}\mathcal{T}^0 : H^{-\frac{1}{2}}(\partial B) &\to H^{\frac{1}{2}}(\partial B)\\ \mathbf{f} &\mapsto \int_{\partial B} \mathbf{G}(a(\cdot - \mathbf{s}))\mathbf{f}(\mathbf{s})\, d\mathbf{s}\,,\end{aligned}$$

and define for $l = 1, 2, 3$ the operators

$$\begin{aligned}\mathcal{S}_l : H^{-\frac{1}{2}}(\partial B) &\to H^{\frac{1}{2}}(\partial B)\\ \mathbf{f} &\mapsto \int_{\partial B} \mathbf{K}_l(\mathbf{x}_i, \mathbf{x}_i)\mathbf{f}(\mathbf{s})\, d\mathbf{s}\,,\end{aligned}$$

and eventually

$$\begin{aligned}\mathcal{S}_{i,j} : H^{-\frac{1}{2}}(\partial B) &\to H^{\frac{1}{2}}(\partial B)\\ \mathbf{f} &\mapsto \int_{\partial B} \mathbf{K}(\mathbf{x}_i, \mathbf{x}_j)\mathbf{f}(\mathbf{s})\, d\mathbf{s}\,.\end{aligned}$$

(Notice that for all $\mathbf{f} \in H^{-\frac{1}{2}}(\partial B)$, $\mathcal{S}_l\mathbf{f}$ and $\mathcal{S}_{i,j}\mathbf{f}$ are in fact constant maps.)

That these operators are continuous operators from $H^{-\frac{1}{2}}(\partial B)$ into $H^{\frac{1}{2}}(\partial B)$ is classical. We hereafter are only interested into the estimation of their norms, and more precisely the way they depend on a, δ and y in the limit $a \to 0$. Notice that since the kernel $\mathbf{G}$ is homogeneous of degree -1, one has

$$\|\mathcal{T}^0\|_{\mathcal{L}(\mathcal{H}^{-1/2},\mathcal{H}^{1/2})} = O\left(\frac{1}{a}\right) \text{ and } \left\|\left(\mathcal{T}^0\right)^{-1}\right\|_{\mathcal{L}(\mathcal{H}^{1/2},\mathcal{H}^{-1/2})} = O\left(a\right)\,. \tag{3.36}$$

As far as $\mathcal{S}_l$ is concerned, we get that (since $|\mathbf{K}_l(\mathbf{x}_i, \mathbf{x}_i)| = O(1)$)

$$\|\mathcal{S}_l\|_{\mathcal{L}(\mathcal{H}^{-1/2},\mathcal{H}^{1/2})} = O\left(1\right)\,, \tag{3.37}$$

and similarly

$$\|\mathcal{S}_{i,j}\|_{\mathcal{L}(\mathcal{H}^{-1/2},\mathcal{H}^{1/2})} = O\left(1\right)\,. \tag{3.38}$$

When $a \to 0$ this enables us to invert (4.29) leading to (4.30).

3.5.4 Asymptotic expansion of the motion equation

We now use the fact that the spheres are non-deformable and may only move following a rigid body motion. In other words, the velocity of each point $\mathbf{r}$ of the $i-$sphere expresses as a sum of a translation and a rotation as

$$\mathbf{u}_i(\mathbf{r}) = \mathbf{u}_{T_i} + \mathbf{u}_{R_i}(\mathbf{r})\,, \tag{3.39}$$

where $\mathbf{u}_{T_i}$ is constant on ∂B while $\mathbf{u}_{R_i}(\mathbf{r}) = \omega_i \times a\mathbf{r}$ for a suitable angular velocity ω_i (remember that all quantities are expressed on the unit sphere ∂B). This is of particular importance for the computation of the total force and the total torque, which, due to self-propulsion, should vanish. This implies

$$\sum_i \int_{\partial B} \mathbf{f}_i = \sum_i \int_{\partial B} \left(\mathcal{T}_{\mathbf{x}}^{-1}\mathbf{u}\right)_i = 0\,. \tag{3.40}$$

Plugging (4.39) in (4.40) and using (4.30) leads to

$$\begin{aligned}\sum_i \int_{\partial B} (\mathcal{T}^0)^{-1}\left(\mathbf{u}_{Ti} + \mathbf{u}_{Ri} - \sum_{k=1}^{3} \mathbf{K}_k(\mathbf{x}_i, \mathbf{x}_i)\langle(\mathcal{T}^0)^{-1}(\mathbf{u}_{Ti} + \mathbf{u}_{Ri}), \mathrm{Id}\rangle_{\partial B}\right) -\\ (\mathcal{T}^0)^{-1}\left(\sum_{j\neq i} \mathbf{K}(\mathbf{x}_i, \mathbf{x}_j)\langle(\bar{\mathcal{T}}^0)^{-1}(\mathbf{u}_{Tj} + \mathbf{u}_{Rj}), \mathbf{Id}\rangle_{\partial B}\right) = O\left(a^3\right)||\mathbf{u}||\,.\end{aligned} \tag{3.41}$$

It is well known that both translations and rotations are eigenfunctions of the Dirichlet to Neumann map of the three dimensional Stokes operator outside a sphere. Namely

$$\left(\mathcal{T}^0\right)^{-1}\mathbf{u}_{Ti}=\lambda_T\mathbf{u}_{Ti}\text{ and }\left(\mathcal{T}^0\right)^{-1}\mathbf{u}_{Ri}=\lambda_R\mathbf{u}_{Ri}\,.$$

It is well-known that $\lambda_T=\frac{3\mu a}{2}$ leading in particular to the celebrated Stokes formula

$$\int_{\partial B}\left(\mathcal{T}^0\right)^{-1}\mathbf{u}_{T_i}\mathrm{d}\mathbf{s}=6\pi\mu a\,\mathbf{u}_{T_i}$$

while $\lambda_R=3\mu a$. We also remark that due to $\int_{\partial B}\mathbf{u}_{R_i}\mathrm{d}\mathbf{s}=0$, we have

$$\int_{\partial B}\left(\mathcal{T}^0\right)^{-1}\mathbf{u}_{R_i}\mathrm{d}\mathbf{s}=0\,.$$

We therefore obtain

$$6\pi\mu a\sum_i\left(\mathbf{u}_{Ti}-6\pi\mu a\sum_{k=1}^3\mathbf{K}_k(\mathbf{x}_i,\mathbf{x}_i)\mathbf{u}_{Ti}-6\pi\mu a\sum_{j\neq i}\mathbf{K}(\mathbf{x}_i,\mathbf{x}_j)\mathbf{u}_{Tj}\right)=O\left(a^3\right)||\mathbf{u}||\,. \tag{3.42}$$

We now compute the torque with respect to the center $\mathbf{x}_2$ of the first ball B_2. Self-propulsion of the swimmer implies that this torque vanishes:

$$0=\int_{\partial B}(\mathbf{x}_1-\mathbf{x}_2+a\mathbf{r})\times\mathbf{f}_1(\mathbf{r})+\int_{\partial B}a\mathbf{r}\times\mathbf{f}_2(\mathbf{r})+\int_{\partial B}(\mathbf{x}_3-\mathbf{x}_2+a\mathbf{r})\times\mathbf{f}_3(\mathbf{r})=\mathbf{I}_1+\mathbf{I}_2+\mathbf{I}_3\,, \tag{3.43}$$

where, calling $\mathbf{e}_\theta=\begin{pmatrix}\cos\theta\\ \sin\theta\\ 0\end{pmatrix}$ the direction of the swimmer, the quantities $\mathbf{I}_1$, $\mathbf{I}_2$ and $\mathbf{I}_3$ are respectively given below.

$$\begin{aligned}
\mathbf{I}_1 &= \int_{\partial B}(\mathbf{x}_1-\mathbf{x}_2+a\mathbf{r})\times\mathbf{f}_1(\mathbf{r})=\int_{\partial B}(\xi_1\mathbf{e}_\theta+a\mathbf{r})\times(\mathcal{T}_{\mathbf{x}})^{-1}\mathbf{u}_1\\
&= \int_{\partial B}(-\xi_1\mathbf{e}_\theta+a\mathbf{r})\times(\mathcal{T}^0)^{-1}\left(\mathbf{u}_{T1}+\mathbf{u}_{R1}-6\pi\mu a\sum_{l=1}^3\mathbf{K}_l(\mathbf{x}_1,\mathbf{x}_1)\mathbf{u}_{T1}\right.\\
&\qquad\left.-6\pi\mu a\sum_{j\neq 2}\mathbf{K}(\mathbf{x}_1,\mathbf{x}_j)\mathbf{u}_{Tj}+O\left(a^2\right)||\mathbf{u}||\right)\\
&= -6\pi\mu a\xi_1\mathbf{e}_\theta\times\left(\mathbf{u}_{T1}-6\pi\mu a\sum_{l=1}^3\mathbf{K}_l(\mathbf{x}_1,\mathbf{x}_1)\mathbf{u}_{T1}-6\pi\mu a\sum_{j\neq 1}\mathbf{K}(\mathbf{x}_1,\mathbf{x}_j)\mathbf{u}_{Tj}\right)+O\left(a^3\right)||\mathbf{u}||\,.
\end{aligned}$$

Similarly, we get,

$$\begin{aligned}
\mathbf{I}_2 &= a\int_{\partial B}\mathbf{r}\times\mathbf{f}_2(\mathbf{r})=a\int_{\partial B}\mathbf{r}\times(\mathcal{T}_{\mathbf{x}})^{-1}\mathbf{u}_2\\
&= a\int_{\partial B}\mathbf{r}\times(\mathcal{T}^0)^{-1}\left(\mathbf{u}_{T2}+\mathbf{u}_{R2}-6\pi\mu a\sum_{l=1}^3\mathbf{K}_l(\mathbf{x}_2,\mathbf{x}_2)\mathbf{u}_{T2}\right.\\
&\qquad\left.-6\pi\mu a\sum_{j\neq 2}\mathbf{K}(\mathbf{x}_2,\mathbf{x}_j)\mathbf{u}_{Tj}+O\left(a^2\right)||\mathbf{u}||\right)\\
&= a\int_{\partial B}\mathbf{r}\times(\mathcal{T}^0)^{-1}\left(\mathbf{u}_{R1}\right)+O\left(a^4\right)||\mathbf{u}||\,.
\end{aligned}$$

But since $\left(\mathcal{T}^0\right)^{-1}\mathbf{u}_{R1} = \lambda_R \mathbf{u}_{R1} = \lambda_R \omega_1 \times a\mathbf{r}$, we have

$$\begin{aligned} a\int_{\partial B} \mathbf{r}\times\left(\mathcal{T}^0\right)^{-1}(\mathbf{u}_{R2}) &= a^2\lambda_R \int_{\partial B} \mathbf{r}\times(\omega_1\times\mathbf{r})\,d\mathbf{r} \\ &= \frac{8\pi}{3}\mu a^3\omega_1\,. \end{aligned}$$

This leads to

$$\mathbf{I}_2 = \frac{8\pi}{3}\mu a^3\omega_1 + O\left(a^4\right)||\mathbf{u}||\,.$$

Correspondingly,

$$\begin{aligned} \mathbf{I}_3 &= \int_{\partial B}(\mathbf{x}_3-\mathbf{x}_2+a\mathbf{r})\times\mathbf{f}_3(\mathbf{r}) \\ &= 6\pi\mu a\xi_2\mathbf{e}_\theta\times\left(\mathbf{u}_{T3} - 6\pi\mu a\sum_{l=1}^{3}\mathbf{K}_l(\mathbf{x}_3,\mathbf{x}_3)\mathbf{u}_{T3} - 6\pi\mu a\sum_{j\neq 3}\mathbf{K}(\mathbf{x}_3,\mathbf{x}_j)\mathbf{u}_{Tj}\right) + O\left(a^3\right)||\mathbf{u}||\,. \end{aligned}$$

Denoting by $\mathbf{A}$ the matrix

$$\mathbf{A} = \begin{pmatrix} \mathbf{A}_{11} & \mathbf{A}_{12} & \mathbf{A}_{13} \\ \mathbf{A}_{21} & \mathbf{A}_{22} & \mathbf{A}_{23} \\ \mathbf{A}_{31} & \mathbf{A}_{32} & \mathbf{A}_{33} \end{pmatrix} \tag{3.44}$$

where for $i = 1,2,3$

$$\mathbf{A}_{ii} = \mathbf{Id} - 6\pi\mu a\sum_{l=1}^{3}\mathbf{K}_l(\mathbf{x}_i,\mathbf{x}_i) \tag{3.45}$$

and for $i,j = 1,2,3$ with $i \neq j$

$$\mathbf{A}_{ij} = -6\pi\mu a\,\mathbf{K}(\mathbf{x}_i,\mathbf{x}_j) \tag{3.46}$$

and $\mathbf{S}$ the matrix

$$\mathbf{S} = \begin{pmatrix} \mathbf{Id} & \mathbf{Id} & \mathbf{Id} \\ -\xi_1\mathbf{e}_\theta\times & 0 & +\xi_2\mathbf{e}_\theta\times \end{pmatrix},$$

we can rewrite the self-propulsion assumption (4.43), (4.44) as (notice that angular velocities being involved of higher order disappear)

$$\mathbf{SA}\begin{pmatrix} \mathbf{u}_{T_1} \\ \mathbf{u}_{T_2} \\ \mathbf{u}_{T_3} \end{pmatrix} = O\left(a^2\right)||\mathbf{u}||. \tag{3.47}$$

We end up by expressing $\mathbf{u}_{T_1}, \mathbf{u}_{T_2}, \mathbf{u}_{T_3}$ and $\omega_1, \omega_2, \omega_3$ in terms of $\dot{x}, \dot{y}, \dot{\theta}, \dot{\xi_1}$ and $\dot{\xi_2}$. But, since $\mathbf{u}_{T_i}$ is the velocity of the center of the ball B_i, one has

$$\mathbf{u}_{T_1} = \begin{pmatrix} \dot{x} - \dot{\xi}_1\cos(\theta) + \dot{\theta}\xi_1\sin(\theta) \\ \dot{y} - \dot{\xi}_1\sin(\theta) - \dot{\theta}\xi_1\cos(\theta) \\ 0 \end{pmatrix},\ \mathbf{u}_{T_2} = \begin{pmatrix} \dot{x} \\ \dot{y} \\ 0 \end{pmatrix},$$

and

$$\mathbf{u}_{T_3} = \begin{pmatrix} \dot{x} + \dot{\xi}_2\cos(\theta) - \dot{\theta}\xi_2\sin(\theta) \\ \dot{y} + \dot{\xi}_2\sin(\theta) + \dot{\theta}\xi_2\cos(\theta) \\ 0 \end{pmatrix}.$$

Similarly

$$\omega_1 = \omega_2 = \omega_3 = \begin{pmatrix} 0 \\ 0 \\ \dot{\theta} \end{pmatrix} .$$

We rewrite these formulas as

$$\begin{pmatrix} \mathbf{u}_{T_1} \\ \mathbf{u}_{T_2} \\ \mathbf{u}_{T_3} \end{pmatrix} = \mathbf{T} \begin{pmatrix} \dot{x} \\ \dot{y} \\ \dot{\theta} \end{pmatrix} + \mathbf{U}\dot{\boldsymbol{\xi}} \tag{3.48}$$

with

$$\mathbf{T} = \begin{pmatrix} \mathbf{Id} & -\xi_1 \mathbf{e}_\theta^\perp \\ \mathbf{Id} & 0 \\ \mathbf{Id} & \xi_2 \mathbf{e}_\theta^\perp \end{pmatrix} ,$$

where $\mathbf{e}_\theta^\perp = \begin{pmatrix} -\sin\theta \\ \cos\theta \\ 0 \end{pmatrix}$ and

$$\mathbf{U} = \begin{pmatrix} -\mathbf{e}_\theta & 0 \\ 0 & 0 \\ 0 & \mathbf{e}_\theta \end{pmatrix} .$$

Plugging (3.48) into (4.48) leads to the motion equation

$$(\mathbf{SA} + \mathbf{R}) \left(\mathbf{T} \begin{pmatrix} \dot{x} \\ \dot{y} \\ \dot{\theta} \end{pmatrix} + \mathbf{U}\dot{\boldsymbol{\xi}} \right) = 0 \tag{3.49}$$

where the residual matrix has a norm which is estimated as

$$||\mathbf{R}|| = O\left(a^2\right) .$$

3.5.5 Dimension of Lie algebra under the small spheres hypothesis

Rewriting from (4.45), (4.46) and (4.47) $\mathbf{A} = \mathbf{Id} + a\mathbf{A}_1$, we can expand in power series of a the solution of (3.49). This enables us to write an expansion (still in a) of the two vectorfields $\mathbf{F}_1$ and $\mathbf{F}_2$. To this end, we have used the software MAPLE to symbolically compute those expressions and the Lie brackets $[\mathbf{F}_1, \mathbf{F}_2]$, $[\mathbf{F}_1, [\mathbf{F}_1, \mathbf{F}_2]]$, and $[\mathbf{F}_2, [\mathbf{F}_1, \mathbf{F}_2]]$. Writing the vectorfields in components as

$$\mathbf{F}_1(\xi_1, \xi_2, y, \theta) := \begin{pmatrix} 1 \\ 0 \\ \mathbf{F}_1^3 + O\left(a^2\right) \\ \mathbf{F}_1^4 + O\left(a^2\right) \\ \mathbf{F}_1^5 + O\left(a^2\right) \end{pmatrix} , \mathbf{F}_2(\xi_1, \xi_2, y, \theta) := \begin{pmatrix} 0 \\ 1 \\ \mathbf{F}_2^3 + O\left(a^2\right) \\ \mathbf{F}_2^4 + O\left(a^2\right) \\ \mathbf{F}_2^5 + O\left(a^2\right) \end{pmatrix} , \tag{3.50}$$

we find, after having furthermore expanded the abovementioned components in power series of $\dfrac{1}{y}$,

$$
\begin{aligned}
\mathbf{F}_1^3 &= \frac{1}{3}\cos(\theta) + \frac{a}{6}\cos(\theta)K_1^3(\xi_1,\xi_2,\theta) + \frac{3a}{16y^2}\left(\sin(\theta)\cos(\theta)\left(\xi_2+2\xi_1\right)\right) \\
&\quad + \frac{a}{384y^3}\left(\cos(\theta)K_2^3(\xi_1,\xi_2,\theta)\right) + \frac{a}{512y^4}\left(\sin(\theta)\cos(\theta)K_3^3(\xi_1,\xi_2,\theta)\right) + O\left(\frac{a}{y^5}\right), \\
\mathbf{F}_2^3 &= -\frac{1}{3}\cos(\theta) - \frac{a}{6}\cos(\theta)K_1^3(\xi_2,\xi_1,-\theta) + \frac{3a}{16y^2}\left(\sin(\theta)\cos(\theta)\left(2\xi_2+\xi_1\right)\right) \\
&\quad - \frac{a}{384y^3}\left(\cos(\theta)K_2^3(\xi_2,\xi_1,-\theta)\right) + \frac{a}{512y^4}\left(\sin(\theta)\cos(\theta)K_3^3(\xi_2,\xi_1,-\theta)\right) + O\left(\frac{a}{y^5}\right), \\
\mathbf{F}_1^4 &= \frac{1}{3}\sin(\theta) + \frac{a}{6}\sin(\theta)K_1^4(\xi_1,\xi_2,\theta) - \frac{3a}{32y^2}K_2^4(\xi_1,\xi_2,\theta) \\
&\quad + \frac{a}{192y^3}\sin(\theta)K_3^4(\xi_1,\xi_2,\theta) - \frac{a}{y^4}K_4^4(\xi_1,\xi_2,\theta) + O\left(\frac{a}{y^5}\right), \\
\mathbf{F}_2^4 &= -\frac{1}{3}\sin(\theta) - \frac{a}{6}\sin(\theta)K_1^4(\xi_2,\xi_1,-\theta) - \frac{3a}{32y^2}K_2^4(\xi_2,\xi_1,\theta) \\
&\quad - \frac{a}{192y^3}\sin(\theta)K_3^4(\xi_2,\xi_1,-\theta) - \frac{a}{y^4}K_4^4(\xi_2,\xi_1,-\theta) + O\left(\frac{a}{y^5}\right), \\
\mathbf{F}_1^5 &= \frac{3a}{64y^3}\sin(\theta)\cos(\theta)K_1^5(\xi_1,\xi_2,\theta) - \frac{9a}{512y^4}\cos(\theta)K_2^5(\xi_1,\xi_2,\theta) + O\left(\frac{a}{y^5}\right), \\
\mathbf{F}_2^5 &= \frac{3a}{64y^3}\sin(\theta)\cos(\theta)K_1^5(\xi_2,\xi_1,-\theta) + \frac{9a}{512y^4}\cos(\theta)K_2^5(\xi_2,\xi_1,-\theta) + O\left(\frac{a}{y^5}\right).
\end{aligned}
$$

In those expressions the remaining functions are respectively given by

$$
\begin{aligned}
K_1^3(\boldsymbol{\xi},\theta) &= \frac{\left(\xi_2^2\xi_1^2 - \xi_2^3\xi_1 - \xi_2^4 + 2\xi_1^3\xi_2 + 2\xi_1^4\right)}{\left(\xi_2^2+\xi_1\xi_2+\xi_1^2\right)\xi_1\xi_2\left(\xi_1+\xi_2\right)}, \\
K_2^3(\boldsymbol{\xi},\theta) &= -210\xi_1^2\cos(\theta)^2 + 12\cos(\theta)^4\xi_1^2 + 184\xi_1^2 + 24\cos(\theta)^2\xi_1\xi_2 \\
&\quad -32\xi_1\xi_2 - 6\cos(\theta)^4\xi_1\xi_2 - 92\xi_2^2 + 105\xi_2^2\cos(\theta)^2 - 6\cos(\theta)^4\xi_2^2, \\
K_3^3(\boldsymbol{\xi},\theta) &= \frac{1}{\left(\xi_2^2+\xi_1\xi_2+\xi_1^2\right)}\Big(12\cos(\theta)^4\xi_2^5 + 24\xi_1^5\cos(\theta)^4 - 168\xi_2^5\cos(\theta)^2 - 336\xi_1^5\cos(\theta)^2 \\
&\quad +112\xi_2^5 + 72\xi_1\xi_2^4 - 176\xi_1^2\xi_2^3 - 136\xi_1^3\xi_2^2 + 224\xi_1^5 - 156\xi_1^3\xi_2^2\cos(\theta)^2 \\
&\quad -24\xi_1^2\xi_2^3\cos(\theta)^2 - 240\xi_1^4\xi_2\cos(\theta)^2 + 48\xi_1^4\xi_2 - 156\xi_1\xi_2^4\cos(\theta)^2 \\
&\quad -24\cos(\theta)^4\xi_1^2\xi_2^3 + 9\cos(\theta)^4\xi_1\xi_2^4 - 21\xi_1^3\cos(\theta)^4\xi_2^2\Big), \\
K_1^4(\boldsymbol{\xi},\theta) &= \frac{\left(\xi_2^2\xi_1^2 - \xi_2^3\xi_1 - \xi_2^4 + 2\xi_1^3\xi_2 + 2\xi_1^4\right)}{\left(\xi_2^2+\xi_1\xi_2+\xi_1^2\right)\xi_1\xi_2\left(\xi_1+\xi_2\right)}, \\
K_2^4(\boldsymbol{\xi},\theta) &= 6\cos(\theta)^2\xi_1 + 3\cos(\theta)^2\xi_2 - 4\xi_1 - 2\xi_2,
\end{aligned}
$$

$$
\begin{aligned}
K_3^4(\boldsymbol{\xi},\theta) &= -132\xi_1^2\cos(\theta)^2 + 6\cos(\theta)^4\xi_1^2 + 56\xi_1^2 + 12\cos(\theta)^2\xi_1\xi_2 \\
&\quad -16\xi_1\xi_2 - 3\cos(\theta)^4\xi_1\xi_2 - 28\xi_2^2 + 66\xi_2^2\cos(\theta)^2 - 3\cos(\theta)^4\xi_2^2\,, \\
K_4^4(\boldsymbol{\xi},\theta) &= \frac{1}{(512\xi_2^2 + 512\xi_1\xi_2 + 512\xi_1^2)}\Big(-210\cos(\theta)^4\xi_2^5 - 420\xi_1^5\cos(\theta)^4 + 232\xi_2^5\cos(\theta)^2 \\
&\quad +24\cos(\theta)^6\xi_1^5 - 64\xi_2^5 + 12\cos(\theta)^6\xi_2^5 - 96\xi_1\xi_2^4 - 64\xi_1^2\xi_2^3 \\
&\quad -128\xi_1^5 + 104\xi_1^3\xi_2^2\cos(\theta)^2 - 56\xi_1^2\xi_2^3\cos(\theta)^2 \\
&\quad -96\xi_1^4\xi_2 + 216\xi_1\xi_2^4\cos(\theta)^2 - 66\cos(\theta)^4\xi_1^2\xi_2^3 \\
&\quad -318\xi_1^4\cos(\theta)^4\xi_2 - 240\xi_1^3\cos(\theta)^4\xi_2^2 - 24\cos(\theta)^6\xi_1^2\xi_2^3 \\
&\quad -21\cos(\theta)^6\xi_1^3\xi_2^2 + 464\xi_1^5\cos(\theta)^2 - 128\xi_1^3\xi_2^2 \\
&\quad +264\xi_1^4\xi_2\cos(\theta)^2 - 204\cos(\theta)^4\xi_1\xi_2^4 + 9\cos(\theta)^6\xi_1\xi_2^4\Big),
\end{aligned}
$$

$$
\begin{aligned}
K_1^5(\boldsymbol{\xi},\theta) &= -8\xi_1 - 4\xi_2 + 2\cos(\theta)^2\xi_1 + \cos(\theta)^2\xi_2\,, \\
K_2^5(\boldsymbol{\xi},\theta) &= \frac{1}{(\xi_2^2 + \xi_1\xi_2 + \xi_1^2)}\Big(20\cos(\theta)^2\xi_2^4 - 40\cos(\theta)^2\xi_1^4 - 4\cos(\theta)^4\xi_2^4 + 8\xi_1^4\cos(\theta)^4 \\
&\quad -40\xi_2^3\xi_1 - 8\xi_2^2\xi_1^2 + 32\xi_1^3\xi_2 - 16\xi_2^4 + 32\xi_2^3\cos(\theta)^2\xi_1 - 7\cos(\theta)^4\xi_2^3\xi_1 \\
&\quad + \cos(\theta)^4\xi_1^2\xi_2^2 - 40\cos(\theta)^2\xi_1^3\xi_2 + 8\xi_1^3\cos(\theta)^4\xi_2 + 32\xi_1^4 - 8\xi_2^2\xi_1^2\cos(\theta)^2\Big)\,.
\end{aligned}
$$

As one can see, the use of a software for symbolic computation seems unavoidable. Subsequently, we get the expansion of the Lie bracket $[\mathbf{F}_1,\mathbf{F}_2](\xi_1,\xi_2,y,\theta)$

$$
[\mathbf{F}_1,\mathbf{F}_2](\boldsymbol{\xi},y,\theta) := \begin{pmatrix} 0 \\ 0 \\ [\mathbf{F}_1,\mathbf{F}_2]_3 + O\left(a^2\right) \\ [\mathbf{F}_1,\mathbf{F}_2]_4 + O\left(a^2\right) \\ [\mathbf{F}_1,\mathbf{F}_2]_5 + O\left(a^2\right) \end{pmatrix}, \tag{3.51}
$$

where the components are given by the following expressions

$$
\begin{aligned}
[\mathbf{F}_1,\mathbf{F}_2]_3 &= -\frac{a}{3}\cos(\theta)\frac{(\xi_1^4 + 2\xi_1^3\xi_2 + \xi_2^2\xi_1^2 + 2\xi_2^3\xi_1 + \xi_2^4)}{(\xi_1+\xi_2)^2\xi_2^2\xi_1^2} \\
&\quad -\frac{27\,a}{512\,y^4}a\cos(\theta)\sin(\theta)\frac{\xi_1\xi_2\left(\cos(\theta)^4 - 4\cos(\theta)^2 + 8\right)\left(-\xi_2^2+\xi_1^2\right)}{(\xi_2^2+\xi_1\xi_2+\xi_1^2)} \\
&\quad +O\left(\frac{a}{y^5}\right), \\
[\mathbf{F}_1,\mathbf{F}_2]_4 &= -\frac{a}{3}\sin(\theta)\frac{\left(\xi_1^4 + 2\xi_1^3\xi_2 + \xi_2^2\xi_1^2 + 2\xi_2^3\xi_1 + \xi_2^4\right)}{\left(\xi_1+\xi_2\right)^2\xi_2^2\xi_1^2} \\
&\quad +\frac{27\,a}{512\,y^4}\cos(\theta)^2\frac{\xi_1\xi_2\left(\cos(\theta)^4 - 4\cos(\theta)^2 + 8\right)\left(-\xi_2^2+\xi_1^2\right)}{(\xi_2^2+\xi_1\xi_2+\xi_1^2)} \\
&\quad +O\left(\frac{a}{y^5}\right),
\end{aligned}
$$

$$
[\mathbf{F}_1,\mathbf{F}_2]_5 = \frac{81\,a}{512\,y^4}\cos(\theta)\frac{\xi_1\xi_2\left(\xi_1+\xi_2\right)\left(\cos(\theta)^4 - 4\cos(\theta)^2 + 8\right)}{(\xi_2^2+\xi_1\xi_2+\xi_1^2)} + O\left(\frac{a}{y^5}\right).
$$

Notice that since the two first coordinates of $\mathbf{F}_1$ and $\mathbf{F}_2$ are constant, the corresponding first coordinates of the Lie bracket vanish. Similarly, the asymptotic expansion for the second order Lie bracket $[\mathbf{F}_1,[\mathbf{F}_1,\mathbf{F}_2]]\,(\boldsymbol{\xi},y,\theta)$ reads

$$[\mathbf{F}_1,[\mathbf{F}_1,\mathbf{F}_2]](\boldsymbol{\xi},y,\theta) := \begin{pmatrix} 0 \\ 0 \\ [\mathbf{F}_1,[\mathbf{F}_1,\mathbf{F}_2]]_3 + O\left(a^2\right) \\ [\mathbf{F}_1,[\mathbf{F}_1,\mathbf{F}_2]]_4 + O\left(a^2\right) \\ [\mathbf{F}_1,[\mathbf{F}_1,\mathbf{F}_2]]_5 + O\left(a^2\right) \end{pmatrix}, \tag{3.52}$$

where

$$\begin{aligned}
[\mathbf{F}_1,[\mathbf{F}_1,\mathbf{F}_2]]_3 &= -\frac{2\,a}{3}\cos(\theta)\frac{\xi_2\left(3\xi_1^2+3\xi_1\xi_2+\xi_2^2\right)}{\xi_1^3(\xi_1+\xi_2)^3} \\
&\quad +\frac{27\,a}{512\,y^4}\cos(\theta)\sin(\theta)L_3(\boldsymbol{\xi},\theta)+O\left(\frac{a}{y^5}\right), \\
[\mathbf{F}_1,[\mathbf{F}_1,\mathbf{F}_2]]_4 &= -\frac{2\,a}{3}\sin(\theta)\frac{\xi_2\left(3\xi_1^2+3\xi_1\xi_2+\xi_2^2\right)}{\xi_1^3\left(\xi_1+\xi_2\right)^3} \\
&\quad -\frac{27\,a}{512\,y^4}\cos(\theta)^2L_3(\boldsymbol{\xi},\theta)+O\left(\frac{a}{y^5}\right), \\
[\mathbf{F}_1,[\mathbf{F}_1,\mathbf{F}_2]]_5 &= -\frac{81\,a}{512\,y^4}\cos(\theta)L_4(\boldsymbol{\xi},\theta)+O\left(\frac{a}{y^5}\right).
\end{aligned}$$

There, L_3 and L_4 are respectively given by

$$\begin{aligned}
L_3(\boldsymbol{\xi},\theta) &= \frac{\xi_2^3\left(8-4\cos(\theta)^2+\cos(\theta)^4\right)\left(2\xi_1^2-\xi_1\xi_2-\xi_2^2\right)}{(\xi_2^2+\xi_1\xi_2+\xi_1^2)^2}, \\
L_4(\boldsymbol{\xi},\theta) &= \frac{\xi_2^3\left(8-4\cos(\theta)^2+\cos(\theta)^4\right)(2\xi_1+\xi_2)}{(\xi_2^2+\xi_1\xi_2+\xi_1^2)^2}.
\end{aligned}$$

Eventually, the expansion of the vector field $[\mathbf{F}_2,[\mathbf{F}_1,\mathbf{F}_2]]$ is given by

$$[\mathbf{F}_2,[\mathbf{F}_1,\mathbf{F}_2]](\xi_1,\xi_2,y,\theta) := \begin{pmatrix} 0 \\ 0 \\ [\mathbf{F}_2,[\mathbf{F}_1,\mathbf{F}_2]]_3 + O\left(a^2\right) \\ [\mathbf{F}_2,[\mathbf{F}_1,\mathbf{F}_2]]_4 + O\left(a^2\right) \\ [\mathbf{F}_2,[\mathbf{F}_1,\mathbf{F}_2]]_5 + O\left(a^2\right) \end{pmatrix}, \tag{3.53}$$

where

$$\begin{aligned}
[\mathbf{F}_2,[\mathbf{F}_1,\mathbf{F}_2]]_3 &= -\frac{2}{3}a\cos(\theta)\frac{\xi_1\left(\xi_1^2+3\xi_1\xi_2+3\xi_2^2\right)}{\left(\xi_2^3\left(\xi_1+\xi_2\right)^3\right)} \\
&\quad -\frac{27\,a}{512\,y^4}a\cos(\theta)\sin(\theta)L_3(\xi_2,\xi_1,-\theta)+O\left(\frac{a}{y^5}\right), \\
[\mathbf{F}_2,[\mathbf{F}_1,\mathbf{F}_2]]_4 &= \frac{2\,a}{3}\sin(\theta)\frac{\xi_1\left(\xi_1^2+3\xi_1\xi_2+3\xi_2^2\right)}{\left(\xi_2^3\left(\xi_1+\xi_2\right)^3\right)} \\
&\quad -\frac{27\,a}{512\,y^4}\cos(\theta)^2L_3(\xi_2,\xi_1,-\theta)+O\left(\frac{a}{y^5}\right), \\
[\mathbf{F}_2,[\mathbf{F}_1,\mathbf{F}_2]]_5 &= -\frac{81\,a}{512\,y^4}\cos(\theta)L_4(\xi_2,\xi_1,-\theta)+O\left(\frac{a}{y^5}\right).
\end{aligned}$$

Having an expansion of $\det\left(\mathbf{F}_1,\mathbf{F}_2,[\mathbf{F}_1,\mathbf{F}_2],[\mathbf{F}_1,[\mathbf{F}_1,\mathbf{F}_2]],[\mathbf{F}_2,[\mathbf{F}_1,\mathbf{F}_2]]\right)$ which does not vanish implies the local controllability of our model swimmer. It can be readily checked that we have

$$\begin{aligned}\det\left(\mathbf{F}_1,\mathbf{F}_2,[\mathbf{F}_1,\mathbf{F}_2],[\mathbf{F}_1,[\mathbf{F}_1,\mathbf{F}_2]],[\mathbf{F}_2,[\mathbf{F}_1,\mathbf{F}_2]]\right) &= \\ &= \begin{vmatrix} [\mathbf{F}_1,\mathbf{F}_2]_3 & [\mathbf{F}_1,[\mathbf{F}_1,\mathbf{F}_2]]_3 & [\mathbf{F}_2,[\mathbf{F}_1,\mathbf{F}_2]]_3 \\ [\mathbf{F}_1,\mathbf{F}_2]_4 & [\mathbf{F}_1,[\mathbf{F}_1,\mathbf{F}_2]]_4 & [\mathbf{F}_2,[\mathbf{F}_1,\mathbf{F}_2]]_4 \\ [\mathbf{F}_1,\mathbf{F}_2]_5 & [\mathbf{F}_1,[\mathbf{F}_1,\mathbf{F}_2]]_5 & [\mathbf{F}_2,[\mathbf{F}_1,\mathbf{F}_2]]_5 \end{vmatrix} \\ &= \frac{81\,a^3(\xi_1-\xi_2)}{131072\,y^9}\sin\theta(\cos\theta)^2 R(\boldsymbol{\xi},\theta) + O\left(\frac{1}{y^{10}}\right), \qquad (3.54)\end{aligned}$$

with,

$$\begin{aligned}R(\boldsymbol{\xi},\theta) &= \frac{\left(6\xi_1^6+27\xi_1^5\xi_2+50\xi_1^4\xi_2^2+55\xi_1^3\xi_2^3+50\xi_1^2\xi_2^4+27\xi_1\xi_2^5+6\xi_2^6\right)}{(\xi_1+\xi_2)\left(\xi_2^2+\xi_1\xi_2+\xi_1^2\right)^2\xi_1\xi_2} \\ &\quad\times\left(64-64\cos(\theta)^2+32\cos(\theta)^4-8\cos(\theta)^6+\cos(\theta)^8\right).\end{aligned}$$

It is easily seen that R never vanishes. Therefore, the previous determinant has a non-vanishing first coefficient (in $\frac{1}{y^9}$) which does not vanish for $\xi_1 \neq \xi_2$ and $\theta \notin \{0, \frac{\pi}{2}, \pi, \frac{3\pi}{2}\}$. Since it is an analytic function of $(\xi_1, \xi_2, y, \theta)$ we deduce that it does not vanish except at most on a negligible set. This is sufficient to conclude that

$$d_{(\xi_1,\xi_2,y,\theta)} = 5$$

almost everywhere and the local controllability of the Three-sphere swimmer around such points.

Remark 3.5.8 *Quite strikingly, when $\xi_1 = \xi_2$ the first term of the expansion vanishes and one has to go one step further. We find in that case*

$$det\left(\mathbf{F}_1,\mathbf{F}_2,[\mathbf{F}_1,\mathbf{F}_2],[\mathbf{F}_1,[\mathbf{F}_1,\mathbf{F}_2]],[\mathbf{F}_2,[\mathbf{F}_1,\mathbf{F}_2]]\right)(\xi,\xi,y,\theta) = T(\xi,y,\theta)\frac{1}{y^{10}} + O\left(\frac{1}{y^{11}}\right),$$

where

$$T(\xi,y,\theta) = -\frac{945}{524288}a^3\sin(\theta)^2\cos(\theta)^2\xi\left(\cos(\theta)^4+8-4\cos(\theta)^2\right)^2.$$

This coefficient does not vanish unless $\theta \notin \{0, \frac{\pi}{2}, \pi, \frac{3\pi}{2}\}$.

We already know from symmetry that when $\theta = \frac{\pi}{2}$ or $\theta = \frac{3\pi}{2}$, one has $d_{(\xi_1,\xi_2,y,\theta)} \leq 3$. Therefore, it remains to understand the case $\theta = 0$ (or π by symmetry). The preceding computation does not allow us to conclude about the dimension of the Lie algebra at such points. Indeed, the 2 first coefficients of the expansion of the determinant vanish, and it might well be the case at all orders. Nevertheless, in that case, we can expand the subdeterminant

$$\Delta = \begin{vmatrix} [\mathbf{F}_1,\mathbf{F}_2]_3 & [\mathbf{F}_1,[\mathbf{F}_1,\mathbf{F}_2]]_3 \\ [\mathbf{F}_1,\mathbf{F}_2]_5 & [\mathbf{F}_1,[\mathbf{F}_1,\mathbf{F}_2]]_5 \end{vmatrix}$$

in order to obtain informations. Indeed, one gets

$$\Delta = \frac{45}{512\,y^4}a^2(\xi_1-\xi_2)\xi_1 R'(\boldsymbol{\xi}) + O\left(\frac{1}{y^5}\right),$$

with,

$$R'(\boldsymbol{\xi}) = \frac{2\xi_2^5+11\xi_1\xi_2^4+16\xi_1^2\xi_2^3+19\xi_1^3\xi_2^2+12\xi_1^4\xi_2+3\xi_1^5}{\left(\xi_1+\xi_2\right)^2\xi_2^2\left(\xi_2^2+\xi_1^2+\xi_1\xi_2\right)^2}.$$

As a direct consequence, we get that the dimension of the Lie algebra, $d_{(\boldsymbol{\xi},y,0)} \geq 4$, for almost every $(\boldsymbol{\xi}, y) \in (\mathbf{R}^+)^3$.

This finishes the proof of Lemma 3.3.6 and thus of Theorem 3.2.2.

Remark 3.5.9 *As usual, it is possible to pass from local to global controllability on each of the connected components where the determinant given by (3.54) does not vanish. More precisely, let* $\mathcal{A} := \big\{(\boldsymbol{\xi}, \mathbf{p})$ *s. t.* $d_{(\boldsymbol{\xi},\mathbf{p})} \leq 4\big\}$*, we define by* $\mathcal{S}_{(\boldsymbol{\xi},\mathbf{p})}$ *the connected component of the subset* $\mathcal{S} \setminus \mathcal{A}$ *which contains* $(\boldsymbol{\xi}, \mathbf{p})$*. Applying Chow's Theorem 3.3.3 on* $\mathcal{S}_{(\boldsymbol{\xi},\mathbf{p})}$*, gives that for every initial configuration* $(\boldsymbol{\xi}^i, \mathbf{p}^i)$*, any final configuration* $(\boldsymbol{\xi}^f, \mathbf{p}^f)$ *in* $\mathcal{S}_{(\boldsymbol{\xi},\mathbf{p})}$*, and any final time* $T > 0$*, there exists a stroke* $\boldsymbol{\xi} \in \mathcal{W}^{1,\infty}([0,T])$*, satisfying* $\boldsymbol{\xi}(0) = \boldsymbol{\xi}^i$ *and* $\boldsymbol{\xi}(T) = \boldsymbol{\xi}^f$ *and such that the self-propelled swimmer starting in position* $\mathbf{p}^i$ *with the shape* $\boldsymbol{\xi}^i$ *at time* $t = 0$*, ends at position* $\mathbf{p}^f$ *and shape* $\boldsymbol{\xi}^f$ *at time* $t = T$ *by changing its shape along* $\boldsymbol{\xi}(t)$ *and staying in* $\mathcal{S}_{(\boldsymbol{\xi},\mathbf{p})}$ *for all time* $t \in [0,T]$*. In other words,* $\mathcal{S}_{(\boldsymbol{\xi},\mathbf{p})}$ *is exactly equal to the orbit of the point* $(\boldsymbol{\xi}, \mathbf{p})$*.*

3.6 Conclusion

The aim of the present paper was to examine how the controllability of low Reynolds number artificial swimmers is affected by the presence of a plane boundary on the fluid. The systems are those classically studied in the literature (see [7] for instance) but are usually not confined. This is the first in-depth control study of how the presence of the plane wall affects the reachable set of a peculiar micro-swimmer.

Firstly, Theorem 3.2.1 shows that the controllability on the whole space implies the controllability in the half space. Although the proof is applied on the Four-sphere swimmer, it is based on general arguments which can be appropriate for any finite dimensional linear control systems.

Secondly, the Theorem 3.2.2 deals with the controllability of the Three-sphere swimmer in the presence of the plane wall. We prove that, at least for this example, the hydrodynamics perturbation due to the wall surprisingly makes the swimmer more controllable. This result is not in contradiction with the several scientific studies which show that the wall seems to attract the swimmer (see [74], [91], [81], [38], [17]). Although, the Theorem 3.2.2 leads to the fact that the wall contributes to increase the swimmer's reachable set, we can conjecture that some of them are easier to reach than others.

The quantitative approach to this question together with the complete understanding of the situation in view of controllability of the underlying systems is far beyond reach and thus still under progress as is, in another direction, the consideration of more complex situations like, e.g. rough or non planar wall. This is the purpose of ongoing work.

Chapitre 4

Rough wall effect on micro-swimmers

Abstract : We study the effect of a rough wall on the controllability of micro-swimmers made of several balls linked by thin jacks: the so-called 3-sphere and 4-sphere swimmers. Our work completes the previous work [11] dedicated to the effect of a flat wall. We show that a controllable swimmer (the 4-sphere swimmer) is not impacted by the roughness. On the contrary, we show that the roughness changes the dynamics of the 3-sphere swimmer, so that it can reach any direction almost everywhere.

4.1 Introduction

Micro-swimming is a subject of growing interest, notably for its biological and medical implications: one can mention the understanding of reproduction processes, the description of infection mechanisms, or the conception of micro-propellers for drug delivery in the body. As regards its mathematical modeling and analysis, the studies by Taylor [84], Lighthill [54] and Purcell [70] have been pioneering contributions to a constantly increasing field: we refer to the recent work of T. Powers and E. Lauga [53] for an extensive bibliography.

Among the many aspects of micro-swimming, the influence of the environment on swimmers dynamics has been recognized by many biological studies (see for instance [17], [68], [81], [82], [74], [91], [92]). One important factor in this dynamics is the presence of confining walls. For example, experiments have shown that some microorganisms, like E. Coli, are attracted to surfaces.

The focus of this paper is *the effect of wall roughness on micro-swimming*. Such effect has been already recognized in the context of microfluidics, in connection with superhydrophobic surfaces ([94]). Moreover, recent studies have highlighted the role of roughness in the dynamics of passive spherical particles in a Stokes flow: we refer for instance to the study of S. H. Rad and A. Najafi [71] or to the one of D. Gérard-Varet and M. Hillairet [43].

We want here to study the impact of a rough wall on the displacement of micro-swimmers, at low Reynolds number. Our point of view will be theoretical, more precisely based on control theory. Connection between swimming at low Reynolds number and control theory has been emphasized over the last years (see [63], [27], [60], [59]). We shall ponder here on the recent studies [7] and [11], dedicated to the controllability analysis of particular Stokesian robots, in the whole space and in the presence of a plane wall respectively. We shall here incorporate roughness at the wall, and focus on two classical models of swimmers: the 3-sphere swimmer (see [47],[8], [7], [11]) and the 4-sphere swimmer (see [7], [11]). First, we will show that the controllability of the 4-sphere swimmer (already true near a flat wall) persists with roughness. Then, we will prove that the rough wall leads the 3-sphere swimmer to reach any space direction. The underlying mechanism is the symmetry-breaking generated by the roughness.

The paper is divided into three parts. In Section 4.2, we introduce the mathematical model for the fluid-swimmer coupling, and we derive from there an ODE for the swimmer dynamics. In Section 4.3, we show that the force field in this ODE is analytic with respect to the roughness amplitude and swimmer size and position. Combining this property with the results of [11] yields the controllability of the 4-sphere swimmer "almost everywhere". Section 4.4 provides an asymptotic expansion of the Dirichlet-to-Neumann operator, with respect to the roughness amplitude and swimmer's size. This operator is naturally involved in the expansion of the force fields. Eventually, we use this expansion and make it truly explicit in Section 4.5, in the special case of the 3-sphere swimmer. This allows us to show its controllability.

4.2 Mathematical setting

In this part, we present our mathematical model for the swimming problem.

4.2.1 Swimmers

We carry on the study of specific swimmers that were considered in [7] in $\mathbf{R}^3$ and in [11] in an half plane. These swimmers consist of N spheres $\cup_{l=1}^{N} B_l$ of radii a connected by k thin jacks which are supposed free of viscous resistance. The position of the swimmer is described by a variable $\mathbf{p} \in \mathbf{R}^3_+ \times SO(3)$, which gives both the coordinates of one point over the swimmer and the swimmer's orientation. Moreover, the shape variable is denoted by a k-tuple $\boldsymbol{\xi}$: its ith component ξ_i gives the length of ith arm, that can stretch or elongate through time. Nevertheless, the directions of the arms are only modified by global rotation of the swimmer. Let us stress that all the variables above depend implicitly on time, through the transport and deformation of the swimmer. Finally, we call $\mathcal{S} \subset \mathbf{R}^M$ (for a suitable $M \in \mathbf{N}$) the set of admissible states $(\boldsymbol{\xi}, \mathbf{p})$. Typically, this admissible set encodes geometrical constraints, like a no-contact condition between the swimmer and the confining wall, or the fact that the balls can not touch each other. We assume that $\mathcal{S}$ is a connected smooth submanifold of $\mathbf{R}^M$.

Many results of our paper apply to the general class of swimmers just described. Nevertheless, we will pay a special attention to two examples:

- *The 4-sphere swimmer.* We consider a regular tetrahedron $(\mathbf{S}_1, \mathbf{S}_2, \mathbf{S}_3, \mathbf{S}_4)$ with center $\mathbf{O} \in \mathbf{R}^3_+$. The 4-sphere swimmer consists of four balls linked by four arms of fixed directions $\vec{\mathbf{OS}}_i$ which are able to elongate and shrink (in a referential associated to the swimmer). The four ball cluster is completely described by the list of parameters $(\boldsymbol{\xi}, \mathbf{p}) = (\xi_1, \ldots, \xi_4, \mathbf{x}_c, \boldsymbol{\mathcal{R}}) \in \mathcal{S} = (\sqrt{\frac{3}{2}}a, \infty)^4 \times \mathbf{R}^3_+ \times SO(3)$. It is known that the 4-sphere swimmer is controllable in $\mathbf{R}^3$ and remains controllable in presence of a plane wall (see [7], [11]). This means that it is able to move to any point and with any orientation under the constraint of being self-propelled, when the surrounding flow is dominated by viscosity (Stokes flow). This swimmer is depicted in Fig. 4.1.

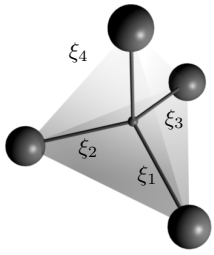

Figure 4.1: The Four-sphere swimmer.

- *The 3-sphere swimmer* (see [66], [8],[7] and [11]). It is composed of three aligned spheres, linked by two arms, see Fig. 3.2. The dynamics of the swimmer is described through the lengths of the two arms ξ_1, ξ_2, the coordinates of the center of the middle ball: $\mathbf{x}_c = (x_c, y_c, z_c)$, and some matrix $\mathcal{R} \in SO(3)$ describing the orientation of the swimmer. Thus,

$$(\boldsymbol{\xi}, \mathbf{p}) = (\xi_1, \xi_2, \mathbf{x}_c, \mathcal{R}) \in \mathcal{S} = (2a, \infty)^2 \times \mathbb{R}^3 \times SO(3).$$

  As regards the position and elongation of the swimmer, the angle of the rotation $\mathcal{R}$ around the symmetry axis of the 3-sphere is irrelevant. As a matter of fact, we will not show controllability for this angle: our result, Theorem 4.2.4, yields controllability

of the swimmer up to rotation around its axis. Still, the associated angular velocity is not zero, and will appear in the dynamics.

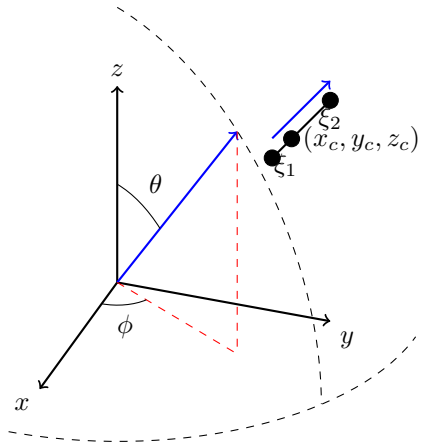

Figure 4.2: Coordinates of the 3-sphere swimmer

4.2.2 Fluid flow

We consider a fluid confined by a rough boundary. This boundary is modelled by a surface with equation $z = \varepsilon h(x, y)$, for some Lipschitz positive function h. Here, $\varepsilon > 0$ denotes the amplitude of the roughness, that is $\|h\|_\infty = 1$. The swimmer evolves in the half-space $\mathcal{O} = \{(x, y, z) \in \mathbf{R}^3 \text{ s. t. } z > \varepsilon h(x, y)\}$. The fluid domain is then $\mathcal{F} := \mathcal{O} \setminus \cup_{l=1}^N B_l$, and again it depends implicitly on time. Finally, we assume that the flow is governed there by the Stokes equation. Thus, the velocity $\mathbf{u}^S$ and the pressure p^S of the fluid satisfy:

$$-\mu\Delta\mathbf{u}^S + \nabla p^S = 0\,, \quad \text{div } \mathbf{u}^S = 0 \quad \text{in } \mathcal{F}, \tag{4.1}$$

where μ is the viscosity of the fluid. We complement the Stokes equation (4.1) by standard no-slip boundary conditions, that read:

$$\begin{cases} \mathbf{u}^S = \Omega \times (\mathbf{x} - \mathbf{x}_c) + \mathbf{v} + \mathbf{u}_d & \text{at } \cup_{l=1}^N \partial B_l, \\ \mathbf{u}^S = 0 & \text{at } \partial\mathcal{O}. \end{cases} \tag{4.2}$$

In other words, we impose the continuity of the velocity both at the fixed wall and at the boundary of the moving swimmer. Note that the velocity field of the swimmer is made of two parts:

- one corresponding to an (unknown) rigid movement, with angular velocity Ω and linear velocity $\mathbf{v}$. If $\mathbf{x}_c$ is the point over the swimmer encoded in $\mathbf{p}$, the velocity $\mathbf{v}$ is its speed. The vector $(\Omega, \mathbf{v})^t$ can be identified with $\dot{\mathbf{p}}$ (everything will be made explicit in due course).
- one corresponding to the (known) deformation of the jacks, with associated velocity $\mathbf{u}^d$, depending on $\dot{\boldsymbol{\xi}}$.

Introducing the Hilbert space

$$\mathcal{V} = \left\{ \mathbf{u} \in \mathcal{D}'(\mathcal{F}, \mathbf{R}^3) \,|\, \nabla\mathbf{u} \in L^2(\mathcal{F}),\ \frac{\mathbf{u}(\mathbf{r})}{\sqrt{1 + |\mathbf{r}|^2}} \in L^2(\mathcal{F}) \right\}, \tag{4.3}$$

we get (for any configuration of the swimmer $\cup B_l$ and velocities $(\Omega, \mathbf{v}, \mathbf{u}^d)$) a unique solution $(\mathbf{u}^S, p^S)$ of (4.1) -(4.2) in $\mathcal{V} \times L^2(\mathcal{F})$.

4.2.3 Dynamics

Of course, the previous relations describe the equilibrium of the fluid flow at any given instant t. To close the model (that is the fluid-swimmer coupling), we still need to specify the dynamics of the swimmer, based on Newton's laws. The description is by now classical (see for instance [7], [59]), and can be expressed by an affine control system without drift. Let us recall the principle of derivation. Neglecting inertia, Newton's laws become

$$\left\{ \begin{array}{l} \displaystyle\sum_{l=1}^{N} \int_{\partial B_l} \boldsymbol{\sigma}(\mathbf{u}^S, p^S) \cdot \mathbf{n} \, \mathrm{d}s = 0 \,, \\ \displaystyle\sum_{l=1}^{N} \int_{\partial B_l} \boldsymbol{\sigma}(\mathbf{u}^S, p^S) \cdot \mathbf{n} \times (\mathbf{x} - \mathbf{x}_c) \, \mathrm{d}s = 0 \,, \end{array} \right. \tag{4.4}$$

where $\boldsymbol{\sigma}(\mathbf{u}, p) = \mu(\nabla \mathbf{u} + \nabla^t \mathbf{u}) - p\mathbf{Id}$ is the Cauchy tensor.

Moreover, if we introduce an orthonormal basis $(\mathbf{e}_1, \mathbf{e}_2, \mathbf{e}_3)$ and use linearity, $\mathbf{u}^S$ decomposes into

$$\mathbf{u}^S = \sum_{i=1}^{3} \Omega_i \mathbf{u}_i + \sum_{i=4}^{6} v_{i-3} \mathbf{u}_i \, + \mathbf{u}^d. \tag{4.5}$$

Here, the $\mathbf{u}_i$'s and $\mathbf{u}^d$ are solutions of the Stokes equation, with zero Dirichlet condition at the wall, and inhomogeneous Dirichlet conditions at the ball. The Dirichlet data is $\mathbf{e}_i \times (\mathbf{x} - \mathbf{x}_c)$ for $i = 1, 2, 3$, $\mathbf{e}_{i-3}$ for $i = 4, 5, 6$, $\mathbf{u}_d$ for $\mathbf{u}^d$. Note also that the speed $\mathbf{u}^d$ can be expressed as a linear combination of $(\dot{\xi}_i)_{i=1}^k$:

$$\mathbf{u}^d = \sum_{i=1}^{k} \mathbf{u}_i^d \dot{\xi}_i. \tag{4.6}$$

Identifying $(\Omega, \mathbf{v})^t$ with $\dot{\mathbf{p}}$ (everything will be made explicit in due course), the system (4.4) reduces to the following ODE:

$$\mathbf{M}(\boldsymbol{\xi}, \mathbf{p}) \, \dot{\mathbf{p}} + \mathbf{N}(\boldsymbol{\xi}, \mathbf{p}) = 0 \tag{4.7}$$

where the matrix $\mathbf{M}(\boldsymbol{\xi}, \mathbf{p})$ is defined by,

$$\mathbf{M}_{i,j}(\boldsymbol{\xi}, \mathbf{p}) := \left\{ \begin{array}{l} \displaystyle\sum_{l=i}^{N} \int_{\partial B_l} ((\mathbf{x} - \mathbf{x}_c) \times \mathbf{e}_i) \cdot \boldsymbol{\sigma}(\mathbf{u}_j, p_j) \, \mathbf{n} \, \mathrm{d}s \quad (1 \le i \le 3, 1 \le j \le 6) \,, \\ \displaystyle\sum_{i=i}^{N} \int_{\partial B_l} \mathbf{e}_{i-3} \cdot \boldsymbol{\sigma}(\mathbf{u}_j, p_j) \, \mathbf{n} \, \mathrm{d}s \quad (4 \le i \le 6, 1 \le j \le 6) \,, \end{array} \right.$$

and $\mathbf{N}(\boldsymbol{\xi}, \mathbf{p})$ is the vector of $\mathbb{R}^6$ whose entries are,

$$\mathbf{N}_i(\boldsymbol{\xi}, \mathbf{p}) := \left\{ \begin{array}{l} \displaystyle\sum_{l=1}^{N} \int_{\partial B_l} ((\mathbf{x} - \mathbf{x}_c) \times \mathbf{e}_i) \cdot \boldsymbol{\sigma}(\mathbf{u}^d, p^d) \, \mathbf{n} \, \mathrm{d}s \quad (1 \le i \le 3) \,, \\ \displaystyle\sum_{l=1}^{N} \int_{\partial B_l} \mathbf{e}_{i-3} \cdot \boldsymbol{\sigma}(\mathbf{u}^d, p^d) \, \mathbf{n} \, \mathrm{d}s \quad (4 \le i \le 6) \,. \end{array} \right.$$

The matrix $\mathbf{M}(\boldsymbol{\xi}, \mathbf{p})$ is checked to be symmetric and negative definite. By inverting it in (4.7), we end up with the following relation for the swimmer's dynamics:

$$\dot{\mathbf{p}} = -\mathbf{M}^{-1}(\boldsymbol{\xi}, \mathbf{p})\mathbf{N}(\boldsymbol{\xi}, \mathbf{p})\,. \tag{4.8}$$

By using (4.6), we deduce that there are vector fields $\mathbf{F}_i$, $i = 1..k$, such that the equation (4.8) reads

$$\dot{\mathbf{p}} = \sum_{i=1}^{k} \mathbf{F}_i(\boldsymbol{\xi}, \mathbf{p})\dot{\xi}_i\,. \tag{4.9}$$

4.2.4 Main results

Before turning to our mathematical analysis, we synthetize here our main results.

The controllability properties of the swimmers will follow from a careful study of the properties of the $\mathbf{F}_i$'s in (4.9). As a first consequence of this study, we will obtain the analyticity of these vector fields with respect to all parameters: the typical height of the roughness ε, the radius of the balls a, the vector of arms lengths $\boldsymbol{\xi}$ and the position of the swimmer p. More precisely, defining

$$\mathcal{A} := \{(\varepsilon, a, \boldsymbol{\xi}, \mathbf{p}) \in \mathbb{R} \times \mathbb{R}_+^* \times (\mathbb{R}_+^*)^k \times (\mathbb{R}^3 \times SO(3)) \text{ such that } B_i \cap B_j = \emptyset\ \forall i \neq j, \text{ and } B_i \cap \partial\mathcal{O} = \emptyset\ \forall i\},$$

we have the following

Theorem 4.2.1 *For all $i = 1 \dots k$, the field $\mathbf{F}^i(\boldsymbol{\xi}, p)$ (which depends also implicitly on ε and a) is an analytic function of $(\varepsilon, a, \boldsymbol{\xi}, p)$ over $\mathcal{A}$.*

Then, as a consequence of Theorem 4.2.1, we will prove that the roughness does not change the controllability of the 4-sphere swimmer. We restrict here to local controllability "almost everywhere": this terminology refers to the following

Definition 4.2.2 ("almost everywhere") *We say that a property holds for almost every $(\varepsilon, a, \boldsymbol{\xi}, \mathbf{p})$ in $\mathcal{A}$ if it holds for all $(\varepsilon, a, \boldsymbol{\xi}, \mathbf{p})$ outside the zero set of a (non-trivial) analytic function over $\mathcal{A}$.*

We have

Theorem 4.2.3 *The 4-sphere swimmer is controllable almost everywhere, in the following sense: for almost every $(\varepsilon, a, \boldsymbol{\xi}^i, \mathbf{p}^i)$, with $(\boldsymbol{\xi}^i, \mathbf{p}^i) \in \mathcal{S}$, one has local controllability from the initial configuration $(\boldsymbol{\xi}^i, \mathbf{p}^i)$. This means that for any final configuration $(\boldsymbol{\xi}^f, \mathbf{p}^f)$ in a suitable neighborhood of $(\boldsymbol{\xi}^i, \mathbf{p}^i)$ and any final time $T > 0$, there exists a stroke $\boldsymbol{\xi} \in \mathcal{W}^{1,\infty}([0, T])$, satisfying $\boldsymbol{\xi}(0) = \boldsymbol{\xi}^i$ and $\boldsymbol{\xi}(T) = \boldsymbol{\xi}^f$ and such that if the self-propelled swimmer starts in position $\mathbf{p}^i$ with the shape $\boldsymbol{\xi}^i$ at time $t = 0$, it ends at position $\mathbf{p}^f$ and shape $\boldsymbol{\xi}^f$ at time $t = T$ by changing its shape along $\boldsymbol{\xi}(t)$.*

In the last Section 4.5, we shall address the controllability of the 3-sphere swimmer. In the case of a flat boundary, as shown in [11], symmetries constrain the swimmer to move in a plane. Also, it does not rotate around its own axis. As we will see, the roughness at the wall breaks (in general) such symmetries, allowing for local controllability almost everywhere. Let us point here a subtlety regarding our controllability result. To express the dynamics of the swimmer through the equation (4.9), we have included in variable $\mathbf{p}$ (more precisely in its $SO(3)$ component) an angle describing rotation of the 3-sphere around its own axis. We are not able to show controllability for this angle: we only show controllability for the other components of $\mathbf{p}$. Of course, this is not a problem with regards to the effective movement of the swimmer: this angle is indeed irrelevant with regards to the swimmer's orientation and position. The analysis of Section 4.5 leads to the

Theorem 4.2.4 *There exists a surface $h \in C_c^\infty(\mathbb{R}^2)$ such that the 3-sphere swimmer is locally controllable almost everywhere (up to rotation around its axis).*

Refined statements will be provided in Section 4.5. This controllability result requires a careful asymptotic asymptotic expansion of the force fields $\mathbf{F}^i$. This expansion is related to an expansion of a Dirichlet-to-Neumann map, performed in section 4.4. Eventually, the dimension of the Lie algebra generated by the force fields is computed numerically, and the controllability result follows from application of Chow's theorem.

4.3 Analyticity of the dynamics

4.3.1 Regularity

This paragraph is devoted to the proof of Theorem 4.2.1. Let $\overline{\mathbf{Y}} = (\overline{\varepsilon}, \overline{a}, \overline{\boldsymbol{\xi}}, \overline{\mathbf{p}}) \in \mathcal{A}$. We must prove analyticity of the $\mathbf{F}^i$'s with respect to $\mathbf{Y} = (\varepsilon, a, \boldsymbol{\xi}, \mathbf{p})$, in a neighborhood of $\overline{\mathbf{Y}}$. It will follow from the analyticity of $\mathbf{M}$ and $\mathbf{N}$ defined after (4.7). Their definitions involve functionals of the type

$$\mathbf{I} := \sum_{l=1}^{N} \int_{\partial B_l} \left(\begin{smallmatrix} 1 \\ \mathbf{x} \end{smallmatrix}\right) \otimes \sigma(\mathbf{u}, p) n \, ds$$

where $(\mathbf{u}, p)$ satisfies the Stokes equation in $\mathcal{F}$, with Dirichlet conditions of the type:

$$\mathbf{u} = 0 \quad \text{at } \partial\mathcal{O}, \quad \mathbf{u} = \mathbf{u}_l \quad \text{at } \partial B_l, \quad l = 1, \dots, N$$

for some family of rigid fields $\mathbf{u}_l$'s taken in the "elementary set" $\{\mathbf{e}_i \times \mathbf{x}, \mathbf{e}_i,\ i = 1...3\}$.

We denote by $\mathbf{x}_l$, resp. $\overline{\mathbf{x}}_l$ the center of the ball B_l, resp. the center of the ball $\overline{B}_l$ corresponding to $\overline{\mathbf{Y}}$. We introduce the diffeomorphisms

$$\varphi_l(\mathbf{x}) := \frac{a}{\overline{a}}(\mathbf{x} - \overline{\mathbf{x}}_l) + \mathbf{x}_l.$$

Then, we have

$$\int_{\partial B_l} \left(\begin{smallmatrix} 1 \\ \mathbf{x} \end{smallmatrix}\right) \otimes \sigma(\mathbf{u}, p) n \, ds = \left(\frac{a}{\overline{a}}\right)^2 \int_{\partial \overline{B}_l} \left(\begin{smallmatrix} 1 \\ \varphi_l(\mathbf{x}) \end{smallmatrix}\right) \otimes \sigma(\mathbf{u} \circ \varphi_l, p \circ \varphi_l) n \, ds.$$

Hence, in order to prove Theorem 4.2.1, it is enough to show that for all $l = 1...N$, for $\delta, \eta > 0$ small enough:

$$B(\overline{\mathbf{Y}}, \delta) \mapsto H^1\left(\mathcal{F} \cap B(\overline{\mathbf{x}}_l, a + \eta)\right) \times L^2\left(\mathcal{F} \cap B(\overline{\mathbf{x}}_l, a + \eta)\right), \quad \mathbf{Y} \mapsto (\mathbf{u} \circ \varphi_l, p \circ \varphi_l)$$

is analytic. Indeed, $\mathbf{Y} \mapsto \sigma(\mathbf{u} \circ \varphi_l, p \circ \varphi_l)$ will be analytic with values in $H^{-1/2}(\partial B_l)$, and the surface integral will be analytic as well.

Therefore, we define the change of variable

$$\varphi(\mathbf{x}) = \mathbf{x} + \sum_l \chi(\mathbf{x} - \overline{\mathbf{x}}_l)\left(\varphi_l(\mathbf{x}) - \mathbf{x}\right) + (\varepsilon - \overline{\varepsilon})\chi_h(\mathbf{x})(0, 0, h(x_1, x_2))$$

with $\chi, \chi_h \in C_c^\infty(\mathbb{R}^3)$, $\chi = 1$ near $B(0, \overline{a})$, $\chi_h = 1$ near $x_3 = h(x_1, x_2)$. For χ and χ_h with small enough supports, and for $\mathbf{Y} \in B(\overline{\mathbf{Y}}, \delta)$, $\delta > 0$ small enough, it is easily seen that φ is a smooth diffeomorphism, which depends analytically on $\mathbf{Y}$, and such that $\varphi(\overline{\mathcal{F}}) = \mathcal{F}$. Moreover, one has $\varphi = \varphi_l$ in a small enough δ'-neighborhood of $\overline{B}_l$. Introducing $\mathbf{U} := \mathbf{u} \circ \varphi$

and $P := p \circ \varphi$, it remains to prove the following

Claim: $\mathbf{Y} \mapsto \mathbf{U}$ is analytic from $B(\bar{\mathbf{Y}}, \delta)$ to $\overline{\mathcal{V}}_0$, where

$$\overline{\mathcal{V}}_0 := \left\{ \mathbf{U} \in \mathcal{D}'(\overline{\mathcal{F}}, \mathbf{R}^3) \,|\, \nabla \mathbf{U} \in L^2(\overline{\mathcal{F}}),\ \frac{\mathbf{U}(\mathbf{r})}{\sqrt{1+|\mathbf{r}|^2}} \in L^2(\overline{\mathcal{F}}), \quad \mathbf{U}|_{\partial\bar{\mathcal{O}}} = 0. \right\}.$$

To prove this claim, one first needs to write down the system satisfied by $\mathbf{U}, P$. A simple computation yields

$$\begin{cases} -\text{ div } (A\nabla \mathbf{U}) + B\nabla P = 0 & \text{in } \overline{\mathcal{F}}, \\ \text{div } (B^t \mathbf{U}) = 0 & \text{in } \overline{\mathcal{F}}, \\ \mathbf{U} = 0 \quad \text{at } \partial\overline{\mathcal{O}}, \quad \mathbf{U} = \mathbf{U}_l \quad \text{at } \partial\overline{\mathcal{B}}_l, \end{cases} \tag{4.10}$$

where

$$A = A(\mathbf{x}) := |\det \nabla\phi(\mathbf{x})| (\nabla\phi^{-1})^t (\nabla\phi^{-1})(\phi(\mathbf{x})),$$
$$B = B(\mathbf{x}) := |\det \nabla\phi(\mathbf{x})| (\nabla\phi^{-1})(\phi(\mathbf{x})), \quad \mathbf{U}_l := \mathbf{u}_l \circ \varphi_l.$$

Note that $A, B, \mathbf{U}_l$ depend analytically on the parameter $\mathbf{Y}$. We now consider the mapping

$$\mathcal{L}: \ B(\overline{\mathbf{Y}}, \delta) \times \overline{\mathcal{V}}_0 \times L^2(\overline{\mathcal{F}}) \ \mapsto \ \big(\overline{\mathcal{V}}_0\big)' \times L^2(\overline{\mathcal{F}}) \times \prod_l H^{1/2}(\partial\overline{B}_l),$$
$$(\mathbf{Y}, \mathbf{V}, Q) \mapsto \big(-\text{ div } (A\nabla\mathbf{V}) + B\nabla Q,\ \text{div } (B^t\mathbf{V}), \big(\mathbf{V}|_{\partial\overline{\mathcal{B}}_l} - \mathbf{U}_l\big)_{l=1}^N\big).$$

$\mathcal{L}$ is clearly well-defined, and it is analytic in $(\mathbf{Y}, \mathbf{V})$: we refer to [89] for the definition of analytic functions over Banach spaces. Moreover, $\mathbf{U} = \mathbf{U}_{\mathbf{Y}}$ and $P = P_{\mathbf{Y}}$ satisfy

$$\mathcal{L}(\mathbf{Y}, \mathbf{U}, P) = 0$$

By the analytic version of the implicit function theorem, see again [89], $\mathbf{U}$ and P will be analytic in $\mathbf{Y}$ near $\overline{\mathbf{Y}}$ if

$$\frac{\partial \mathcal{L}}{\partial(\mathbf{V}, Q)}|_{(\overline{\mathbf{Y}}, \mathbf{U}, P)} \text{ is an isomorphism from } \overline{\mathcal{V}}_0 \times L^2(\overline{\mathcal{F}}) \text{ to } \big(\overline{\mathcal{V}}_0\big)' \times L^2(\overline{\mathcal{F}}) \times \prod_l H^{1/2}(\partial\overline{B}_l).$$

In other words, analyticity of $\mathbf{U}$ and P follows from the existence and uniqueness in $\overline{\mathcal{V}}_0 \times L^2(\overline{\mathcal{F}})$ of a solution $(\mathbf{V}, Q)$ for the Stokes system

$$\begin{aligned} -\Delta\mathbf{V} + \nabla Q = \mathbf{F} \quad & \text{in } \overline{\mathcal{F}}, \\ \text{div } \mathbf{V} = G \quad & \text{in } \overline{\mathcal{F}}, \\ \mathbf{V} = 0 \quad \text{at } \partial\overline{\mathcal{O}}, \quad \mathbf{V} = \mathbf{V}_l \quad & \text{at } \partial\overline{B}_l, \quad l = 1...N \end{aligned}$$

where $\mathbf{F} \in \big(\overline{\mathcal{V}}_0\big)'$, $G \in L^2(\overline{\mathcal{F}})$ and $\mathbf{V}_l \in H^{1/2}(\partial\overline{B}_l)$ are prescribed data. Such well-posedness is proved in the appendix. This ends the proof of Theorem 4.2.1.

4.3.2 Application to the 4-sphere swimmer

From the analyticity shown above and the results of [11], we can deduce Theorem 4.2.3. First, by (4.9), we can write the swimmer's dynamics as

$$\begin{pmatrix} \dot{\boldsymbol{\xi}} \\ \dot{\mathbf{p}} \end{pmatrix} = \sum_{i=1}^{4} \mathbf{G}_i \left(\begin{pmatrix} \boldsymbol{\xi} \\ \mathbf{p} \end{pmatrix} \right) u_i$$

where $(u_i := \dot{\xi}_i)_{i=1}^4$ is the family of controls, and $\mathbf{G}_i := \begin{pmatrix} \mathbf{e}_i \\ \mathbf{F}_i \end{pmatrix}$ ($(\mathbf{e}_1, ..., \mathbf{e}_4)$ is the canonical basis of $\mathbb{R}^4$). By the analyticity of the $\mathbf{G}_i$'s and Chow's theorem, it is then enough to prove that for some $(\varepsilon, a, \boldsymbol{\xi}, \mathbf{p}) \in \mathbb{R}_+ \times \mathbb{R}_+^* \times \mathcal{S}$,

$$\dim Lie_{(\boldsymbol{\xi},\mathbf{p})}(\mathbf{G}_1, ..., \mathbf{G}_{10}) = 10.$$

We write

$$\partial^\alpha \mathbf{G}_i(\boldsymbol{\xi}, \mathbf{p}) = \partial^\alpha \mathbf{G}_i^0(\boldsymbol{\xi}, \mathbf{p}) \ + \ O(\varepsilon), \quad \forall \alpha \in \mathbb{N}^7,$$

where the $\mathbf{G}_i^0$'s are force fields corresponding to the flat case $h = 0$. In particular, for ε small enough

$$\dim Lie_{(\boldsymbol{\xi},\mathbf{p})}(\mathbf{G}_1, ..., \mathbf{G}_{10}) \ \geq \ \dim Lie_{(\boldsymbol{\xi},\mathbf{p})}(\mathbf{G}_1^0, ..., \mathbf{G}_{10}^0).$$

But from [11] we know that for almost every $(a, \boldsymbol{\xi}, \mathbf{p})$

$$\dim Lie_{(\boldsymbol{\xi},\mathbf{p})}(\mathbf{G}_1^0, ..., \mathbf{G}_{10}^0) = 10.$$

This concludes the proof.

4.4 Asymptotic expansion of the Dirichlet-to-Neumann

We now turn to the controllability properties of the 3-sphere swimmer. As before, the key point is to determine the dimension of the Lie algebra generated by the force fields $\mathbf{F}^i$. Therefore, we need to derive an asymptotic expansion of the $\mathbf{F}^i$'s, in a and ε.

A preliminary step is to derive an asymptotic expansion of the so-called Dirichlet-to-Neumann map of the Stokes operator. Indeed, the force fields $\mathbf{F}^i$ involve this map: that is, the definition of the coefficients $\mathbf{M}_{ij}$ and $\mathbf{N}_i$ involves

$$DN : \prod_{l=1}^N H^{1/2}(\partial B_l) \mapsto \prod_{l=1}^N H^{-1/2}(\partial B_l), \quad (\mathbf{u}_l) \mapsto (\mathbf{f}_l \ := \ \sigma(\mathbf{u}, p)n|_{\partial B_l}),$$

where $(\mathbf{u}, p)$ is the solution of the Stokes equation

$$-\Delta \mathbf{u} + \nabla p = 0, \quad \text{div } \mathbf{u} = 0 \quad \text{in } \mathcal{F}, \quad \mathbf{u}|_{\partial \mathcal{O}} = 0, \quad \mathbf{u}|_{\partial B_l} = \mathbf{u}_l.$$

More precisely, it involves *DN in restriction to N-uplets of rigid vector fields over B_l*, $l = 1...N$. We denote by R the (finite-dimensional) space of such N-uplets.

Even restricted to R, this operator is not very explicit: to derive directly an expansion in terms of the parameters of the swimmer and wall is not easy. Hence, we follow the same path as in [7, 11]: we write that for all $(\mathbf{u}_l)_{l=1}^N \in R$,

$$DN\left((\mathbf{u}_l)\right) \ = \ T^{-1}\left((\mathbf{u}_l)\right)$$

where

$$T : \prod_{l=1}^N H^{-1/2}(\partial B_l) \mapsto \prod_{l=1}^N H^{1/2}(\partial B_l), \quad (\mathbf{f}_l) \mapsto (\mathbf{u}_l \ := \ \mathbf{u}|_{\partial B_l})$$

and $\mathbf{u}$ is the solution of the following Stokes system in $\mathcal{O}$:

$$-\Delta \mathbf{u} + \nabla p \ = \ \sum_{l=1}^N 1_{\partial B_l} \mathbf{f}_l, \quad \text{div } \mathbf{u} = 0 \quad \text{in} \quad \mathcal{O}, \quad \mathbf{u}|_{\partial \mathcal{O}} = 0.$$

Equivalently, this last system can be written:

$$-\Delta \mathbf{u} + \nabla p = 0, \quad \text{div } \mathbf{u} = 0 \quad \text{in} \quad \mathcal{O} \setminus \cup_l \partial B_l, \quad [\mathbf{u}]|_{\partial B_l} = 0, \quad [\sigma(\mathbf{u}, p)n]|_{\partial B_l} = \mathbf{f}_l,$$

where $[]|_{\partial B_l}$ denotes the jump across ∂B_l. Let us remind that $\mathcal{O} = \{z > \varepsilon h(x, y)\}$ is the domain without the balls. In particular, the operator T (associated to a transmission condition) is not the Neumann-to-Dirichlet operator. The latter one would correspond to the Stokes problem

$$-\Delta \mathbf{u} + \nabla p = 0, \quad \text{div } \mathbf{u} = 0 \quad \text{in} \quad \mathcal{O} \setminus \cup_l B_l, \quad \sigma(\mathbf{u}, p)n|_{\partial B_l} = \mathbf{f}_l,$$

associated to a Neumann type condition. However, *in restriction to the space R, the operators DN and T^{-1} coincide*, due to the fact that a rigid vector field is a solution of the Stokes equation, with zero pressure and zero stress tensor.

The advantage of T over the Neumann-to-Dirichlet operator is its more explicit representation. Indeed, one has for all $i = 1...N$

$$T(\mathbf{f})_i(\mathbf{x}) \; = \; \sum_{l=1}^{n} \int_{\partial B_l} \mathbf{K}^{\varepsilon}(\mathbf{x}, \mathbf{y}) \mathbf{f}_l(\mathbf{y}) d\mathbf{y}, \quad \mathbf{x} \in \partial B_i,$$

where the kernel $\mathbf{K}^{\varepsilon}$ is simply the Green function associated to the Stokes equation in $\mathcal{O}$: in other words, $(\mathbf{K}^{\epsilon}, \mathbf{q}^{\epsilon})$ is the solution of the problem:

$$\begin{cases} -\mu \Delta_{\mathbf{x}} \mathbf{K}^{\epsilon}(\mathbf{x}, \mathbf{x}_0) + \nabla_{\mathbf{x}} \mathbf{q}^{\epsilon}(\mathbf{x}) = \delta_{\mathbf{x}_0}(\mathbf{x}) \, \mathbf{I}, \quad \mathbf{x} \text{ in } \mathcal{O}, \\ \text{div}_{\mathbf{x}} \, \mathbf{K}^{\varepsilon}(\mathbf{x}, \mathbf{x}_0) = 0, \quad \mathbf{x} \text{ in } \mathcal{O}, \\ \mathbf{K}^{\epsilon}(\mathbf{x}, \mathbf{x}_0) = 0 \quad \mathbf{x} \text{ on } \partial \mathcal{O}, \end{cases} \tag{4.11}$$

where $\mathbf{I}$ stands for the identity matrix. This will make easier the derivation of an asymptotic expansion, through an expansion of T. Still, there is one little technical difficulty: the domain of definition and range of T, that are $\prod_l H^{\pm 1/2}(\partial B_l)$ depend on the parameter a (and also on $(\mathbf{p}, \boldsymbol{\xi})$). Let us denote $B := B(0, 1)$ the unit ball, and $H_N^{\pm 1/2} := \left(H^{\pm 1/2}(\partial B)\right)^N$. We introduce

$$\phi : \prod_{l=1}^{N} H^{1/2}(\partial B_l) \to H_N^{1/2}, \quad \mathbf{u} = (\mathbf{u}_l) \mapsto \mathbf{U} = (\mathbf{U}_l : \mathbf{r} \mapsto \mathbf{u}_l(\mathbf{x}_l + a\mathbf{r})),$$

as well as the adjoint map

$$\phi^* : H_N^{-1/2} \to \prod_{l=1}^{N} H^{-1/2}(\partial B_l), \quad \mathbf{F} = (\mathbf{F}_l) \mapsto \mathbf{f} = (\mathbf{f}_l),$$

defined through the duality relation: $< \phi^*(\mathbf{F}), \mathbf{u} > = < \mathbf{F}, \phi(\mathbf{u}) >$. Finally, we set $\mathcal{T} := \phi \circ T \circ \phi^* : H_N^{-1/2} \mapsto H_N^{1/2}$. We shall use $\mathcal{T}$ rather than T to compute the expansion of the force field in section 4.5.2. Note that $\mathcal{T}$ depends implicitly on ε, a and on $(\mathbf{p}, \boldsymbol{\xi})$. *In what follows, we will always consider configurations in which the swimmer stays away from the rough wall:*

$$dist(B_l, \partial \mathcal{O}) \geq \delta > 0, \quad \forall l = 1...N, \tag{4.12}$$

for some given δ.

4.4.1 Expansion for small ε

Under the constraint (4.12), we prove

Proposition 4.4.1

$$\mathcal{T} \,:=\, \mathcal{T}^0 \,+\, \varepsilon\mathcal{T}^1 \,+\, O(\varepsilon^2) \quad \textit{in} \quad \mathcal{L}(H_N^{-1/2}, H_N^{1/2})$$

where $\mathcal{T}^0$ and $\mathcal{T}^1$ are defined in (4.20) *and* (4.21)-(4.22) *respectively.*

Proof. For $\mathbf{f} = (\mathbf{f}_l) \in H_N^{-1/2}$, we can write

$$\mathcal{T}(\mathbf{f})_i(r) \,=\, \sum_j \int_{\partial B} \mathbf{K}^\varepsilon(x_i + a\mathbf{r}, x_j + a\mathbf{s})\mathbf{f}_j(\mathbf{s})d\mathbf{s}$$

(with a classical and slightly abusive notation: the integral should be understood as a duality bracket). Thus, the whole point is to expand the kernel $\mathbf{K}^\varepsilon$ defined in (4.11). Of course, the first term should be $\mathbf{K}^0$, that is the Green function in the flat case. This Green function can be computed in terms of the Stokeslet by the method of images (see [20]): one has

$$\mathbf{K}^0(\mathbf{r}, \mathbf{r}_0) = \mathbf{G}(\mathbf{r} - \mathbf{r}_0) + \mathbf{K}_1(\mathbf{r}, \mathbf{r}_0) + \mathbf{K}_2(\mathbf{r}, \mathbf{r}_0) + \mathbf{K}_3(\mathbf{r}, \mathbf{r}_0)\,, \tag{4.13}$$

the four functions $\mathbf{G}$, $\mathbf{K}_1$, $\mathbf{K}_2$ and $\mathbf{K}_3$ being respectively the Stokeslet

$$\mathbf{G}(\mathbf{r}) = \frac{1}{8\pi\mu}\left(\frac{\mathbf{Id}}{|\mathbf{r}|} + \frac{\mathbf{r}\otimes\mathbf{r}}{|\mathbf{r}|^3}\right) \tag{4.14}$$

and the three "images"

$$\mathbf{K}_1(\mathbf{r}, \mathbf{r}_0) = -\frac{1}{8\pi\mu}\left(\frac{\mathbf{Id}}{|\mathbf{r}'|} + \frac{\mathbf{r}'\otimes\mathbf{r}'}{|\mathbf{r}'|^3}\right), \tag{4.15}$$

$$K_{2,ij}(\mathbf{r}, \mathbf{r}_0) = \frac{1}{4\pi\mu} z_0^2\,(1 - 2\delta_{j3})\left(\frac{\delta_{ij}}{|\mathbf{r}'|^3} - \frac{3r'_i r'_j}{|\mathbf{r}'|^5}\right), \tag{4.16}$$

$$K_{3,ij}(\mathbf{r}, \mathbf{r}_0) = -\frac{1}{4\pi\mu} z_0\,(1 - 2\delta_{j3})\left(\frac{r'_3}{|\mathbf{r}'|^3}\delta_{ij} - \frac{r'_j}{|\mathbf{r}'|^3}\delta_{i3} + \frac{r'_i}{|\mathbf{r}'|^3}\delta_{j3} - \frac{3r'_i r'_j r'_3}{|\mathbf{r}'|^5}\right). \tag{4.17}$$

Here $\mathbf{r}_0 = (x_0, y_0, z_0)$ and $\mathbf{r}' = \mathbf{r} - \tilde{\mathbf{r}}_0$, where $\tilde{\mathbf{r}}_0 = (x_0, y_0, -z_0)$ stands for the "image" of $\mathbf{r}_0$, that is to say, the point symmetric to $\mathbf{r}_0$ with respect to the flat wall.

We now consider $\mathbf{u}^\varepsilon(\mathbf{x}, \mathbf{x}_0) = \mathbf{K}^\varepsilon(\mathbf{x}, \mathbf{x}_0) - \mathbf{K}^0(\mathbf{x}, \mathbf{x}_0)$, for $\mathbf{x}_0 \in \cup_l B_l$. As a function of $\mathbf{x}$, it satisfies the Stokes equation in $\mathcal{O}$:

$$-\Delta\mathbf{u}^\varepsilon(\,\cdot\,, \mathbf{x}_0) + \nabla\mathbf{p}(\,\cdot\,, \mathbf{x}_0) = 0, \qquad \text{div}\ \mathbf{u}^\varepsilon(\,\cdot\,, \mathbf{x}_0) = 0 \quad \text{in}\ \mathcal{O}$$

with Dirichlet condition

$$\mathbf{u}^\varepsilon(\,\cdot\,, \mathbf{x}_0) = -\mathbf{K}^0(\,\cdot\,, \mathbf{x}_0), \quad \text{at} \quad \partial\mathcal{O}.$$

We can then expand the boundary data: for $\mathbf{x} = (x, y, \varepsilon h(x, y)) \in \mathcal{O}$

$$-\mathbf{K}^0(\mathbf{x}, \mathbf{x}_0) \,=\, -\sum_{k=1}^{n} \varepsilon^k \frac{h(x,y)^k}{k!}\partial_z^k \mathbf{K}^0(x, y, 0, \mathbf{x}_0) \,+\, O(\varepsilon^{n+1}).$$

More precisely, under the constraint (4.12), one has

$$\| - \mathbf{K}^0(\,\cdot\,, x_0) + \sum_{k=1}^{n} \varepsilon^k \left(\mathbf{x} \mapsto \frac{h(x,y)^k}{k!}\partial_z^k \mathbf{K}^0(x, y, 0, \mathbf{x}_0)\right) \|_{H^s(\partial\mathcal{O})} \,\le\, C_{\delta,s}\,\varepsilon^{n+1}, \quad \forall\, s.$$

We deduce from this inequality that

$$\|\nabla\big(\mathbf{u}^\varepsilon(\,\cdot\,,\mathbf{x}_0)-\sum_{k=1}^{n}\varepsilon^k\mathbf{u}^k(\,\cdot\,,\mathbf{x}_0)\big)\|_{L^2(\mathcal{O})}\ \le\ C\varepsilon^{n+1} \tag{4.18}$$

where $\mathbf{u}^k$ is the solution of

$$-\Delta\mathbf{u}^k(\,\cdot\,,\mathbf{x}_0)+\nabla\mathbf{p}(\,\cdot\,,\mathbf{x}_0)=0,\quad \text{div }\mathbf{u}^k(\,\cdot\,,\mathbf{x}_0)=0\quad\text{in}\quad\mathcal{O},$$
$$\mathbf{u}^k(\mathbf{x},\mathbf{x}_0)=-\frac{h(x,y)^k}{k!}\partial_z^k\mathbf{K}^0(x,y,0,\mathbf{x}_0),\quad \mathbf{x}\in\partial\mathcal{O}.$$

The existence of the $\mathbf{u}^k$'s and the estimate (4.18) are obtained by classical arguments (see the appendix for the more difficult case of a rough half-space minus the balls). In particular, we have

$$\|\nabla\big(\mathbf{u}^\varepsilon(\,\cdot\,,\mathbf{x}_0)-\varepsilon\mathbf{u}^1(\,\cdot\,,\mathbf{x}_0)\big)\|_{L^2(\mathcal{O})}\ \le\ C\varepsilon^2. \tag{4.19}$$

The last step consists in replacing $\mathbf{u}^1$ by the solution $\mathbf{K}^1$ of

$$-\Delta\mathbf{K}^1(\,\cdot\,,\mathbf{x}_0)+\nabla\mathbf{p}(\,\cdot\,,\mathbf{x}_0)=0,\quad \text{div }\mathbf{K}^1(\,\cdot\,,\mathbf{x}_0)=0,\quad z>0,$$
$$\mathbf{K}^1(x,y,0,\mathbf{x}_0)=-h(x,y)\partial_z\mathbf{K}^0(x,y,0,\mathbf{x}_0),\quad (x,y)\in\mathbb{R}^2,$$

that is replacing the rough half-space by the flat half-space. We claim that

$$||\nabla(\mathbf{u}^1(\,\cdot\,,\mathbf{x}_0)-\mathbf{K}^1(\,\cdot\,,\mathbf{x}_0))\|_{L^2(\mathcal{O}\cap\{z>0\})}\ =\ O(\varepsilon^2).$$

With no loss of generality, we can assume that $h>0$ (meaning that the flat wall is below the rough wall). Otherwise, we can make an intermediate comparison with the solution $\tilde{\mathbf{K}}^1$ of the same Stokes problem in $\{z>-\varepsilon(\sup|h|+1)\}$. Now, an easy but important remark is that

$$\|\mathbf{K}^1(\,\cdot\,,\mathbf{x}_0)\|_{H^s(\{0<z<Z\})}\ \le\ C_{s,Z},\quad \forall s\in\mathbb{N},\ \forall Z>0.$$

This comes from Poincaré inequality and standard elliptic regularity results. Hence,

$$\mathbf{K}^1(\mathbf{x},\mathbf{x}_0)=-h(x,y)\partial_z\mathbf{K}^0(x,y,0,\mathbf{x}_0)\ +\ O(\varepsilon)\quad\text{in}\quad H^s(\partial\mathcal{O}).$$

By a simple estimate on $\mathbf{u}^1-\mathbf{K}^1$, we deduce the claim.

Back to the definition of $\mathbf{u}^\varepsilon$, we obtain thanks to standard elliptic regularity in variable $\mathbf{x}$: for all $\alpha\in\mathbb{N}^3$,

$$|\partial_{\mathbf{x}}^\alpha\left(\mathbf{K}^\varepsilon(\mathbf{x},\mathbf{x}_0)-\mathbf{K}^0(\mathbf{x},\mathbf{x}_0)-\varepsilon\mathbf{K}^1(\mathbf{x},\mathbf{x}_0)\right)|=O(\varepsilon^2),$$

uniformly in $\mathbf{x},\mathbf{x}_0\in\cup_l B_l$. The same reasoning as above can then be applied to the fields $\mathbf{u}^\varepsilon_\beta=\partial^\beta_{\mathbf{x}_0}(\mathbf{K}^\varepsilon-\mathbf{K}^0)$, for all $\beta\in\mathbb{N}^3$. Hence,

$$|\partial_{\mathbf{x}}^\alpha\partial^\beta_{\mathbf{x}_0}\left(\mathbf{K}^\varepsilon(\mathbf{x},\mathbf{x}_0)-\mathbf{K}^0(\mathbf{x},\mathbf{x}_0)-\varepsilon\mathbf{K}^1(\mathbf{x},\mathbf{x}_0)\right)|=O(\varepsilon^2),$$

uniformly in $\mathbf{x},\mathbf{x}_0\in\cup_l B_l$. The theorem follows straightforwardly, considering

$$\mathcal{T}^0(\mathbf{f})_i(r)\ :=\ \sum_j\int_{\partial B}\mathbf{K}^0(x_i+a\mathbf{r},x_j+a\mathbf{s})\mathbf{f}_j(\mathbf{s})d\mathbf{s} \tag{4.20}$$

and

$$\mathcal{T}^1(\mathbf{f})_i(r)\ :=\ \sum_j\int_{\partial B}\mathbf{K}^1(x_i+a\mathbf{r},x_j+a\mathbf{s})\mathbf{f}_j(\mathbf{s})d\mathbf{s}. \tag{4.21}$$

Expressing $\mathbf{K}^1(\mathbf{x},\mathbf{x}_0)$ with a Poisson kernel yields

$$\mathbf{K}^1(\mathbf{x},\mathbf{x}_0)\ :=\ -\int_{\partial\mathbb{R}^3_+}h(\mathbf{s})\,\frac{\partial}{\partial z}\left(\mathbf{s}\mapsto\mathbf{K}^0(\mathbf{s},\mathbf{x})\right)\,\frac{\partial}{\partial z}\left(\mathbf{s}\mapsto\mathbf{K}^0(\mathbf{s},\mathbf{x}_0)\right)\mathrm{d}\mathbf{s}\,. \tag{4.22}$$

4.4.2 Expansion for small a

We go one step further in the asymptotics of $\mathcal{T}$, by considering the regime of small radius a. The expression of $\mathcal{T}$ involves the maps

$$\begin{array}{rcl} \mathcal{T}_{i,j} : H^{-1/2}(\partial B) & \to & H^{1/2}(\partial B) \\ \mathbf{f}_j & \mapsto & \displaystyle\int_{\partial B} \mathbf{K}(\mathbf{x}_i + a\,\cdot\,, \mathbf{x}_j + a\mathbf{s})\,\mathbf{f}_j(\mathbf{s})\,\mathrm{d}\mathbf{s}\,, \end{array} \tag{4.23}$$

with the Green kernel $\mathbf{K}$ given by Proposition 4.4.1:

$$\mathbf{K}(\mathbf{r},\mathbf{r}') := \mathbf{G}(\mathbf{r}-\mathbf{r}') + \mathbf{K}_1(\mathbf{r},\mathbf{r}') + \mathbf{K}_2(\mathbf{r},\mathbf{r}') + \mathbf{K}_3(\mathbf{r},\mathbf{r}') + \mathbf{K}_4(\mathbf{r},\mathbf{r}').$$

We recall that $\mathbf{K}_1, \mathbf{K}_2$ and $\mathbf{K}_3$ are defined in (4.13), whereas $\mathbf{K}_4$ is defined by (see (4.22)):

$$\mathbf{K}_4(\mathbf{r},\mathbf{r}') := -\varepsilon \int_{\partial\mathbb{R}^3_+} h(\mathbf{s})\,\frac{\partial}{\partial z}\left(\mathbf{s}\mapsto \mathbf{K}^0(\mathbf{s},\mathbf{r})\right)\,\frac{\partial}{\partial z}\left(\mathbf{s}\mapsto \mathbf{K}^0(\mathbf{s},\mathbf{r}')\right)\mathrm{d}\mathbf{s}\,.$$

Eventually, we call $\mathcal{T}^G$ the Neumann to Dirichlet map associated to $\mathbf{G}$

$$\begin{array}{rcl} \mathcal{T}^G : H^{-1/2}(\partial B) & \to & H^{1/2}(\partial B) \\ \mathbf{f} & \mapsto & \displaystyle\int_{\partial B} \mathbf{G}(a(\,\cdot\,-\mathbf{s}))\,\mathbf{f}(\mathbf{s})\,\mathrm{d}\mathbf{s}\,. \end{array}$$

Proposition 4.4.2 *Let $(i,j) \in \{1,\cdots,N\}^2$. We have the following expansions, valid for $a \ll 1$:*

- *if $i \neq j$ then*
$$\mathcal{T}_{i,j} = \mathbf{K}(\mathbf{x}_i,\mathbf{x}_j)\langle\,\cdot\,,\mathbf{I}_d\rangle_{\partial B} + \mathbf{R}_1 \tag{4.24}$$
where $||\mathbf{R}_1||_{\mathcal{L}(H^{-1/2},H^{1/2})} = O(a)$,
- *otherwise*
$$\mathcal{T}_{i,i} = \mathcal{T}^G + \sum_{k=1}^{4} \mathbf{K}_k(\mathbf{x}_i,\mathbf{x}_i)\langle\,\cdot\,,\mathbf{I}_d\rangle_{\partial B} + \mathbf{R}_2 \tag{4.25}$$
where $||\mathbf{R}_2||_{\mathcal{L}(H^{-1/2},H^{1/2})} = O(a)$.

Proof: Let $(i,j) \in \{1,\cdots,N\}^2$ be such that $i \neq j$. For all $\mathbf{f}_j \in H^{-1/2}(\partial B)$, we write

$$\left(\mathcal{T}_{i,j} - \mathbf{K}(\mathbf{x}_i,\mathbf{x}_j)\langle\,\cdot\,,\mathbf{I}_d\rangle\right)(\mathbf{f}_j)(\mathbf{r}) = \int_{\partial B} \left(\mathbf{K}(\mathbf{x}_i + a\mathbf{r}, \mathbf{x}_j + a\mathbf{s}) - \mathbf{K}(\mathbf{x}_i,\mathbf{x}_j)\right)\mathbf{f}_j(\mathbf{s})\mathrm{d}\mathbf{s}\,. \tag{4.26}$$

The point is that, as $i \neq j$, the kernel $\mathbf{K}$ is smooth in a neighborhood of $B_i \times B_j$. Hence,

$$|\mathbf{K}(\mathbf{x}_i + a\mathbf{r}, \mathbf{x}_j + a\mathbf{s}) - \mathbf{K}(\mathbf{x}_i,\mathbf{x}_j)| = O(a)\ , |\nabla\mathbf{K}(\mathbf{x}_i + a\mathbf{r}, \mathbf{x}_j + a\mathbf{s}) - \mathbf{K}(\mathbf{x}_i,\mathbf{x}_j)| = O(a) \tag{4.27}$$

uniformly for $\mathbf{r},\mathbf{s} \in B$. Estimate (4.24) follows straightforwardly.

The proof of (4.25) is similar: we have for all $\mathbf{f}_i \in H^{-1/2}(\partial B)$

$$\left(\mathcal{T}_{i,i} - \mathcal{T}^G - \mathbf{K}(\mathbf{x}_i,\mathbf{x}_j)\langle\,\cdot\,,\mathbf{I}_d\rangle\right)(\mathbf{f}_i)(\mathbf{r}) = \int_{\partial B} \sum_{k=1}^{4} \left(\mathbf{K}_k(\mathbf{x}_i + a\mathbf{r}, \mathbf{x}_i + a\mathbf{s}) - \mathbf{K}_k(\mathbf{x}_i,\mathbf{x}_i)\right)\mathbf{f}_i(\mathbf{s})\mathrm{d}\mathbf{s}\,, \tag{4.28}$$

where none of the $\mathbf{K}_k$'s is singular near $B_i \times B_i$. □

As a simple consequence of the previous propositions, we have

Proposition 4.4.3 *For every* $\mathbf{f} \in H_N^{-1/2}$*, for all* $(\mathbf{x}, \boldsymbol{\xi}) \in \mathcal{S}$*,*

$$(\mathcal{T}\mathbf{f})_i(\mathbf{r}) = \mathcal{T}^G \mathbf{f}_i + \sum_{l=1}^{4} \mathbf{K}_l(\mathbf{x}_i, \mathbf{x}_i)\langle \mathbf{f}_i, \mathbf{Id}\rangle_{\partial B} + \sum_{j\neq i} \mathbf{K}(\mathbf{x}_i, \mathbf{x}_j)\langle \mathbf{f}_j, \mathbf{Id}\rangle_{\partial B} + \mathcal{R}_i(\mathbf{f}), \qquad (4.29)$$

with $\|\mathcal{R}_i\|_{\mathcal{L}(H_N^{-1/2}, H_N^{1/2})} = O\left(a + \varepsilon^2\right)$*, and* $i = 1...N$*.*

Proof: By Proposition 4.4.1: for all $i = 1...N$, and all $\mathbf{r} \in \partial B$

$$\begin{aligned}(\mathcal{T}\mathbf{f})_i(\mathbf{r}) &:= \int_{\partial B} \mathbf{K}(\mathbf{x}_i + a\mathbf{r}, \mathbf{x}_i + a\mathbf{s})\,\mathbf{f}_i(\mathbf{s})\mathrm{d}\mathbf{s} + \sum_{i\neq j} \int_{\partial B} \mathbf{K}(\mathbf{x}_i + a\mathbf{r}, \mathbf{x}_j + a\mathbf{s})\,\mathbf{f}_j(\mathbf{s})\mathrm{d}\mathbf{s} + \mathcal{R}^\varepsilon(\mathbf{f}) \\ &= \mathcal{T}_{i,i}\mathbf{f}_i + \sum_{j\neq i} \mathcal{T}_{i,j}\mathbf{f}_j + \mathcal{R}^\varepsilon(\mathbf{f}), \qquad \|\mathcal{R}^\varepsilon\|_{\mathcal{L}(H_N^{-1/2}, H_N^{1/2})} = O(\varepsilon^2)\end{aligned}$$

and the result follows from the application of (4.24) and (4.25) of Proposition 4.4.2. □

Proposition 4.4.4 *For every* $\mathbf{u} \in H_N^{1/2}$*, for all* $(\mathbf{p}, \boldsymbol{\xi}) \in \mathcal{S}$*, one has*

$$\begin{aligned}\left(\mathcal{T}^{-1}\mathbf{u}\right)_i = \quad & (\mathcal{T}^G)^{-1}\left(\mathbf{u}_i - \sum_{k=1}^{4} \mathbf{K}_k(\mathbf{x}_i, \mathbf{x}_i)\langle (\mathcal{T}^G)^{-1}\mathbf{u}_i, \mathbf{Id}\rangle_{\partial B}\right) - \\ & (\mathcal{T}^G)^{-1}\left(\sum_{j\neq i} \mathbf{K}(\mathbf{x}_i, \mathbf{x}_j)\langle (\mathcal{T}^G)^{-1}\mathbf{u}_j, \mathbf{Id}\rangle_{\partial B}\right) + \tilde{\mathcal{R}}_i(\mathbf{u})\end{aligned} \qquad (4.30)$$

with $\|\tilde{\mathcal{R}}_i\|_{\mathcal{L}(H_N^{1/2}, H_N^{-1/2})} = O\left(a^3 + a^2\varepsilon^2\right)$*,* $i = 1...N$*.*

Proof: We recall that

$$\mathcal{T}^G : H^{-\frac{1}{2}}(\partial B) \to H^{\frac{1}{2}}(\partial B), \quad \mathbf{f} \mapsto \int_{\partial B} \mathbf{G}(a(\,\cdot - \mathbf{s}))\mathbf{f}(\mathbf{s})\,d\mathbf{s}\,,$$

and define for $l = 1, \ldots, 4$ the operators

$$\mathcal{S}_l : H^{-\frac{1}{2}}(\partial B) \to H^{\frac{1}{2}}(\partial B), \quad \mathbf{f} \mapsto \int_{\partial B} \mathbf{K}_l(\mathbf{x}_i, \mathbf{x}_i)\mathbf{f}(\mathbf{s})\,d\mathbf{s}\,,$$

and eventually

$$\mathcal{S}_{i,j} : H^{-\frac{1}{2}}(\partial B) \to H^{\frac{1}{2}}(\partial B), \quad \mathbf{f} \mapsto \int_{\partial B} \mathbf{K}(\mathbf{x}_i, \mathbf{x}_j)\mathbf{f}(\mathbf{s})\,d\mathbf{s}\,.$$

Notice that for all $\mathbf{f} \in H^{-\frac{1}{2}}(\partial B)$, $\mathcal{S}_l\mathbf{f}$ and $\mathcal{S}_{i,j}\mathbf{f}$ are constant applications.

That these operators are continuous operators from $H^{-\frac{1}{2}}(\partial B)$ into $H^{\frac{1}{2}}(\partial B)$ is classical. We are only interested in estimating their norms, and more precisely in the way they depend on a in the limit $a \to 0$. Notice that since the kernel $\mathbf{G}$ is homogeneous of degree -1, one has

$$\|\mathcal{T}^G\|_{\mathcal{L}(H^{-1/2}, H^{1/2})} = O\left(\frac{1}{a}\right) \text{ and } \left\|\left(\mathcal{T}^G\right)^{-1}\right\|_{\mathcal{L}(H^{1/2}, H^{-1/2})} = O(a)\,. \qquad (4.31)$$

As far as $\mathcal{S}_l$ is concerned, we get that (since $|\mathbf{K}_l(\mathbf{x}_i, \mathbf{x}_i)| = O(1)$)

$$\|\mathcal{S}_l\|_{\mathcal{L}(H^{-1/2}, H^{1/2})} = O(1) \ , \tag{4.32}$$

and similarly

$$\|\mathcal{S}_{i,j}\|_{\mathcal{L}(H^{-1/2}, H^{1/2})} = O(1) \ . \tag{4.33}$$

When $a \to 0$ this enables us to invert (4.29) leading to (4.30). □

4.5 Controllability of the Three-sphere swimmer

We deal in this section with the controllability of the 3-sphere swimmer, namely Theorem 4.2.4.

4.5.1 Preliminary remarks on the 3-sphere dynamics

We must first come back to equation (4.7) (4.9), in the particular case of the 3-sphere swimmer. Remember that the writing in this equation was slightly abusive: we had denoted by $\dot{\mathbf{p}}$ the vector $\left(\begin{smallmatrix}\Omega\\ \mathbf{v}\end{smallmatrix}\right)$ associated to the rigid movement of the swimmer, see (4.5). In our case, $\Omega = \left(\begin{smallmatrix}\Omega_1\\ \Omega_2\\ \Omega_3\end{smallmatrix}\right)$ and $\mathbf{v} = \dot{\mathbf{x}}_c = \left(\begin{smallmatrix}v_1\\ v_2\\ v_3\end{smallmatrix}\right)$ are respectively the angular velocity and the linear velocity of the middle sphere, decomposed in an arbitrary orthonormal basis $(\mathbf{e}_i)$. Moreover, it is natural to take for $\mathbf{e}_1$ the unit vector of the 3-sphere axis. Let θ be the angle between the swimmer's axis and $\mathbf{e}_z$, while ϕ is the angle between the y-axis and the projection of the swimmer in Oxy plane (see figure 4.2). Then, the unit vector of the 3-sphere axis reads (in the canonical basis) $\mathbf{e}_1 = \begin{pmatrix} \cos(\phi)\sin(\theta) \\ \sin(\phi)\sin(\theta) \\ \cos(\theta) \end{pmatrix}$. It is completed into an orthonormal basis by defining

$$\mathbf{e}_2 = \begin{pmatrix} \cos(\phi)\cos(\theta) \\ \sin(\phi)\cos(\theta) \\ -\sin(\theta) \end{pmatrix} , \qquad \mathbf{e}_3 = \begin{pmatrix} -\sin(\phi) \\ \cos(\phi) \\ 0 \end{pmatrix} .$$

Hence, a rigorous writing of (4.7) or (4.9) is

$$\mathbf{M}\left(\begin{smallmatrix}\Omega\\ \mathbf{v}\end{smallmatrix}\right) + \mathbf{N} = 0, \quad \text{or } \left(\begin{smallmatrix}\Omega\\ \mathbf{v}\end{smallmatrix}\right) = -\mathbf{M}^{-1}\mathbf{N}. \tag{4.34}$$

A crucial remark is that $\mathbf{M}$ and $\mathbf{N}$ do not depend on the whole of $\mathbf{p}$. The angle θ_1 of rotation around the swimmer's axis is not involved, as it is irrelevant to the swimmer's position, orientation or elongation. In particular, keeping only the five bottom lines of the last system, we end up with a closed relation of the type

$$\begin{pmatrix} \dot{\theta}_2 \\ \dot{\theta}_3 \\ \dot{\mathbf{x}}_c \end{pmatrix} = \sum_{i=1}^{2} \tilde{\mathbf{F}}_i \left(\begin{pmatrix} \theta_2 \\ \theta_3 \\ \mathbf{x}_c \end{pmatrix} \right) \dot{\xi}_i \tag{4.35}$$

where θ_2 and θ_3 are the rotation angles around $\mathbf{e}_2$ and $\mathbf{e}_3$ respectively. Then, by the analyticity of the $\tilde{\mathbf{F}}_i$'s and Chow's theorem, it remains to prove that there exists some $(\varepsilon, a, \theta_2, \theta_3, \mathbf{x}_c)$ such that

$$\dim Lie_{(\theta_2,\theta_3,\mathbf{x}_c)} \left(\begin{pmatrix} 1 \\ 0 \\ \tilde{\mathbf{F}}_1 \end{pmatrix}, \begin{pmatrix} 0 \\ 1 \\ \tilde{\mathbf{F}}_2 \end{pmatrix} \right) = 7.$$

Actually, we shall not work directly with angles θ_2, θ_3. We find it more convenient to work with the angles θ, ϕ introduced above (see Figure **??**). From the relation $\frac{d}{dt}\mathbf{e}_1 = \Omega \times \mathbf{e}_1$, we infer that

$$\Omega_2 = -\sin\theta\dot{\phi}, \quad \Omega_3 = \dot{\theta}.$$

Note that in the special case $\sin\theta = 0$, the angle ϕ coincides with the useless angle θ_1. Moreover, the mapping $(\theta_2, \theta_3) \to (\theta, \phi)$ is not a diffeomorphism in the vicinity of $\theta \equiv 0[\pi]$. *Thus, we shall restrict to orientations of the swimmer for which*

$$|\sin\theta| \geq \delta > 0. \tag{4.36}$$

We shall establish the maximality of the Lie algebra at points satisfying this condition.

Before entering the computation of this Lie algebra, we state a technical lemma, that will somehow allow us to neglect the rotation around the swimmer's axis. As mentioned before, we assume inequality (4.36). We have

Lemma 4.5.1 *There exists a constant C which does not depend on a and ϵ such that*

$$|\Omega_1| \leq C\,\left(|\dot{\theta}| + |\dot{\phi}| + |\dot{\mathbf{x}}_c| + |\dot{\boldsymbol{\xi}}|\right)\,.$$

Proof: We go back to the first identity in (4.34). The first line gives

$$\mathbf{M}_{1,1}\,\Omega_1 = -\mathbf{N}_1\dot{\boldsymbol{\xi}} + \mathbf{M}_{1,2}\,\sin(\theta)\dot{\phi} - \mathbf{M}_{1,3}\,\dot{\theta} - \mathbf{M}_{1,4}\,v_1 - \mathbf{M}_{1,5}\,v_2 - \mathbf{M}_{1,6}\,v_3\,. \tag{4.37}$$

We recall that, in the definitions of $\mathbf{M}$ and $\mathbf{N}$, we denoted by $\mathbf{u}_i$ and $\mathbf{u}^d$ some solutions of the Stokes equation, with zero Dirichlet condition at the wall, and inhomogeneous Dirichlet conditions at the ball. The Dirichlet data is $\mathbf{e}_i \times (\mathbf{x} - \mathbf{x}_c)$ for $i = 1, 2, 3$, $\mathbf{e}_{i-3}$ for $i = 4, 5, 6$, and $\mathbf{u}_d$ for $\mathbf{u}^d$. In the case of the 3-sphere swimmer, $\mathbf{u}_d$ is $-\dot{\xi}_1\mathbf{e}_1$ on the sphere ∂B_1, 0 on the middle sphere and $\dot{\xi}_2\mathbf{e}_2$ on the sphere ∂B_3.

Let us first examine

$$\begin{aligned}\mathbf{M}_{1,1} \;&=\; \sum_{l=1}^{3}\int_{\partial B}(\mathbf{x}_l - \mathbf{x}_c + a\mathbf{r}) \times \mathbf{e}_1 \cdot \mathcal{T}^{-1}(\mathbf{e}_1 \times a\mathbf{r}, \mathbf{e}_1 \times a\mathbf{r}, \mathbf{e}_1 \times a\mathbf{r})\mathrm{d}\sigma \\ &=\; 3\int_{\partial B} a\mathbf{r} \times \mathbf{e}_1 \cdot \mathcal{T}^{-1}(\mathbf{e}_1 \times a\mathbf{r}, \mathbf{e}_1 \times a\mathbf{r}, \mathbf{e}_1 \times a\mathbf{r})\mathrm{d}\sigma\end{aligned} \tag{4.38}$$

using that $(\mathbf{x}_l - \mathbf{x}_c) \times \mathbf{e}_1 = 0$. We then use the expansion (4.30). We recall the well-known fact that the rotation are eigenfunctions of $\left(\mathcal{T}^G\right)^{-1}$, with associated eigenvalue $3\mu a$. In particular,

$$\left(\mathcal{T}^G\right)^{-1}(\mathbf{e}_1 \times a\mathbf{r}) \;=\; 3\mu a\mathbf{e}_1 \times a\mathbf{r}, \quad \text{and } \langle\left(\mathcal{T}^G\right)^{-1}(\mathbf{e}_1 \times a\mathbf{r}), \mathbf{Id}\rangle_{\partial B} = 0.$$

We find then easily that $\mathbf{M}_{1,1} = -3\mu a^3 \;+\; O(a^5 + \varepsilon^2 a^3)$.

Then, we examine

$$\mathbf{N}_1 = \sum_{l=1}^{3}\int_{\partial B}(\mathbf{x}_l - \mathbf{x}_c + a\mathbf{r}) \times \mathbf{e}_1 \cdot \mathcal{T}^{-1}(-\dot{\xi}_1\,\mathbf{e}_1, 0, \dot{\xi}_2\,\mathbf{e}_2)\,\mathrm{d}\sigma.$$

Again, we can expand $\mathcal{T}^{-1}$ using (4.30). This time, we use that translations are eigenfunctions of $\left(\mathcal{T}^G\right)^{-1}$ with associated eigenvalue $\frac{3}{2}\mu a$. Thus,

$$\left(\mathcal{T}^G\right)^{-1}(\mathbf{e}_1) \;=\; \frac{3}{2}\mu a\,\mathbf{e}_1.$$

It follows that the first terms in the expansion vanish, and we find

$$\mathbf{N}_1 = O((a^4 + a^3\varepsilon^2)\,|\dot{\boldsymbol{\xi}}|)$$

The remaining terms $M_{1,j}$, $j = 2, ..., 4$ can be handled with similar arguments. The lemma follows straightforwardly.

□

4.5.2 Asymptotics of the 3-sphere dynamics

We shall now provide an accurate description of the 3-sphere dynamics: broadly speaking, the point is to obtain an explicit expansion of the $\mathbf{F}_i$'s in (4.35) (with angles θ_2, θ_3 replaced by θ, ϕ, see remark above). We remind that the dynamics (that is the 6x6 system in (4.34)) is governed by self-propulsion: it corresponds to

- The sum of the forces on the swimmer being zero.
- The sum of the torques on the swimmer being zero.

Forces. By the definition of the swimmer, each sphere obeys a rigid body motion. More precisely, the velocity of each point $\mathbf{r}$ of the lth sphere expresses as a sum of a translation and a rotation as

$$\mathbf{u}_l^S(\mathbf{r}) = \mathbf{u}_{T_l} + \mathbf{u}_{R_l}(\mathbf{r})\,, \tag{4.39}$$

where $\mathbf{u}_{T_l}$ is constant on ∂B while $\mathbf{u}_{R_l}(\mathbf{r}) = \Omega \times a\mathbf{r}$ (remember that all quantities are expressed on the unit sphere ∂B). The vanishing of the total force, due to self-propulsion, reads

$$\sum_l \int_{\partial B} \mathbf{f}_l = \sum_l \int_{\partial B} \left(\mathcal{T}^{-1}\left(\mathbf{u}_1^S, \mathbf{u}_2^S, \mathbf{u}_3^S\right)\right)_l = 0\,. \tag{4.40}$$

Plugging (4.39) in (4.40) and using (4.30) leads to

$$\sum_l \int_{\partial B} (\mathcal{T}^G)^{-1}\left(\mathbf{u}_{Tl} + \mathbf{u}_{Rl} - \sum_{k=1}^{4} \mathbf{K}_k(\mathbf{x}_l, \mathbf{x}_l)\langle(\mathcal{T}^G)^{-1}(\mathbf{u}_{Tl} + \mathbf{u}_{Rl}), \mathrm{Id}\rangle_{\partial B}\right) -$$
$$(\mathcal{T}^G)^{-1}\left(\sum_{j\neq i} \mathbf{K}(\mathbf{x}_i, \mathbf{x}_j)\langle(\mathcal{T}^G)^{-1}(\mathbf{u}_{Tl} + \mathbf{u}_{Rl}), \mathbf{Id}\rangle_{\partial B}\right) = \left(O\left(a^3\right) + O\left(a^2\epsilon^2\right)\right)||\mathbf{u}||\,. \tag{4.41}$$

where $\|\mathbf{u}\| = \|(\mathbf{u}_i^S)\|$ is any norm on the n-uplets of rigid vector fields over the ball. Here,

$$\|u\| \;=\; O(|\dot{\theta}| + |\dot{\phi}| + |\dot{\mathbf{x}}_c| + |\Omega_1|) \;=\; O(|\dot{\theta}| + |\dot{\phi}| + |\dot{\mathbf{x}}_c|) \tag{4.42}$$

where the last equality comes from Lemma 4.5.1. As mentioned earlier, it is well known that both translations and rotations are eigenfunctions of the Dirichlet to Neumann map of the three dimensional Stokes operator outside a sphere. Namely

$$\left(\mathcal{T}^G\right)^{-1}\mathbf{u}_{Tl} = \lambda_T\mathbf{u}_{Tl} \text{ and } \left(\mathcal{T}^G\right)^{-1}\mathbf{u}_{Rl} = \lambda_R\mathbf{u}_{Rl}\,.$$

It is also well-known that $\lambda_T = \frac{3\mu a}{2}$, $\lambda_R = 3\mu a$, leading in particular to the celebrated Stokes formula

$$\int_{\partial B} \left(\mathcal{T}^G\right)^{-1}\mathbf{u}_{T_l}\mathrm{d}\mathbf{s} = 6\pi\mu a\,\mathbf{u}_{T_l}$$

We also remark that due to $\int_{\partial B} \mathbf{u}_{R_l} \mathrm{d}\mathbf{s} = 0$, we have $\int_{\partial B} \left(\mathcal{T}^G\right)^{-1} \mathbf{u}_{R_l} \mathrm{d}\mathbf{s} = 0$. We therefore obtain

$$6\pi\mu a \sum_l \left(\mathbf{u}_{Tl} - 6\pi\mu a \sum_{k=1}^{4} \mathbf{K}_k(\mathbf{x}_l, \mathbf{x}_l)\mathbf{u}_{Tl} - 6\pi\mu a \sum_{j\neq i} \mathbf{K}(\mathbf{x}_l, \mathbf{x}_j)\mathbf{u}_{Tj} \right) = \left(O\left(a^3\right) + O\left(a^2\epsilon^2\right)\right) ||\mathbf{u}|| \,. \quad (4.43)$$

Torques. We now compute the torque with respect to the center $\mathbf{x}_c$ of the middle ball B_2. Self-propulsion of the swimmer implies that this torque vanishes:

$$0 = \int_{\partial B} (\mathbf{x}_1 - \mathbf{x}_2 + a\mathbf{r}) \times \mathbf{f}_1(\mathbf{r}) + \int_{\partial B} a\mathbf{r} \times \mathbf{f}_2(\mathbf{r}) + \int_{\partial B} (\mathbf{x}_3 - \mathbf{x}_2 + a\mathbf{r}) \times \mathbf{f}_3(\mathbf{r}) = \mathbf{I}_1 + \mathbf{I}_2 + \mathbf{I}_3 \,, \quad (4.44)$$

with the quantities $\mathbf{I}_1$, $\mathbf{I}_2$ and $\mathbf{I}_3$ given below.

$$\begin{aligned}
\mathbf{I}_1 &= \int_{\partial B} (\mathbf{x}_1 - \mathbf{x}_2 + a\mathbf{r}) \times \mathbf{f}_1(\mathbf{r}) = \int_{\partial B} (\xi_1 \mathbf{e}_\xi^1 + a\mathbf{r}) \times \left(\mathcal{T}^{-1}\left(\mathbf{u}_1^S, \mathbf{u}_2^S, \mathbf{u}_3^S\right)\right)_1 \\
&= \int_{\partial B} (-\xi_1 \mathbf{e}_1 + a\mathbf{r}) \times (\mathcal{T}^G)^{-1} \left(\mathbf{u}_{T1} + \mathbf{u}_{R1} - 6\pi\mu a \sum_{k=1}^{4} \mathbf{K}_k(\mathbf{x}_1, \mathbf{x}_1)\mathbf{u}_{T1} \right. \\
&\qquad \left. - 6\pi\mu a \sum_{j\neq 1} \mathbf{K}(\mathbf{x}_1, \mathbf{x}_j)\mathbf{u}_{Tj} + O\left(a^2 + a\varepsilon^2\right) ||\mathbf{u}|| \right) \\
&= -6\pi\mu a \xi_1 \mathbf{e}_\xi^1 \times \left(\mathbf{u}_{T1} - 6\pi\mu a \sum_{k=1}^{4} \mathbf{K}_k(\mathbf{x}_1, \mathbf{x}_1)\mathbf{u}_{T1} - 6\pi\mu a \sum_{j\neq 1} \mathbf{K}(\mathbf{x}_1, \mathbf{x}_j)\mathbf{u}_{Tj} \right) \\
&\qquad + \left(O\left(a^3\right) + O\left(a^2\epsilon^2\right)\right) ||\mathbf{u}|| \,.
\end{aligned}$$

Similarly, we get,

$$\begin{aligned}
\mathbf{I}_2 &= a \int_{\partial B} \mathbf{r} \times \mathbf{f}_2(\mathbf{r}) = a \int_{\partial B} \mathbf{r} \times \left(\mathcal{T}^{-1}\left(\mathbf{u}_1^S, \mathbf{u}_2^S, \mathbf{u}_3^S\right)\right)_2 \\
&= a \int_{\partial B} \mathbf{r} \times (\mathcal{T}^G)^{-1} \left(\mathbf{u}_{T2} + \mathbf{u}_{R2} - 6\pi\mu a \sum_{k=1}^{4} \mathbf{K}_k(\mathbf{x}_2, \mathbf{x}_2)\mathbf{u}_{T2} \right. \\
&\qquad \left. - 6\pi\mu a \sum_{j\neq 2} \mathbf{K}(\mathbf{x}_2, \mathbf{x}_j)\mathbf{u}_{Tj} + O\left(a^2 + a\varepsilon^2\right) ||\mathbf{u}|| \right) \\
&= O\left(a^3 + a^3\epsilon^2\right) ||\mathbf{u}|| \,.
\end{aligned}$$

Finally,

$$\begin{aligned}
\mathbf{I}_3 &= \int_{\partial B} (\mathbf{x}_3 - \mathbf{x}_2 + a\mathbf{r}) \times \mathbf{f}_3(\mathbf{r}) \\
&= 6\pi\mu a \xi_2 \mathbf{e}_1 \times \left(\mathbf{u}_{T3} - 6\pi\mu a \sum_{k=1}^{4} \mathbf{K}_k(\mathbf{x}_3, \mathbf{x}_3)\mathbf{u}_{T3} - 6\pi\mu a \sum_{j\neq 3} \mathbf{K}(\mathbf{x}_3, \mathbf{x}_j)\mathbf{u}_{Tj} \right) \\
&\qquad + \left(O\left(a^3\right) + O\left(a^2\epsilon^2\right)\right) ||\mathbf{u}|| \,.
\end{aligned}$$

Denoting by $\mathbf{A}$ the matrix

$$\mathbf{A} = \begin{pmatrix} \mathbf{A}_{11} & \mathbf{A}_{12} & \mathbf{A}_{13} \\ \mathbf{A}_{21} & \mathbf{A}_{22} & \mathbf{A}_{23} \\ \mathbf{A}_{31} & \mathbf{A}_{32} & \mathbf{A}_{33} \end{pmatrix} \tag{4.45}$$

where for $i = 1, 2, 3$

$$\mathbf{A}_{ii} = \mathbf{Id} - 6\pi\mu a \sum_{l=1}^{4} \mathbf{K}_l(\mathbf{x}_i, \mathbf{x}_i) \tag{4.46}$$

and for $i, j = 1, 2, 3$ with $i \neq j$

$$\mathbf{A}_{ij} = -6\pi\mu a\, \mathbf{K}(\mathbf{x}_i, \mathbf{x}_j) \tag{4.47}$$

and $\mathbf{S}$ the matrix

$$\mathbf{S} = \begin{pmatrix} \mathbf{Id} & \mathbf{Id} & \mathbf{Id} \\ -\xi_1 \mathbf{e}_1 \times & 0 & +\xi_2 \mathbf{e}_1 \times \end{pmatrix},$$

we can rewrite the self-propulsion assumption (4.43), (4.44) as

$$\mathbf{SA} \begin{pmatrix} \mathbf{u}_{T_1} \\ \mathbf{u}_{T_2} \\ \mathbf{u}_{T_3} \end{pmatrix} = \left(O\left(a^2\right) + O\left(a\epsilon^2\right) \right) ||\mathbf{u}||. \tag{4.48}$$

Terms involving the $\mathbf{u}_{R_l}$'s are included in the r.h.s.

We now express $\mathbf{u}_{T_1}, \mathbf{u}_{T_2}$ and $\mathbf{u}_{T_3}$ in terms of $\dot{\mathbf{x}}_c, \dot{\theta}, \dot{\phi}$ and $\dot{\boldsymbol{\xi}}$. Since $\mathbf{u}_{T_2}$ is the velocity of the center of the ball B_2, one has

$$\mathbf{u}_{T_2} = \dot{\mathbf{x}}_c = \begin{pmatrix} \dot{x} \\ \dot{y} \\ \dot{z} \end{pmatrix} \quad \text{in the canonical basis of } \mathbb{R}^3.$$

Then, by using $\frac{d}{dt}\mathbf{e}_1 = \dot{\theta}\, \mathbf{e}_2 + \sin(\theta)\dot{\phi}\, \mathbf{e}_3$, we get

$$\mathbf{u}_{T_1} = \mathbf{u}_{T_2} - \xi_1 \left(\dot{\theta}\mathbf{e}_2 + \sin(\theta)\dot{\phi}\, \mathbf{e}_3 \right) - \dot{\xi}_1 \mathbf{e}_1\,, \quad \mathbf{u}_{T_3} = \mathbf{u}_{T_2} + \xi_2 \left(\dot{\theta}\mathbf{e}_2 + \sin(\theta)\dot{\phi}\, \mathbf{e}_3 \right) + \dot{\xi}_2 \mathbf{e}_1\,.$$

In matrix form, all this reads Then, the speed $\mathbf{u}_{T_i}$ $(i = 1, 2, 3)$ is expressed as

$$\begin{pmatrix} \mathbf{u}_{T_1} \\ \mathbf{u}_{T_2} \\ \mathbf{u}_{T_3} \end{pmatrix} = \mathbf{T} \begin{pmatrix} \Omega_1 \\ \dot{\theta} \\ \dot{\phi} \\ \dot{x} \\ \dot{y} \\ \dot{z} \end{pmatrix} + \mathbf{U}\, \dot{\boldsymbol{\xi}}\,. \tag{4.49}$$

with

$$\mathbf{T} = \begin{pmatrix} 0 & -\xi_1 \mathbf{e}_2 & -\xi_1 \sin(\theta)\mathbf{e}_3 & \mathbf{Id} \\ & 0 & 0 & \\ \vdots & 0 & 0 & \mathbf{Id} \\ & 0 & 0 & \\ 0 & +\xi_2 \mathbf{e}_2 & +\xi_2 \sin(\theta)\mathbf{e}_3 & \mathbf{Id} \end{pmatrix}, \quad \text{and} \quad \mathbf{U} = \begin{pmatrix} 0 & 0 \\ -\mathbf{e}_1 & 0 \\ 0 & \vdots \\ \vdots & 0 \\ 0 & \mathbf{e}_1 \end{pmatrix}.$$

Combining with (4.48), the motion equation (4.34) becomes

$$(\mathbf{SA} + \mathbf{R}_1) \left(\mathbf{T} \begin{pmatrix} \Omega_1 \\ \dot{\theta} \\ \dot{\phi} \\ \dot{x} \\ \dot{y} \\ \dot{z} \end{pmatrix} + (\mathbf{U} + \mathbf{R}_2)\, \dot{\boldsymbol{\xi}} \right) = 0 \tag{4.50}$$

where the residual matrices $\mathbf{R}_1, \mathbf{R}_2$ satisfy

$$|\mathbf{R}_1| + |\mathbf{R}_2| = \left(O\left(a^2\right) + O(a\epsilon^2)\right)$$

using (4.42). Finally, we only keep the five bottom lines of this system. It yields the following 5x5 system

$$\left(\tilde{\mathbf{S}}\mathbf{A} + \tilde{\mathbf{R}}\right)\left(\tilde{\mathbf{T}}\begin{pmatrix}\dot\theta\\ \dot\phi\\ \dot x\\ \dot y\\ \dot z\end{pmatrix} + \tilde{\mathbf{U}}\,\dot{\boldsymbol{\xi}}\right) = 0\,, \tag{4.51}$$

where

$$\tilde{\mathbf{S}} := (S_{i,j})_{2\le i\le 6, 1\le j\le 9}\,, \quad \tilde{\mathbf{T}} := \begin{pmatrix} -\xi_1\mathbf{e}_2 & -\xi_1\sin(\theta)\mathbf{e}_3 & \mathbf{Id}\\ 0 & 0 & \\ 0 & 0 & \mathbf{Id}\\ 0 & 0 & \\ +\xi_2\mathbf{e}_2 & +\xi_2\sin(\theta)\mathbf{e}_3 & \mathbf{Id}\end{pmatrix}, \qquad \tilde{\mathbf{U}} := \begin{pmatrix} -\mathbf{e}_1 & 0\\ 0 & \vdots\\ \vdots & 0\\ 0 & \mathbf{e}_1\end{pmatrix},$$

and where the residual matrices still satisfy $|\tilde{\mathbf{R}}_1| + |\tilde{\mathbf{R}}_2| = O\left(a^2\right) + O(a\epsilon^2)$. We leave to the reader to check that $\tilde{\mathbf{S}}\mathbf{A}\tilde{\mathbf{T}} = \tilde{\mathbf{S}}\tilde{\mathbf{T}} + O(a)$ is invertible, with $|(\tilde{\mathbf{S}}\mathbf{A}\tilde{\mathbf{T}})^{-1}| = O(1)$ uniformly in a and ε. Then, we can write system (4.51) as

$$\begin{pmatrix}\dot\theta\\ \dot\phi\\ \dot x\\ \dot y\\ \dot z\end{pmatrix} = -(\tilde{\mathbf{S}}\mathbf{A}\tilde{\mathbf{T}})^{-1}\tilde{\mathbf{S}}\mathbf{A}\tilde{\mathbf{U}}\dot{\boldsymbol{\xi}} \;+\; \tilde{\mathbf{R}}\dot{\boldsymbol{\xi}} \tag{4.52}$$

with $|\tilde{\mathbf{R}}| = O(a^2 + \varepsilon^2 a)$.

4.5.3 Reachable set

We are now ready to prove Theorem 4.2.4. We drop the tilda in the ODE (4.52) and express it as

$$\dot{\mathbf{X}} \;=\; \mathbf{F}_1(\mathbf{X})\dot\xi_1 \;+\; \mathbf{F}_2(\mathbf{X})\dot\xi_2, \quad \mathbf{X} \;:=\; \begin{pmatrix}\xi_1\\ \xi_2\\ \theta\\ \phi\\ x\\ y\\ z\end{pmatrix}. \tag{4.53}$$

To expand the $\mathbf{F}_i$'s, we decompose the matrix $\mathbf{A}$ into three matrices: $\mathbf{A} := \mathbf{Id} + \mathbf{A}^1 + \mathbf{A}^2$ where

$$\mathbf{A}^1_{ii} = -6\pi\mu a\sum_{k=1}^{3}\mathbf{K}_k(\mathbf{x}_i,\mathbf{x}_i)\;\forall\, i \quad \mathbf{A}^1_{ij} = -6\pi\mu a\left(\mathbf{G}(\mathbf{x}_i,\mathbf{x}_j) + \sum_{k=1}^{3}\mathbf{K}_k(\mathbf{x}_i,\mathbf{x}_j)\right)\;\forall\, i\neq j$$

and where

$$\mathbf{A}^2_{i,j} = -6\pi\mu a\,\mathbf{K}_4(\mathbf{x}_i,\mathbf{x}_j) \quad \forall\, i,j.$$

Thanks to (4.51), we get an expansion of the form $\mathbf{F}_i := \mathbf{F}_i^0 + \mathbf{F}_i^1 + \mathbf{F}_i^2 + \mathbf{R}_i$ where $\mathbf{F}_i^0$, $\mathbf{F}_i^1$ and $\mathbf{F}_i^2$ are respectively the zero order term, the term of order a and the term of order εa. The remainder is $\mathbf{R}_i = \left(O\left(a^2\right) + O(a\epsilon^2)\right)$. These vector fields are given by

$$\begin{aligned}
\mathbf{F}_i^0 &= \begin{pmatrix}\mathbf{e}_i\\ -(\mathbf{ST})^{-1}(\mathbf{SU})\mathbf{e}_i\end{pmatrix},\\
\mathbf{F}_i^1 &= \begin{pmatrix}\mathbf{e}_i\\ \left((\mathbf{ST})^{-1}\mathbf{SA}^1\mathbf{T}(\mathbf{ST})^{-1}\mathbf{SU} - (\mathbf{ST})^{-1}\mathbf{SA}^1\mathbf{U}\right)\mathbf{e}_i\end{pmatrix},\\
\mathbf{F}_i^2 &= \begin{pmatrix}\mathbf{e}_i\\ \left((\mathbf{ST})^{-1}\mathbf{SA}^2\mathbf{T}(\mathbf{ST})^{-1}\mathbf{SU} - (\mathbf{ST})^{-1}\mathbf{SA}^2\mathbf{U}\right)\mathbf{e}_i\end{pmatrix}.
\end{aligned}$$

where $\mathbf{e}_1 = \left(\begin{smallmatrix}1\\0\end{smallmatrix}\right)$ and $\mathbf{e}_2 = \left(\begin{smallmatrix}0\\1\end{smallmatrix}\right)$.

Now, we want to find some $(\varepsilon, a, \mathbf{X})$ in $\mathbb{R}_+ \times \mathbb{R}_+^* \times \mathcal{S}$ for which the determinant

$$\det(\mathbf{X}) := \Big|\mathbf{F}_1, \mathbf{F}_2,\, [\mathbf{F}_1, \mathbf{F}_2],\, [\mathbf{F}_1, [\mathbf{F}_1, \mathbf{F}_2]],\, [\mathbf{F}_2, [\mathbf{F}_1, \mathbf{F}_2]],\, [\mathbf{F}_1, [\mathbf{F}_1, [\mathbf{F}_1, \mathbf{F}_2]]],\, [\mathbf{F}_2, [\mathbf{F}_2, [\mathbf{F}_1, \mathbf{F}_2]]]\Big|(\mathbf{X}) \neq 0. \quad (4.54)$$

As the l.h.s. defines an analytic function of $\mathbf{X}$, it will be non-zero almost everywhere. Thus, the Lie algebra generated by $\mathbf{F}_1$ and $\mathbf{F}_2$ will be maximal (of dimension 7) at almost every $\mathbf{X}$, and local controllability will follow from Chow's theorem, see [51].
For all $\mathbf{G} \in \mathrm{Lie}(\mathbf{F}_1, \mathbf{F}_2)$, let us denote $\mathbf{G}^0$, $\mathbf{G}^1$ and $\mathbf{G}^2$ the zero order term, the term of order a and the term of order $a\varepsilon$ in the expansion of the vector field $\mathbf{G}$ respectively. Thus,

$$\mathbf{G} = \mathbf{G}^0 + \mathbf{G}^1 + \mathbf{G}^2 + O\left(a^2\right) + O(a\epsilon^2)\,.$$

For instance the expansion of the first Lie bracket reads

$$[\mathbf{F}_1, \mathbf{F}_2] = [\mathbf{F}_1, \mathbf{F}_2]^0 + [\mathbf{F}_1, \mathbf{F}_2]^1 + [\mathbf{F}_1, \mathbf{F}_2]^2 + O\left(a^2\right) + O(a\epsilon^2)\,.$$

with

$$[\mathbf{F}_1, \mathbf{F}_2]^0 = [\mathbf{F}_1^0, \mathbf{F}_2^0]\,, \quad [\mathbf{F}_1, \mathbf{F}_2]^1 = [\mathbf{F}_1^1, \mathbf{F}_2^0] + [\mathbf{F}_1^0, \mathbf{F}_2^1]\,, \quad [\mathbf{F}_1, \mathbf{F}_2]^2 = [\mathbf{F}_1^2, \mathbf{F}_2^0] + [\mathbf{F}_1^0, \mathbf{F}_2^2].$$

Note that for all $\mathbf{G} \in \mathrm{Lie}(\mathbf{F}_1, \mathbf{F}_2)$, $\mathbf{G}^0 + \mathbf{G}^1$ is a "flat wall" expansion, first order in a. Meanwhile, $\mathbf{G}^2$ is the first term which takes into account the roughness.

Without including this extra term, the three-sphere swimmer would not be controllable (see [11]), meaning that the determinant would vanish. We have notably

Lemma 4.5.2 *For all* $\mathbf{G} \in Lie(\mathbf{F}_1, \mathbf{F}_2) \setminus \{\mathbf{F}_1, \mathbf{F}_2\}$, $\mathbf{G}^0 = 0$.

Proof: A simple calculation yields

$$\mathbf{F}_1^0(\mathbf{X}) = \begin{pmatrix} 1 \\ 0 \\ 0 \\ 0 \\ \frac{1}{3}\cos(\phi)\sin(\theta) \\ \frac{1}{3}\sin(\phi)\sin(\theta) \\ \frac{1}{3}\cos(\theta) \end{pmatrix}, \qquad \mathbf{F}_2^0(\mathbf{X}) = \begin{pmatrix} 0 \\ 1 \\ 0 \\ 0 \\ -\frac{1}{3}\cos(\phi)\sin(\theta) \\ -\frac{1}{3}\sin(\phi)\sin(\theta) \\ -\frac{1}{3}\cos(\theta) \end{pmatrix}.$$

It implies that $[\mathbf{F}_1^0, \mathbf{F}_2^0]$ is zero. The lemma is proved. □

As regards the $O(a)$ term, we have

Lemma 4.5.3 *Let* $Lie(\mathbf{F}_1, \mathbf{F}_2)^1 := \left\{\mathbf{G}^1 \ s.t. \ \mathbf{G} \in Lie(\mathbf{F}_1, \mathbf{F}_2)\right\}$. *For all* $\mathbf{X} \in \mathcal{S}$, *the dimension of the subspace* $Lie(\mathbf{F}_1, \mathbf{F}_2)^1(\mathbf{X})$ *is less than* 5.

Proof: As said above, for all $\mathbf{G} \in Lie(\mathbf{F}_1, \mathbf{F}_2)$, the sum $\mathbf{G}^0 + \mathbf{G}^1$ is a $O(a)$ expansion of the "flat wall field", corresponding to the case $h = 0$. But in such flat case, symmetries constrain the swimmer within a plane. Thus, the associated manifold has at most dimension 5 (ξ_1, ξ_2, two coordinates for the center of the middle ball, one angle). This implies the result. □

Remark 4.5.4 *Since without roughness the swimmer evolves in a plane, it follows that the angle ϕ cannot change with time. Consequently, for all $\mathbf{F}(\mathbf{X}) \in Lie(\mathbf{F}_1, \mathbf{F}_2)^1(\mathbf{X})$ the fourth component of the vector $\mathbf{F}(\mathbf{X})$ is zero.*

Remark 4.5.5 *The lemma also 4.5.3 applies to the vector fields which does not take into account the roughness i.e., the ones which appear in the expansion without ε.*

From this, we will get that the non-zero leading term in the expansion of det has power $a^5\epsilon^2$. Theorem 4.2.4 follows directly from

Proposition 4.5.6 *In the regime $1 \gg \varepsilon \gg a$, one can find a surface $h \in C_c^\infty(\mathbb{R}^2)$ and a non-trivial analytic function $\mathcal{A}$ on $\mathcal{S}$ such that for all $\mathbf{X} \in \mathcal{S}$*

$$\det(\mathbf{X}) = a^5\,\epsilon^2\,\mathcal{A}(\mathbf{X}) + O(a^6\varepsilon^2 + a^5\epsilon^3)\,.$$

Proof: For all vector $\mathbf{G}$, we denote $(\mathbf{G})_{j'}^{j} := (\mathbf{G}_k)_{j\le k\le j'}$. Since $\mathbf{F}_i$, $i = 1, 2$, is of the type $\begin{pmatrix} \mathbf{e}_i \\ * \\ \vdots \\ * \end{pmatrix}$, we get easily that

$$\det(\mathbf{X}) = |\mathbf{Z}_1, \mathbf{Z}_2, \mathbf{Z}_3, \mathbf{Z}_4, \mathbf{Z}_5|$$

where

$$\left\{\begin{array}{l} \mathbf{Z}_1 := ([\mathbf{F}_1, \mathbf{F}_2])_3^7\,, \\ \mathbf{Z}_2 := ([\mathbf{F}_1, [\mathbf{F}_1, \mathbf{F}_2]])_3^7\,, \\ \mathbf{Z}_3 := ([\mathbf{F}_2, [\mathbf{F}_1, \mathbf{F}_2]])_3^7\,, \\ \mathbf{Z}_4 := ([\mathbf{F}_1, [\mathbf{F}_1, [\mathbf{F}_1, \mathbf{F}_2]]])_3^7\,, \\ \mathbf{Z}_5 := ([\mathbf{F}_2, [\mathbf{F}_2, [\mathbf{F}_1, \mathbf{F}_2]]])_3^7\,. \end{array}\right. \tag{4.55}$$

From Lemma 4.5.2, $\mathbf{Z}_i^0 = 0$ for all $i = 1...5$. Moreover, by Lemma 4.5.3, any determinant of the type

$$\left|\mathbf{Z}_{k_1}^1, \mathbf{Z}_{k_2}^1, \mathbf{Z}_{k_3}^1, *\right|, \quad k_i \in \{1, ..., 5\} \quad \text{is zero.}$$

Expanding the function det by 5-linearity, we obtain

$$\det(\mathbf{X}) \;=\; a^5\,\epsilon^2\,\mathcal{A}(\mathbf{X}) + O(a^6\varepsilon^2 + a^5\epsilon^3)\,,$$

where the function $\mathcal{A}(\mathbf{X})$ is defined as follows. Let

$$\mathcal{I} \;:=\; \left\{\mathbf{k} \in \{1, ..., 5\}^5 \quad \text{with } k_1 < k_2 \quad \text{and} \quad k_3 < k_4 < k_5 \quad \text{distinct of } k_1 \text{ and } k_2\right\}.$$

We set

$$\mathcal{A}(\mathbf{X}) \;:=\; \sum_{\mathbf{k}\in\mathcal{I}} \pm \left|\mathbf{Z}_{k_1}^2,\, \mathbf{Z}_{k_2}^2,\, \mathbf{Z}_{k_3}^1,\, \mathbf{Z}_{k_3}^1,\, \mathbf{Z}_{k_4}^1,\, \mathbf{Z}_{k_5}^1\right|,$$

where the $\pm$ is the signature of the permutation $i \to k_i$.

It remains to prove that there exists $\mathbf{X}_0 \in \mathcal{S}$ such that $\mathcal{A}(\mathbf{X}_0)$ is non-zero. By calling $\mathbf{K}_4^{int}$ the function $(\mathbf{s}, \mathbf{r}, \mathbf{r}') \mapsto \frac{\partial}{\partial z}\left(\mathbf{s} \mapsto \mathbf{K}^0(\mathbf{s}, \mathbf{r})\right)\, \frac{\partial}{\partial z}\left(\mathbf{s} \mapsto \mathbf{K}^0(\mathbf{s}, \mathbf{r}')\right)$, we have (see (4.22))

$$\mathbf{K}_4(\mathbf{r}, \mathbf{r}') = -\varepsilon \int_{\partial\mathbb{R}^3_+} h(s_1, s_2)\, \mathbf{K}_4^{int}(\mathbf{s}, \mathbf{r}, \mathbf{r}')\, \mathrm{d}\mathbf{s}\,.$$

We then define the 3x3 block matrix $\mathbf{A}_{int}^2(\mathbf{s})$ through

$$(\mathbf{A}_{int}^2(\mathbf{s}))_{ij} = -6\pi\mu a\, \mathbf{K}_4^{int}(\mathbf{s}, \mathbf{x}_i, \mathbf{x}_j), \quad i, j = 1...3.$$

By using the linearity of the integral, the vector fields $\mathbf{F}_i^2$, $i = 1, 2$ read

$$\mathbf{F}_i^2 = \left(-\varepsilon \int_{\partial \mathbb{R}^3_+} h(\mathbf{s}) \left(\mathbf{F}_{i,int}^2(\mathbf{s}) \right) \mathrm{d}\mathbf{s} \right) ,$$

where,

$$\mathbf{F}_{i,int}^2(\mathbf{s}) = - \left(-(\mathbf{ST})^{-1} \mathbf{S} \mathbf{A}_{int}^2(\mathbf{s}) \mathbf{T} (\mathbf{ST})^{-1} \mathbf{SU} + (\mathbf{ST})^{-1} \mathbf{S} \mathbf{A}_{int}^2(\mathbf{s}) \mathbf{U} \right) \mathbf{e}_i \, . \tag{4.56}$$

Then, denoting

$$\mathbf{Z}_{1,int}^2(\mathbf{s}) \; := \; [\mathbf{F}_{1,int}^2(\mathbf{s}), \mathbf{F}_2^0] + [\mathbf{F}_1^0, \mathbf{F}_{2,int}^2(\mathbf{s})]$$

leads to

$$\mathbf{Z}_1^2 = -\varepsilon \int_{\partial \mathbb{R}^3_+} h(s_1, s_2) \, \mathbf{Z}_{1,int}^2(\mathbf{s}) \, \mathrm{d}\mathbf{s} \, . \tag{4.57}$$

We can go on with this process and find explicitly functions $\mathbf{Z}_{i,int}^2(\mathbf{s})$ for $i = 2, \ldots, 5$ such that

$$\forall i \in \{2, \ldots, 5\} \, , \qquad \mathbf{Z}_i^2 = -\varepsilon \int_{\partial \mathbb{R}^3_+} h(s_1, s_2) \left(\mathbf{Z}_{i,int}^2(\mathbf{s}) \right) \mathrm{d}\mathbf{s} \, .$$

Finally,

$$\begin{aligned} \mathcal{A}(\mathbf{X}) = -\varepsilon^2 \int_{\partial \mathbb{R}^3_+} \int_{\partial \mathbb{R}^3_+} & h(s_1, s_2) \, h(s_1', s_2') \\ & \sum_{\mathcal{I}} \pm \left| \mathbf{Z}_{k_1,int}^2(s_1, s_2) \; \mathbf{Z}_{k_2,int}^2(s_1', s_2') \; \mathbf{Z}_{k_3}^1 \; \mathbf{Z}_{k_4}^1 \; \mathbf{Z}_{k_5}^1 \, (\mathbf{X}) \right| \, \mathrm{d}\mathbf{s} \, \mathrm{d}\mathbf{s}' . \end{aligned} \tag{4.58}$$

We call $\det_{int}$ the function $(\mathbf{X}, \mathbf{s}, \mathbf{s}') \mapsto \sum_{\mathcal{I}} \pm \left| \mathbf{Z}_{k_1,int}^2(\mathbf{s}) \; \mathbf{Z}_{k_2,int}^2(\mathbf{s}') \; \mathbf{Z}_{k_3}^1 \; \mathbf{Z}_{k_4}^1 \; \mathbf{Z}_{k_5}^1 \, (\mathbf{X}) \right|$. Clearly, for Theorem 4.5.6 to hold, it is enough that there exists $\mathbf{X}_0 \in \mathcal{S}$ and $(\mathbf{s}, \mathbf{s}') \in (\partial \mathbb{R}^3_+)^2$ such that $\det_{int}(\mathbf{X}_0, \mathbf{s}, \mathbf{s}')$ is not zero for some $(\mathbf{s}, \mathbf{s}') \in \mathbb{R}^4$. Indeed, we can then adjust the function h to make the integral non-zero. The calculation of $\det_{int}$ can be carried out using Maple. More precisely, one can derive an equivalent as z goes to infinity, and check that $\det_{int}(\mathbf{X}_0, \cdot, \cdot) \neq 0$ for $\mathbf{X}_0 = \left(1, 2, \frac{\pi}{3}, \frac{\pi}{3}, 1, 2, z\right)$ for z large enough. This concludes the proof.

4.6 Conclusions and perspectives

The aim of this present paper was to examine how the controllability of low Reynolds number artificial swimmers is affected by the presence of a rough wall on a fluid. This study generalizes the one made by F. Alouges and L. Giraldi in [11] which deals with the effect of a plane wall on the controllability of this particular swimmers.

Firstly, we show Theorem 4.2.1. It deals with the regularity of the dynamics of the swimmers. Indeed, we prove that the equation of motion of such particular swimmers are analytic with respect to the parameters defining the swimmer (radius of the ball, position and length of the arms) and the typical height of roughness of the wall. Then, we deduce Theorem 4.2.3 which claims that the 4-sphere swimmer remains controllable with the presence of roughness. The proof is based on general arguments which could be used for other models of micro-swimmer.

Secondly, Theorem 4.2.4 examines the controllability of the Three-sphere swimmer in the presence of a rough wall. More precisely, we show that there exists a roughness such that the

swimmer can locally reach any direction. We recall that the previous studies made on the 3-sphere swimmer allow to show that it can reach only one direction (see [7] when it evolves in a whole space and three directions with the presence of a plane wall (see [11]). In our case, the roughness leads to break the symmetry of the system "fluids-swimmer". As a result, it allows the swimmer to reach any direction. The proof is an in-depth study which associates several tools both in hydrodynamics and control theory. The general "idea" emphasizes here is the fact that in the real life all the micro-organism, regardless how symmetric it is, can move in any direction.

The quantitative approach to this question together with the complete understanding in a view of controllability of underlying systems is far beyond reach and thus still under progress as in a another direction, the consideration of an confined environment, e.g. when the fluid is bounded. Future work will also explore which are the directions easier to reach than the others by varying the rough wall.

4.7 Appendix: A well-posedness result for the Stokes system

We show here the well-posedness of the inhomogeneous Stokes system involved in the proof of Theorem 4.2.1. We refer to this proof for notations, and shall drop here all bars for brevity. What we want to show is

Proposition 4.7.1 *Let $(F, G, V_1, ..., V_N)$ given in $(\mathcal{V}_0)' \times L^2(\mathcal{F}) \times \prod_l H^{1/2}(B_l)$. There exists a unique solution (V, Q) in $\mathcal{V}_0 \times L^2(\mathcal{F})$ of*

$$\begin{aligned} -\Delta V + \nabla Q &= F \quad \text{in } \mathcal{F}, \\ \text{div } V &= G \quad \text{in } \mathcal{F}, \\ V = 0 \quad \text{at } \partial\mathcal{O}, \quad V &= V_l \quad \text{at } \partial B_l, \quad l = 1...N. \end{aligned}$$

Proof of the Proposition. In the "standard" case where $G = 0$ and all V_l's are zero, the result follows from a direct variational argument. Thus the whole point is to find a $W \in \mathcal{V}_0$ satisfying

$$\text{div } W = G \quad \text{in } \mathcal{F}, \quad V = 0 \quad \text{at } \partial\mathcal{O}, \quad V = V_l \quad \text{at } \partial B_l, \quad l = 1...N. \tag{4.59}$$

Indeed, setting $V' := V - W$, one comes back to the standard case with $F + \Delta W$ replacing F.

To build such W, a key ingredient is

Lemma 4.7.2 *Given $G \in L^2(\mathcal{O})$, there exists a field $W \in L^2_{loc}(\mathcal{O}), \nabla W \in L^2(O)$ such that*

$$\text{div } W = G, \quad W|_{\partial\mathcal{O}} = 0 \quad \|\nabla W\|_{L^2} \leq C \|G\|_{L^2}.$$

Note that this lemma is only about the domain $\mathcal{O}$, that is without the balls. Let us postpone its proof, and show how it implies the existence of a W satisfying (4.59).

- First step: we lift the boundary data V_l. One can find $\overline{W} \in H^1(\mathcal{F})$ compactly supported near the balls, such that $\overline{W} = V_l$ at ∂B_l. Up to replace W by $W - \overline{W}$ and G by $G -$ div $\overline{W}$, we can assume $V_l = 0$ for all l.
- Second step (assuming now $V_l = 0$ for all l): we extend G by 0 in the balls and apply the Lemma: it provides a $\tilde{W}$ satisfying div $\tilde{W} = G$, $\tilde{W}|_{\partial\mathcal{O}} = 0$. However, the boundary data at the balls is non-zero: $\tilde{W}|_{\partial B_l} \neq 0$.

- Third step: we correct this non-zero boundary data. We observe that

$$\int_{\partial B_l} \tilde{W} \cdot n \, ds = 0 = \int_{B_l} \text{div } \tilde{W} = 0,$$

as G was extended by zero inside the balls. Thanks to this "compatibility" condition, we can use a standard result of Bogovskii, see [, Exercice III.3.5, p176]: for all l, there exists a field W_l defined over the annulus $\{a < |x - x_l| < a + \eta\}$, satisfying

$$\text{div } W_l = 0, \quad W_l|_{\partial B_l} = -\tilde{W}|_{\partial B_l}, \quad W_l|_{\{|x-x_l|=a+\eta\}} = 0.$$

We take η small enough so that the annuli do not intersect. Then, we extend the W_l's by 0 outside the annuli and set $W := \tilde{W} + \sum W_l$. This new field W satisfies (4.59), as expected.

Proof of the Lemma. In the case where $h = cst$, that is for a flat half-space, the result is classical: *cf* [, Corollary 4.3.1, p261]. In particular, if the support of G is included in $\{x_3 > \sup |h|\}$, the problem is solved: one can take the solution W of

$$\text{div } W = G \quad \text{for} \quad x_3 > \sup |h|, \quad W|_{\{x_3=\sup |h|\}} = 0$$

and extend it by zero below $\{x_3 = \sup |h|\}$.

For general G, we can decompose $G = G\,1_{\{x_3>\sup |h|\}} + G\,1_{\{x_3<\sup |h|\}}$, and handle the first part as previously. In other words, *it remains to consider the case where G is compactly supported in x_3.* From there, we proceed in three steps:

- Step 1. Let R such that $G = 0$ for $x_3 \geq R$. We introduce $W^1 := \nabla\psi\, 1_{\{x_3<R\}}$ where ψ satisfies

$$\Delta\psi = G \quad \text{for } \varepsilon h < x_3 < R, \quad \partial_n\psi|_{\partial\mathcal{O}} = 0, \quad \psi|_{x_3=R} = 0.$$

This Poisson equation has a unique solution in $H^2(\{\varepsilon h < x_3 < R\})$: note that Poincaré inequality applies thanks to the Dirichlet condition at $x_3 = R$. Hence, W^1 satisfies $\text{div } W^1 = G$ in the strip $\{\varepsilon h < x_3 < R\}$, and also trivially in the half-space $\{x_3 > R\}$. However, two problems remain: the normal component of W^1 jumps at $x_3 = R$, and it has non-zero boundary data at $\{x_3 = \varepsilon h\}$.

- Step 2. Correction of the jump at $x_3 = R$. We just introduce the field $W^2 := \tilde{W}\, 1_{\{x_3>R\}}$, where $\tilde{W}$ satisfies

$$\text{div } \tilde{W} = 0 \quad \text{for} \quad x_3 > R, \quad \tilde{W}|_{\{x_3=R\}} = \nabla\Psi|_{x_3=R},$$
$$\|\nabla\tilde{W}\|_{L^2} \leq C\|\nabla\psi\|_{H^{1/2}(\{x_3=R\})} \,(\leq C\,\|G\|_{L^2}).$$

The existence of such $\tilde{W}$ is classical, see [39, Theorem IV.3.3].

- Step 3. Correction of the boundary data. Thanks to the Neumann condition on ψ, we have $W^1 \cdot n|_{\partial\mathcal{O}} = 0$. We introduce some partition of unity $(\chi_k = \chi_k(x_1, x_2))_{k\in\mathbb{Z}^2}$ associated to a covering of $\mathbb{R}^2$ by rectangles R_k. More precisely, we assume that the lengths of R_k are uniformly bounded in k, and that the C^1 norms of χ^k are uniformly bounded in k (we leave the construction of examples to the reader). Thanks to the tangency condition on W^1, we can apply the Bogovskii's result seen above on slices $S_k := \{(x_1, x_2) \in R_k, \quad \varepsilon h(x_1, x_2) < x_3 < R\}$, $k \in \mathbb{Z}^2$. Hence, there exists some $W_k \in H^1(S_k)$ such that

$$\text{div } W_k = 0 \quad \text{in} \quad S_k, \quad W_k = -\chi_k W^1 \quad \text{at} \quad \partial S_k \cap \partial\mathcal{O},$$
$$W_k = 0 \quad \text{at} \quad \partial S_k \setminus \mathcal{O},$$

and $\|\nabla W_k\|_{L^2} \leq C \|\chi_k W^1\|_{H^{1/2}(\partial\mathcal{O})}$. Extending all W_k's by 0 outside S_k, and setting $W^3 := \sum_{k\in\mathbb{Z}^2} W_k$, we find that

$$\text{div } W^3 = 0 \quad \text{in} \quad \mathcal{O}, \quad W^3|_{\partial\mathcal{O}} = -W^1|_{\partial\mathcal{O}},$$
$$\|\nabla W^3\|_{L^2(\mathcal{O})} \leq C\|W^1\|_{H^{1/2}(\partial\mathcal{O})} \, (\leq C\|W^1\|_{H^1(\mathcal{O})}).$$

Finally, $W = W^1 + W^2 + W^3$ fulfills all requirements, which concludes the proof of the lemma.

Troisième partie

Problèmes optimaux associés au déplacement d'un micro-nageur

Chapitre 5

Optimal strokes for driftless swimmers : a geometrical approach

---

This work is done in collaboration with T. Chambrion and A. Munnier. The aim of this study is to provide a general framework to examine optimal controllability of driftless swimmer. We focus on the analyze on the optimal strokes i.e., periodic shape changes. More precisely, we prove the existence of optimal strokes, minimizing or maximizing various cost functionals (related to the energy of the system, the efficiency, the time). Then, we demonstrate some properties of the optimal strokes. In particular, we show how the optimal controls corresponding to different cost functionals can actually be deduced one from the others. Finally, we analyze the regularity and the monotony of the value functions. We prove that the cost *increases* along with the covered distance. Numerical simulations are presented on a particular swimmer which has an explicit dynamics.

5.1 Introduction

Understanding the mechanics of swimming has been an issue in Mathematical Physics for a long time. Aside from improving the academic understanding of locomotion in fluid, this interest growth from the observation that fish and aquatic mammals evolved swimming capabilities far superior to those achieved by human technology and consequently provide an attractive model for the design of biomimetic robots.

Significant contributions to this matter are due to Taylor [84], J. Lighthill [54], E.M. Purcell [70] and T. Y. Wu [93].

Among the many models available in the literature, let us focus on those for which the Reynolds number of the fluid is either very low or very high. The main interest of these cases lies in the fact that the dynamics governing the fluid-swimmer system are simple enough to allow theoretical results to be proved. Theses two cases are usually referred to as "driftless models". The first one for which the fluid is assumed to be very viscous is called "resistive model". It is relevant for microswimmers (like microorganisms) and consists in neglecting the inertial effects in the modeling. The second one, called "reactive model", is obtained by neglecting rather the viscous forces and is supposed to be relevant for swimmers with elongated bodies (like eels). Surprisingly, the dynamics are very close for both cases and their study fall under the same general abstract framework.

The well-posedness of the system of equations for these models was established for instance in [32], [22] and [59] in a Stokesian flow and in [27] in a perfect fluid. The controllability is addressed in [27] and [59] where the authors prove the generic controllability of 3D driftless swimmers in a perfect and Stokesian flow respectively. An earlier result was established in [8] and next improved in [11], in which 3D three or four- sphere mechanisms are shown to be controllable.

To our knowledge, still few theoretical studies have been conducted about optimal swimming (although more numerical approach of the problem are many). In [60], J. Loheac et al. are interested in optimizing the swimming of a 3D slightly deformable sphere in order to minimize its displacement time. In [7], the authors describe an algorithm allowing optimizing the strokes for a three-sphere swimmer, based on the theory of calculus of variations.

5.1.1 Contribution

The aim of this work is to provide a general framework to study optimal controllability of driftless swimmers. In particular, every aforementioned paper falls within this framework. After recalling minimal hypotheses ensuring the controllability of the system under consideration, we shall focus on the study of optimal strokes i.e. periodic shape changes. More precisely, we will be interested in the following points:

- Existence of optimal strokes, minimizing or maximizing various cost functionals (related to the energy of the system, the efficiency, the time). As in [60], contraints on the state of the system are taken into account (for instance, the deformations are required to be *not too large*).
- Qualitative properties of the optimal strokes (or, differently stated, of the corresponding optimal controls). In particular, we will show how the optimal controls corresponding to different cost functionals can actually be deduced one from the others.
- Regularity and monotony of the value functions (does the cost increases along with the covered distance?).

Most of the proofs rely on the following arguments:

- The analyticity of the system;

- The Riemannian and sub-Riemannian underlying structure.

For pedagogical purposes, the results will be applied to the toy model introduced in [27] and [65]. The main interest of this model, dealing with a swimmer in a 2D potential flow, is that the governing equations, although not trivial, can be made fully explicit by means of complex calculus.

5.1.2 Abstract Framework and Notation

We introduce in this subsection the general framework of our study. In the sequel, we call *swimmer* any 5-uple $\mathfrak{S} = (\mathcal{S}, \mathbf{g}, \mathbf{Q}^{\mathcal{S}}, \mathbf{s}^{\dagger}, \mathcal{L})$, where:

- $(\mathcal{S}, \mathbf{g})$ is a N-dimensional ($N \geq 1$), connected, analytic manifold endowed with an analytic Riemannian structure $\mathbf{g}$. Every element $\mathbf{s}$ of $\mathcal{S}$ stands for a possible shape of the swimmer. The shape changes of the swimmer over a time interval $[0, T]$ will be described by a function $\mathbf{s} : [0, T] \mapsto \mathbf{s}(t) \in \mathcal{S}$.

- The metric $\mathbf{g}$ will be used to measure the cost required to achieve this shape change. The cost of a shape change $\mathbf{s} : [0, T] \mapsto \mathbf{s}(t) \in \mathcal{S}$ could be, for instance, the length of the curve parameterized by the function $\mathbf{s}$, i.e.

$$\int_0^T \sqrt{\mathbf{g}_{\mathbf{s}(t)}(\dot{\mathbf{s}}(t), \dot{\mathbf{s}}(t))} \mathrm{d}t, \tag{5.1a}$$

  or something more energy-like, usually called the action:

$$\frac{1}{2} \int_0^T \mathbf{g}_{\mathbf{s}(t)}(\dot{\mathbf{s}}(t), \dot{\mathbf{s}}(t)) \mathrm{d}t. \tag{5.1b}$$

- The reference shape $\mathbf{s}^{\dagger}$ is a point of $\mathcal{S}$ which could be thought of as the natural shape of the swimmer, when it is at rest for instance. It will be the starting point for every shape change we will consider.

- The mapping $\mathbf{Q}^{\mathcal{S}} : T\mathcal{S} \to \mathbb{R}^n$ is an analytic vector valued 1-form. It accounts for the physical constraints that every shape change has to satisfy to physically make sense. Let us be more specific:

  Definition 5.1.1 *An admissible shape change is any absolutely continuous curve* $\mathbf{s} : [0, T] \to \mathcal{S}$, *with essentially bounded first derivative, and which satisfies for almost every time,*

$$\mathbf{Q}^{\mathcal{S}}_{\mathbf{s}(t)} \dot{\mathbf{s}}(t) = 0. \tag{5.2}$$

  This last identity means that for a given shape (i.e. a given element of $\mathcal{S}$), not every direction on $\mathcal{S}$ is admissible. For instance, by self-deforming, the swimmer will not be allowed to modify the position of its center of mass.

  Among admissible shape changes, we will mostly focus on strokes:

  Definition 5.1.2 *An admissible shape change* $\mathbf{s} : [0, T] \mapsto \mathcal{S}$ *will be termed a stroke if* $\mathbf{s}(0) = \mathbf{s}(T)$.

- We are only interested in the motion of the swimmer in one given direction. The displacement in this direction is measured thanks to the analytic differential 1-form $\mathcal{L}$ on $\mathcal{S}$. When undergoing the admissible shape change $\mathbf{s} : [0, T] \to \mathcal{S}$, the displacement of the swimmer is given by:

$$\int_0^T \mathcal{L}_{\mathbf{s}(t)}(\dot{\mathbf{s}}(t)) \mathrm{d}t. \tag{5.3}$$

Most of our results will rest on the following elementary but fundamental observation:

Remark 5.1.3 *The constraint* (5.2) *as well as the quantities* (5.1a) *and* (5.3) *are time reparameterization invariant. They depend only on the oriented curve* $\Gamma \subset \mathcal{S}$*, a parameterization of which being* $\mathbf{s} : [0, T] \to \mathcal{S}$*.*

The famous *Scallop Theorem* (see for instance [70]) can be seen as a straightforward consequence of this remark. Indeed, it states that if the shape change is nothing more than a parameterization back and forth of a curve on $\mathcal{S}$, then the resulting displacement is null.

5.1.3 Outline and Main Achievements

In Section 5.2, we show that two important cases of locomotion in a fluid (namely the locomotion of a single swimmer in an infinite extent of fluid at infinite and zero Reynolds number) fit within the framework of Section 5.1.2. In Section 5.3, we establish minimal hypotheses (based on the computation of Lie brackets) ensuring the controllability of the system. Section 5.4 is dedicated to the study of optimal strokes. After stating 5 classical optimization problems, we show that every one admits minimizers or maximizers. We prove that most of these problems are actually equivalent (for instance, it is completely equivalent to minimize the time, as in [60] and to minimize the efficiency as in [8]). Then we focus on two values functions: the first one associates to every covered distance the minimal cost necessary to achieve this displacement and the other associates to every given cost, the maximum distance that can be covered with no greater cost. Among others properties, we prove the continuity and study the monotony of these functions. In Section 5.5, we restrict our study to the case where the shape manifold $\mathcal{S}$ is 2 dimensional. We show that the stroke optimization problem turns into an isoperimetric problem on the shape manifold. The sub-Riemannian structure becomes a *contact* sub-Riemannian structure and applying results from [1], we give a precise description of all the "small" optimal strokes. Some numerics applications on the example of swimmer in a potential flow are displayed in the last section.

5.2 Modeling

In this Section we aim to establish the dynamics governing the motion of low and high Reynolds numbers swimmers and show that they fall within the abstract framework introduced in Section 5.1.2.

Our purpose it to highlight that, although the properties of the fluid are different in both cases, the equations of motion turn out to have the exact same general form. The modeling is carried out in 3D, the 2D case being similar.

We assume that the swimmer is alone in the fluid and that the fluid-swimmer system fills the whole space. The buoyant force is not taken into account.

We consider a Galilean fixed frame $(\mathbf{E}_1, \mathbf{E}_2, \mathbf{E}_3)$ and an attached coordinate system $\mathcal{R}_f := (O, \mathbf{E}_1, \mathbf{E}_2, \mathbf{E}_3)$ where O is a fixed point of $\mathbb{R}^3$. In $\mathcal{R}_f$, coordinates will be written with capital letters (as $X := (X_1, X_2, X_3)$). Since we are interested in seeking optimal strokes, we will consider only shape changes that make the center of mass of the swimmer remains on the X_1-axis. Thus, the swimmer is compelled to swim along a straight line.

Kinematics

We denote by $\mathbf{r}$ the center of mass of the swimmer (lying on the X_1-axis) and we consider the coordinate system $\mathcal{R}_m := (\mathbf{r}, \mathbf{E}_1, \mathbf{E}_2, \mathbf{E}_3)$, attached to the swimmer.

We assume that every possible shape of the swimmer, when described in $\mathcal{R}_m$, can be characterized by a so-called shape variable $\mathbf{s}$ belonging to some connected analytic hypersurface $\mathcal{S}$ of $\mathbb{R}^{N+1}$ (for some integer $N \geq 1$).

Thus, we denote by $\mathcal{A}_m(\mathbf{s})$ the domain of $\mathbb{R}^3$ occupied by the swimmer, in the coordinate system $\mathcal{R}_m$, and hence $\mathcal{A}_f(\mathbf{s}) = \mathbf{r} + \mathcal{A}_m(\mathbf{s})$ is the same domain expressed in $\mathcal{R}_f$. For every $\mathbf{s} \in \mathcal{S}$, the set $\mathcal{A}_m(\mathbf{s})$ is the image of the unit ball B by a C^1 diffeomorphism $\chi(\mathbf{s}, \cdot)$ depending on the parameter $\mathbf{s}$. Knowing every diffeomorphism $\chi(\mathbf{s}, \cdot)$ for every shape variable $\mathbf{s}$, the shape changes over a time interval $[0, T]$ can be merely described by means of a (shape) function:

$$t \in [0, T] \mapsto \mathbf{s}(t) \in \mathcal{S}.$$

The Eulerian velocity $\mathbf{W}$ at any point $X \in \mathcal{A}_f(\mathbf{s})$ of the swimmer is the sum of the rigid velocity $\dot{\mathbf{r}} := \dot{r}\mathbf{E}_1$ ($\dot{r} \in \mathbb{R}$) and the velocity of deformation

$$\mathbf{W}_d(\mathbf{s}, \dot{\mathbf{s}}, X) := \nabla_{\mathbf{s}} \chi \left(\mathbf{s}, \chi(\mathbf{s}, (X - \mathbf{r}))^{-1}\right) \cdot \dot{\mathbf{s}}.$$

Thus, we get:

$$\mathbf{W} = \dot{\mathbf{r}} + \mathbf{W}_d \qquad \text{in } \mathcal{A}_f(\mathbf{s}).$$

In the coordinate system $\mathcal{R}_m$, this equality turns out to be:

$$\mathbf{w} = \dot{\mathbf{r}} + \mathbf{w}_d \qquad \text{in } \mathcal{A}_m(\mathbf{s}),$$

where, for every $x \in \mathcal{A}_m(\mathbf{s})$ we have set $\mathbf{w}(x) := \mathbf{W}(x + \mathbf{r})$ and $\mathbf{w}_d(\mathbf{s}, \dot{\mathbf{s}}, x) := \mathbf{W}_d(\mathbf{s}, \dot{\mathbf{s}}, x + \mathbf{r})$.

Dynamics

In $\mathcal{R}_m$, the density $\varrho(\mathbf{s}, \cdot)$ of the body can be deduced from a given constant density $\varrho_0 > 0$, defined in B, according to the conservation of mass principle:

$$\varrho(\mathbf{s}, \chi(\mathbf{s}, x)) = \frac{\varrho_0}{|\det \nabla_x \chi(\mathbf{s}, x)|}, \qquad x \in B.$$

The volume of the swimmer is $\mathrm{Vol}(\mathbf{s}) = \int_B |\det \nabla_x \chi(\mathbf{s}, x)| \mathrm{d}x$ and its mass $m = \varrho_0 \mathrm{Vol}(B)$.

Although prescribed, the deformations should be interpretable as produced by some internal forces. It means that in the absence of fluid, the swimmer is not able to modify its linear momentum, which reads:

$$\int_{\mathcal{A}_m(\mathbf{s})} \varrho(\mathbf{s}, x) \mathbf{w}_d(\mathbf{s}, \dot{\mathbf{s}}, x) \mathrm{d}x = \varrho_0 \int_B \nabla_{\mathbf{s}} \chi(\mathbf{s}, x) \cdot \dot{\mathbf{s}} \, \mathrm{d}x = \mathbf{0}. \tag{5.4}$$

We introduce the $3 \times N$ matrix:

$$\mathbf{Q}^{\mathcal{S}}(\mathbf{s}) := \varrho_0 \int_B \nabla_{\mathbf{s}} \chi(\mathbf{s}, x) \mathrm{d}x, \tag{5.5}$$

and we rewrite (5.2) as:

$$\mathbf{Q}^{\mathcal{S}}(\mathbf{s}) \dot{\mathbf{s}} = \mathbf{0}. \tag{5.6}$$

This equation has to be understood as a constraint on the shape variable and is referred to as the *self-propulsion hypothesis*.

The fluid obeys, in the whole generality, to the Navier-Stokes equations for incompressible fluid:

$$\varrho_f \frac{D}{Dt} \mathbf{U}(t, X) - \nabla_X \cdot \mathbb{T}_f(\mathbf{U}, P)(t, X) = 0 \qquad t > 0,\ X \in \mathcal{F}_f(\mathbf{s}(t)); \tag{5.7a}$$

$$\nabla_X \cdot \mathbf{U}(t, X) = 0 \qquad t > 0,\ X \in \mathcal{F}_f(\mathbf{s}(t)); \tag{5.7b}$$

where

1. For every $\mathbf{s} \in \mathcal{S}$, $\mathcal{F}_f(\mathbf{s}) := \mathbb{R}^3 \setminus \overline{\mathcal{A}_f(\mathbf{s})}$ is the domain of the fluid;

2. $\varrho_f > 0$ is the fluid's density;
3. $\mathbf{U}(t, X)$ is the Eulerian velocity of the fluid at the time $t > 0$ and the point $X \in \mathcal{F}_f(\mathbf{s}(t))$;
4. $D/Dt := \partial/\partial t + (\mathbf{U}(t, X) \cdot \nabla_X)$ is the convective derivative;
5. $\mathbb{T}_f(\mathbf{U}, P)(t, X) := \mu(\nabla_X \mathbf{U}(t, X) + \nabla_X \mathbf{U}^T(t, X)) - P(t, X)\mathbb{I}\mathrm{d}$ is the stress tensor, μ the dynamic viscosity and P the pressure.

The rigid displacement of the body is governed by Newton's laws for the linear momentum:

$$m\ddot{r}(t) = -\int_{\partial\mathcal{A}_f(\mathbf{s})} \mathbf{E}_1 \cdot \mathbb{T}_f(\mathbf{U}, P)(t, X)\mathbf{n}\, \mathrm{d}\sigma_X, \qquad (t > 0),$$

where $\mathbf{n}$ is the unit normal vector to $\partial\mathcal{A}_f(\mathbf{s})$ directed towards the interior of $\mathcal{A}_f(\mathbf{s})$.

These equations have to be supplemented with boundary conditions on $\partial\mathcal{A}_f(\mathbf{s})$, which can be either

$$\mathbf{U} \cdot \mathbf{n} = \mathbf{W} \cdot \mathbf{n} \qquad \text{on } \partial\mathcal{A}_f(\mathbf{s}),$$

known as *slip* or Navier boundary conditions or

$$\mathbf{U} = \mathbf{W} \qquad \text{on } \partial\mathcal{A}_f(\mathbf{s}),$$

referred to as *no-slip* boundary conditions. Eventually, for the system to be well-posed, initial data are needed:

$$\mathbf{U}(0) = \mathbf{U}_0,\ \mathbf{r}(0) = \mathbf{r}_0 \text{ and } \dot{\mathbf{r}}(0) = \dot{\mathbf{r}}_0.$$

As mentioned in the introduction, we focus on two limit problems connecting to the value of the Reynolds number $\mathrm{Re} := \varrho\bar{\mathbf{U}}L/\mu$ ($\bar{\mathbf{U}}$ is the mean fluid velocity and L is a characteristic linear dimension). The first case $\mathrm{Re} \ll 1$ concerns low Reynolds swimmers like bacteria (or more generally so-called micro swimmers whose size is about $1\mu m$). For the second $\mathrm{Re} \gg 1$, we will restrain our study to irrotational flows and so it is relevant for large animals swimming quite slowly, a case where vorticity can be neglected.

5.2.1 Low Reynolds number swimmers

For micro-swimmers, scientists agree that inertia (for both the fluid and the body) can be neglected in the dynamics. It means that in the modeling, we can set $\varrho_0 = \varrho_f = 0$. In this case, the Navier-Stokes equations reduce to the steady Stokes equations

$$\begin{aligned} -\nabla_X \cdot \mathbb{T}_f(\mathbf{U}, P)(t, X) &= 0 \qquad t > 0,\ X \in \mathcal{F}_f(\mathbf{s}(t)); \\ \nabla_X \cdot \mathbf{U}(t, X) &= 0 \qquad t > 0,\ X \in \mathcal{F}_f(\mathbf{s}(t)); \end{aligned}$$

supplemented with no-slip boundary conditions

$$\mathbf{U} = \mathbf{W} \text{ on } \partial\mathcal{A}_f(\mathbf{s}).$$

Introducing, for all $x \in \mathcal{F}_m(\mathbf{s}) := \mathbb{R}^3 \setminus \overline{\mathcal{A}_m(\mathbf{s})}$,

$$\mathbf{u}(t, x) := \mathbf{U}(t, x + \mathbf{r}(t)) \quad \text{ and } \quad p(t, x) := P(t, x + \mathbf{r}(t)),$$

the equations keep the same form when expressed in the coordinate system $\mathcal{R}_m$, namely, with evident notation:

$$-\nabla_x \cdot \mathbb{T}_m(\mathbf{u}, p)(t, x) = 0 \qquad t > 0,\ x \in \mathcal{F}_m(\mathbf{s}(t)); \tag{5.8a}$$

$$\nabla_x \cdot \mathbf{u}(t, x) = 0 \qquad t > 0,\ x \in \mathcal{F}_m(\mathbf{s}(t)); \tag{5.8b}$$

$$\mathbf{u}(t, x) = \mathbf{w}(t, x) \qquad t > 0,\ x \in \partial\mathcal{A}_m(\mathbf{s}(t)). \tag{5.8c}$$

From a mathematical point of view, the advantage is two folds:

1. The equations are now linear;
2. The fluid has no more proper degree of freedom. Indeed, the fluid equations simplify from an initial and boundary value problem into merely a boundary value problem. In particular, no more initial data is required.

Newton's law for linear momentum reads:

$$\int_{\partial\mathcal{A}_m(\mathbf{s})} \mathbf{E}_1 \cdot \mathbb{T}_m(\mathbf{u},p)(t,x)\mathbf{n}\mathrm{d}\sigma = 0.$$

The solution $(\mathbf{u},p)$ being linear with respect to the boundary data $\mathbf{w}$ it can be decomposed as follows:

$$\begin{aligned}
\mathbf{u}(t,x) &= \dot{r}(t)\mathbf{u}_r(\mathbf{s}(t),x) + \sum_{j=1}^{N} \dot{s}_j u_d^j(\mathbf{s}(t),x);\\
p(t,x) &= \dot{r}(t)p_r(\mathbf{s}(t),x) + \sum_{j=1}^{N} \dot{s}_j p_d^j(\mathbf{s}(t),x); \qquad (t>0,\, x\in\mathcal{F}_m(\mathbf{s})),
\end{aligned}$$

where we are written $\mathbf{s}=(s_1,\dots,s_N)$ in a local chart of $\mathcal{S}$ and $\dot{s}=(\dot{s}_1,\dots,\dot{s}_N)$ in the basis $(\partial_{s_1},\dots,\partial_{s_N})$ of the tangent space $T_{\mathbf{s}}\mathcal{S}$. It entails that the stress tensor:

$$\mathbb{T}_m(\mathbf{u},p) := \mu(\nabla_x\mathbf{u} + \nabla_x\mathbf{u}^T) - p\,\mathbb{I}\mathrm{d},$$

can also be decomposed as:

$$\mathbb{T}_m(\mathbf{u},p) = \dot{r}\mathbb{T}_m(\mathbf{u}_r,p_r) + \sum_{j=1}^{N} \dot{s}_j \mathbb{T}_m(\mathbf{u}_d^j,p_d^j).$$

The *elementary solutions* $(\mathbf{u}_r,p_r)$ and $(\mathbf{u}_d,p_d^j)$ satisfy the Stokes system (5.8a-5.8b) with the boundary conditions:

$$\begin{aligned}
&\mathbf{u}_r(t,x) = \mathbf{E}_1 && t>0,\, x\in\partial\mathcal{A}_m(\mathbf{s}(t));\\
&\mathbf{u}_d^j(t,x) = \mathbf{w}_d(\mathbf{s}(t),\partial_{s_j},x) && t>0,\, x\in\partial\mathcal{A}_m(\mathbf{s}(t)),\, j=1,\dots,N.
\end{aligned}$$

Notice that the elementary solutions $(\mathbf{u}_r,p_r)$ and $(\mathbf{u}_d^j,p_d^j)$ $(j=1,\dots,N)$ depend on the time through the shape variable $\mathbf{s}$ only. We next introduce the scalar:

$$M^r(\mathbf{s}) := \int_{\partial\mathcal{A}(\mathbf{s})} \mathbf{E}_1 \cdot \left(\mathbb{T}_m(\mathbf{u}_r,p_r)\right)\mathbf{n}\mathrm{d}\sigma,$$

and the row vector $\mathbf{N}(\mathbf{s})$ whose entries are:

$$N_j(\mathbf{s}) = \int_{\partial\mathcal{A}(\mathbf{s})} \mathbf{E}_1 \cdot \left(\mathbb{T}_m(\mathbf{u}_d^j,p_d^j)\right)\mathbf{n}\mathrm{d}\sigma.$$

We can rewrite Newton's laws as

$$\dot{r}M^r(\mathbf{s}) + \mathbf{N}(\mathbf{s})\dot{\mathbf{s}} = 0.$$

Upon an integration by parts, we get the equivalent definition $M^r(\mathbf{s})$:

$$M^r(\mathbf{s}) := \mu\int_{\mathcal{F}_m(\mathbf{s})} D(\mathbf{u}_r) : D(\mathbf{u}_r)\mathrm{d}x, \tag{5.9a}$$

where $D(\mathbf{u}_r) := (\nabla_x \mathbf{u} + \nabla_x \mathbf{u}^T)$. We deduce that $M^r(\mathbf{s})$ is always positive. The same arguments for $\mathbf{N}(\mathbf{s})$ lead to the identity:

$$N_j(\mathbf{s}) = \mu \int_{\mathcal{F}_m(\mathbf{s})} D(\mathbf{u}^r) : D(\mathbf{u}_d^j) \mathrm{d}x. \tag{5.9b}$$

Later on, we will also need the matrix:

$$\mathbb{M}^d(\mathbf{s}) = \left(\mu \int_{\mathcal{F}_m(\mathbf{s})} D(\mathbf{u}_d^i) : D(\mathbf{u}_d^j) \mathrm{d}x \right)_{\substack{1 \le i \le N \\ 1 \le j \le N}}. \tag{5.9c}$$

We eventually obtain the Euler-Lagrange equation governing the rigid displacement with respect to the shape changes:

$$\dot{r} = \mathcal{L}_{\mathbf{s}} \dot{\mathbf{s}} \qquad t > 0, \tag{5.10}$$

where we have set set, for every $\mathbf{s} \in \mathcal{S}$:

$$\mathcal{L}_{\mathbf{s}} = -M^r(\mathbf{s})^{-1} \mathbf{N}(\mathbf{s}).$$

Considering the expressions (5.9) and (5.10), we deduce:

Proposition 5.2.1 *The dynamics of a micro-swimmer is independent of the viscosity of the fluid. Or, in other words, the same shape changes produce the same rigid displacement, whatever the viscosity of the fluid is.*

Proof. Let $(\mathbf{u}, p)$ be an elementary solution (as defined in the modeling above) to the Stokes equations corresponding to a viscosity $\mu > 0$, then $(\mathbf{u}, (\tilde{\mu}/\mu)p)$ is the solution corresponding to the viscosity $\tilde{\mu} > 0$. Since the Euler-Lagrange equation depends only on the Eulerian velocities $\mathbf{u}$, the proof is completed. In the sequel, we will set $\mu = 1$.

The self-propelled constraint (5.2) does not make sense any longer for low Reynolds number swimmers because $\varrho_0 = 0$. However, since we still do not want the swimmer to be able to translate itself just by self-deforming, we require the shape function to satisfy (5.2) in which we define the matrix $\mathbf{Q}^{\mathcal{S}}(\mathbf{s})$ by:

$$\mathbf{Q}^{\mathcal{S}}(\mathbf{s}) := \int_{\Sigma} \nabla_{\mathbf{s}} \chi(\mathbf{s}, x) \, \mathrm{d}x, \tag{5.11}$$

where $\Sigma = \partial B$.

5.2.2 High Reynolds number swimmers

Assume now that the inertia is preponderant with respect to the viscous force (it is the case when $\mathrm{Re} \ll 1$). The Navier-Stokes equations (5.7) simplify into the Euler equations:

$$\varrho_f \frac{D}{Dt} \mathbf{U}(t, X) - \nabla_X \cdot \mathbb{T}_f(\mathbf{U}, P)(t, X) = 0 \qquad t > 0,\ X \in \mathcal{F}_f(\mathbf{s}(t)); \tag{5.12a}$$

$$\nabla_X \cdot \mathbf{U}(t, X) = 0 \qquad t > 0,\ X \in \mathcal{F}_f(\mathbf{s}(t)); \tag{5.12b}$$

$$\mathbf{U}(t, X) \cdot \mathbf{n} - \mathbf{W}(t, X) \cdot \mathbf{n} = 0 \qquad t > 0,\ X \in \partial \mathcal{A}_f(\mathbf{s}(t)). \tag{5.12c}$$

where the stress tensor reads:

$$\mathbb{T}_f(\mathbf{U}, P)(t, X) = -P(t, X) \mathrm{I}d \qquad t > 0,\ X \in \mathcal{F}_f(\mathbf{s}(t)).$$

Like in the preceding Subsection, we will assume that According to Kelvin's circulation theorem, if the flow is irrotational at some moment (i.e. $\nabla \times \mathbf{U} = 0$) then, it has always

been and will always remain irrotational. Hence, we can suppose that $\nabla \times \mathbf{U} = 0$ for all times and then, according to the Helmholtz decomposition, that there exists for all time $t > 0$ a potential scalar function $\Phi(t, \cdot)$ defined in $\mathcal{F}_f(\mathbf{s})$, such that

$$\mathbf{U}(t, X) = \nabla_X \Phi(t, X) \qquad t > 0,\ X \in \mathcal{F}_f(\mathbf{s}(t)).$$

The divergence-free condition leads to

$$\Delta_X \Phi(t, X) = 0 \qquad t > 0,\ X \in \mathcal{F}_f(\mathbf{s}(t)),$$

and the boundary condition reads:

$$\partial_{\mathbf{n}} \Phi(t, X) = \mathbf{W}(t, X) \cdot \mathbf{n} \qquad t > 0,\ X \in \partial\mathcal{A}_f(\mathbf{s}(t)).$$

The function $\varphi(t, \cdot)$ defined by:

$$\varphi(t, x) := \Phi(t, x - \mathbf{r}) \qquad t > 0,\ x \in \mathcal{F}_m(\mathbf{s}(t)),$$

is harmonic in $\mathcal{F}_m(\mathbf{s}(t))$ and satisfies the boundary condition:

$$\partial_{\mathbf{n}} \varphi(t, x) = \mathbf{w}(t, x) \cdot \mathbf{n} \qquad t > 0,\ x \in \partial\mathcal{A}_m(\mathbf{s}(t)).$$

The potential φ is linear in $\mathbf{w}$, so it can be decomposed into

$$\varphi(t, x) = \dot{r}\varphi_r(t, x) + \sum_{j=1}^{N} \dot{s}_j \varphi_d(t, x) \qquad t > 0,\ x \in \mathcal{F}_m(\mathbf{s}(t)),$$

where at every moment the elementary potentials $\varphi_r(t, \cdot)$ and $\varphi_d(t, \cdot)$ are harmonics in $\mathcal{F}_m(\mathbf{s}(t))$ and satisfy the boundary conditions:

$$\begin{aligned} &\partial_{\mathbf{n}} \varphi_r(t, x) = \mathbf{E}_1 \cdot \mathbf{n}, \\ &\partial_{\mathbf{n}} \varphi_d(t, x) = \mathbf{w}_d(\mathbf{s}(t), \partial_{s_j}, x) \qquad t > 0,\ x \in \partial\mathcal{A}_m(\mathbf{s}(t)). \end{aligned}$$

This process is usually referred to as Kirchhoff's law. At this point, we do not invoke Newton's laws to derive the Euler-Lagrange equation but rather use the formalism of Analytic Mechanics. Both approaches (Newton's laws of Classical Mechanics and the Least Action principle of Analytic Mechanics) are equivalent, as proved in [64], but the latter is simpler and shorter.

In the absence of buoyant force, the Lagrangian function L of the body-fluid system coincides with the kinetic energy:

$$L = m\frac{1}{2}|\dot{r}|^2 + \frac{1}{2}\int_{\mathcal{A}_m(\mathbf{s})} \varrho(\mathbf{s}, x)|\mathbf{w}_d(t, x)|^2 \mathrm{d}x + \frac{1}{2}\int_{\mathcal{F}_m(\mathbf{s})} \varrho_f |\mathbf{u}(t, x)|^2 \mathrm{d}x.$$

In this sum, one can identify, from the left to the right: the kinetic energy of the body connecting to the rigid motion, the kinetic energy resulting from the deformations and the kinetic energy of the fluid. We can next compute that, upon a change of variables:

$$\int_{\mathcal{A}_m(\mathbf{s})} \varrho(\mathbf{s}, x)|\mathbf{w}_d(t, x)|^2 \mathrm{d}x = \varrho_0 \int_B |\nabla_{\mathbf{s}} \chi(\mathbf{s}, x) \cdot \dot{\mathbf{s}}|^2 \, \mathrm{d}x,$$

and

$$\int_{\mathcal{F}_m(\mathbf{s})} \varrho_f |\mathbf{u}(t, x)|^2 \mathrm{d}x = \varrho_f \int_{\mathcal{F}_m(\mathbf{s})} |\nabla\varphi(t, x)|^2 \mathrm{d}x.$$

It leads us to introduce the scalar:

$$M^r(\mathbf{s}) = m + \varrho_f \int_{\mathcal{F}_m(\mathbf{s})} |\nabla \varphi_r(\mathbf{s}, x)|^2 \mathrm{d}x, \tag{5.13a}$$

the row vector $\mathbf{N}(\mathbf{s})$ whose entries are:

$$N_j(\mathbf{s}) = \varrho_f \int_{\mathcal{F}_m(\mathbf{s})} \nabla \varphi_r(\mathbf{s}, x) \cdot \nabla \varphi_d^j(\mathbf{s}, x) \mathrm{d}x, \qquad j = 1, \dots, N, \tag{5.13b}$$

and the matrix $\mathbb{M}^d(\mathbf{s})$:

$$\mathbb{M}^d(\mathbf{s}) = \varrho_0 \int_B \nabla_{\mathbf{s}} \chi(\mathbf{s}, x) \otimes \nabla_{\mathbf{s}} \chi(\mathbf{s}, x) \, \mathrm{d}x + \varrho_f \left(\int_{\mathcal{F}_m(\mathbf{s})} \nabla \varphi_d^i(\mathbf{s}, x) \cdot \nabla \varphi_d^j(\mathbf{s}, x) \mathrm{d}x \right)_{\substack{1 \le i \le N \\ 1 \le j \le N}}.$$

Observe the similarity between relations (5.9) and (5.13). We can rewrite the Lagrangian function as:

$$L(\dot{r}, \mathbf{s}, \dot{\mathbf{s}}) = \frac{1}{2} M^r(\mathbf{s}) |\dot{r}|^2 + \dot{r} \mathbf{N}(\mathbf{s}) \dot{\mathbf{s}} + \dot{\mathbf{s}} \cdot \mathbb{M}^d(\mathbf{s}) \dot{\mathbf{s}}.$$

Invoking now the Least Action principle, we claim that the Euler-Lagrange equation is:

$$\frac{d}{dt} \frac{\partial L}{\partial \dot{r}}(\dot{r}, \mathbf{s}, \dot{\mathbf{s}}) - \frac{\partial L}{\partial r}(\dot{r}, \mathbf{s}, \dot{\mathbf{s}}) = 0,$$

which reduces to, since L does not depend on r:

$$\frac{d}{dt} \left(M^r(\mathbf{s}) \dot{r} + \mathbf{N}(\mathbf{s}) \dot{\mathbf{s}} \right) = 0.$$

Assuming that the impulse $M^r(\mathbf{s}) \dot{r} + \mathbf{N}(\mathbf{s}) \dot{\mathbf{s}}$ is zero at the initial time, we get eventually for the dynamics the exact same expression as (5.10):

$$\dot{r} = \mathcal{L}_{\mathbf{s}} \dot{\mathbf{s}} \qquad t > 0,$$

where, for every $\mathbf{s} \in \mathcal{S}$:

$$\mathcal{L}_{\mathbf{s}} = -M^r(\mathbf{s})^{-1} \mathbf{N}(\mathbf{s}). \tag{5.14}$$

It is easy to verify that the dynamics does not depend on ϱ_0 and ϱ_f independently but only on the relative density ϱ_0/ϱ_f, which is assumed to be equal to 1 in the sequel.

5.2.3 Examples of cost functionals

For low Reynolds number swimmers, a classical notion of swimming efficiency (see [56] and [8]) is defined as the inverse of the ratio between the average power expended by the swimmer during a stroke starting and ending at the shape $\mathbf{s}^\dagger$ and the power that an external force would spend to translate the system rigidly at the same average speed:

$$\mathrm{Eff}^{-1} := \frac{\frac{1}{T} \int_0^T \left(\int_{\partial \mathcal{A}_m(\mathbf{s})} \mathbf{F}(\mathbf{s}, \dot{\mathbf{s}}, \dot{r}, x) \cdot \mathbf{u}(\mathbf{s}, \dot{\mathbf{s}}, \dot{r}, x) \mathrm{d}\sigma_x \right) \mathrm{d}t}{\bar{\mathbf{v}} \cdot \int_{\partial \mathcal{A}_m(\mathbf{s})} \mathbf{F}(\mathbf{s}^\dagger, \mathbf{0}, \bar{\mathbf{v}}, x) \mathrm{d}\sigma_x},$$

where

$$\mathbf{F}(\mathbf{s}, \dot{\mathbf{s}}, \dot{r}, x) := \left(\dot{r} \mathbb{T}_m(\mathbf{u}_r, p_r)(\mathbf{s}, x) + \sum_{j=1}^N \dot{s}_j \mathbb{T}_m(\mathbf{u}_j^d, p_d^j)(\mathbf{s}, x) \right) \mathbf{n}$$

is the force in the normal direction exerted by the fluid at the point x of the surface of the swimmer, with shape $\mathbf{s}$, shape change rate $\dot{\mathbf{s}}$ and rigid velocity $\dot{r}$. In the same way:

$$\mathbf{u}(\mathbf{s}, \dot{\mathbf{s}}, x) := \dot{r}\mathbf{E}_1 + \sum_{j=1}^{N} \dot{s}_j \mathbf{w}_d(\mathbf{s}, \partial_{s_j}, x),$$

is the velocity of the swimmer. Eventually $\bar{\mathbf{v}}$ is the average speed:

$$\bar{\mathbf{v}} := \left(\frac{1}{T} \int_0^T \dot{r} \mathrm{d}t \right) \mathbf{E}_1.$$

With the notation (5.9), the efficiency can be rewritten as:

$$\mathrm{Eff}^{-1} := \frac{\frac{1}{T}\int_0^T \left(M^r(\mathbf{s})|\dot{r}|^2 + \dot{r}\mathbf{N}(\mathbf{s})\dot{\mathbf{s}} + \dot{\mathbf{s}} \cdot \mathbb{M}^d(\mathbf{s})\dot{\mathbf{s}} \right) \mathrm{d}t}{|\bar{\mathbf{v}}|^2 M^r(\mathbf{s}^\dagger)}. \tag{5.15}$$

It can easily be verified that:

$$M^r(\mathbf{s})|\dot{r}|^2 + \dot{r}\mathbf{N}(\mathbf{s})\dot{\mathbf{s}} + \dot{\mathbf{s}} \cdot \mathbb{M}^d(\mathbf{s})\dot{\mathbf{s}} = \int_{\mathcal{F}_m(\mathbf{s})} D(\mathbf{u}, p) : D(\mathbf{u}, p) \mathrm{d}x > 0,$$

where $(\mathbf{u}, p)$ is the solution to the Stokes system (5.8).

For high Reynolds number swimmers, we can choose the same expression (5.15) for the efficiency, in which we use the definitions (5.13). In this case, the efficiency is the inverse of the ratio between the mean energy expended by the swimmer divided by the energy required to translate rigidly the swimmer at the same average speed.

Taking into account the dynamics and replacing $\dot{r}$ by $-M^r(\mathbf{s})^{-1}\mathbf{N}(\mathbf{s})\dot{\mathbf{s}}$ in (5.15), it leads us to consider on $T_{\mathbf{s}}\mathcal{S}$ the following scalar product:

$$\mathbf{g}_{\mathbf{s}}(\dot{\mathbf{s}}_1, \dot{\mathbf{s}}_2) = \dot{\mathbf{s}}_1 \cdot \left(\mathbb{M}^d(\mathbf{s}) - \frac{\mathbf{N}(\mathbf{s}) \otimes \mathbf{N}(s)}{M^r(\mathbf{s})} \right) \dot{\mathbf{s}}_2, \quad (\dot{\mathbf{s}}_1, \dot{\mathbf{s}}_2 \in T_{\mathbf{s}}\mathcal{S}). \tag{5.16}$$

According to the abstract framework introduced in Section 5.1.2, the cost of an admissible shape change $\mathbf{s} : [0, T] \mapsto \mathcal{S}$ will be:

$$\frac{1}{2} \int_0^T \mathbf{g}_{\mathbf{s}(t)}(\dot{\mathbf{s}}(t), \dot{\mathbf{s}}(t)) \mathrm{d}t. \tag{5.17}$$

5.2.4 Regularity results

In Section 5.1.2, the manifold $\mathcal{S}$ and the differential forms are all of them assumed to be analytic. The following Lemma ensures that, under a simple hypothesis, this regularity is ensured for swimmers in a perfect fluid and Stokesian swimmers.

We denote by $M(N_1, N_2)$ the Euclidian space of the $N_1 \times N_2$ matrices and we claim:

Lemma 5.2.2 *Assume that the map $\mathbf{s} \in \mathcal{S} \mapsto \chi(\mathbf{s}, \cdot) \in C^1(\bar{B}, \mathbb{R}^3)$ is analytic (we refer to [90] for the definitions and the properties of analytic functions valued in Banach spaces), then for both cases (low and high Reynolds number swimmers) the maps $\mathbf{s} \in \mathcal{S} \mapsto \mathbf{Q}^{\mathcal{S}}(\mathbf{s}) \in M(3, N)$, $\mathbf{s} \in \mathcal{S} \mapsto M^r(\mathbf{s}) \in \mathbb{R}$, $\mathbf{s} \in \mathcal{S} \mapsto \mathbf{N}(\mathbf{s}) \in \mathbb{R}^N$ and $\mathbf{s} \in \mathcal{S} \mapsto \mathbb{M}^d(\mathbf{s}) \in M(N, N)$ are analytic.*

The proofs can be found in [28] for swimmers in a perfect fluid and in [59] for Stokesian swimmers.

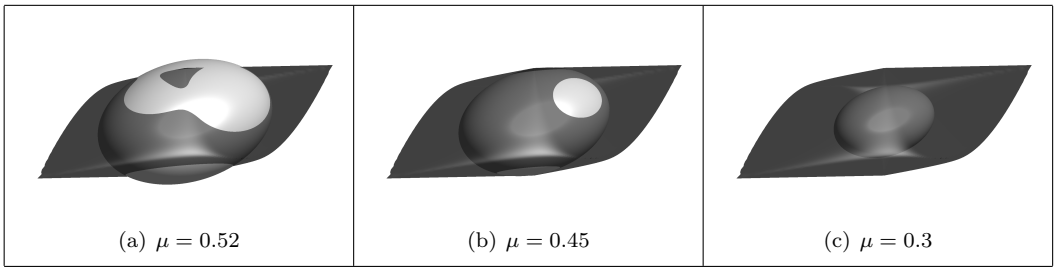

(a) $\mu = 0.52$ (b) $\mu = 0.45$ (c) $\mu = 0.3$

Figure 5.1: Examples of manifolds $\mathcal{S}_\mu$ for different values of μ. For small values of μ, $\mathcal{S}_\mu$ turns out to be merely the surface of the ellipsoid since it is entirely included in the unit ball.

5.2.5 An example of swimmer in a potential flow

All along the paper, we will illustrate our purpose by applying our approach to a concrete example. We have chosen to deal with a simplified version of a 2D swimmer in a perfect fluid introduced in [27] and improved in [65].

Shape changes

Recall that in 2D, at every time, $\mathcal{A}_m(\mathbf{s})$ is the image of the unit disk D by a diffeomorphism $\chi(\mathbf{s}, \cdot)$ depending on the parameter $\mathbf{s}$, and whose form (with complex notation) is:

$$\chi(\mathbf{s}, z) = z + s_1\bar{z} + s_2\bar{z}^2 + s_3\bar{z}^3, \qquad (z \in \mathbb{C},\, \mathbf{s} = (s_1, s_2, s_3) \in \mathbb{R}^3). \tag{5.18}$$

We define the following norm in $\mathbb{R}^3$:

$$\|\mathbf{s}\|_{\mathcal{S}} = \sup_{z \in \partial D} |s_1 + 2s_2 z + 3s_3 z^2|, \qquad (\mathbf{s} \in \mathbb{R}^3).$$

and we claim (see [27] for details):

Lemma 5.2.3 *1. The mapping $\chi(\mathbf{s}, \cdot)$ is a C^∞ diffeormorphism from the the unit ball D onto its image $\mathcal{A}_m(\mathbf{s})$ if and only if $\|\mathbf{s}\|_{\mathcal{S}} < 1$.*

2. The measure of the area of $\mathcal{A}_m(\mathbf{s})$ is $\pi(1 - s_1^2 + 2s_2^2 + 3s_3^2)$.

Since we want both conditions (i) the mapping $\chi(\mathbf{s}, \cdot)$ is a diffeomorphism and (ii) the area of $\mathcal{A}_m(\mathbf{s}, \cdot)$ is of constant (and nonzero) measure, to be fulfilled, we introduce for every $0 < \mu < 1$ the set (see Fig. 5.1):

$$\mathcal{S}_\mu = \{\mathbf{s} \in \mathbb{R}^3 \,:\, \|\mathbf{s}\|_{\mathcal{S}} < 1 \text{ and } s_1^2 + 2s_2^2 + 3s_3^2 = \mu^2\}.$$

For any $0 < \mu < 1$, $\mathcal{S}_\mu$ is a 2D analytic submanifold of $\mathbb{R}^3$. It consists in the parts the ellipsoid surface $s_1^2 + 2s_2^2 + 3s_3^2 = \mu^2$ lying inside the unit ball $\|\mathbf{s}\|_{\mathcal{S}} < 1$.

To simplify, we will consider in the following that μ is small enough. In this case, the ellipsoid $s_1^2 + 2s_2^2 + 3s_3^2 \leq \mu^2$ is included in the unit ball $\|\mathbf{s}\|_{\mathcal{S}} < 1$, and hence $\mathcal{S}_\mu$ reduces merely to the surface of the ellipsoid.

As a conclusion, once μ (and therefore the measure of the swimmer) has be chosen and fixed, the shape changes over a time interval $[0, T]$ are described by means of a function:

$$t \in [0, T] \mapsto \mathbf{s}(t) \in \mathcal{S}_\mu.$$

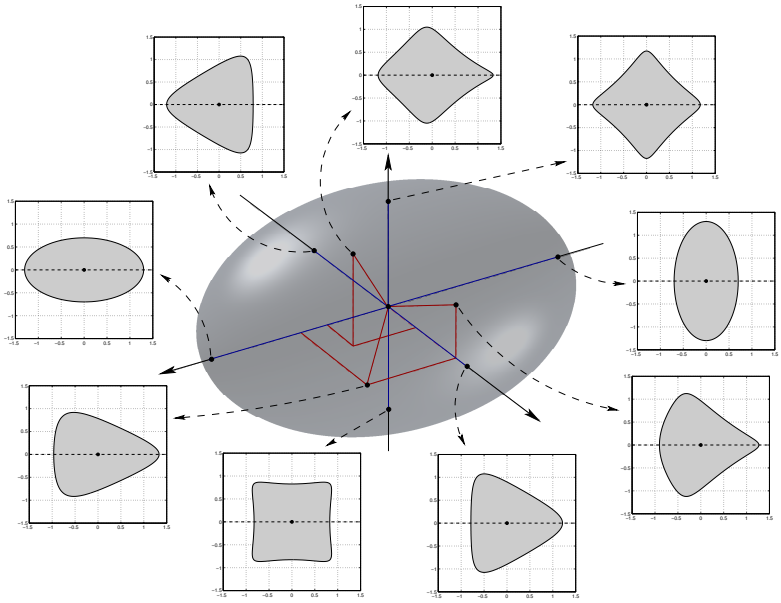

Figure 5.2: Some points on the ellipsoid $\mathcal{S}_\mu$ ($\mu = 0.3$) and the corresponding shapes of the swimmer.

By direct computations, one verifies that the self-propelled constraints (5.2), ensuring that the swimmer can not modified its linear momentum by self-deforming, are automatically satisfied in this simplified case.

In Fig. 5.2, we have pictured some points of the the ellipsoid and the corresponding shapes for the swimmer.

Using the conformal mapping

$$\phi(\mathbf{s}, z) := z + \frac{s_1}{z} + \frac{s_2}{z^2} + \frac{s_3}{z^3}, \qquad (z \in \mathbb{C} \setminus \bar{D},\, \mathbf{s} = (s_1, s_2, s_3) \in \mathcal{S}_\mu),$$

which maps the exterior of the unit disk onto the fluid domain $\mathcal{F}_m(\mathbf{s})$, we can compute explicitly the elementary kirchhoff's potentials $\varphi_r(\mathbf{s}, \cdot\,)$ and $\varphi_d(\mathbf{s}, \cdot\,)$ (again, we refer to [27] or [65] for the details). We finally get the following expressions for the mass matrices introduced in (5.13):

$$M^r(\mathbf{s}) = 2 - 2s_1 \tag{5.19a}$$

$$\mathbf{N}(\mathbf{s}) = \begin{bmatrix} -3s_2 + 2s_2 s_1 + 3s_2 s_3 & -s_1 - 4s_3 + {s_1}^2 + 3s_1 s_3 & -2s_2 + 3s_2 s_1 \end{bmatrix} \tag{5.19b}$$

$$\mathbb{M}^d(\mathbf{s}) = \begin{bmatrix} 4{s_2}^2 - 3s_3 + \frac{9}{2}{s_3}^2 + 1 & 2s_1 s_2 + 6s_2 s_3 & 4{s_2}^2 - \frac{1}{2}s_1 + \frac{3}{2}s_1 s_3 \\ 2s_1 s_2 + 6s_2 s_3 & {s_1}^2 + 6s_1 s_3 + 9{s_3}^2 + \frac{2}{3} & 2s_1 s_2 + 6s_2 s_3 \\ 4{s_2}^2 - \frac{1}{2}s_1 + \frac{3}{2}s_1 s_3 & 2s_1 s_2 + 6s_2 s_3 & 4{s_2}^2 + \frac{1}{2}{s_1}^2 + \frac{1}{2} \end{bmatrix} \tag{5.19c}$$

The 1-form $\mathcal{L}$ defined in (5.14) as well as the scalar product $\mathbf{g}$ defined in (5.16) and the cost functional (5.17) can now be explicitly computed. Instead of writing out their (complicated) expressions, we compute rather the Ricci-curvature induced by $\mathbf{g}$ on the ellipsoid. The result is displayed on Fig 5.3.

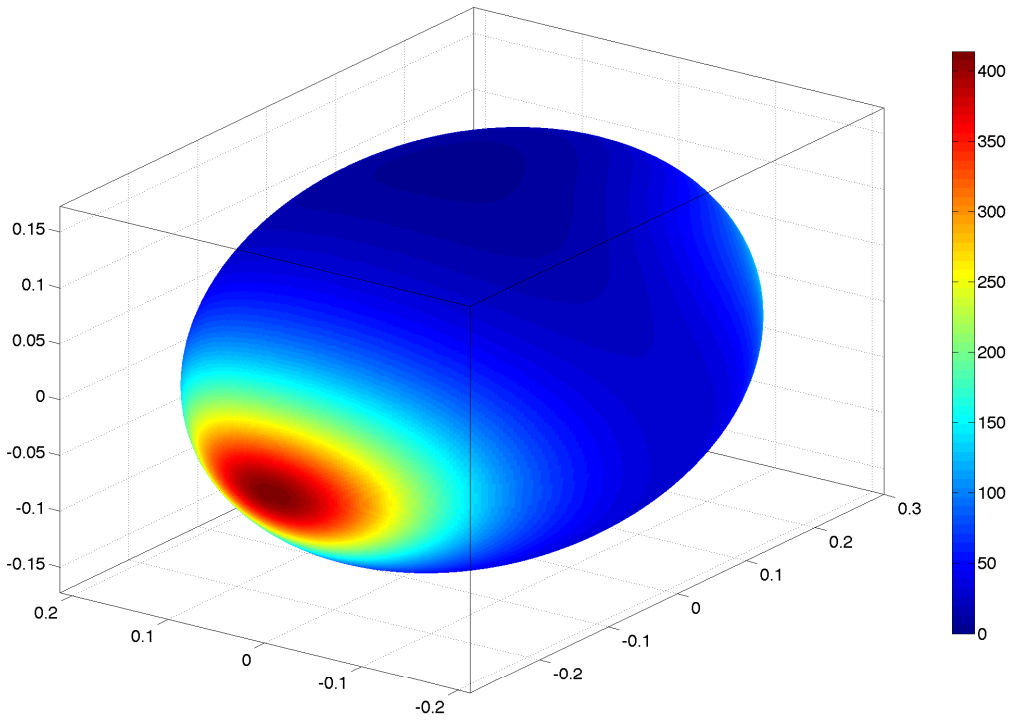

Figure 5.3: The Ricci curvature corresponding to the Riemannian metric $\mathbf{g}$ defined in (5.16), on the ellipsoid.

5.3 Controllability

5.3.1 General results

Let us consider an abstract swimmer $\mathfrak{S} = (\mathcal{S}, \mathbf{g}, \mathbf{Q}^{\mathcal{S}}, \mathbf{s}^\dagger, \mathcal{L})$ as described in Section 5.1.2, denote, for every $\mathbf{s} \in \mathcal{S}$:

$$\ker \mathbf{Q}^{\mathcal{S}} = \Delta^{\mathcal{S}}_{\mathbf{s}} \subset T_{\mathbf{s}}\mathcal{S}.$$

Assume that the dimension of $\Delta^{\mathcal{S}}_{\mathbf{s}}$ is not always zero (otherwise, it would mean that there is no shape change satisfying the self-propelled constraints (5.2)). For every $\mathbf{s} \in \mathcal{S}$, we denote by $\{\mathbf{X}_1(\mathbf{s}), \dots, \mathbf{X}_p(\mathbf{s})\}$ $(p > 0)$ a spanning set of $\Delta^{\mathcal{S}}_{\mathbf{s}}$ where the vector fields $\mathbf{s} \in \mathcal{S} \mapsto \mathbf{X}_j(s) \in T_{\mathbf{s}}\mathcal{S}$ $(1 \leq j \leq p)$ are assumed to be analytic. We denote $\mathcal{X} := \{\mathbf{X}_j,\, j = 1, \dots, p\} \subset \mathfrak{X}(\mathcal{S})$ and we shall call $\mathcal{X}$ an analytic spanning family of the distribution $\Delta^{\mathcal{S}}$. Notice that is general, the spanning family $\mathcal{X}$ cannot be required to be a basis of $\Delta^{\mathcal{S}}_{\mathbf{s}}$ at every point $\mathbf{s}$ of $\mathcal{S}$ because the analytic vector fields $\mathbf{X}_j$ cannot be prevented from vanishing at some point of the manifold (see for instance the example in Subsection 5.3.2).

Proposition 5.3.1 *Any absolutely continuous function with essentially bounded derivatives $\mathbf{s} : [0, T] \to \mathcal{S}$ is an admissible shape change if and only if it is solution (in the sense of Carathéodory) of a Cauchy problem*

$$\dot{\mathbf{s}}(t) = \sum_{j=1}^{p} u_j(t)\mathbf{X}_j(\mathbf{s}(t)) \quad (t > 0), \tag{5.20a}$$

$$\mathbf{s}(0) = \mathbf{s}^\dagger, \tag{5.20b}$$

for some $\mathbf{u} = (u_1, \dots, u_p) \in L^\infty([0, T], \mathbb{R}^p)$.

Proof. The proof is elementary: For every admissible shape change, the function $\mathbf{u} = (u_1, \dots, u_p) \in L^\infty([0, T], \mathbb{R}^p)$ gives the coordinates of $\dot{\mathbf{s}}$ in the spanning family $\mathcal{X}(\mathbf{s})$.

System (5.20) allows associating with every measurable function $\mathbf{u} \in L^\infty([0, T], \mathbb{R}^p)$ an admissible shape change, at least for times small enough.

We define $\mathcal{M}$ as being the analytic $(N+1)$-dimensional manifold $\mathcal{S}\times\mathbb{R}$. Then, we introduce the projectors $\pi_{\mathcal{S}}$ and $\pi_{\mathbb{R}}$ by:

$$\pi_{\mathcal{S}} : \begin{array}{ccc} \mathcal{M} & \to & \mathcal{S} \\ (\mathbf{s}, r) & \mapsto & \pi_{\mathcal{S}}(\boldsymbol{\xi}) = \mathbf{s} \end{array} \quad \text{and} \quad \pi_{\mathbb{R}} : \begin{array}{ccc} \mathcal{M} & \to & \mathbb{R} \\ (\mathbf{s}, r) & \mapsto & \pi_{\mathbb{R}}(\boldsymbol{\xi}) = r. \end{array}$$

On $\mathcal{M}$, we define the analytic vectors fields:

$$\mathbf{Z}_j(\boldsymbol{\xi}) := \begin{pmatrix} \mathbf{X}_j(\pi_{\mathcal{S}}\boldsymbol{\xi}) \\ \mathcal{L}_{\mathbf{s}}\mathbf{X}_j(\pi_{\mathcal{S}}\boldsymbol{\xi}) \end{pmatrix}, \qquad (j = 1, \dots, p), \tag{5.21}$$

we denote $\mathcal{Z} := \{\mathbf{Y}_j,\, j = 1, \dots, p\} \subset \mathfrak{X}(\mathcal{M})$ and we define the distribution

$$\Delta^{\mathcal{M}}_{\boldsymbol{\xi}} = \operatorname{span} \mathcal{Z}(\boldsymbol{\xi}), \qquad \boldsymbol{\xi} \in \mathcal{M}.$$

System (5.20) and the dynamics (5.10) can now be gathered as a unique dynamical system on $\mathcal{M}$:

$$\dot{\boldsymbol{\xi}}(t) = \sum_{j=1}^{p} u_j(t)\mathbf{Z}_j(\boldsymbol{\xi}(t)) \quad (t > 0), \tag{5.22a}$$

$$\boldsymbol{\xi}(0) = \boldsymbol{\xi}^\dagger \tag{5.22b}$$

where $\boldsymbol{\xi}^\dagger = (\mathbf{s}^\dagger, 0)$.

Remark 5.3.2 *The choice of the initial condition* $(\mathbf{s}^\dagger, 0)$ *(and not* $(\mathbf{s}^\dagger, r_0)$ *for some* $r_0 \neq 0$*) is physically irrelevant, since the vector fields* $\mathbf{Z}_j$ *(*$1 \leq j \leq p$*), and hence the dynamics* (5.22)*, do not depend upon the* $\mathbb{R}$ *component of the variable* $\boldsymbol{\xi}$*.*

Definition 5.3.3 *For every positive time* T*, every swimmer* $\mathfrak{S} = (\mathcal{S}, \mathbf{g}, \mathbf{Q}^{\mathcal{S}}, \mathbf{s}^\dagger, \mathcal{L})$ *and every analytic spanning family* $\mathcal{X}$ *of* $\Delta^{\mathcal{S}}$*, we denote by* $\mathcal{U}^{\mathcal{X}}_{\mathfrak{S}}(T)$ *the set of all the controls* $\mathbf{u} = (u_j)_{1\leq j\leq p} \in L^\infty([0,T], \mathbb{R}^p)$ *for which the solution of* (5.20) *(and hence of* (5.22)*) is defined on* $[0,T]$*.*

For any given control $\mathbf{u} \in \mathcal{U}^{\mathcal{X}}_{\mathfrak{S}}(T)$, we denote

$$t \in [0,T] \mapsto \boldsymbol{\xi}^{\mathcal{X}}_{\mathfrak{S}}(t, \mathbf{u}) \in \mathcal{M},$$

the solution to (5.22) with control $\mathbf{u}$.

Remark 5.3.4 *According to this notation, we have:*

$$\pi_{\mathbb{R}}\boldsymbol{\xi}^{\mathcal{X}}_{\mathfrak{S}}(T, \mathbf{u}) = \int_0^T \mathcal{L}_{\pi_{\mathcal{S}}\boldsymbol{\xi}^{\mathcal{X}}_{\mathfrak{S}}(t,\mathbf{u})} \frac{\mathrm{d}}{\mathrm{d}t} \pi_{\mathcal{S}}\boldsymbol{\xi}^{\mathcal{X}}_{\mathfrak{S}}(t, \mathbf{u}) \mathrm{d}t.$$

One hypothesis required in order to ensure that the swimmer is controllable is that $\mathcal{X}$ is bracket generating on $\mathcal{S}$. Observe that this condition does not depend on the particular choice of the spanning family $\mathcal{X}$ but only on the distribution $\Delta^{\mathcal{S}}$ and hence on the vector valued 1-form $\mathbf{Q}^{\mathcal{S}}$. It can be easily verified that if $\mathcal{X}$ and $\mathcal{X}'$ are two smooth spanning families of $\Delta^{\mathcal{S}}$, then for every $\mathbf{s} \in \mathcal{S}$:

$$\mathrm{Lie}_{\mathbf{s}}\mathcal{X} = \mathrm{Lie}_{\mathbf{s}}\mathcal{X}' = \mathrm{Lie}_{\mathbf{s}}\Delta^{\mathcal{S}}.$$

Taking into account this obversation, we define:

Hypothesis 5.3.5 *The swimmer* $\mathfrak{S} = (\mathcal{S}, \mathbf{g}, \mathbf{Q}^{\mathcal{S}}, \mathbf{s}^\dagger, \mathcal{L})$ *is such that*

1. *The distribution* $\Delta^{\mathcal{S}}$ *is bracket generating on* $\mathcal{S}$*, i.e.*

$$\dim \mathrm{Lie}_{\mathbf{s}}\Delta^{\mathcal{S}} = \dim \mathcal{S}, \quad \forall\, \mathbf{s} \in \mathcal{S};$$

2. *There exists* $\boldsymbol{\xi} \in \mathcal{M}$ *such that* $\dim \mathrm{Lie}_{\boldsymbol{\xi}}\Delta^{\mathcal{M}} = \dim \mathcal{M}$*.*

Lemma 5.3.6 *Hypothesis 5.3.5 leads to:*

$$\dim \mathrm{Lie}_{\boldsymbol{\xi}}\Delta^{\mathcal{M}} = \dim \mathcal{M}, \quad \forall\, \boldsymbol{\xi} \in \mathcal{M}.$$

Proof. Let $\boldsymbol{\xi}^* = (\mathbf{s}^*, 0)$ be such that $\dim \mathrm{Lie}_{\boldsymbol{\xi}^*}\Delta^{\mathcal{M}} = \dim \mathcal{M}$. As already mentioned, the choice of 0 for the $\mathbb{R}$ component of $\boldsymbol{\xi}^*$ is irrelevant regarding the Lie algebra $\mathrm{Lie}_{\boldsymbol{\xi}^*}\Delta^{\mathcal{M}} = \mathrm{Lie}_{\boldsymbol{\xi}^*}\mathcal{Z}$ since, for every $j = 1, \ldots, p$, $\mathbf{Z}_j(\boldsymbol{\xi}) = \mathbf{Z}_j(\pi_{\mathcal{S}}\boldsymbol{\xi})$. Consider now any $\boldsymbol{\xi} = (\mathbf{s}, r) \in \mathcal{M}$ and denote $\mathcal{O}(\boldsymbol{\xi})$ the orbit of $\mathcal{Z}$ through $\boldsymbol{\xi}$. Since $\Delta^{\mathcal{S}}$ is bracket generating on $\mathcal{S}$, Rashevsky-Chow Theorem ensures that for any $T > 0$, there exists a control $\mathbf{u} \in L^\infty([0,T], \mathbb{R}^p)$ such that the solution to the EDO (5.20) with Cauchy data $\mathbf{s}$ is equal to $\mathbf{s}^*$ at the final time T. Using this control in EDO (5.22) with Cauchy data $\boldsymbol{\xi} = (\mathbf{s}, r)$, we deduce that the solution reaches a point $\tilde{\boldsymbol{\xi}}^* = (\mathbf{s}^*, r^*)$ at the time T for some $r^* \in \mathbb{R}$ ($\boldsymbol{\xi}$ and $\tilde{\boldsymbol{\xi}}^*$ are both in $\mathcal{O}(\boldsymbol{\xi})$). But since $\pi_{\mathcal{S}}\tilde{\boldsymbol{\xi}}^* = \pi_{\mathcal{S}}\boldsymbol{\xi}^*$, we have the equality $\dim \mathrm{Lie}_{\tilde{\boldsymbol{\xi}}^*}\mathcal{Z} = \dim \mathrm{Lie}_{\boldsymbol{\xi}^*}\mathcal{Z} = \dim \mathcal{M}$. According to the Orbit Theorem, the dimension of the Lie algebra of $\mathcal{Z}$ is constant on $\mathcal{O}(\boldsymbol{\xi})$ and hence we have also $\dim \mathrm{Lie}_{\boldsymbol{\xi}}\mathcal{Z} = \dim \mathcal{M}$. The proof is now complete.

Assuming only, in the second point of Hypothesis 5.3.5, that the equality holds for one point of $\mathcal{M}$ may seem a somehow useless mathematical refinement. Quite the reverse, the explicit computation of $\mathrm{Lie}_{\boldsymbol{\xi}}\Delta^{\mathcal{M}}$ in concrete cases is often very involved and can still be hardly carry out for one particular $\boldsymbol{\xi}$ (see for instance []).

Definition 5.3.7 *A swimmer satisfying Hypothesis 5.3.5 will be called controllable.*

This definition is justified by the following Theorem:

Theorem 5.3.8 *Let $\mathfrak{S}$ be a swimmer satisfying Hypothesis 5.3.5. Then, for every $T > 0$, every analytic spanning family $\mathcal{X}$ of $\Delta^{\mathcal{S}}$, every $\boldsymbol{\xi}^{\ddagger}$ in $\mathcal{M}$ and every open, connected set $\mathcal{O} \subset \mathcal{M}$ containing $\boldsymbol{\xi}^{\dagger}$ and $\boldsymbol{\xi}^{\ddagger}$, there exists a control $\mathbf{u} \in L^{\infty}([0,T], \mathbb{R}^p)$ such that $\boldsymbol{\xi}^{\mathcal{X}}_{\mathfrak{S}}(T, \mathbf{u}) = \boldsymbol{\xi}^{\ddagger}$ and $\boldsymbol{\xi}^{\mathcal{X}}_{\mathfrak{S}}(t, \mathbf{u}) \in \mathcal{O}$ for every $t \in [0,T]$.*

Proof. This is a straightforward consequence of the analytic Orbit theorem.

Notice that this theorem applies for the models (high and low Reynolds numbers swimmers) introduced in Section 5.2. For these models, controllability is ensured as soon as Hypothesis 5.3.5 is fulfilled.

Let us enter more into details for the example presented in Subsection 5.2.5.

5.3.2 Swimmer in a potential flow

In this case, as already mentioned before, we have $\mathbf{Q}^{\mathcal{S}} = \mathbf{0}$ (the self-propelled constraints are always fulfilled) and hence $\Delta^{\mathcal{S}} = T\mathcal{S}_{\mu}$. We define the following vector fields which are, for every $\mathbf{s} \in \mathcal{S}_{\mu}$, an analytic spanning set of $T_{\mathbf{s}}\mathcal{S}_{\mu}$:

$$\mathbf{X}_1(\mathbf{s}) := \begin{bmatrix} 3s_3(1-s_1) \\ 0 \\ s_1(s_1-1) \end{bmatrix}, \quad \mathbf{X}_2(\mathbf{s}) := \begin{bmatrix} 2s_2(1-s_1) \\ s_1(s_1-1) \\ 0 \end{bmatrix}, \quad \mathbf{X}_3(\mathbf{s}) := \begin{bmatrix} 0 \\ 3s_3(1-s_1) \\ 2s_2(s_1-1) \end{bmatrix}.$$

Notice that, for all $\mathbf{s} \in \mathcal{S}$, $2s_2\mathbf{X}_1(\mathbf{s}) - 3s_3\mathbf{X}_2(\mathbf{s}) - s_1\mathbf{X}_3(\mathbf{s}) = \mathbf{0}$. From this family of vectors, we build the vectors $\mathbf{Z}_j$ $(j = 1, 2, 3)$ according to the definition (5.21) and the expressions (5.19). We get:

$$\mathbf{Z}_1(\boldsymbol{\xi}) := \begin{bmatrix} 3s_3(1-s_1) \\ 0 \\ s_1(s_1-1) \\ \frac{9}{2}s_2s_3 - 3s_1s_2s_3 - \frac{9}{2}s_2s_3^2 - s_1s_2 + \frac{3}{2}s_1^2s_2 \end{bmatrix}$$

$$\mathbf{Z}_2(\boldsymbol{\xi}) := \begin{bmatrix} 2s_2(1-s_1) \\ s_1(s_1-1) \\ 0 \\ 3s_2^2 - 2s_1s_2^2 - 3s_2^2s_3 - \frac{1}{2}s_1^2 - 2s_1s_3 + \frac{1}{2}s_1^3 + \frac{3}{2}s_1^2s_3 \end{bmatrix}$$

$$\mathbf{Z}_3(\boldsymbol{\xi}) := \begin{bmatrix} 0 \\ 3s_3(1-s_1) \\ 2s_2(s_1-1) \\ \frac{3}{2}s_1s_3 + 6s_3^3 - \frac{3}{2}s_1^2s_3 - \frac{9}{2}s_1s_3^2 - 2s_2^2 + 3s_1s_2^2 \end{bmatrix}.$$

Obviously, we have again that $2s_2\mathbf{Z}_1(\boldsymbol{\xi}) - 3s_3\mathbf{Z}_2(\boldsymbol{\xi}) - s_1\mathbf{Z}_3(\boldsymbol{\xi}) = \mathbf{0}$ for all $\boldsymbol{\xi} = (\mathbf{s}, r) \in \mathcal{M}$. By direct calculation, one can check that for all $\boldsymbol{\xi} \in \mathcal{M}$:

$$[\mathbf{Z}_1(\boldsymbol{\xi}), \mathbf{Z}_2(\boldsymbol{\xi})] = \begin{bmatrix} 0 \\ 3s_3(2s_1-1)(s_1-1) \\ -2s_2(2s_1-1)(s_1-1) \\ -\frac{3}{2}s_1s_3 - 3s_1^2s_2^2 + \frac{3}{2}s_1^3s_3 + \frac{9}{2}s_1^2s_3^2 - \frac{21}{2}s_1s_3^2 - s_1^2 + 6s_3^2 + s_1^3 + 5s_1s_2^2 - 2s_2^2 \end{bmatrix}.$$

For $\boldsymbol{\xi}^{\dagger} := (\mu, 0, 0, 0) \in \mathcal{M}$, we have:

$$[\mathbf{Z}_1(\boldsymbol{\xi}^{\dagger}), \mathbf{Z}_2(\boldsymbol{\xi}^{\dagger}), [\mathbf{Z}_1(\boldsymbol{\xi}^{\dagger}), \mathbf{Z}_2(\boldsymbol{\xi}^{\dagger})]] = \mu(\mu-1) \begin{bmatrix} 0 & 0 & 0 \\ 0 & 1 & 0 \\ 1 & 0 & 0 \\ 0 & \frac{1}{2}\mu^2 & \mu^2 \end{bmatrix},$$

and hence $\dim \mathrm{Lie}_{\boldsymbol{\xi}^\dagger}\{\mathbf{Z}_j,\, j=1,2,3\} = 3$. According to Theorem 5.3.8, we deduce that our example of swimmer in a perfect fluid is controllable.

5.4 Seeking of Optimal Strokes

In this section, we address the main problems that we are interested in. A controllable swimmer $\mathfrak{S}$ being given, and a cost being chosen (among those presented in (5.1)), what is the *best* possible stroke? By *best*, it is understood that the swimmer is wished to swim as far as possible with a corresponding cost as low as possible.

To be rigorously stated, the question has to be split into several closely related but not always equivalent problems:

1. What is the stroke minimizing the cost among those allowing traveling a given, fixed distance?
2. What is the stroke maximizing the travelled distance among those whose cost is not greater than a given fixed bound?

In case the cost is not important, we can also be interested in seeking the stroke maximizing the mean swimming velocity.

We shall conduct a detailed study on every one of these problems, focusing on the existence of optimal strokes and deriving their main properties.

5.4.1 Statement of optimal problems

To begin with, let us restrict slightly the scope of our study by introducing a new hypothesis that the swimmer has to satisfy:

Hypothesis 5.4.1 *The swimmer $\mathfrak{S} = (\mathcal{S}, \mathbf{g}, \mathbf{Q}^{\mathcal{S}}, \mathbf{s}^\dagger, \mathcal{L})$ is such that there exists an analytic basis $\mathcal{X} = \{\mathbf{X}_j, j = 1, \dots, p\}$ of the distribution $\Delta^{\mathcal{S}}$.*

Definition 5.4.2 *A swimmer $\mathfrak{S}$ satisfying Hypothesis 5.4.1 will be termed trivialized.*

Applying a Gram-Schmidt process, we can assume that for every $\mathbf{s} \in \mathcal{S}$, the family $\{\mathbf{X}_j(\mathbf{s}), j = 1, \dots, p\}$ in Hypothesis 5.4.1 is an orthonormal basis (for the Riemannian scalar product $\mathbf{g}$ of $\mathcal{S}$) of $\Delta^{\mathcal{S}}_{\mathbf{s}}$. As already mentioned before, it is in general not possible to extract from any smooth spanning family of $\Delta^{\mathcal{S}}$ a smooth basis on the whole manifold $\mathcal{S}$ (see also the computations in Subsection 5.3.2). Nevertheless, any swimmer can be locally trivialized:

Proposition 5.4.3 *Let $\mathfrak{S} = (\mathcal{S}, \mathbf{g}, \mathbf{Q}^{\mathcal{S}}, \mathbf{s}^\dagger, \mathcal{L})$ be a swimmer. Then, there exists an open connected subset $\mathcal{S}'$ (for the topology of $\mathcal{S}$) containing $\mathbf{s}^\dagger$ such that $\mathfrak{S}' = (\mathcal{S}', \mathbf{g}, \mathbf{Q}^{\mathcal{S}}, \mathbf{s}^\dagger, \mathcal{L})$ is a trivialized swimmer.*

Notice in particular that any open subset of an analytic manifold is still an analytic manifold.

Let $\mathfrak{S} = (\mathcal{S}, \mathbf{g}, \mathbf{Q}^{\mathcal{S}}, \mathbf{s}^\dagger, \mathcal{L})$ be a trivialized, controllable swimmer, $\mathcal{K}$ be a compact of $\mathcal{S}$ containing $\mathbf{s}^\dagger$ and $\mathcal{X}$ be an orthonormal basis of $\Delta^{\mathcal{S}}$. For every $\boldsymbol{\xi}^\ddagger$ in $\mathcal{M}$ and $T \geq 0$, we define

$$
\begin{aligned}
\mathcal{U}^{\mathcal{X}}_{\mathfrak{S}}(\boldsymbol{\xi}^\ddagger, T) &:= \left\{ \mathbf{u} \in \mathcal{U}^{\mathcal{X}}_{\mathfrak{S}}(T) \,:\, \boldsymbol{\xi}^{\mathcal{X}}_{\mathfrak{S}}(T, \mathbf{u}) = \boldsymbol{\xi}^\ddagger \right\};\\
\widehat{\mathcal{U}}^{\mathcal{X}}_{\mathfrak{S}}(\boldsymbol{\xi}^\ddagger, T) &:= \left\{ \mathbf{u} \in \mathcal{U}^{\mathcal{X}}_{\mathfrak{S}}(\boldsymbol{\xi}^\ddagger, T) \,:\, \|\mathbf{u}(t)\|_{\mathbb{R}^p} = 1 \ \forall\, t \in [0,T] \right\};\\
\mathcal{U}^{\mathcal{X}}_{\mathfrak{S},\mathcal{K}}(T) &:= \left\{ \mathbf{u} \in \mathcal{U}^{\mathcal{X}}_{\mathfrak{S}}(T) \,:\, \pi_{\mathcal{S}} \boldsymbol{\xi}^{\mathcal{X}}_{\mathfrak{S}}(t, \mathbf{u}) \in \mathcal{K} \quad \forall t \in [0,T] \right\};\\
\mathcal{U}^{\mathcal{X}}_{\mathfrak{S},\mathcal{K}}(\boldsymbol{\xi}^\ddagger, T) &:= \left\{ \mathbf{u} \in \mathcal{U}^{\mathcal{X}}_{\mathfrak{S}}(\boldsymbol{\xi}^\ddagger, T) \,:\, \pi_{\mathcal{S}} \boldsymbol{\xi}^{\mathcal{X}}_{\mathfrak{S}}(t, \mathbf{u}) \in \mathcal{K} \quad \forall t \in [0,T] \right\};\\
\widehat{\mathcal{U}}^{\mathcal{X}}_{\mathfrak{S},\mathcal{K}}(\boldsymbol{\xi}^\ddagger, T) &:= \left\{ \mathbf{u} \in \mathcal{U}^{\mathcal{X}}_{\mathfrak{S},\mathcal{K}}(\boldsymbol{\xi}^\ddagger, T) \,:\, \|\mathbf{u}(t)\|_{\mathbb{R}^p} = 1 \ \forall\, t \in [0,T] \right\}.
\end{aligned}
$$

The following Lemma

Lemma 5.4.4 *If there exist an orthonormal basis $\mathcal{X}$ of $\Delta^{\mathcal{S}}$ and $T > 0$ such that the set $\mathcal{U}^{\mathcal{X}}_{\mathfrak{S},\mathcal{K}}(T, \boldsymbol{\xi}^{\ddagger})$ is empty, then it is empty for every orthonormal basis $\mathcal{X}$ of $\Delta^{\mathcal{S}}$ and every $T > 0$.*

Proof. Assume that for some $\mathcal{X}$ and $T > 0$, the set $\mathcal{U}^{\mathcal{X}}_{\mathfrak{S},\mathcal{K}}(T, \boldsymbol{\xi}^{\ddagger})$ is nonempty and denote by $\mathbf{u}$ one of its elements. Then, for any $T' > 0$, define:

$$\alpha = \frac{\|\mathbf{u}\|_{L^1([0,T],\mathbb{R}^p)}}{T'}; \tag{5.23a}$$

$$\phi(t) = \frac{1}{\alpha}\int_0^t \|\mathbf{u}(s)\|_{\mathbb{R}^p}\mathrm{d}s, \qquad t \in [0,T]; \tag{5.23b}$$

$$\tilde{\mathbf{u}}(t) = \alpha\frac{\mathbf{u}(\phi^{-1}(t))}{\|\mathbf{u}(\phi^{-1}(t))\|_{\mathbb{R}^p}}, \qquad t \in [0,T']. \tag{5.23c}$$

It can be easily verified that $\tilde{\mathbf{u}} \in \mathcal{U}^{\mathcal{X}}_{\mathfrak{S},\mathcal{K}}(T', \boldsymbol{\xi}^{\ddagger})$. Notice that $t \in [0,T'] \mapsto \boldsymbol{\xi}^{\mathcal{X}}_{\mathfrak{S}}(t, \tilde{\mathbf{u}}) \in \mathcal{M}$ is nothing but a time reparameterization of the curve, also parameterized by $t \in [0,T] \mapsto \boldsymbol{\xi}^{\mathcal{X}}_{\mathfrak{S}}(t, \mathbf{u}) \in \mathcal{M}$. Saying that $\mathcal{U}^{\mathcal{X}}_{\mathfrak{S},\mathcal{K}}(T, \boldsymbol{\xi}^{\ddagger})$ is nonempty means that there exist an allowable curve on $\mathcal{M}$, whose projection on $\mathcal{S}$ is contained in $\mathcal{K}$ and which links $\boldsymbol{\xi}^{\dagger}$ to $\boldsymbol{\xi}^{\ddagger}$. The existence of such a curve depends neither on $\mathcal{X}$ nor on T.

In every one of the problems stated below, we make the convention that the infimum of an empty set is equal to $+\infty$ while the supremum is equal to $-\infty$.

Problem 5.4.5 (Minimizing the Riemannian length) *For any $\delta^{\dagger} \in \mathbb{R}$ and $T > 0$, set $\boldsymbol{\xi}^{\ddagger} = (\mathbf{s}^{\dagger}, \delta^{\dagger})$ and determine:*

$$\Phi^{\mathcal{X}}_{\mathfrak{S},\mathcal{K}}(\delta^{\dagger}, T) = \inf\left\{\int_0^T \|\mathbf{u}(t)\|_{\mathbb{R}^p}\mathrm{d}t \,:\, \mathbf{u} \in \mathcal{U}^{\mathcal{X}}_{\mathfrak{S},\mathcal{K}}(\boldsymbol{\xi}^{\ddagger}, T)\right\}. \tag{5.24}$$

Notice that, since $\mathcal{X}$ is assumed to be orthonormal, we have also:

$$\int_0^T \|\mathbf{u}(t)\|_{\mathbb{R}^p}\mathrm{d}t = \int_0^T \sqrt{\mathbf{g}(\pi_{\mathcal{S}}\boldsymbol{\xi}^{\mathcal{X}}_{\mathfrak{S}}(t,\mathbf{u}), \pi_{\mathcal{S}}\boldsymbol{\xi}^{\mathcal{X}}_{\mathfrak{S}}(t,\mathbf{u}))}\mathrm{d}t,$$

which is the length of the curve $\Gamma \subset \mathcal{K}$ parameterized by $t \in [0,T] \mapsto \pi_{\mathcal{S}}\boldsymbol{\xi}^{\mathcal{X}}_{\mathfrak{S}}(t,\mathbf{u}) \in \mathcal{S}$. The lengths of the curves on $\mathcal{S}$ do not depend on the parameterization, so Problem 5.4.5 is time parameterization invariant.

Modifying the cost leads to:

Problem 5.4.6 (Minimizing the action) *For any $\delta^{\dagger} \in \mathbb{R}$ and $T > 0$, set $\boldsymbol{\xi}^{\ddagger} = (\mathbf{s}^{\dagger}, \delta^{\dagger})$ and determine:*

$$\Theta^{\mathcal{X}}_{\mathfrak{S},\mathcal{K}}(\delta^{\dagger}, T) = \inf\left\{\frac{1}{2}\int_0^T \|\mathbf{u}(t)\|^2_{\mathbb{R}^p}\mathrm{d}t \,:\, \mathbf{u} \in \mathcal{U}^{\mathcal{X}}_{\mathfrak{S},\mathcal{K}}(\boldsymbol{\xi}^{\ddagger}, T)\right\}. \tag{5.25}$$

Remark that, unlike the cost in (5.24), the cost in (5.25) is not time parameterization independent.

Before stating results about these problems, let us introduce a last related optimal problem, studied for instance in []:

Problem 5.4.7 (Optimizing the time) *For any $\delta^{\dagger} \in \mathbb{R}$, denote $\boldsymbol{\xi}^{\ddagger} = (\mathbf{s}^{\dagger}, \delta^{\dagger})$ and determine:*

$$T^{\mathcal{X}}_{\mathfrak{S},\mathcal{K}}(\delta^{\dagger}) = \inf\{T \,:\, \widehat{\mathcal{U}}^{\mathcal{X}}_{\mathfrak{S},\mathcal{K}}(\boldsymbol{\xi}^{\ddagger}, T) \neq \emptyset\}.$$

Problem 5.4.8 (Maximizing traveling distance with bounded Riemannian lenght) *For any $l \geq 0$ and $T \geq 0$, determine:*

$$\Psi^{\mathcal{X}}_{\mathfrak{S},\mathcal{K}}(l,T) = \sup\left\{\pi_{\mathbb{R}}\boldsymbol{\xi}^{\mathcal{X}}_{\mathfrak{S}}(T,\mathbf{u}) \,:\, \mathbf{u}\in\mathcal{U}^{\mathcal{X}}_{\mathfrak{S},\mathcal{K}}(T),\, \pi_{\mathcal{S}}\xi^{\mathcal{X}}_{\mathfrak{S}}(T,\mathbf{u}) = \mathbf{s}^{\dagger},\right.$$
$$\left. \text{and } \int_0^T \|\mathbf{u}(t)\|_{\mathbb{R}^p}\mathrm{d}t \leq l\right\}. \quad (5.26)$$

Problem 5.4.9 (Maximizing traveling distance with bounded action) *For any $l \geq 0$ and $T \geq 0$, determine:*

$$\Lambda^{\mathcal{X}}_{\mathfrak{S},\mathcal{K}}(l,T) = \sup\left\{\pi_{\mathbb{R}}\boldsymbol{\xi}^{\mathcal{X}}_{\mathfrak{S}}(T,\mathbf{u}) \,:\, \mathbf{u}\in\mathcal{U}^{\mathcal{X}}_{\mathfrak{S},\mathcal{K}}(T),\, \pi_{\mathcal{S}}\xi^{\mathcal{X}}_{\mathfrak{S}}(T,\mathbf{u}) = \mathbf{s}^{\dagger},\right.$$
$$\left. \text{and } \frac{1}{2}\int_0^T \|\mathbf{u}(t)\|^2_{\mathbb{R}^p}\mathrm{d}t \leq l\right\}. \quad (5.27)$$

Using the control $\mathbf{u} = \mathbf{0}$ in the last two problems, we deduce that $\Psi^{\mathcal{X}}_{\mathfrak{S},\mathcal{K}}(l,T) \geq 0$ and $\Lambda^{\mathcal{X}}_{\mathfrak{S},\mathcal{K}}(l,T) \geq 0$.

5.4.2 Firsts Properties of the Optimal Strokes

In this Subsection, we will derive properties of the optimal strokes resting on the Riemannian structure of $\mathcal{S}$. Then, in the following Subsection, we will introduce an make use of the sub-Riemannian structure of $\mathcal{M}$.

To begin with, let us focus on the firsts three problems:

Theorem 5.4.10 *Let $\mathfrak{S} = (\mathcal{S}, \mathbf{g}, \mathbf{Q}^{\mathcal{S}}, \mathbf{s}^{\dagger}, \mathcal{L})$ be a controllable, trivialized swimmer, and $\mathcal{K}$ be a compact of $\mathcal{S}$ containing $\mathbf{s}^{\dagger}$. Then*

1. *For every $\delta^{\dagger} \in \mathbb{R}$, the quantities $\Phi^{\mathcal{X}}_{\mathfrak{S},\mathcal{K}}(\delta^{\dagger},T)$, $\Theta^{\mathcal{X}}_{\mathfrak{S},\mathcal{K}}(\delta^{\dagger},T)$, and $T^{\mathcal{X}}_{\mathfrak{S},\mathcal{K}}(\delta^{\dagger})$ are either all of them infinite or all of them finite, for every $T \geq 0$ and every orthonormal basis $\mathcal{X}$ of $\Delta^{\mathcal{S}}$.*
2. *If $\mathbf{s}^{\dagger} \in \mathring{\mathcal{K}}$ then $\Phi^{\mathcal{X}}_{\mathfrak{S},\mathcal{K}}(\delta^{\dagger},T)$, $\Theta^{\mathcal{X}}_{\mathfrak{S},\mathcal{K}}(\delta^{\dagger},T)$, and $T^{\mathcal{X}}_{\mathfrak{S},\mathcal{K}}(\delta^{\dagger})$ are all of them finite, for every $T \geq 0$, every orthonormal basis $\mathcal{X}$ of $\Delta^{\mathcal{S}}$ and every $\delta^{\dagger} \in \mathbb{R}$.*
3. *If $\Phi^{\mathcal{X}}_{\mathfrak{S},\mathcal{K}}(\delta^{\dagger},T)$, $\Theta^{\mathcal{X}}_{\mathfrak{S},\mathcal{K}}(\delta^{\dagger},T)$, and $T^{\mathcal{X}}_{\mathfrak{S},\mathcal{K}}(\delta^{\dagger})$ are finite, then there exist minimizers or maximizers to every Problem 5.4.5, 5.4.6 and 5.4.7.*
4. *For every $T \geq 0$ and every $\delta^{\dagger} \in \mathbb{R}$, $\Phi^{\mathcal{X}}_{\mathfrak{S},\mathcal{K}}(\delta^{\dagger},T)$, $\Theta^{\mathcal{X}}_{\mathfrak{S},\mathcal{K}}(\delta^{\dagger},T)$ and $T^{\mathcal{X}}_{\mathfrak{S},\mathcal{K}}(\delta^{\dagger})$ do not depend on $\mathcal{X}$. So from now on, we drop $\mathcal{X}$ in the notation.*
5. *$\Phi_{\mathfrak{S},\mathcal{K}}(\delta^{\dagger},T)$ does not depend on T. So from now on, we drop T in the notation.*
6. *The following identities hold for every $\delta^{\dagger} \in \mathbb{R}$, and every $T > 0$:*

$$\Phi_{\mathfrak{S},\mathcal{K}}(\delta^{\dagger}) = T_{\mathfrak{S},\mathcal{K}}(\delta^{\dagger}) \quad (5.28a)$$
$$\Theta_{\mathfrak{S},\mathcal{K}}(\delta^{\dagger},T) = (1/2)(T_{\mathfrak{S},\mathcal{K}}(\delta^{\dagger}))^2/T \quad (5.28b)$$

7. *Any minimizer $\mathbf{u} \in \mathcal{U}^{\mathcal{X}}_{\mathfrak{S},\mathcal{K}}(\boldsymbol{\xi}^{\ddagger},T)$ to Problem 5.4.6:*
   (a) *is such that $\|\mathbf{u}(t)\|_{\mathbb{R}^p}$ is constant at every moment;*
   (b) *is also a minimizer to Problem 5.4.5;*

(c) is proportional to a minimizer of Problem 5.4.7.

Proof.

1. Let $\delta^\dagger$ be given. According to Lemma 5.4.4, if $\mathcal{U}^{\mathcal{X}}_{\mathfrak{S},\mathcal{K}}(T,\boldsymbol{\xi}^\ddagger)$ is empty for some $T>0$, then it is empty for every $T>0$ and therefore every quantity $\Phi^{\mathcal{X}}_{\mathfrak{S},\mathcal{K}}(\delta^\dagger,T)$, $\Theta^{\mathcal{X}}_{\mathfrak{S},\mathcal{K}}(\delta^\dagger,T)$, and $T^{\mathcal{X}}_{\mathfrak{S},\mathcal{K}}(\delta^\dagger)$ is infinite. Reciprocally, if for some $T>0$ there exists $\mathbf{u}\in\mathcal{U}^{\mathcal{X}}_{\mathfrak{S},\mathcal{K}}(T,\boldsymbol{\xi}^\ddagger)$, then, for every $T>0$, the set $\mathcal{U}^{\mathcal{X}}_{\mathfrak{S},\mathcal{K}}(T,\boldsymbol{\xi}^\ddagger)$ is nonempty as well and $\Phi^{\mathcal{X}}_{\mathfrak{S},\mathcal{K}}(\delta^\dagger,T)$ and $\Theta^{\mathcal{X}}_{\mathfrak{S},\mathcal{K}}(\delta^\dagger,T)$ are both finite. Moreover, from the control $\mathbf{u}$, we can build $\tilde{\mathbf{u}}\in\widehat{\mathcal{U}}^{\mathcal{X}}_{\mathfrak{S},\mathcal{K}}(\|\mathbf{u}\|_{L^1([0,T],\mathbb{R}^p)},\boldsymbol{\xi}^\ddagger)$ by setting $\alpha=1$ in (5.23). We deduce that $T^{\mathcal{X}}_{\mathfrak{S},\mathcal{K}}(\delta^\dagger)$ is finite and the first assertion of the Theorem is proved.

2. Denote $\mathcal{O}_1$ the connected component of $\mathring{\mathcal{K}}$ containing $\mathbf{s}^\dagger$ and for every $\delta^\dagger\in\mathbb{R}$, take $\mathcal{O}=\mathcal{O}_1\times]-|\delta^\dagger|-1,|\delta^\dagger|+1[$ in Theorem 5.3.8. The Theorem ensures that for every $T>0$ and every orthonormal basis $\mathcal{X}$ of $\Delta^{\mathcal{S}}$, the set $\mathcal{U}^{\mathcal{X}}_{\mathfrak{S},\mathcal{K}}(\boldsymbol{\xi}^\ddagger,T)$ is nonempty.

3. We prove now all the remaining points of the Theorem. Let $\mathcal{X}$ (an orthonormal basis of $\Delta^{\mathcal{S}}$), $T>0$ and $\delta^\dagger\in\mathbb{R}$ be given. For any control $\mathbf{u}\in\mathcal{U}^{\mathcal{X}}_{\mathfrak{S},\mathcal{K}}(\boldsymbol{\xi}^\ddagger,T)$, denote $\tilde{\mathbf{u}}\in\mathcal{U}^{\mathcal{X}}_{\mathfrak{S},\mathcal{K}}(\boldsymbol{\xi}^\ddagger,T)$ the control defined in (5.23) with $T'=T$. One can easily verify that:

$$\int_0^T\|\mathbf{u}(s)\|_{\mathbb{R}^p}\mathrm{d}s=\int_0^T\|\tilde{\mathbf{u}}(s)\|_{\mathbb{R}^p}\mathrm{d}s \tag{5.29}$$

and

$$\begin{aligned}\int_0^T\|\mathbf{u}(s)\|^2_{\mathbb{R}^p}\mathrm{d}s&\geq\frac{1}{T}\left(\int_0^T\|\mathbf{u}(s)\|_{\mathbb{R}^p}\mathrm{d}s\right)^2\\&=\int_0^T\|\tilde{\mathbf{u}}(s)\|^2_{\mathbb{R}^p}\mathrm{d}s,\end{aligned} \tag{5.30}$$

with equality in (5.30) if and only if $\|\mathbf{u}(s)\|_{\mathbb{R}^p}$ is constant, i.e. $\mathbf{u}=\tilde{\mathbf{u}}$. So, replacing $\mathbf{u}$ by $\tilde{\mathbf{u}}$ does not modify the cost functional of Problem 5.4.5 and does not increase the cost functional of Problem 5.4.6. Moreover, since

$$\int_0^T\|\tilde{\mathbf{u}}(s)\|^2_{\mathbb{R}^p}\mathrm{d}s=\frac{1}{T}\left(\int_0^T\|\tilde{\mathbf{u}}(s)\|_{\mathbb{R}^p}\mathrm{d}s\right)^2, \tag{5.31}$$

if $(\mathbf{u}_n)_n$ is a minimizing sequence for either Problem 5.4.5 or Problem 5.4.6, then $(\tilde{\mathbf{u}}_n)_n$ is a minimizing sequence for both Problem 5.4.5 and Problem 5.4.6. By construction, the sequence $(\tilde{\mathbf{u}}_n)_n$ is bounded in $L^\infty([0,T],\mathbb{R}^p)$. Hence, up to a subsequence extraction, we can assume that $(\tilde{\mathbf{u}}_n)_n$ weakly converges, for instance, in $L^2([0,T],\mathbb{R}^p)$ toward $\mathbf{u}^*$. In particular, the following inequality holds:

$$\int_0^T\|\mathbf{u}^*(s)\|^2_{\mathbb{R}^p}\mathrm{d}s\leq\liminf_{n\to+\infty}\int_0^T\|\tilde{\mathbf{u}}_n(s)\|^2_{\mathbb{R}^p}\mathrm{d}s. \tag{5.32}$$

Let us verify that $\mathbf{u}^*\in\mathcal{U}^{\mathcal{X}}_{\mathfrak{S},\mathcal{K}}(\boldsymbol{\xi}^\ddagger,T)$.

The functions $t\in[0,T]\mapsto\boldsymbol{\xi}^{\mathcal{X}}_{\mathfrak{S}}(t,\tilde{\mathbf{u}}_n)\in\mathcal{M}$ are equi-Lipschitz continuous on $[0,T]$, because the vector fields $\mathbf{Z}_i$ are analytic on the compact $\mathcal{K}$ and hence bounded. According to Ascoli Theorem, we can assume that, up to a subsequence extraction, the sequence $(t\mapsto\boldsymbol{\xi}^{\mathcal{X}}_{\mathfrak{S}}(t,\tilde{\mathbf{u}}_n))_n$ converges uniformly on $[0,T]$ toward a Lipschitz continuous

function $t \in [0,T] \mapsto \boldsymbol{\xi}^* \in \mathcal{M}$. Furthermore, the curve $t \in [0,T] \mapsto \pi_{\mathcal{S}}\boldsymbol{\xi}^* \in \mathcal{S}$ is absolutely continuous, with bounded derivative and thus is an admissible shape change (with support in $\mathcal{K}$). For every $t \in [0,T]$ and every $n \in \mathbb{N}$, we have:

$$\boldsymbol{\xi}^{\mathcal{X}}_{\mathfrak{S}}(t, \tilde{\mathbf{u}}_n) = \boldsymbol{\xi}^\dagger + \sum_{i=1}^{p} \int_0^t \tilde{u}_i^n(s) \mathbf{Z}_i(\boldsymbol{\xi}^{\mathcal{X}}_{\mathfrak{S}}(s, \tilde{\mathbf{u}}_n)) \mathrm{d}s. \tag{5.33}$$

Since $\tilde{u}_i^n \rightharpoonup u_i^*$ in $L^2([0,T],\mathbb{R})$ and $\mathbf{Z}_i(\boldsymbol{\xi}^{\mathcal{X}}_{\mathfrak{S}}(\,\cdot\,, \tilde{\mathbf{u}}_n)) \to \mathbf{Z}_i(\boldsymbol{\xi}^*)$ uniformly on $[0,T]$ (and hence also in $L^2([0,T], T\mathcal{M})$), passing to the limit as $n \to +\infty$ in (5.33) leads to:

$$\boldsymbol{\xi}^*(t) = \boldsymbol{\xi}^\dagger + \sum_{i=1}^{p} \int_0^t u_i^*(s) \mathbf{Z}_i(\boldsymbol{\xi}^*(s)) \mathrm{d}s, \quad t \in [0,T].$$

We have now proved that $\mathbf{u}^*$ is indeed a minimizer to Problems 5.4.6. Moreover, since equality in (5.30) holds if and only if $\|\mathbf{u}^*(t)\|_{\mathbb{R}^p}$ is constant for every $t \in [0,T]$, we infer that $\mathbf{u}^* = \tilde{\mathbf{u}}^*$. This equality leads to the following estimates:

$$\begin{aligned}
\int_0^T \|\mathbf{u}^*(s)\|_{\mathbb{R}^p} \mathrm{d}s &= \sqrt{T} \left(\int_0^T \|\mathbf{u}^*(s)\|^2_{\mathbb{R}^p} \mathrm{d}s \right)^{1/2} \\
&\leq \liminf_{n \to +\infty} \sqrt{T} \left(\int_0^T \|\tilde{\mathbf{u}}_n(s)\|^2_{\mathbb{R}^p} \mathrm{d}s \right)^{1/2} \\
&= \liminf_{n \to +\infty} \int_0^T \|\tilde{\mathbf{u}}_n(s)\|_{\mathbb{R}^p} \mathrm{d}s,
\end{aligned}$$

and $\mathbf{u}^*$ is also a minimizer to Problem 5.4.5. Using this control in (5.31), we obtain the equality:

$$\Theta^{\mathcal{X}}_{\mathfrak{S},\mathcal{K}}(\delta^\dagger, T) = \frac{1}{2T} (\Phi^{\mathcal{X}}_{\mathfrak{S},\mathcal{K}}(\delta^\dagger, T))^2. \tag{5.34}$$

Eventually, as already mentioned earlier, for every $T > 0$ and from any control $\mathbf{u} \in \mathcal{U}^{\mathcal{X}}_{\mathfrak{S},\mathcal{K}}(\boldsymbol{\xi}^\ddagger, T)$, we can build $\tilde{\mathbf{u}} \in \widehat{\mathcal{U}}^{\mathcal{X}}_{\mathfrak{S},\mathcal{K}}(\|\mathbf{u}\|_{L^1([0,T],\mathbb{R}^p)}, \boldsymbol{\xi}^\ddagger)$ by setting $\alpha = 1$ in (5.23). The identity (5.29) becomes:

$$\int_0^T \|\mathbf{u}(s)\|_{\mathbb{R}^p} \mathrm{d}s = \int_0^{\|\mathbf{u}\|_{L^1([0,T],\mathbb{R}^p)}} \mathrm{d}s,$$

whence we deduce that

$$T^{\mathcal{X}}_{\mathfrak{S},\mathcal{K}}(\delta^\dagger) = \Phi^{\mathcal{X}}_{\mathfrak{S},\mathcal{K}}(\delta^\dagger, T).$$

This equality tells us that $\Phi^{\mathcal{X}}_{\mathfrak{S},\mathcal{K}}(\delta^\dagger, T)$ does not depend on T. We conclude the proof of the theorem by observing again that $\Phi^{\mathcal{X}}_{\mathfrak{S},\mathcal{K}}(\delta^\dagger, T)$ is the length of the curve on $\mathcal{S}$ parameterized by $t \in [0,T] \mapsto \pi_{\mathcal{S}}\boldsymbol{\xi}^{\mathcal{X}}_{\mathfrak{S},\mathcal{K}}(t, \mathbf{u}^*) \in \mathcal{S}$ and that this length does not depend on $\mathcal{X}$.

We address now Problems 5.4.8 and 5.4.9:

Theorem 5.4.11 *Let $\mathfrak{S} = (\mathcal{S}, \mathbf{g}, \mathbf{Q}^{\mathcal{S}}, \mathbf{s}^\dagger, \mathcal{L})$ be a controllable, trivialized swimmer, and $\mathcal{K}$ be a compact of $\mathcal{S}$ containing $\mathbf{s}^\dagger$. Then*

1. *Problems 5.4.8 and 5.4.9 admit maximizers for every $T \geq 0$, every orthonormal basis $\mathcal{X}$ of $\Delta^{\mathcal{S}}$ and every $l \geq 0$.*
2. *Any maximizer $\mathbf{u} \in \mathcal{U}^{\mathcal{X}}_{\mathfrak{S},\mathcal{K}}(\boldsymbol{\xi}^\ddagger, T)$ to Problem 5.4.9*

(a) is such that $\|\mathbf{u}(t)\|_{\mathbb{R}^p}$ *is constant at every moment;*

(b) is proportional to a maximizer of Problem 5.4.8.

3. $\Psi^{\mathcal{X}}_{\mathfrak{S},\mathcal{K}}(l,T)$ *and* $\Lambda^{\mathcal{X}}_{\mathfrak{S},\mathcal{K}}(l,T)$ *do not depend on* $\mathcal{X}$ *so we drop it in the notation.*

4. $\Psi^{\mathcal{X}}_{\mathfrak{S},\mathcal{K}}(l,T)$ *does not depend on* T *so we drop it in the notation.*

5. *The following identity holds for every* $T>0$ *and* $l\geq 0$*:*

$$\Lambda_{\mathfrak{S},\mathcal{K}}((1/2)l^2/T,T)=\Psi_{\mathfrak{S},\mathcal{K}}(l). \tag{5.35}$$

Proof. To prove the existence of maximizers to Problems 5.4.8 and 5.4.9, we follow the lines of the proof of Theorem 5.4.10: Let $\mathcal{X}$, $l\geq 0$ and $T\geq 0$ be given and consider first a maximizing sequence $(\mathbf{u}_n)_n$ to Problem 5.4.9. Then notice that the renormalized and reparameterized control $(\tilde{\mathbf{u}}_n)_n$ is actually not only a maximizing sequence to Problem 5.4.9 but also to Problem 5.4.8 with $l'=\sqrt{lT}$. Then, up to subsequences extractions and invoking Ascoli Theorem and the weak convergence in $L^2([0,T],\mathbb{R}^p)$ of $(\tilde{\mathbf{u}}_n)_n$, we proves the existence of a common maximizer $\mathbf{u}^*=\tilde{\mathbf{u}}^*$ to Problems 5.4.9 (with l) and 5.4.8 (with $l'=\sqrt{lT}$). Using the control $\mathbf{u}^*$, we also get the equality (5.35).

Once more, the time reparameterization invariance of Problem 5.4.8 leads to infer that $\Psi^{\mathcal{X}}_{\mathfrak{S},\mathcal{K}}$ does not depend neither on $\mathcal{X}$ nor T. Eventually, identity (5.35) ensures that $\Lambda^{\mathcal{X}}_{\mathfrak{S},\mathcal{K}}(l,T)$ does not depend on $\mathcal{X}$.

5.4.3 Further Properties of the Optimal Strokes

In order to prove further properties on Problems 5.4.5-5.4.9, we need to introduce the Sub-Riemannian structure on $\mathcal{M}$.

Let a trivialized swimmer $\mathfrak{S}=(\mathcal{S},\mathbf{g},\mathbf{Q}^{\mathcal{S}},\mathbf{s}^\dagger,\mathcal{L})$ and $\mathcal{X}:=\{\mathbf{X}_j, j=1,\dots,p\}$ an orthonormal basis of $\Delta^{\mathcal{S}}_{\mathbf{s}}$ be given. From the analytic vectors fields $\mathbf{X}_j$ on $\mathcal{S}$, we build the analytic vector fields $\mathbf{Z}_j$ $(j=1,\dots,p)$ on $\mathcal{M}=\mathcal{S}\times\mathbb{R}$ as described in (5.21). Then, we define

$$\mathcal{Z}=\{\mathbf{Z}_j, æ=1,\dots,p\},$$

and the distribution on $\mathcal{M}$:

$$\Delta^{\mathcal{M}}_{\boldsymbol{\xi}}:=\operatorname{span}\mathcal{Z}(\boldsymbol{\xi})\subset T_{\boldsymbol{\xi}}\mathcal{M},\qquad \boldsymbol{\xi}\in\mathcal{M}.$$

We denote by $\mathbb{Z}(\boldsymbol{\xi})$ the matrix whose column vectors are the $\mathbf{Z}_j(\boldsymbol{\xi})$ and we introduce the Euclidean bundle $\mathbf{U}:=\mathcal{M}\times\mathbb{R}^p$ endowed with the Euclidean norm of $\mathbb{R}^p$ and the morphism of vector bundles

$$f:(\boldsymbol{\xi},\mathbf{u})\in\mathbf{U}\mapsto(\boldsymbol{\xi},\mathbb{Z}(\boldsymbol{\xi})\mathbf{u})\in T\mathcal{M}.$$

Following [4, Definition 3.1], we claim that the manifold $\mathcal{M}$ endowed with the triple $(\mathcal{M},\mathbf{U},f)$ is an analytic sub-Riemannian manifold. According to Definition 3.6 from the same booklet, we define the admissible curves as being the Lipschitz curves $\boldsymbol{\xi}:[0,T]\mapsto\mathcal{M}$ for which there exists a control function $\mathbf{u}\in L^\infty([0,T],\mathbb{R}^p)$ such that, for a.e. $t\in[0,T]$:

$$\dot{\boldsymbol{\xi}}=\mathbb{Z}(\boldsymbol{\xi})\mathbf{u}.$$

Notice that it is exactly the dynamics (5.22) that we are dealing with. The sub-Riemannian manifold can be equipped with the so-called *Carnot-Caratheodory distance* (see [4, Definition 3.13]) denoted by $\mathrm{d}(\,\cdot\,,\,\cdot\,)$. In particular, the following identity holds for any $\delta^\dagger\in\mathbb{R}$ and $\boldsymbol{\xi}=(\mathbf{s}^\dagger,\delta^\dagger)$:

$$\mathrm{d}(\boldsymbol{\xi}^\dagger,\boldsymbol{\xi}^\ddagger)=\inf\left\{\int_0^T\|\mathbf{u}(s)\|_{\mathbb{R}^p}\mathrm{d}s,\ \mathbf{u}\in\mathcal{U}^{\mathcal{X}}_{\mathfrak{S}}(T,\boldsymbol{\xi}^\ddagger)\right\}.$$

Be aware that actually, neither $\mathcal{X}$ nor T matters in this definition.

Theorem 5.4.12 *Let $\mathfrak{S} = (\mathcal{S}, \mathbf{g}, \mathbf{Q}^{\mathcal{S}}, \mathbf{s}^\dagger, \mathcal{L})$ be a controllable, trivialized swimmer, and $\mathcal{K}$ be a compact of $\mathcal{S}$ such that $\mathbf{s}^\dagger \in \mathring{\mathcal{K}}$. Then:*

1. *For every $l > 0$, we have $\Psi_{\mathfrak{S},\mathcal{K}}(l) > 0$. For every $l > 0$ and $T > 0$, we have $\Lambda_{\mathfrak{S},\mathcal{K}}(l,T) > 0$.*
2. *The functions*
$$l \in \mathbb{R}_+ \mapsto \Psi_{\mathfrak{S},\mathcal{K}}(l) \in \mathbb{R}_+ \tag{5.36a}$$
is increasing and right continuous.
3. *For every $T > 0$, the function*
$$l \in \mathbb{R}_+ \mapsto \Lambda_{\mathfrak{S},\mathcal{K}}(l,T) \in \mathbb{R}_+ \tag{5.36b}$$
is increasing and right continuous.
4. *For every maximizer to Problems 5.4.8 or 5.4.9, the constraints are saturated.*
5. *The function*
$$\delta \in \mathbb{R} \mapsto \Phi_{\mathfrak{S},\mathcal{K}}(\delta) \in \mathbb{R} \tag{5.36c}$$
is even and uniformly continuous.
6. *For every $T > 0$, the function*
$$\delta \in \mathbb{R} \mapsto \Theta_{\mathfrak{S},\mathcal{K}}(\delta,T) \in \mathbb{R} \tag{5.36d}$$
is even and uniformly continuous.
7. *For every $l \geq 0$ and every $T \geq 0$:*
$$\Phi_{\mathfrak{S},\mathcal{K}}(\Psi_{\mathfrak{S},\mathcal{K}}(l)) = l \tag{5.37a}$$
$$\Theta_{\mathfrak{S},\mathcal{K}}(\Lambda_{\mathfrak{S},\mathcal{K}}(l,T),T) = l. \tag{5.37b}$$

Regarding the last point of the theorem, notice that, for every $\delta^\dagger \in \mathbb{R}_+$, we have $\Psi_{\mathfrak{S},\mathcal{K}}(\Phi_{\mathfrak{S},\mathcal{K}}(\delta^\dagger)) \geq \delta^\dagger$ but it may happen that $\Psi_{\mathfrak{S},\mathcal{K}}(\Phi_{\mathfrak{S},\mathcal{K}}(\delta^\dagger)) > \delta^\dagger$ for some $\delta^\dagger$. Indeed, according to the definition of $\Psi_{\mathfrak{S},\mathcal{K}}(\Phi_{\mathfrak{S},\mathcal{K}}(\delta^\dagger))$, we have:

$$\Psi_{\mathfrak{S},\mathcal{K}}(\Phi_{\mathfrak{S},\mathcal{K}}(\delta^\dagger)) = \max\Big\{\pi_{\mathbb{R}}\boldsymbol{\xi}^{\mathcal{X}}_{\mathfrak{S}}(T,\mathbf{u}) \,:\, \mathbf{u} \in \mathcal{U}^{\mathcal{X}}_{\mathfrak{S},\mathcal{K}}(T),\, \pi_{\mathcal{S}}\boldsymbol{\xi}^{\mathcal{X}}_{\mathfrak{S}}(T,\mathbf{u}) = \mathbf{s}^\dagger, \int_0^T \|\mathbf{u}(s)\|_{\mathbb{R}^p}\mathrm{d}s \leq \Phi_{\mathfrak{S},\mathcal{K}}(\delta^\dagger)\Big\}. \tag{5.38}$$

Proof.

1. For any $a \geq 0$ and $\boldsymbol{\xi} \in \mathcal{M}$, denote by $B^{\mathcal{M}}(\boldsymbol{\xi}, a)$ the sub-Riemannian ball, of radius a and centered at $\boldsymbol{\xi}$. According to [4, Theorem 3.8], the Carnot-Caratheodory distance induces the manifold topology on $\mathcal{M}$. We deduce that, for every $l > 0$, the set $B(\boldsymbol{\xi}^\dagger, l) \cap (\mathring{\mathcal{K}} \times \mathbb{R})$ is open an nonempty (it contains $\mathbf{s}^\dagger$) and hence
$$(\{\mathbf{s}\} \times \mathbb{R}) \cap B(\boldsymbol{\xi}^\dagger, l) \cap (\mathring{\mathcal{K}} \times \mathbb{R})$$
contains an open set $\{\mathbf{s}^\dagger\} \times]-\varepsilon, \varepsilon[$ for some $\varepsilon > 0$. We infer that, for every $l > 0$, we have $\Psi_{\mathfrak{S},\mathcal{K}}(l) > \varepsilon > 0$. We use the relation (5.35) to deduce that, for every $l > 0$ and $T > 0$, we also have $\Lambda_{\mathfrak{S},\mathcal{K}}(l,T) > 0$.

2. The function (5.36a) is clearly nondecreasing. Moreover, for every $l, l' \geq 0$, we have:

$$\Psi_{\mathfrak{S},\mathcal{K}}(l+l') \geq \Psi_{\mathfrak{S},\mathcal{K}}(l) + \Psi_{\mathfrak{S},\mathcal{K}}(l'). \tag{5.39}$$

Indeed, recall that every minimizer to Problem 5.4.8 is time parameterization invariant and consider the curves $\Gamma \subset \mathcal{S}$ of length l and $\Gamma' \subset \mathcal{S}$ of length l' corresponding to the maximizers of Problem 5.4.8 for l and l' respectively. Then denote $\Gamma'' = \Gamma \cup \Gamma'$. This curve is admissible, closed, of length $l + l'$ and produces a displacement no greater than $\Psi_{\mathfrak{S},\mathcal{K}}(l+l')$. Inequality (5.39) together with the first point of the Theorem yield the increasing property of function (5.36a).

In order to prove the right continuity, let $l \in \mathbb{R}_+$ be given and consider a decreasing sequence $(l_n)_n$ converging to l. For every l_n ($n \in \mathbb{N}$), denote by $\mathbf{u}_n$ the minimizer to Problem 5.4.8 such that $\|\mathbf{u}_n(t)\|_{\mathbb{R}^p}$ is constant for every $t \in [0,T]$. The sequence $(\mathbf{u}_n)_n$ is bounded in $L^2([0,T],\mathbb{R}^p)$ and the sequence $(\boldsymbol{\xi}^{\mathcal{X}}_{\mathfrak{S}}(\,\cdot\,,\mathbf{u}_n))_n$ is bounded in $C^0([0,T],\mathcal{M})$, therefore there exists a subsequence $(l_{n_k})_k$ such that $(\Psi_{\mathfrak{S},\mathcal{K}}(l_{n_k}))_k$ converges to $\limsup \Psi_{\mathfrak{S},\mathcal{K}}(l_n)$ while $(\mathbf{u}_{n_k})_k$ weakly converges in $L^2([0,T],\mathbb{R}^p)$ to $\mathbf{u}^*$ and $(\boldsymbol{\xi}^{\mathcal{X}}_{\mathfrak{S}}(\,\cdot\,,\mathbf{u}_{n_k}))_k$ uniformly converges to $\boldsymbol{\xi}^*$.

On the one hand, arguing as for (5.33), we deduce that $\boldsymbol{\xi}^* = \boldsymbol{\xi}^{\mathcal{X}}_{\mathfrak{S}}(\,\cdot\,,\mathbf{u}^*)$ and then that

$$\Psi_{\mathfrak{S},\mathcal{K}}(l_{n_k}) \to \pi_{\mathbb{R}}\boldsymbol{\xi}^{\mathcal{X}}_{\mathfrak{S}}(T,\mathbf{u}^*) \quad \text{as } k \to +\infty$$

with $\|\mathbf{u}^*\|_{L^1([0,T],\mathbb{R}^p)} \leq \liminf l_n = l$. Therefore we obtain that:

$$\limsup \Psi_{\mathfrak{S},\mathcal{K}}(l_n) \leq \Psi_{\mathfrak{S},\mathcal{K}}(l).$$

On the other hand, since $\Psi_{\mathfrak{S},\mathcal{K}}$ is increasing and $l \leq l_n$ for every n, we deduce that

$$\Psi_{\mathfrak{S},\mathcal{K}}(l) \leq \Psi_{\mathfrak{S},\mathcal{K}}(l_n),$$

and the conclusion arises by taking the limit inf in both sides of the inequality.

3. The proof of this point is a straightforward consequence of the preceding point and relation (5.35).

4. The same reasoning as for the second point proves that the constraints are saturated in Problems 5.4.8 or 5.4.9 for the maximizers. Indeed, if the constraints were not saturated, then it would be possible to add to the optimal curve on $\mathcal{S}$ a small loop that would produce an extra displacement (according to the first point).

5. For ε small enough, we have $B^{\mathcal{M}}(\boldsymbol{\xi}^\dagger,\varepsilon) \subset \mathring{\mathcal{K}}$ (because the sub-Riemannian topology coïncides with the manifold topology). In this case, for every $\delta^\dagger \in \pi_{\mathbb{R}}^{-1}B^{\mathcal{M}}(\boldsymbol{\xi}^\dagger,\varepsilon)$, we have:

$$\Phi_{\mathfrak{S},\mathcal{K}}(\delta^\dagger) = \mathrm{d}(\boldsymbol{\xi}^\dagger,\boldsymbol{\xi}^\ddagger).$$

According to [4, Theorem 3.18], the Carnot-Caratheodory distance is continuous for the manifold topology, so we deduce that the function (5.36c) is continuous in a neighborhood of 0. It is even because, for every δ and every minimizer $\mathbf{u}$ on $[0,T]$, the control $t \mapsto \mathbf{u}(T-t)$ is a minimizer with the same Riemannian length, associated to $-\delta$.

Observe now that for every $\delta^\dagger, h \in \mathbb{R}$:

$$\Phi_{\mathfrak{S},\mathcal{K}}(\delta^\dagger + h) \leq \Phi_{\mathfrak{S},\mathcal{K}}(\delta^\dagger) + \Phi_{\mathfrak{S},\mathcal{K}}(h),$$

whence we infer that:

$$\Phi_{\mathfrak{S},\mathcal{K}}(\delta^\dagger + h) - \Phi_{\mathfrak{S},\mathcal{K}}(\delta^\dagger) \leq \Phi_{\mathfrak{S},\mathcal{K}}(h).$$

Writing that

$$\Phi_{\mathfrak{S},\mathcal{K}}(\delta^\dagger) \leq \Phi_{\mathfrak{S},\mathcal{K}}(\delta^\dagger + h) + \Phi_{\mathfrak{S},\mathcal{K}}(-h),$$

and since the function is even, we finally get:

$$|\Phi_{\mathfrak{S},\mathcal{K}}(\delta^\dagger + h) - \Phi_{\mathfrak{S},\mathcal{K}}(\delta^\dagger)| \leq \Phi_{\mathfrak{S},\mathcal{K}}(h),$$

which, with the continuity in 0, proves that the function is uniformly continuous on $\mathbb{R}$.

6. The proof of this point is a straightforward consequence of the preceding point and relation (5.28).

7. For every $l \geq 0$, we clearly have $\Phi_{\mathfrak{S},\mathcal{K}}(\Psi_{\mathfrak{S},\mathcal{K}}(l)) \leq l$. The inequality $\Phi_{\mathfrak{S},\mathcal{K}}(\Psi_{\mathfrak{S},\mathcal{K}}(l)) < l$ for some $l \geq 0$ and the existence of minimizers to Problem 5.4.5 would contradict the fact that the constraint is saturated for every maximizer of Problem 5.4.8.

The function (5.36a) has no reason to be monotone in the general case. Let us define:

Hypothesis 5.4.13 *The swimmer $\mathfrak{S} = (\mathcal{S}, \mathbf{g}, \mathbf{Q}^{\mathcal{S}}, \mathbf{s}^\dagger, \mathcal{L})$ is such that $\mathbf{Q}^{\mathcal{S}} = \mathbf{0}$ (there is no self-propelled constraints).*

Every swimmer satisfying (5.4.13) is called *unconstrained* . For unconstrained swimmers, every absolutely continuous curve on $\mathcal{S}$, with essentially bounded first derivative, is an admissible shape change. Under Hypothesis 5.4.13, we can state:

Theorem 5.4.14 *Let $\mathfrak{S} = (\mathcal{S}, \mathbf{g}, \mathbf{Q}^{\mathcal{S}}, \mathbf{s}^\dagger, \mathcal{L})$ be a controllable, trivialized, unconstrained swimmer, and $\mathcal{K}$ be a compact of $\mathcal{S}$ such that $\mathbf{s}^\dagger \in \mathring{\mathcal{K}}$. Then there exists $\varepsilon > 0$ such that the function* (5.36a) *is increasing on* $]-\varepsilon, \varepsilon[$.

Proof. Denote by $B^{\mathcal{S}}(\mathbf{s}^\dagger, r)$ the Riemannian ball on $\mathcal{S}$, where the radius r is given by Lemma 5.7.1. Let $\varepsilon > 0$ be small enough such that $B^{\mathcal{M}}(\boldsymbol{\xi}^\dagger, \varepsilon) \subset \mathring{\mathcal{K}}$ (it is always possible because the sub-Riemannian topology coïncides with the manifold topology) and $\pi_{\mathcal{S}} B^{\mathcal{M}}(\boldsymbol{\xi}^\dagger, \varepsilon) \subset B^{\mathcal{S}}(\mathbf{s}^\dagger, r)$.

Assume now that there exist $0 < \delta_0 < \delta_1 < \varepsilon$ such that

$$\Phi_{\mathfrak{S},\mathcal{K}}(\delta_1) \leq \Phi_{\mathfrak{S},\mathcal{K}}(\delta_0). \tag{5.40}$$

Denote $\boldsymbol{\xi}^1 = (\mathbf{s}^\dagger, \delta_1)$ and for some $\mathcal{X} = \{\mathbf{X}_j,\, j = 1, \ldots, p\}$ (an orthonormal basis of $\Delta^{\mathcal{S}}$) and $T > 0$, denote by $\mathbf{u}^1 \in \mathcal{U}^{\mathcal{X}}_{\mathfrak{S},\mathcal{K}}(\boldsymbol{\xi}^1, T)$ a control minimizing Problem 5.4.5. Introduce as well $\gamma_1 = \pi_{\mathcal{S}}\boldsymbol{\xi}(\,\cdot\,, \mathbf{u}^1)$ and Γ_1 the curve on $\mathcal{S}$ parameterized by γ_1. The following identity holds:

$$\Phi_{\mathfrak{S},\mathcal{K}}(\delta_1) = \int_0^T \|\mathbf{u}^1(t)\|_{\mathbf{R}^p} \mathrm{d}t = \ell(\Gamma_1).$$

According to Lemma 5.7.1 with $x_0 = \mathbf{s}^\dagger$ and $\gamma = \gamma_1$, there exists a continuous function $\psi : [0,1] \times [0,T] \to \mathcal{S}$ such that, for every $s \in [0,1]$, $\psi(s, \cdot)$ is absolutely continuous with essentially bounded first derivative, $\psi(1, \cdot) = \gamma_1$ and $\psi(0, \cdot) = \mathbf{s}^\dagger$. Denoting by $\mathbf{u}^s = (u^s_j)_{1 \leq j \leq p} \in \mathcal{U}^{\mathcal{X}}_{\mathfrak{S},\mathcal{K}}(T)$ the control such that

$$u^s_j(t) = \mathbf{g}_{\psi(s,t)}(\partial_t \psi(s,t), \mathbf{X}_j(\psi(s,t))), \quad t \in [0,T],$$

and by Γ_s the curve parameterized by $t \in [0,T] \mapsto \psi(s,t) = \pi_{\mathcal{S}}\boldsymbol{\xi}(t, \mathbf{u}^s)$ $(s \in [0,1])$, we have, for every $s \in [0,1]$:

$$\Phi_{\mathfrak{S},\mathcal{K}}(\Xi(s)) \leq \int_0^T \|\mathbf{u}^s(t)\|_{\mathbb{R}^p} \mathrm{d}t = \ell(\Gamma_s).$$

where we have set:

$$\Xi : s \in [0,1] \mapsto \pi_{\mathbb{R}} \boldsymbol{\xi}^{\mathcal{X}}_{\mathfrak{S}}(T, \mathbf{u}^s) \in \mathbb{R}.$$

The function Ξ is continuous and such that $\Xi(1) = \delta_1$ and $\Xi(0) = 0$, so there exists $s^* \in]0,1[$ such that $\Xi(s^*) = \delta_0$. Since, according to Lemma 5.7.1, the function $s \in [0,1] \mapsto \ell(\Gamma_s)$ is increasing, we get:

$$\Phi_{\mathfrak{S},\mathcal{K}}(\delta_0) \leq \ell(\Gamma_{s^*}) < \ell(\Gamma_1) = \Phi_{\mathfrak{S},\mathcal{K}}(\delta_1),$$

which is in contradiction with (5.40). The proof is now completed.

5.5 The case $N = 2$

This section is devoted to the study of optimal strokes for controllable, trivialized, unconstrained swimmers, when the dimension N of the manifold $\mathcal{S}$ is equal to 2.

5.5.1 Optimal Strokes and Isoperimetric Inequalities

In this subsection, we wish to give a hint of how the optimal stroke problem can be interpretable as an isoperimetric problem on the manifold $\mathcal{S}$.

Recall that a stroke is a closed (oriented) admissible curve Γ. Let $\mathbf{s} : [0,T] \mapsto \mathcal{S}$ be a parameterization of a Γ. The travelled distance resulting from this stroke is:

$$\int_0^T \mathcal{L}_{\mathbf{s}(t)} \dot{\mathbf{s}}(t) \mathrm{d}t = \int_\Gamma \mathcal{L}.$$

Denoting by Ω the area enclosed by Γ, Stokes formula tells us that:

$$\int_\Gamma \mathcal{L} = \int_\Omega \mathrm{d}\mathcal{L}.$$

Notice that these formula are metric independent but require $\mathcal{S}$ to be orientable. The $2-$form $\mathrm{d}\mathcal{L}$ defined on the 2 dimensional manifold $\mathcal{S}$ can be seen as a signed measure on $\mathcal{S}$. On the other hand, an example of cost functional considered in this paper is just the Riemannian length of Γ.

So, roughly speaking, seeking optimal strokes consists in minimizing the Riemannian length of Γ while maximizing the measure of the area Ω for the signed measure $\mathrm{d}\mathcal{L}$.

In the case of the swimmer in the potential flow, we have drawn on Fig 5.4 the density function of the measure $\mathrm{d}\mathcal{L}$. Notice in particular that, considering small strokes (and hence small closed curves), not only matter the shape of the curve but the position on the ellipsoid is also preponderant.

This approach of optimal stroke problems as isoperimetric problems would be worth some further investigation.

5.5.2 Pontryagin's maximum principle

Let us begin with recalling some notation. We consider a trivialized, unconstrained, controllable swimmer $\mathfrak{S} = (\mathcal{S}, \mathbf{g}, \mathbf{Q}^{\mathcal{S}}, \mathbf{s}^\dagger, \mathcal{L})$ (with $\mathbf{Q}^{\mathcal{S}} = \mathbf{0}$ since it is *unconstrained*) and $\mathcal{X} = \{\mathbf{X}_1, \mathbf{X}_2\}$ an analytic orthonormal basis of $\Delta^{\mathcal{S}} = T\mathcal{S}$. Then we define the analytic vector fiels $\mathcal{Z} = \{\mathbf{Z}_1, \mathbf{Z}_2\}$ on $\mathcal{M}$, according to formula (5.21).

To pursue, we need to strengthened Hypothesis 5.3.5 as follows.

Hypothesis 5.5.1 *For every $\boldsymbol{\xi} \in \mathcal{M}$, we have:*

$$\dim \operatorname{span}\{\mathbf{Z}_1(\boldsymbol{\xi}), \mathbf{Z}_2(\boldsymbol{\xi}), [\mathbf{Z}_1, \mathbf{Z}_2](\boldsymbol{\xi})\} = 3. \tag{5.41}$$

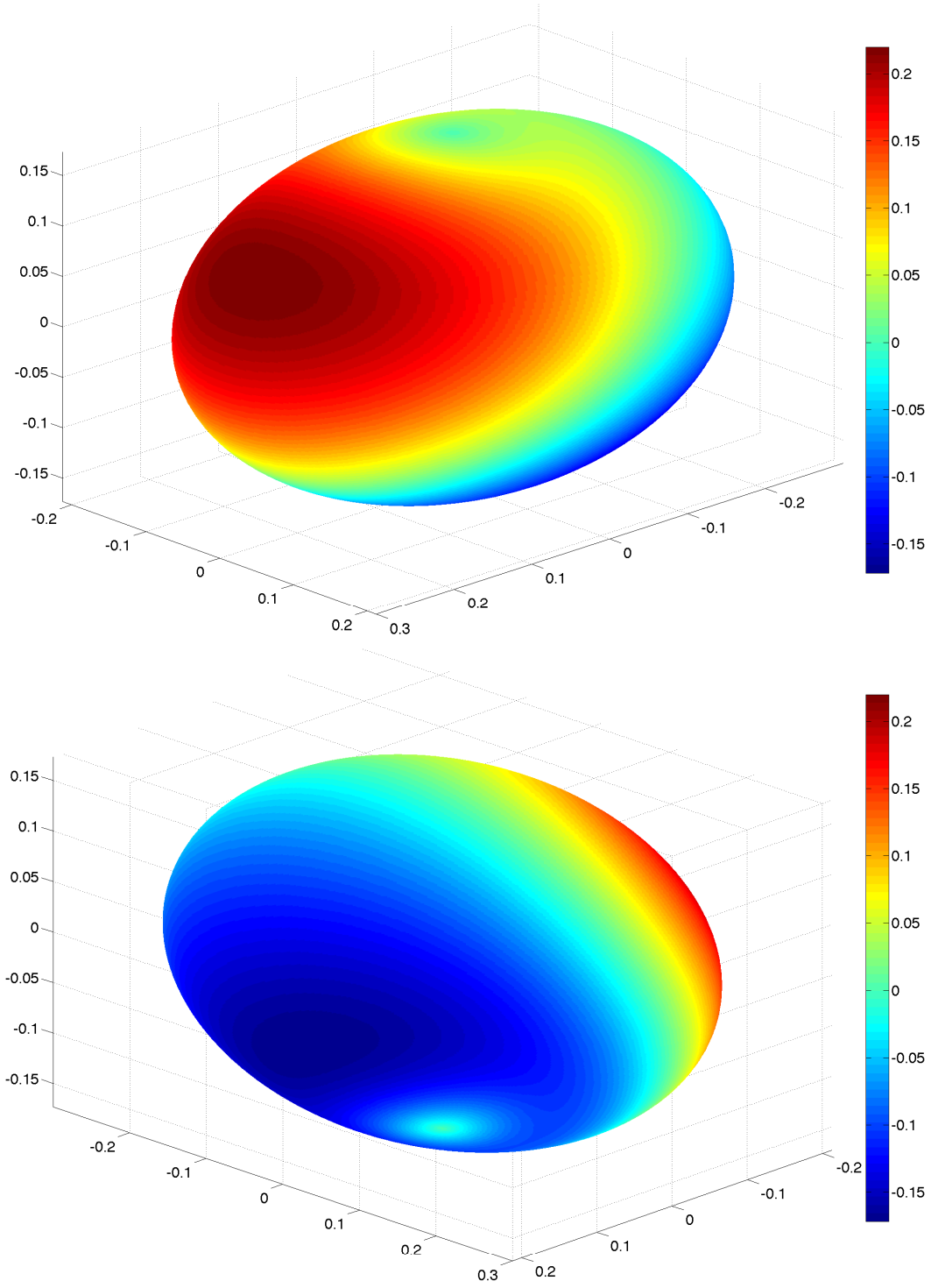

Figure 5.4: Density fonction of the signed measure defined by $d\mathcal{L}$ on the ellipsoid. A stroke being a closed curve on the ellipsoid, the resulting travelled distance is obtained by measuring the area of the enclosed surface for the measure $d\mathcal{L}$. See also Fig 5.5 and 5.9.

As already pointed out, this Hypothesis does not depend on the choice of $\mathcal{Z}$ and hence is independent of the choice of the orthonormal basis $\mathcal{X}$. Actually, (5.41) can be rewritten as:

$$\dim \operatorname{span}\left\{\Delta^{\mathcal{M}}_{\boldsymbol{\xi}}, [\Delta^{\mathcal{M}}_{\boldsymbol{\xi}}, \Delta^{\mathcal{M}}_{\boldsymbol{\xi}}]\right\} = 3.$$

Recall that according to Lemma 5.3.6, Hypothesis 5.3.5 leads to:

$$\dim \operatorname{Lie}_{\boldsymbol{\xi}} \Delta^{\mathcal{M}} = \dim \mathcal{M}, \quad \forall\, \boldsymbol{\xi} \in \mathcal{M}.$$

In Hypothesis 5.5.1, $\operatorname{Lie}_{\boldsymbol{\xi}} \Delta^{\mathcal{M}}$ is required to be spanned by the Lie brackets of order no greater than 1.

In Theorem 5.4.10, it has been proved that Problems 5.4.5-5.4.7 are equivalent. Let us restate a version of this problem in the simplified 2 dimensional case we are considering in this Section:

Problem 5.5.2 *For any given $\boldsymbol{\xi_0}, \boldsymbol{\xi_1}$ in $\mathcal{M}$, find $T \geq 0$ and a measurable bounded function $t \in [0,T] \mapsto (u_1(t), u_2(t)) \in \mathbb{R}^2$ which minimizes the cost*

$$\frac{1}{2}\int_0^T \left(u_1(t)^2 + u_2(t)^2\right) dt,$$

such that there exists an absolutely continuous curve $t \in [0,T] \mapsto \boldsymbol{\xi}(t) \in \mathcal{M}$ satisfying

$$\dot{\boldsymbol{\xi}}(t) = u_1(t)\mathbf{Z}_1(\boldsymbol{\xi}) + u_2(t)\mathbf{Z}_2(\boldsymbol{\xi}) \text{ for almost every } t \text{ in } [0,T], \tag{5.42a}$$

$$\boldsymbol{\xi}(0) = \boldsymbol{\xi}_0, \quad \boldsymbol{\xi}(T) = \boldsymbol{\xi}_1. \tag{5.42b}$$

and,

$$u_1(t)^2 + u_2(t)^2 = 1 \quad \forall t \in [0,T]. \tag{5.42c}$$

In order to apply Pontryagin's maximum principle (see [2]) to this problem, we denote by $T^*\mathcal{M}$ the cotangent bundle of $\mathcal{M}$ and we introduce the Hamiltonian (see [85] Chap.7.1)

$$\begin{array}{rcl} H : \mathbb{R} \times \mathcal{M} \times T^*\mathcal{M} \times \mathbb{R} \times \mathbb{R}^2 & \to & \mathbb{R} \\ \left(t, \boldsymbol{\xi}, \mathbf{p}, p^0, (u_1, u_2)\right) & \mapsto & H\left(t, \boldsymbol{\xi}, \mathbf{p}, p^0, (u_1, u_2)\right) \end{array} \tag{5.43a}$$

defined by:

$$H\left(t, \boldsymbol{\xi}, \mathbf{p}, p_0, \mathbf{U}\right) = \langle \mathbf{p}, u_1(t)\mathbf{Z}_1(\boldsymbol{\xi}) + u_2(t)\mathbf{Z}_2(\boldsymbol{\xi})\rangle - p_0\left(u_1^2(t) + u_2^2(t)\right) \tag{5.43b}$$

where $\langle \cdot\,, \cdot \rangle$ stands for the duality product $T^*\mathcal{M} \times T\mathcal{M}$. For every $\boldsymbol{\xi}$ in $\mathcal{M}$, the quantity $u_1(t)\mathbf{Z}_1(\boldsymbol{\xi}) + u_2(t)\mathbf{Z}_2(\boldsymbol{\xi})$ belongs to the tangent space $T_{\boldsymbol{\xi}}\mathcal{M}$, $\mathbf{p}$ is in the cotangent space $T^*_{\boldsymbol{\xi}}\mathcal{M}$ and p_0, called the cost dual variable, is a time independent real constant.

In this setting and under Hypothesis 5.5.1, the Pontryagin's maximum principle reads (see for instance Theorem 3.28 of [4])

Proposition 5.5.3 *If $(u_1(\,\cdot\,), u_2(\,\cdot\,)) \in L^\infty([0,T], \mathbb{R}^2)$ is a solution to Problem 5.5.2 associated with curve $t \in [0,T] \mapsto \boldsymbol{\xi}(t) \in \mathcal{M}$, then, there exists a non trivial*

$$\mathbf{p} : t \in [0,T] \mapsto \mathbf{p}(t) \in T^*\mathcal{M}$$

solution of the system

$$\dot{\boldsymbol{\xi}} = u_1(t)\mathbf{Z}_1(\boldsymbol{\xi}) + u_2(t)\mathbf{Z}_2(\boldsymbol{\xi}), \tag{5.44a}$$

$$\dot{\mathbf{p}} = -u_1(t)\langle \mathbf{p}, D_{\boldsymbol{\xi}}\mathbf{Z}_1(\boldsymbol{\xi})\rangle - u_2(t)\langle \mathbf{p}, D_{\boldsymbol{\xi}}\mathbf{Z}_2(\boldsymbol{\xi})\rangle. \tag{5.44b}$$

Moreover, for all $t \in [0,T]$,

$$u_i(t) = \langle \mathbf{p}(t)\,,\, \mathbf{Z}_i(\boldsymbol{\xi}(t))\rangle \text{ for } i = 1, 2.$$

Definition 5.5.4 *The exponential map (from $\boldsymbol{\xi}_0$), denoted by $\varepsilon_{\boldsymbol{\xi}_0}$, is the mapping which associates to every $\mathbf{p}_0 \in T^*\mathcal{M}$, the solution of System* (5.44) *with the initial condition $\boldsymbol{\xi}(0) = \boldsymbol{\xi}_0$ and $\mathbf{p}(0) = \mathbf{p}_0$. Such a trajectory is called an* extremal.

We call $\gamma_{\mathbf{p}_0}$ the curve on the manifolds $\mathcal{M}$ of the solution $\varepsilon_{\boldsymbol{\xi}_0}$.

Remark 5.5.5 *The general statement of the Maximum Principle, as it can be found for instance in [2], is more intricate and involves so-called* abnormal *extremals. The study of such extremals is usually far from obvious, from both a theoretical and a numerical point of view. In our case, the distribution is 1-step generating, see Eq. (5.41). Hence, the Goh condition (see Chap. 10.2 of [14]) ensures that all optimal trajectories in $\mathcal{M}$ can be lifted in $T^*\mathcal{M}$ as normal extremals.*

An obvious consequence of Proposition 5.5.3 is

Lemma 5.5.6 *For every solution of* (5.44) $(\boldsymbol{\xi}(\,\cdot\,), \mathbf{p}(\,\cdot\,)) : [0,T] \to T^*\mathcal{M}$, *there exists a continuous function $\theta : [0,T] \to \mathbb{R}$ such that,*

$$\langle \mathbf{p}(\,\cdot\,), \mathbf{Z}_1(\boldsymbol{\xi}(\,\cdot\,))\rangle = \cos(\theta(\,\cdot\,)),$$
$$\langle \mathbf{p}(\,\cdot\,), \mathbf{Z}_2(\boldsymbol{\xi}(\,\cdot\,))\rangle = \sin(\theta(\,\cdot\,)).$$

5.5.3 Contact sub-Riemannian structure

A Riemannian manifold is endowed with a definite 2-form that induces a natural identification between the tangent space and its dual. In general, such an identification cannot be directly generalized to any sub-Riemannian structure, since the definite 2-form that defines the metric is not defined on the whole tangent space, but only on a strict subspace. In our case, from the metric $\mathbf{g}$ on $\mathcal{S}$, we can define the definite 2-form $\mathbf{g}^{\mathcal{M}}$ on $\Delta^{\mathcal{M}}$ by setting:

$$\mathbf{g}^{\mathcal{M}}_{\boldsymbol{\xi}}(\boldsymbol{\zeta}_1, \boldsymbol{\zeta}_2) = \mathbf{g}_{\pi_{\mathcal{S}}\boldsymbol{\xi}}(\pi_{\mathcal{S}}\boldsymbol{\zeta}_1, \pi_{\mathcal{S}}\boldsymbol{\zeta}_1), \quad \boldsymbol{\xi} \in \mathcal{M},\, \boldsymbol{\zeta}_1, \boldsymbol{\zeta}_2 \in \Delta^{\mathcal{M}}_{\boldsymbol{\xi}}.$$

In the particular case of so-called *contact structures* (see definition below), it is possible to define a natural identification between the tangent and the co-tangent spaces. We follow here the procedure exposed by Agrachev in [1], adapted to our special example (for which $\dim \mathcal{M} = 3$).

Definition 5.5.7 *A contact structure in $\mathcal{M}$ is a smooth distribution of 2-planes $\widetilde{\Delta} : \boldsymbol{\xi} \in \mathcal{M} \mapsto \widetilde{\Delta}_{\boldsymbol{\xi}} \in T_{\boldsymbol{\xi}}\mathcal{M}$ that is non-integrable at every point, i.e., $\widetilde{\Delta}_{\boldsymbol{\xi}} + [\widetilde{\Delta}_{\boldsymbol{\xi}}, \widetilde{\Delta}_{\boldsymbol{\xi}}] = T_{\boldsymbol{\xi}}\mathcal{M}$ for every $\boldsymbol{\xi}$ in $\mathcal{M}$.*

This is precisely Hypothesis 5.5.1 and therefore:

Proposition 5.5.8 *The distribution $\Delta^{\mathcal{M}}$ is a contact structure.*

For every $\boldsymbol{\xi}$ in $\mathcal{M}$, $\{\mathbf{Z}_1(\boldsymbol{\xi}), \mathbf{Z}_2(\boldsymbol{\xi})\}$ is a basis of $\Delta^{\mathcal{M}}_{\boldsymbol{\xi}}$. The definite 2-form $\mathbf{g}^{\mathcal{M}}$ induces a natural identification between $\Delta^{\mathcal{M}}_{\boldsymbol{\xi}}$ and $(\Delta^{\mathcal{M}}_{\boldsymbol{\xi}})^*$. Hence the co-vectors $\mathbf{Z}_1(\boldsymbol{\xi})^*$ and $\mathbf{Z}_2(\boldsymbol{\xi})^*$ form a basis of $(\Delta^{\mathcal{M}}_{\boldsymbol{\xi}})^*$. It remains to complete these bases of $\Delta^{\mathcal{M}}_{\boldsymbol{\xi}}$ and $(\Delta^{\mathcal{M}}_{\boldsymbol{\xi}})^*$ by choosing a third vector. It can be done in a canonical way using Stokes fields (see Section 2.1 of [1]).

Lemma 5.5.9 *There exists a unique 1-form ω on $\mathcal{M}$ such that, for every $\boldsymbol{\xi}_0$ in $\mathcal{M}$:*

1. *$\omega_{|\Delta^{\mathcal{M}}_{\boldsymbol{\xi}_0}}$ vanished ,*
2. *$\mathrm{d}\omega_{|\Delta^{\mathcal{M}}_{\boldsymbol{\xi}_0} \times \Delta^{\mathcal{M}}_{\boldsymbol{\xi}_0}}$ is equal to the volume form $\mathbf{g}^{\mathcal{M}}_{\boldsymbol{\xi}_0}$ on the oriented Euclidean space $\Delta^{\mathcal{M}}_{\boldsymbol{\xi}_0}$.*

Proof. The proof of [1] is constructive. Locally, up to a restriction of a local chart, $\mathcal{M} = \mathbb{R}^3$.

For every $\boldsymbol{\xi}$, the vectors $\mathbf{Z}_1(\boldsymbol{\xi})$ and $\mathbf{Z}_2(\boldsymbol{\xi})$ span a 2-dimensional subspace of $T_{\boldsymbol{\xi}}\mathcal{M}$. Since $T^*_{\boldsymbol{\xi}}\mathcal{M}$ is a 3-dimensional vector space, there exists a non-trivial linear form $\tilde{\omega}_{\boldsymbol{\xi}}$ which vanishes on $\mathbf{Z}_1(\boldsymbol{\xi})$ and $\mathbf{Z}_2(\boldsymbol{\xi})$, and hence on $\Delta^{\mathcal{M}}_{\boldsymbol{\xi}}$. Moreover, for any other linear form $\hat{\omega}_{\boldsymbol{\xi}}$ that vanishes on $\Delta^{\mathcal{M}}_{\boldsymbol{\xi}}$, there exists some real number $f_{\boldsymbol{\xi}}$ such that $\hat{\omega}_{\boldsymbol{\xi}} = f(\boldsymbol{\xi})\tilde{\omega}_{\boldsymbol{\xi}}$.

Expressing everything in coordinates, one can see that the coordinates of $\tilde{\omega}$ can be chosen to depend rationally on the coordinates of $\mathbf{Z}_1$ and $\mathbf{Z}_2$, hence we can assume that $\tilde{\omega}$ is smooth on $\mathcal{M}$.

Any other smooth 1-form $\hat{\omega}$ that vanishes on $\Delta^{\mathcal{M}}$ has the form $\hat{\omega} = f\tilde{\omega}$ with $f : \mathcal{M} \to \mathbf{R}$ a smooth function. The problem now is to prove that there exists one, and only one, function f such that $f\tilde{\omega}$ satisfies the second condition of Lemma 5.5.9.

A straightforward computation in coordinates gives, for any smooth function f,

$$\mathrm{d}(f\tilde{\omega})_{|\Delta^{\mathcal{M}}\times\Delta^{\mathcal{M}}} = f\mathrm{d}(\tilde{\omega})_{|\Delta^{\mathcal{M}}\times\Delta^{\mathcal{M}}},$$

what proves the uniqueness of the 1-form ω (if any) satisfying the conditions of Lemma 5.5.9.

As a consequence of Hypothsesis 5.5.1, the 2-form $\mathrm{d}\tilde{\omega}(\mathbf{Z}_1, \mathbf{Z}_2)$ does not vanish (this can be seen with a direct but tedious computation in coordinates by expressing $\det(\mathbf{Z}_1, \mathbf{Z}_2, [\mathbf{Z}_1, \mathbf{Z}_2])$ in terms of $\mathrm{d}\tilde{\omega}(\mathbf{Z}_1, \mathbf{Z}_2)$). Lemma 5.5.9 follows by defining the 1-form $\omega_{\boldsymbol{\xi}} = \dfrac{1}{d\tilde{\omega}_{\boldsymbol{\xi}}(\mathbf{Z}_1(\boldsymbol{\xi}), \mathbf{Z}_2(\boldsymbol{\xi}))}\tilde{\omega}_{\boldsymbol{\xi}}$.

From non on, we denote with ω the 1-form defined in Lemma 5.5.9. Our aim is now to define a vector field $\mathbf{e}$ "dual" to ω in $T\mathcal{M}$.

Lemma 5.5.10 *There exists a unique analytic vector field, called the Stokes field and denoted by $\mathbf{e} : \boldsymbol{\xi} \in \mathcal{M} \mapsto \mathbf{e}_{\boldsymbol{\xi}} \in T_{\boldsymbol{\xi}}\mathcal{M}$ which satisfies, for every $\boldsymbol{\xi}$ in $\mathcal{M}$:*

1. $\omega_{\boldsymbol{\xi}}(\mathbf{e}_{\boldsymbol{\xi}}) = 1$,
2. $\mathrm{d}\omega_{\boldsymbol{\xi}}(\mathbf{e}_{\boldsymbol{\xi}}, \mathbf{Z}_i(\boldsymbol{\xi})) = 0$, *for* $i = 1, 2$.

Proof. For every $\boldsymbol{\xi}$ in $\mathcal{M}$, since the three linear forms $\omega_{\boldsymbol{\xi}}$, $\mathrm{d}\omega_{\boldsymbol{\xi}}(\,\cdot\,, \mathbf{Z}_i(\boldsymbol{\xi}))$, $i = 1, 2$, are independent, there exists an unique vector $\mathbf{e}$ which is solution of the linear system given by the two conditions.

From now on, with a slight abuse of notations, we will denote $\mathbf{Z}^*_i := \mathrm{d}\omega(\,\cdot\,, \mathbf{Z}_i)$. This emphasizes the duality between the bases $(\mathbf{Z}_1(\boldsymbol{\xi}), \mathbf{Z}_2(\boldsymbol{\xi}), \mathbf{e}_{\boldsymbol{\xi}})$ and $(\mathbf{Z}^*_1(\boldsymbol{\xi}), \mathbf{Z}^*_2(\boldsymbol{\xi}), \omega_{\boldsymbol{\xi}})$ of $\mathrm{T}_{\boldsymbol{\xi}}\mathcal{M}$ and $\mathrm{T}^*_{\boldsymbol{\xi}}\mathcal{M}$.

Remark 5.5.11 *An important point in the construction of the bases $(\mathbf{Z}_1(\boldsymbol{\xi}), \mathbf{Z}_2(\boldsymbol{\xi}), \mathbf{e}_{\boldsymbol{\xi}})$ and $(\mathbf{Z}^*_1(\boldsymbol{\xi}), \mathbf{Z}^*_2(\boldsymbol{\xi}), \omega_{\boldsymbol{\xi}})$ is that the construction depends only on $\mathbf{g}^{\mathcal{M}}$ and $\Delta^{\mathcal{M}}$, up to a rotation in the 2-plane $\Delta^{\mathcal{M}}_{\boldsymbol{\xi}}$. In other words, the contact structure in $\mathcal{M}$ is enough to induce an intrinsic isomorphism from the tangent to the cotangent space of $\mathcal{M}$, as if $\mathcal{M}$ were a Riemannian (not only a sub-Riemannian) manifold.*

A direct consequence of the construction done in Lemmas 5.5.9 and 5.5.10 is the possibility to express uniquely any co-vector $\mathbf{p}$ in $T^*_{\boldsymbol{\xi}}\mathcal{M}$ in the basis $(\mathbf{Z}^*_1(\boldsymbol{\xi}), \mathbf{Z}^*_2(\boldsymbol{\xi}), \omega_{\boldsymbol{\xi}})$:

$$\mathbf{p} = \cos(\theta)\mathbf{Z}^*_1 + \sin(\theta)\mathbf{Z}^*_2 + \nu\omega.$$

As a direct consequence, any initial condition $\mathbf{p}_0$ of the Hamiltonian system 5.44 is defined by a couple $(\theta, \nu) \in \mathbb{R}/2\pi\mathbb{R} \times \mathbb{R}$.

5.5.4 Local structure of small geodesics

In this Subsection, we use the adapted bases $(\mathbf{Z}_1(\boldsymbol{\xi}), \mathbf{Z}_2(\boldsymbol{\xi}), \mathbf{e}_{\boldsymbol{\xi}})$ and $(\mathbf{Z}_1^*(\boldsymbol{\xi}), \mathbf{Z}_2^*(\boldsymbol{\xi}), \omega_{\boldsymbol{\xi}})$ of $\mathrm{T}_{\boldsymbol{\xi}}\mathcal{M}$ and $\mathrm{T}^*_{\boldsymbol{\xi}}\mathcal{M}$ in order to describe the geometric behaviour of the geodesics around a point $\boldsymbol{\xi}_0$ of $\mathcal{M}$.

Asymptotic lengths for geodesics

Fix $\boldsymbol{\xi}_0 \in \mathcal{M}$ and consider the exponential map $\varepsilon_{\boldsymbol{\xi}_0}$ starting from $\boldsymbol{\xi}_0$.

Definition 5.5.12 *A point $\boldsymbol{\xi} \neq \boldsymbol{\xi}_0$ is said* conjugate *to $\boldsymbol{\xi}_0$, if $\boldsymbol{\xi}$ is a critical value for $\varepsilon_{\boldsymbol{\xi}_0}$. The conjugate locus is the set which contains all the points to $\boldsymbol{\xi}_0$,*

$$Conj(\boldsymbol{\xi}_0) := \{\boldsymbol{\xi} \ s.\ t.\ \boldsymbol{\xi} \neq \boldsymbol{\xi}_0 \ and \ \boldsymbol{\xi} \ conjugate \ to \ \boldsymbol{\xi}_0\} \ . \tag{5.45}$$

Definition 5.5.13 *Fix $\boldsymbol{\xi}_0 \in \mathcal{M}$, we define the distance,*

$$C_{\mathbf{p}_0} := \sup\left\{t > 0 \,,\ \gamma(t) = \pi_{\mathcal{M}}\left(\varepsilon_{\boldsymbol{\xi}_0}(\mathbf{p}_0)\right) \,,\ d(\boldsymbol{\xi}_0, \gamma(t)) = t\right\} \tag{5.46}$$

The point $\gamma_{\mathbf{p}_0}(C_{\mathbf{p}_0})$ is a cut point of $\boldsymbol{\xi}_0$ along γ.

The cut locus is the set which contains all the cut points of $\mathbf{x}_0$ along all the curve γ,

$$Cut(\boldsymbol{\xi}_0) := \bigcup_{\lambda} \{\boldsymbol{\xi} \ s.\ t.\ \boldsymbol{\xi} \neq \boldsymbol{\xi}_0 \ and \ \boldsymbol{\xi} \ cut \ point \ of \ \mathbf{x}_0 \ along \ \gamma_\lambda\} \ . \tag{5.47}$$

For every point $\boldsymbol{\xi}_0$ in $\mathcal{M}$, the geodesics from $\boldsymbol{\xi}_0$ can lose their optimal property at the set of points defined by the union of the cut locus and the conjugate locus. It is important to know when the geodesics issued from a point $\boldsymbol{\xi}_0$ cut one of these sets. This question is difficult in general and there is no global answer. However, a precise description of short geodesics can be given in our particular setting (see [2]).

Definition 5.5.14 *We call* constants of the structure *the coefficients, denoted by the family $(c_{ij})_{i=1,2}^{j=1,2,3}$ associate with the decomposition of the two-form $d\mathbf{Z}_i^*$ into the basis $(\omega \wedge \mathbf{Z}_1^*, \omega \wedge \mathbf{Z}_2^*, \mathbf{Z}_1^* \wedge \mathbf{Z}_2^*)$. More precisely, for i=1,2, $d\mathbf{Z}_i^*$ reads,*

$$d\mathbf{Z}_i^* = c_{01}^i \, \omega \wedge \mathbf{Z}_1^* + c_{02}^i \, \omega \wedge \mathbf{Z}_2^* + c_{i3} \, \mathbf{Z}_1^* \wedge \mathbf{Z}_2^* \tag{5.48}$$

As the 1-forms $\mathbf{Z}_i^*$, notice that the constants of structure depend also on the point $\boldsymbol{\xi}$ where they are computed. We will introduce the two invariants maps which describe the local geometry around a point of the cut locus and the conjugate locus.

Definition 5.5.15 *We call χ the function from $\mathcal{M}$ to $\mathbb{R}$ defined by*

$$\chi := \sqrt{-\left(c_{01}^1 c_{02}^2 - c_{02}^1 c_{01}^2\right)} \, .$$

Proposition 5.5.16 *For $\mathbf{x}_0 = (\frac{1}{16}\sqrt{3}\sqrt{2}, \frac{1}{4}, \frac{1}{2})$ the value of*

$$\chi_{\mathbf{x}_0} := \frac{1580363335504710039820771085777225033151453265605427 2}{3070472626751170117064260382892590591961941813016409}$$

Proof. This value are calculated by using Maple.

Proposition 5.5.17 *The set $\{\boldsymbol{\xi} \in \mathcal{M} | \chi(\boldsymbol{\xi}) = 0\}$ is closed with measure zero in $\mathcal{M}$.*

Proof. Since the mapping $\boldsymbol{\xi} \in \mathcal{M} \mapsto \mathbf{Z}_i(\mathbf{x})$ is analytic, the function $\boldsymbol{\xi} \mapsto \chi(\boldsymbol{\xi})$ is analytic as well. The result follows from the connectedness of $\mathcal{M}$ and the computation of Proposition 5.5.16.

The fact that $\chi_{\mathbf{x}_0} \neq 0$ gives a asymptotic estimates of the first cut and conjugate lengths by applying the Theorems 3.2 and 4.2 of [2]:

Proposition 5.5.18 *For $\boldsymbol{\xi}$ in $\mathcal{M}$ such that $\chi_{\boldsymbol{\xi}} \neq 0$, for every $\mathbf{p}_0 = (\theta, \nu) \in T_{\boldsymbol{\xi}}\mathcal{M}^*$, the first conjugate length is,*

$$l_1(\theta, \nu) = \frac{2\pi}{|\nu|} + O_{\nu\to\infty}\left(\frac{1}{|\nu|^3}\right), \tag{5.49}$$

and the first cut length is,

$$l_*(\theta, \nu) = \frac{2\pi}{|\nu|} + O_{\nu\to\infty}\left(\frac{1}{|\nu|^3}\right). \tag{5.50}$$

Remark 5.5.19 *Theorems 3.2 and 4.2 in [1] provide also the local geometric behaviour of the cut and conjugate locus. For every $\mathbf{p}_0 = (\theta, \nu)$,*

$$\begin{aligned} Conj_{\mathbf{x}_0}(\theta, \nu) &= \mathbf{x}_0 \pm \tfrac{\pi}{\nu^2}\mathbf{e}_{\mathbf{x}_0} \pm \tfrac{2\pi\chi_{\mathbf{x}}}{\nu^3}\left(\cos(\theta)^3\mathbf{Z}_1(\mathbf{x}_0) - \sin(\theta)^3\mathbf{Z}_2(\mathbf{x}_0)\right) + O_{\nu\to\infty}\left(\tfrac{1}{\nu^4}\right) \\ Cut_{\mathbf{x}_0}(\theta, \nu) &= \mathbf{x}_0 \pm \tfrac{\pi}{\nu^2}\mathbf{e}_{\mathbf{x}_0} \pm \tfrac{2\pi\chi_{\mathbf{x}}\cos(\theta)}{\nu^3}\mathbf{Z}_1(\mathbf{x}_0) + O_{\nu\to\infty}\left(\tfrac{1}{\nu^4}\right). \end{aligned} \tag{5.51}$$

5.6 Swimmer in a potential flow: Numerics

There are basically two methods to compute the optimal strokes corresponding to Problems 5.4.5-5.4.9 for the example of swimmer in a potential flow presented in Subsection (5.2.5).

The first one consists in integrating Pontryagin's maximum principle (5.44) over a time interval $[0, T]$, specifying some initial data $(\boldsymbol{\xi}_0, \mathbf{p}_0)$. Since we are mostly interested in the ending point $\boldsymbol{\xi}(T)$, we can implement a so-called shooting method. For instance, seeking strokes, we want the $\mathcal{S}$ component of the ending point $\pi_{\mathcal{S}}\boldsymbol{\xi}(T)$ to be the same as the $\mathcal{S}$ component of the initial point $\pi_{\mathcal{S}}\boldsymbol{\xi}_0$. Let $\boldsymbol{\xi}_0$ be given and for every $\mathbf{p}_0$ denote by $t \in [0, T] \mapsto \boldsymbol{\xi}(t, \mathbf{p}_0)$ the solution to (5.44) with Cauchy data $(\boldsymbol{\xi}_0, \mathbf{p}_0)$. We seek $\mathbf{p}_0$ as a solution to the equation $F(\mathbf{p}) = 0$ where F is for instance defined (in a chart) by:

$$\mathbf{p} \mapsto \|\pi_{\mathcal{S}}\boldsymbol{\xi}(T, \mathbf{p}) - \pi_{\mathcal{S}}\boldsymbol{\xi}_0\|_{\mathbb{R}^2}.$$

Notice however that not every solution to Pontryagin's maximum principle is an optimal curve. So, rather than determining optimal strokes, we integrate (5.44) a large number of times in order to draw sub-Riemannian wavefronts. Sub-Riemannian wavefronts are precisely the surfaces constituted by the ending points of all the extremal starting at a given point and having the same fixed sub-Riemannian length.

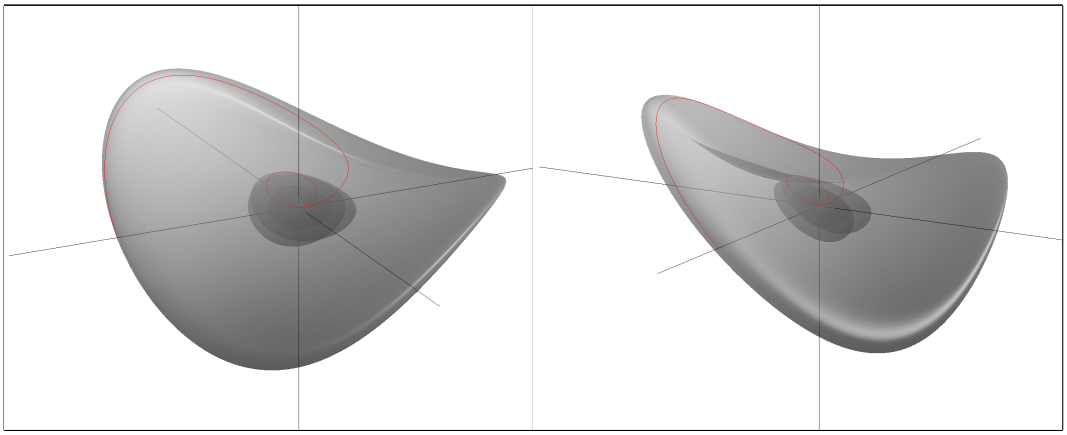

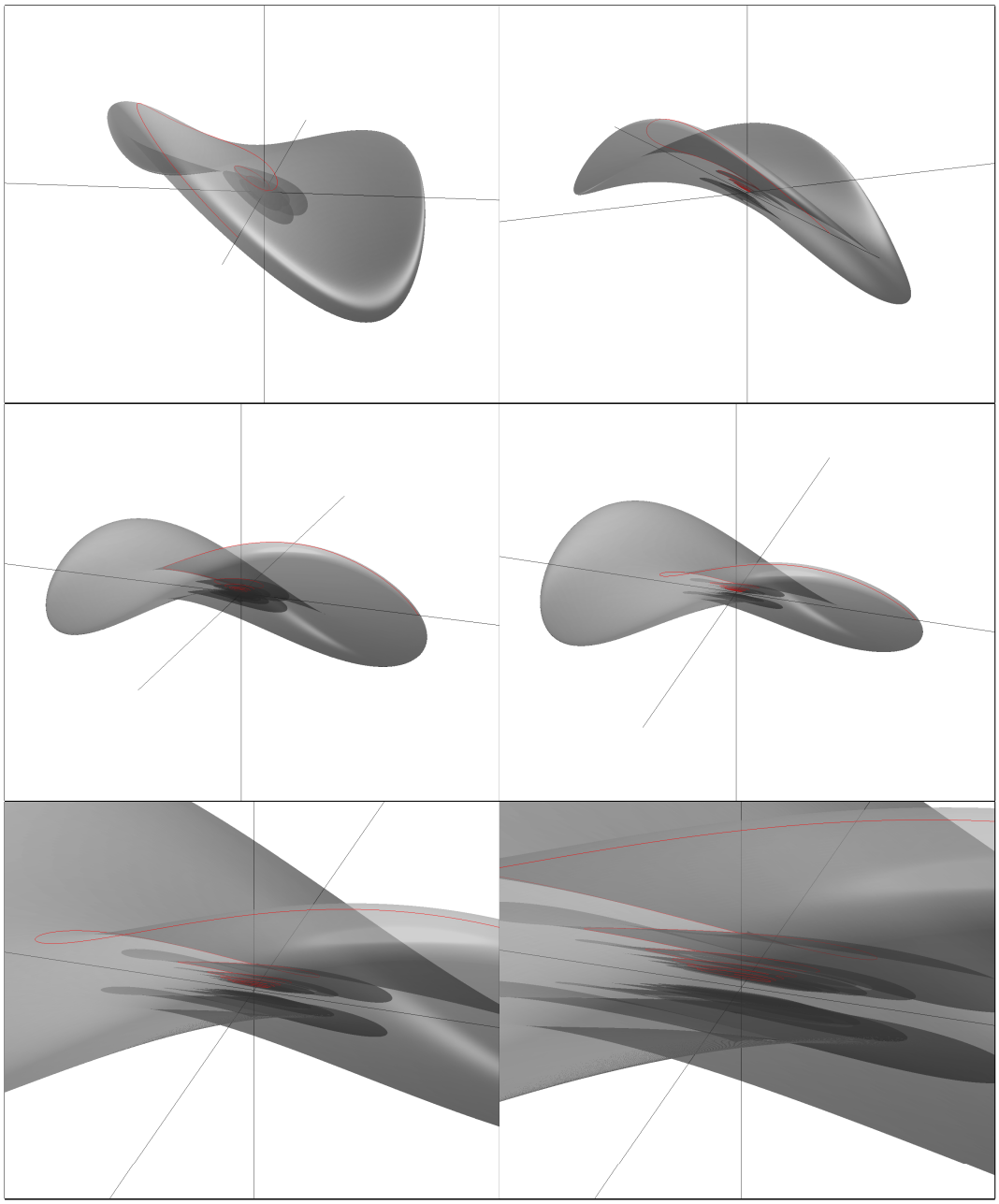

Table 5.1: The sub-Riemannian wavefront of length 0.1 computed by integrating Pontryagin's maximum principle (5.44) with initial data satisfying $\boldsymbol{\xi}_0 = (\mathbf{s}_0, 0)$, $\mathbf{s}_0 = (0.3, 0, 0)$. The picture is draw in a chart, using spherical coordinates.

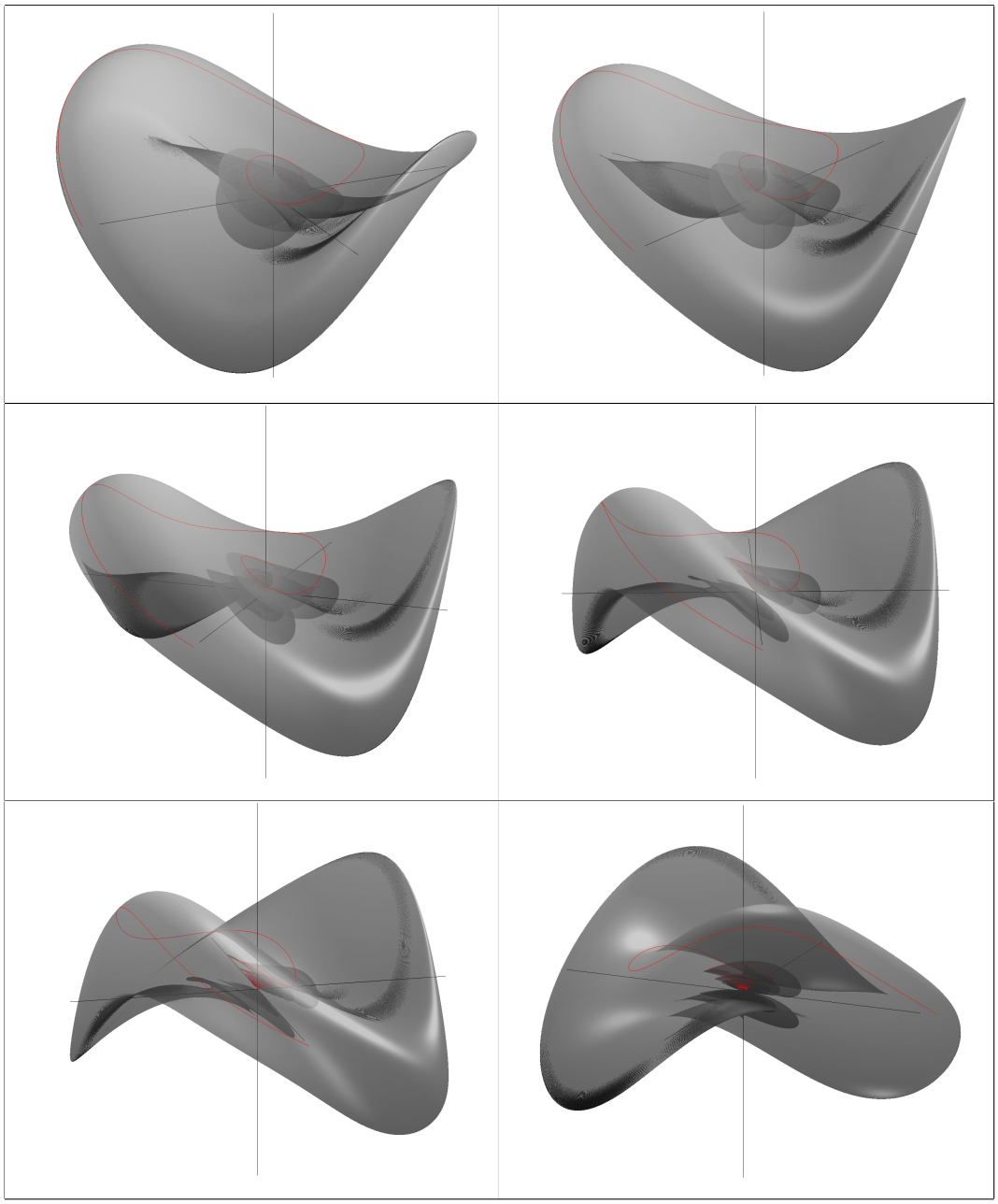

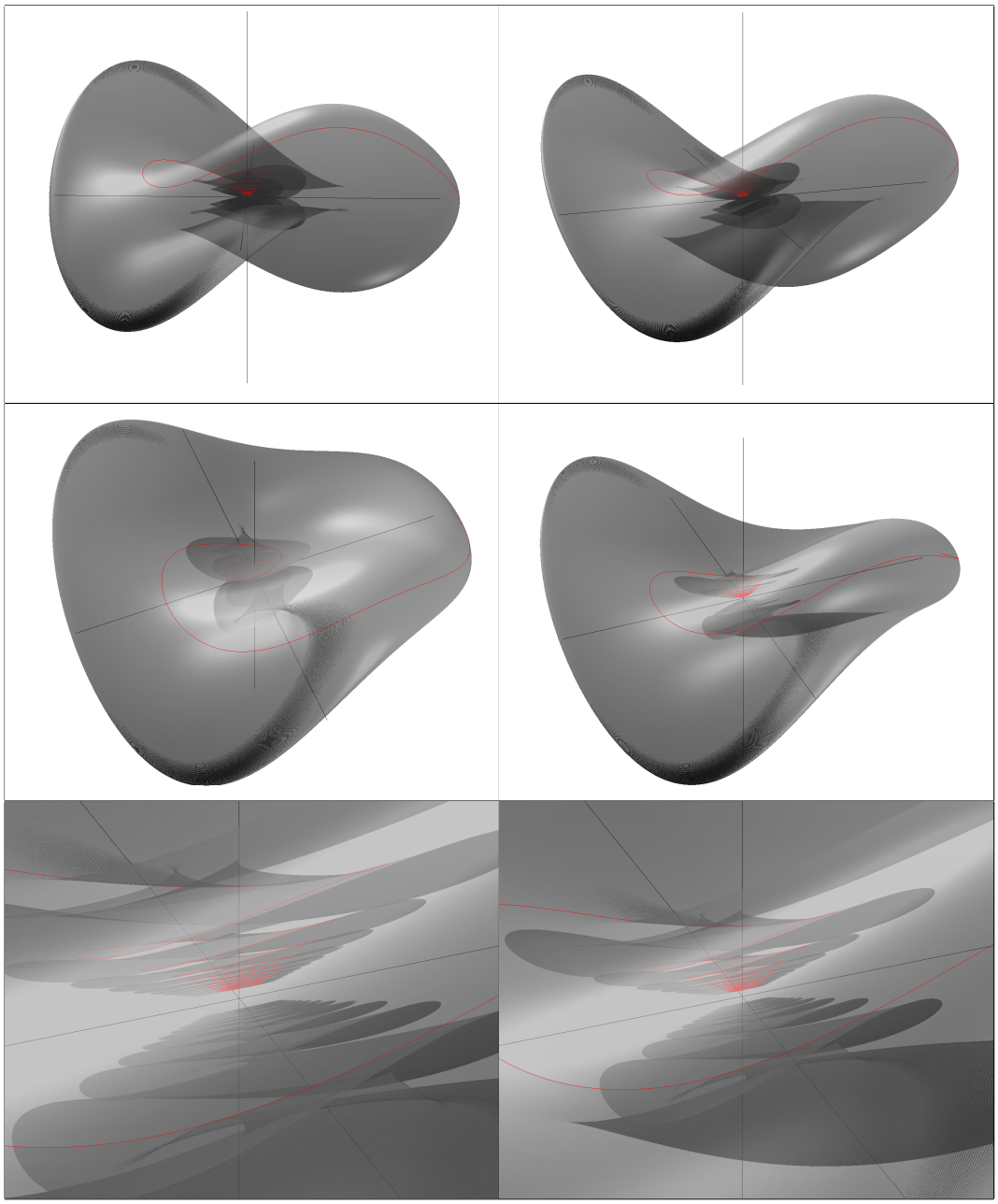

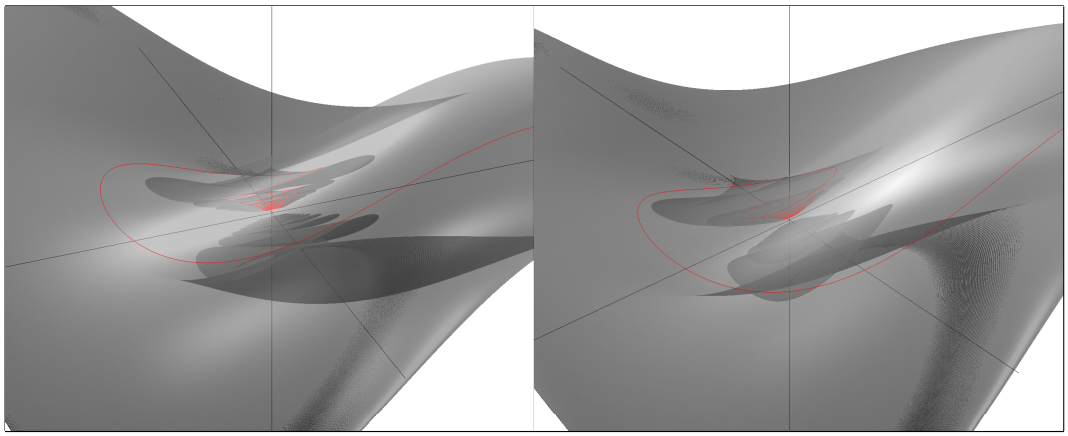

Table 5.2: The sub-Riemannian wavefront of length 0.2 computed by integrating Pontryagin's maximum principle (5.44) with initial data satisfying $\boldsymbol{\xi}_0 = (\mathbf{s}_0, 0)$, $\mathbf{s}_0 = (0.3, 0, 0)$. The picture is drawn in a chart, using spherical coordinates.

The second method consists in approximating any curve on $\mathcal{S}$ by means of cubic splines. In the following examples, we use a basis of 20 cubic splines (actually, two bases since, working in spherical coordinates, we need 20 cubic splines for the polar angle and others 20 for the azimuth angle). So, we dispose of 40 parameters controlling the splines and the optimal problems under consideration turn into finite dimensional optimal problems. To every set of parameters, we can associate a travelled distance and a cost. To solve our optimal problems, we use the optimal toolbox of Matlab. The main difficulty is to manage the change of chart. Indeed, starting with the classical spherical coordinates, a curve cannot pass through the south or north pole of the ellipsoid. So we have to switch the axes, in such a way that the north pole becomes a regular point in spherical coordinates.

First example: optimizing the cost

We consider a closed curve on the ellipsoid and compute the corresponding covered distance by the swimmer. Then, we try to minimize the cost among all the closed curves for which the travelled distance is the same. Notice that it is not exactly what is stated in Problem 5.4.5, because here there is no fixed starting point. The resulting curves on the ellipsoid are pictured on Fig 5.5, while the corresponding sequences of shapes are pictured on Fig 5.6 (initial guess) and 5.7 (optimized swimmer).

Second example: The distance-cost function

Let us draw now the graph of the function defined (5.36c). Considering a shape *at rest* for the swimmer, we compute for every $\delta \in \mathbb{R}_+$, the optimal stroke (i.e. minimizing the cost) allowing the swimmer to cover the distance δ. We choose as shape *at rest*, the converging point of all the curves on Fig 5.9. On the same picture, we drawn all the curves corresponding to the optimal strokes for different values of δ. A sequence of shapes corresponding to the longest curve is given in Fig 5.10. Finally, the graph of the distance-cost function is given in Fig 5.8.

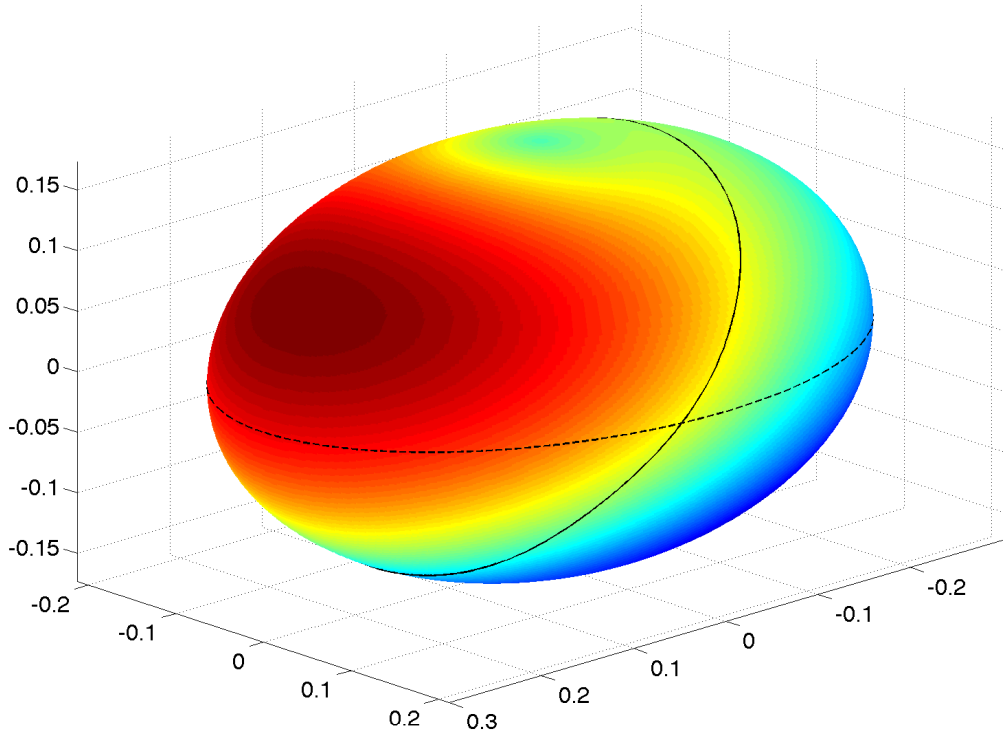

Figure 5.5: The initial closed curve is the equator of the ellipsoid (the dashed line). The optimized curve (the continuous line) is supposed to have the minimum cost for the same travelled distance. The colors are the same of in Fig 5.4.

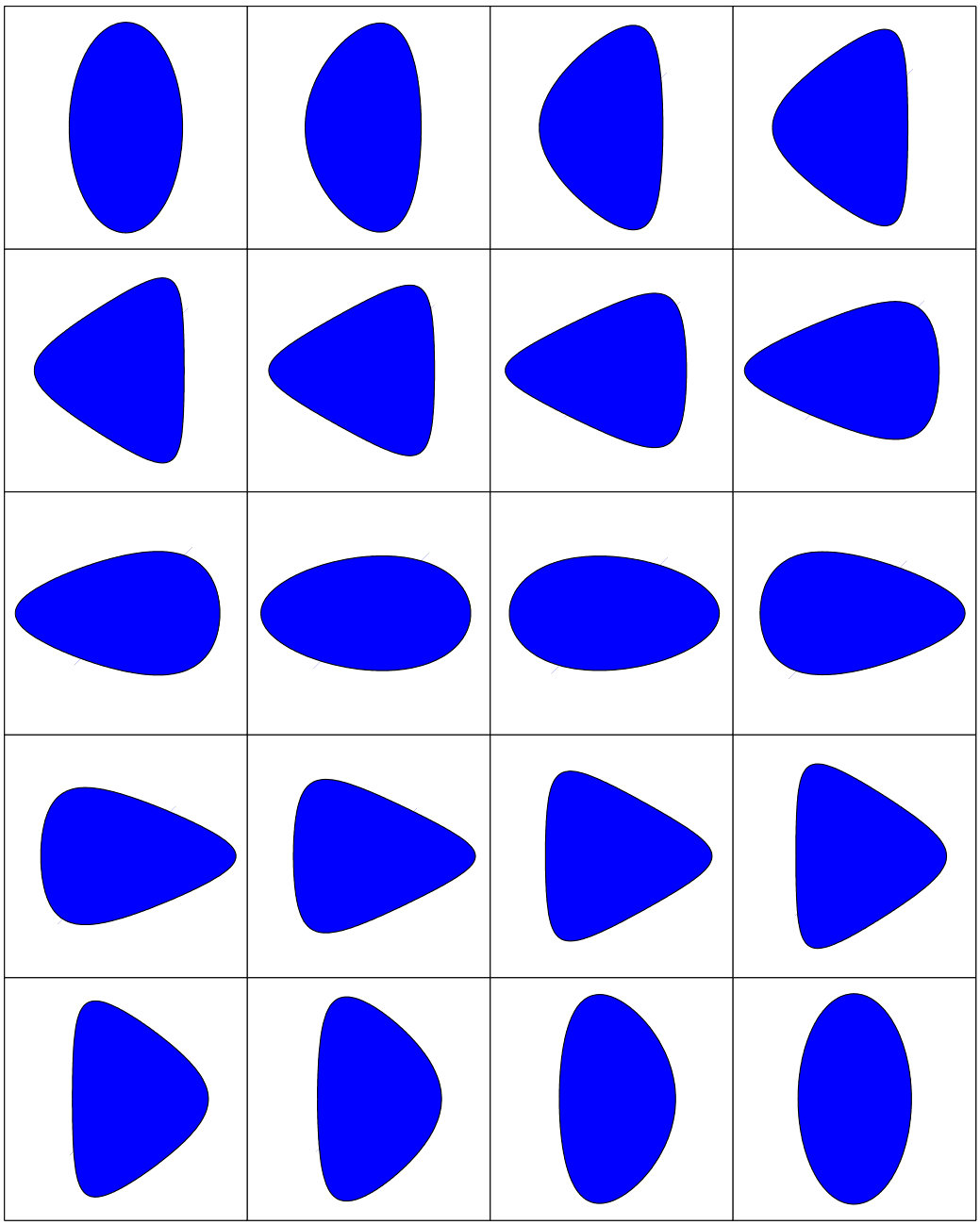

Figure 5.6: Sequence of 20 time equidistributed shapes for the initial guess.

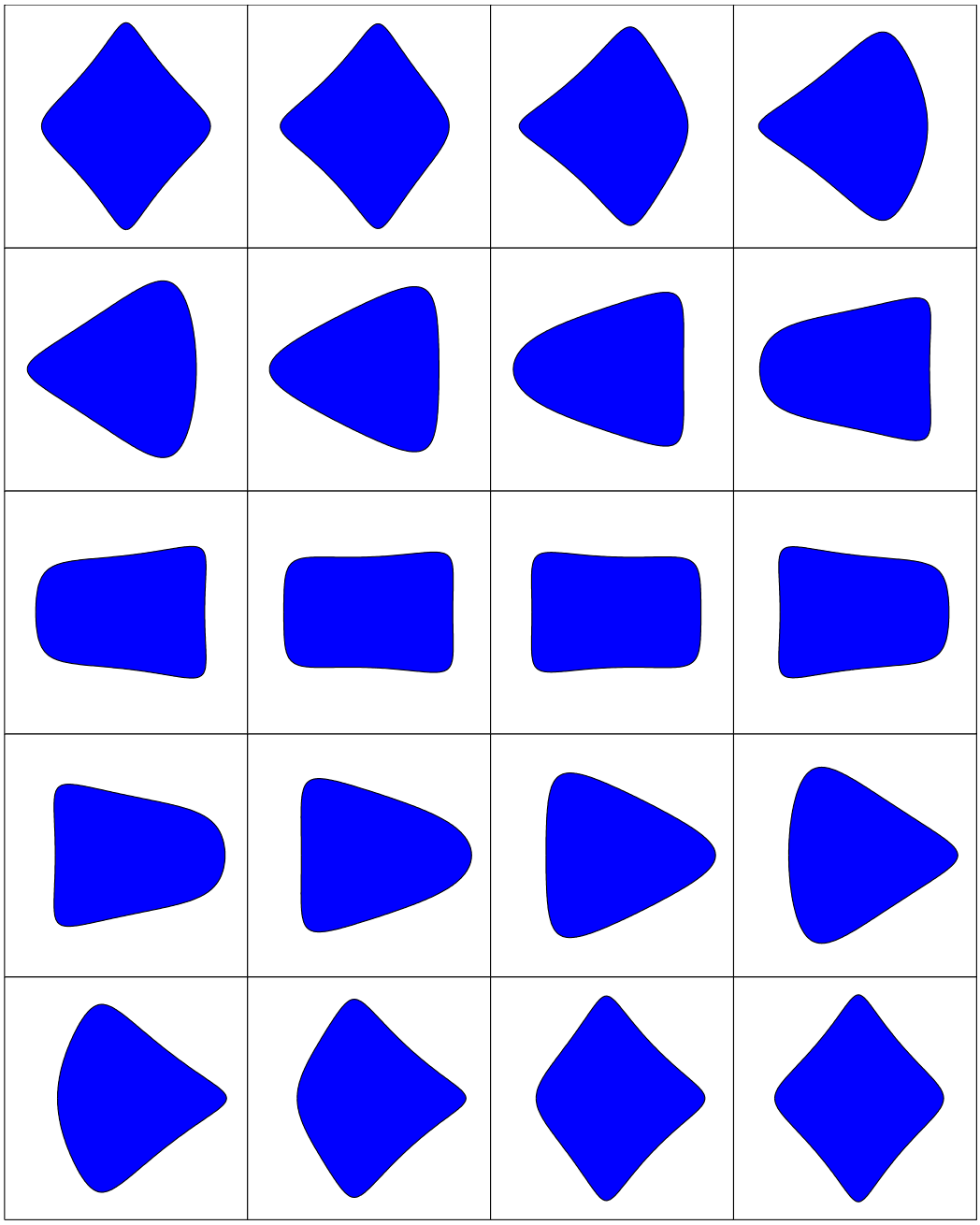

Figure 5.7: Sequence of 20 time equidistributed shapes after optimization.

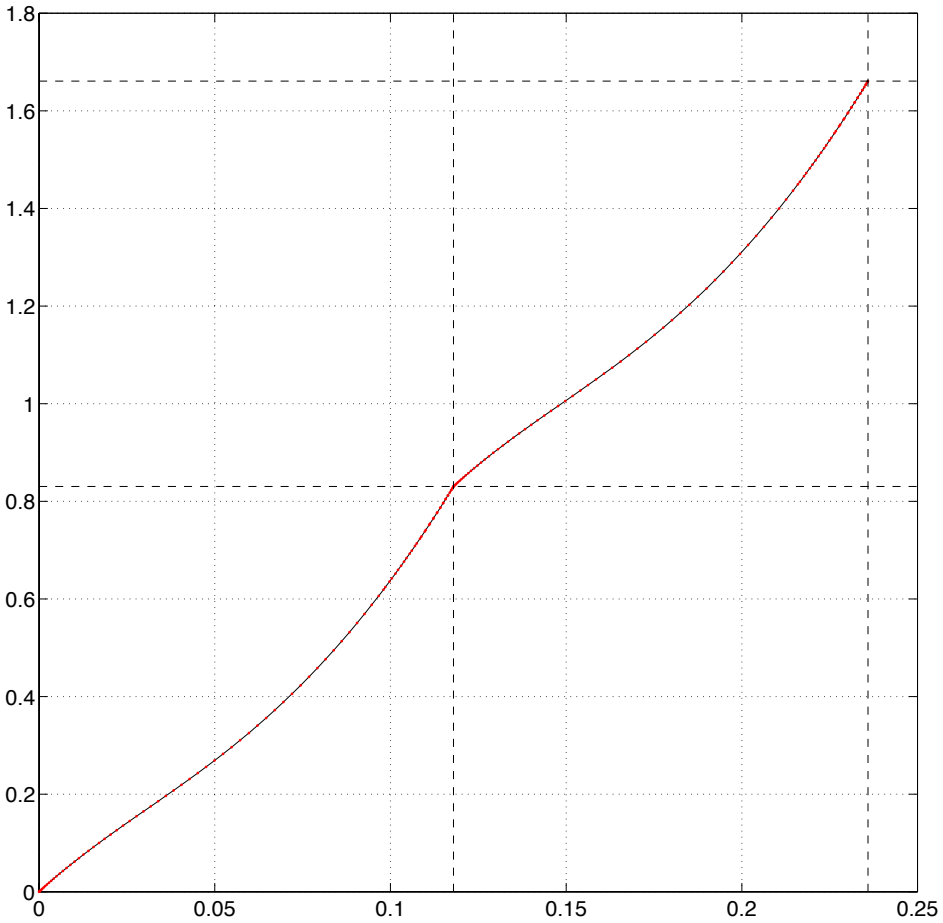

Figure 5.8: For every targeted distance (in abscissa) we compute the corresponding optimal cost (in ordinate). The curve is pseudo-periodic because, above a certain distance, the best stroke is made of two optimal smaller loops.

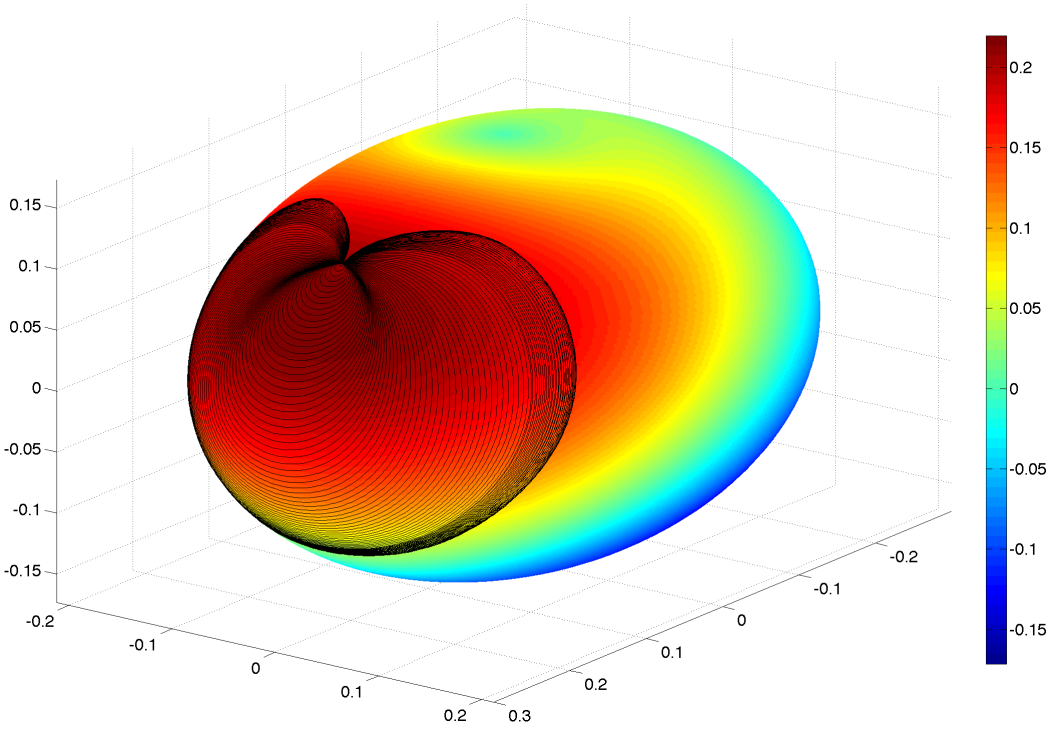

Figure 5.9: Every closed curve corresponds to an optimal stroke (minimizing the cost for a given distance).

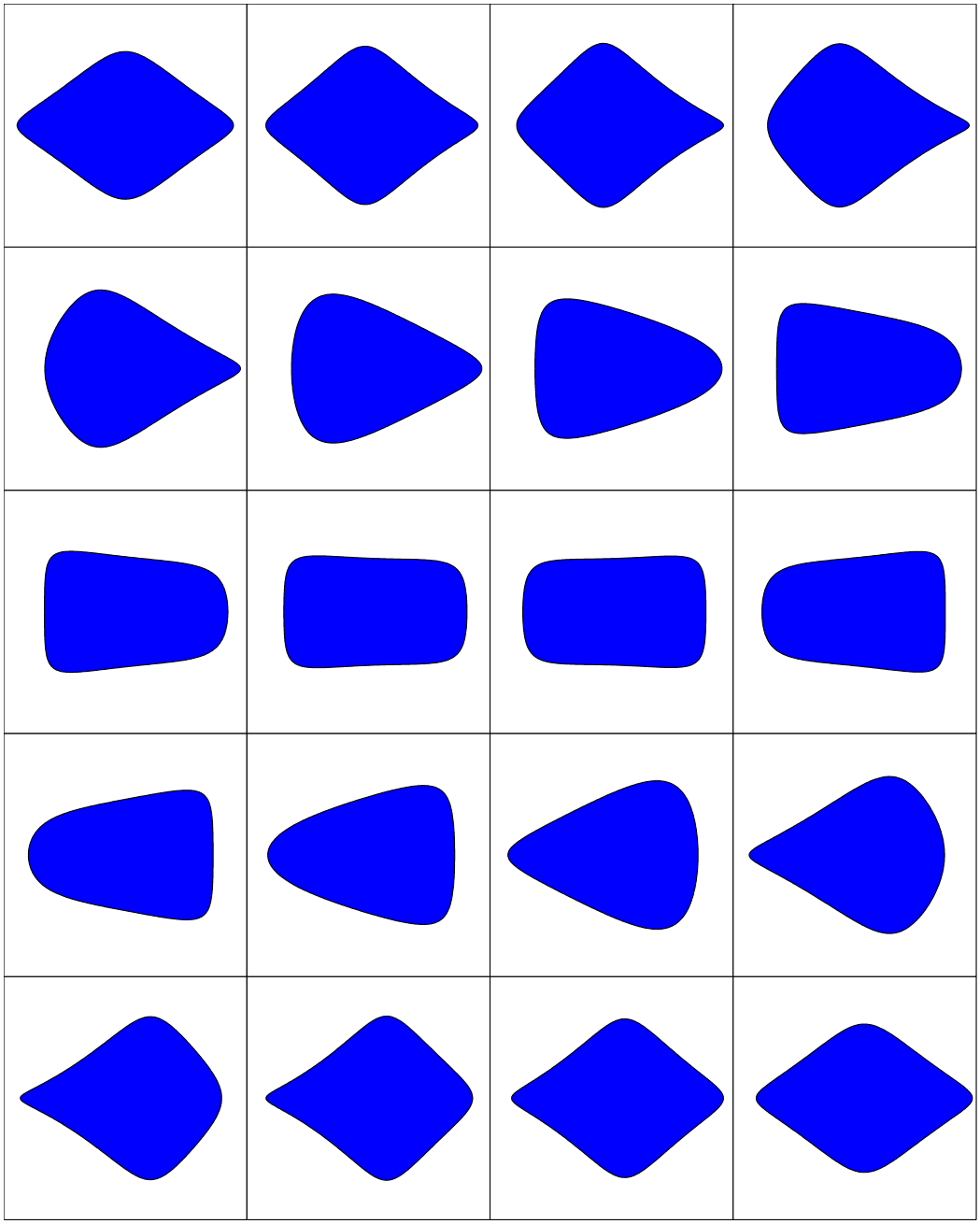

Figure 5.10: Sequence of 20 shapes time equi distributed corresponding to the longest curve on Fig 5.9.

5.7 Appendix A: Riemannian Geometry

Let (M, g) be a Riemannian manifold. We denote $\ell(\Gamma)$ the length of any rectifiable curve $\Gamma \subset M$ and for every $x \in M$ and $r > 0$, we denote by $B(x, r)$ the Riemannian ball centered at x and of radius r. The following Lemma ensures the existence of a small monotone retract at any point of M.

Lemma 5.7.1 *Let x_0 be a point of M. Then there exists $r > 0$ such that, for every path $\gamma : [0, T] \mapsto M$ absolutely continuous with essentially bounded first derivative, such that:*

1. *$\gamma(t) \in B(x_0, r)$ for every $t \in [0, T]$;*
2. *$\gamma(0) = \gamma(T) = x_0$;*

there exists a continuous function $\psi : [0, 1] \times [0, T] \mapsto M$ satisfying:

1. *For every $s \in [0, 1]$, $t \in [0, T] \mapsto \psi(s, t)$ is continuous with essentially bounded first derivative.*
2. *$\psi(1, \cdot\,) = \gamma$;*
3. *$\psi(0, \cdot\,) = x_0$;*
4. *The function $s \in [0, 1] \mapsto \ell(\Gamma_s)$ (where Γ_s is the curve parameterized by $t \in [0, T] \mapsto \psi(s, t)$) is increasing.*

Proof. Let $\mathrm{inj}(x_0)$ be the injectivity radius at x_0 and denote $\mathcal{V} := B(x_0, r)$, for $0 < r < \mathrm{inj}(x_0)$ (the constant r will be fixed later on). Let γ be a path included in $\mathcal{V}$ and satisfying the hypotheses of the lemma. Then define:

$$\zeta : t \in [0, T] \mapsto \zeta(t) := \exp_{x_0}^{-1}(\gamma(t)) \in T_{x_0}M.$$

This function has the same regularity as γ and $\zeta(0) = \zeta(T) = 0$. Define now, for every $(s, t) \in [0, 1] \times [0, T]$:

$$\psi(s, t) = \exp_{x_0}(s\zeta(t)).$$

This function has the required regularity and satisfies the equalities $\psi(1, \cdot\,) = \gamma$ and $\psi(0, \cdot\,) = x_0$. So it remains only to prove that for r small enough, the length of Γ_s is increasing in s.

In the exponential map the metric g have the following Cartan local development:

$$g_{ij}(x) = \delta_i^j - \frac{1}{3}\sum_{k,l} R_{iklj}(0)x_k x_l + \mathcal{O}(\|x\|_E^3), \tag{5.52}$$

where δ_i^j is the Kronecker symbol, R_{ijkl} are the coefficients of the Riemann curvature tensor and $\|x\|_E$ stands for the Euclidean norm. The quantity we are interested in estimating is:

$$\ell(\Gamma_s) = \int_0^T \|\partial_t \psi(s, t)\|_{g(\psi(s,t))}\, \mathrm{d}t, \tag{5.53}$$

and in the local chart, according to (5.52), we have:

$$\begin{aligned}\|\partial_t \psi(s, t)\|^2_{g(\psi(s,t))} = s^2\|\dot\zeta(t)\|_E^2 \\ - s^4\left(\frac{1}{3}\sum_{i,j}\sum_{k,l} R_{iklj}(0)\zeta_k(t)\zeta_l(t)\dot\zeta^i(t)\dot\zeta^j(t)\right) \\ + s^3\left(\|\dot\zeta(t)\|_E^2\mathcal{O}(\|\zeta(t)\|_E^3)\right).\end{aligned}$$

So for r small enough, $\zeta(t)$ is uniformly small and for every $t \in [0, T]$, the function $s \in [0, 1] \mapsto \|\partial_t \psi(s, t)\|^2_{g(\psi(s,t))}$ is increasing. We draw the same conclusion for the quantity (5.53) and proof is completed.

5.8 Appendix B: A brief Survey of the Orbit Theorem

In this Appendix, we aim to recall the statement of the Orbit Theorem. The material presented below is now considered as a classical part of geometric control theory.

Throughout this section, M is a real analytic manifold, and $\mathcal{G}$ a set of analytic vector fields on M. We do not assume in general that the fields from $\mathcal{G}$ are complete.

5.8.1 Attainable sets

Let f be an element of $\mathcal{G}$ and q^* be an element of M. The Cauchy problem

$$\dot{q} = f(q), \qquad q(0) = q^*, \tag{5.54}$$

admits a solution defined on the open interval $I(f, q^*)$ containing 0. For any real t in $I(f, q^*)$ we denote the value of the solution of (5.54) at time t by $e^{tf}(q^*)$. We denote by $I(f, q^*)^+ = I(f, q^*) \cap]0, +\infty[$ the positive elements of $I(f, q^*)$.

For any element q_0 in M and any positive real number T, we define the *attainable set at time* T of $\mathcal{G}$ from q_0 by the set $\mathcal{A}_{q_0}(T)$ of all points of M that can be attained with $\mathcal{G}$ using piecewise constants controls in time T

$$\mathcal{A}_{q_0}(T) = \Big\{ e^{t_p f_p} \circ e^{t_{p-1} f_{p-1}} \circ \cdots \circ e^{t_1 f_1}(q_0) \,:\, p \in \mathbf{N},\, f_i \in \mathcal{G}, \\ t_i \in I(f_i, e^{t_{i-1} f_{i-1}} \circ \cdots \circ e^{t_1 f_1}(q_0))^+,\, t_1 + \cdots + t_p = T \Big\},$$

the times t_i and the fields f_i being chosen in such a way that every written quantity exists. We define also the *orbit* of $\mathcal{G}$ trough q_0 by the set $\mathcal{O}_{q_0}$ of all points of M that can be attained with $\mathcal{G}$ using piecewise constant controls, *at any positive or negative time*

$$\mathcal{O}_{q_0}(T) = \Big\{ e^{t_p f_p} \circ e^{t_{p-1} f_{p-1}} \circ \cdots \circ e^{t_1 f_1}(q_0) \,:\, p \in \mathbf{N},\, f_i \in \mathcal{G}, \\ t_i \in I(f_i, e^{t_{i-1} f_{i-1}} \circ \cdots e^{t_1 f_1}(q_0)) \Big\}.$$

Of course, if $\mathcal{G}$ is a cone, that is if $\lambda f \in \mathcal{G}$ for any positive λ as soon as f belongs to $\mathcal{G}$, the set $\mathcal{A}_{q_0}(T)$ does not depend on the positive T but only on q_0. If $\mathcal{G}$ is assumed to be symmetric, that is if $-f$ belongs to $\mathcal{G}$ as soon as f belongs to $\mathcal{G}$, then the orbit of $\mathcal{G}$ trough a point q_0 is the union of all attainable sets at positive time of $\mathcal{G}$ from q_0.

5.8.2 Lie algebra of vector fields

If f_1 and f_2 are two vector fields on M and q is a point of M, the *Lie bracket* $[f_1, f_2](q)$ of f_1 and f_2 at a point q is the derivative at $t = 0$ of the curve $t \mapsto \gamma(\sqrt{t})$ where γ is defined by $\gamma(t) := e^{-tf_2} e^{-tf_1} e^{tf_2} e^{tf_1}(q)$ for t small enough. The Lie bracket of f_1 and f_2 at a point q is an element of the tangent space T_qM of M at the point q. The Lie bracket is bilinear and skew-symmetric in f_1 and f_2, and measures the non-commutativity of the fields f_1 and f_2 (see [3, Prop 2.6]).

Proposition 5.8.1 *For any f_1, f_2 in $\mathcal{G}$, we have the equivalence:*

$$e^{t_1 f_1} e^{t_2 f_2} = e^{t_2 f_2} e^{t_1 f_1} \Leftrightarrow [f_1, f_2] = 0$$

for all times t_1 and t_2 (if any) for which the expressions written in the left hand side of the above equivalence make sense.

Lie brackets of vectors fields are easy to compute with the following formulas (see [3, Prop 1.3] and [3, Exercise 2.2]).

Proposition 5.8.2 *For any f_1, f_2 in $\mathcal{G}$, for any q in M,*

$$[f_1, f_2](q) = \frac{df_2}{dq} f_1(q) - \frac{df_1}{dq} f_2(q).$$

Further, we have the useful property:

Proposition 5.8.3 *Let f_1 and f_2 be two smooth vector fields on M, and let $a, b : M \to \mathbb{R}$ be two smooth functions. Then*

$$[aX, bY] = ab[X, Y] + \left(\frac{db}{dq} X\right) Y - \left(\frac{da}{dq} Y\right) X.$$

From the Lie brackets, we can define the Lie algebra:

Definition 5.8.4 *The* Lie algebra *of $\mathcal{G}$ is the linear span of all Lie brackets, of any length, of the elements of $\mathcal{G}$*

$$\text{Lie } \mathcal{G} = \text{span}\big\{[f_1, [\dots [f_{k-1}, f_k] \dots]],\ k \in \mathbf{N},\ f_i \in \mathcal{G}\big\},$$

which is a subset of all the vector fields on M.

We denote by $\text{Lie}_q\mathcal{G} := \big\{g(q),\ g \in \text{Lie } \mathcal{G}\big\}$ the evaluation $\text{Lie}_q\mathcal{G}$ of the Lie algebra generated by $\mathcal{G}$ at a point q of M.

5.8.3 The Orbit Theorem

The Orbit Theorem describes the differential structure of the orbit trough a point (see for instance [3, Th 5.1] for a proof).

Theorem 5.8.5 (Orbit Theorem) *For any q and q_0 in M:*

1. *$\mathcal{O}(q_0)$ is a connected immersed submanifold of M.*
2. *If $q \in \mathcal{O}(q_0)$, then $T_q\mathcal{O}(q_0) = \text{Lie}_q\mathcal{G}$.*

Remark 5.8.6 *The conclusion* (1) *of the Orbit Theorem holds true even if M and $\mathcal{G}$ are only assumed to be smooth (and not analytic). The conclusion* (2) *is false in general when $\mathcal{G}$ is only assumed to be smooth.*

The Orbit Theorem has many consequences, among them the following useful properties (see [3, Th 5.2] for a proof and further discussion).

Theorem 5.8.7 (Rashevsky-Chow) *If $\text{Lie}_q\mathcal{G} = T_qM$ for every q in M, then the orbit of $\mathcal{G}$ through q is equal to M.*

Proposition 5.8.8 *If $\mathcal{G}$ is a symmetric cone such that $\text{Lie}_q\mathcal{G} = T_qM$ for every q in M, then the attainable set at any positive time of any point of M is equal to M.*

Bibliographie

[1] A. A. Agrachev. Exponential mappings for contact sub-Riemannian structures. *Journal of dynamical and control systems*, 2(3) :321–358, 1996.

[2] A. A. Agrachev. Introduction to optimal control theory. *Summer School on Mathematical Control Theory, Trieste*, 2001.

[3] A. A. Agrachev. *Non linear and optimal control theory.* Springer Verlag, 2008.

[4] A. A. Agrachev, D. Barilari, and U. Boscain. Introduction to Riemannan and sub-Riemannian geometry. Preprint SISSA 09/2012/M, 2012.

[5] F. Alouges, A. DeSimone, L. Giraldi, and M. Zoppello. Self-propulsion of slender microswimmers by curvature control : N-link swimmers. *To appear in Journal of Non-Linear Mechanics*, 2013.

[6] F. Alouges, A. DeSimone, and L. Heltai. Numerical strategies for stroke optimization of axisymmetric microswimmers. *Math. Models Methods Appl. Sci.*, 21(2), 2011.

[7] F. Alouges, A. DeSimone, L. Heltai, A. Lefebvre, and B. Merlet. Optimally swimming Stokesian robots. *Discrete and Continuous Dynamical Systems Series B*, 18(5), 2013.

[8] F. Alouges, A. DeSimone, and A. Lefebvre. Optimal strokes for low Reynolds number swimmers : an example. *Journal of Nonlinear Science*, 18 :277–302, 2008.

[9] F. Alouges, A. DeSimone, and A. Lefebvre. Biological fluid dynamics, nonlinear partial differential equations. *Encyclopedia of Complexity and Systems Science*, 2009.

[10] F. Alouges, A. DeSimone, and A. Lefebvre. Optimal strokes for axisymmetric microswimmers. *The European Physical Journal E*, 28(279–284), 2009.

[11] F. Alouges and L. Giraldi. Enhanced controllability of low Reynolds number swimmers in the presence of a wall. *Acta Applicandae Mathematicae*, April 2013.

[12] P. R. Amestoy, I. S. Duff, J. Koster, and J. Y. L. Excellent. A fully asynchronous multifrontal solver using distributed dynamic scheduling. *SIAM Journal of Matrix Analysis and Applications*, 23(1) :15–41, 2001.

[13] M. Arroyo, D. Milan, L. Heltai, and A. DeSimone. Reverse engineering the euglenoid movement. *Proc. Nat. Acad. Sciences USA*, 109 :17874–17879, 2012.

[14] D. Barilari. Trace heat kernel asymptotics in 3D contact sub-Riemannian geometry. *to appear in Journal of Mathematical Science.*

[15] L. E. Becker, S. A. Koehler, and H. A. Stone. On self-propulsion of micro-machines at low Reynolds number : Purcell's three-link swimmer. *J. Fluid Mech.*, 2003.

[16] H. Ben Belgacem, S. Conti, A. DeSimone, and S. Müller. Rigorous bounds for the Foeppl-von Karman theory of isotropically compressed plates. *Journal of Nonlinear Science*, 10 :661–683, 2000.

[17] A. P. Berke, L. Turner, H. C. Berg, and E. Lauga. Hydrodynamic attraction of swimming microorganisms by surfaces. *Physical Review Letters*, 101(3), 2008.

[18] L. V. Berlyand, S. D. Ryan, B. M. Haines, and D. A. Karpeev. A kinetic model for semi-dilute bacterial suspensions. *submitted to SIAM MMS*, 2012.

[19] L. V. Berlyand, S. D. Ryan, A. Sokolov, and I. S. Aranson. Collective dynamics in semidilute bacterial suspensions. *submitted to New Journal of Physics*, 2013.

[20] J. R. Blake. A note on the image system for a Stokeslet in a no-slip boundary. *Proc. Gamb. Phil. Soc.*, 70 :303, 1971.

[21] F. Bonnans, P. Martinon, and V. Grélard. Bocop - A collection of examples. Technical report, INRIA, 2012. RR-8053.

[22] M. Bonnivard. On the stability of self-propelled bodies with respect to their shape motion. *Mathematical Models and Methods in Applied Sciences*, 2011.

[23] C. Brennen and H. Winet. Fluid mechanics of propulsion by cilia and flagella. *Ann. Rev. Fluid Mech.*, 9 :339–398, 1977.

[24] H. Brenner and J. Happel. *Low Reynolds number hydrodynamics : with special applications to particulate media.* Springer, 1965.

[25] H. Brezis. *Analyse Fonctionnelle Théorie et Applications.* Editions Dunod, 1999.

[26] C. J. Brokaw. Bending moments in free-swimming flagella. *J. Exp. Biol.*, 53 :445–464, 1970.

[27] T. Chambrion and A. Munnier. Locomotion and control of a self-propelled shape-changing body in a fluid. *Journal of Nonlinear Science*, 21 :325–385, 2011.

[28] T. Chambrion and A. Munnier. Generic controllability of 3D swimmers in a perfect fluid. *SIAM Journal on Control and Optimization*, 50(5) :2814–2835, 2012.

[29] J. M. Coron. *Control and Nonlinearity.* American Mathematical Society, 2007.

[30] S. Court. *Problèmes d'interactions entre une structure déformable et un fluide visqueux et incompressible.* PhD thesis, Université de Toulouse, 2012.

[31] R. G. Cox. The motion of long slender bodies in a viscous fluid. part 1. general theory. *J. Fluid Mech.*, 44 :791–810, 1970.

[32] G. Dal Maso, A. DeSimone, and M. Morandotti. An existence and uniqueness result for the motion of self-propelled micro-swimmers. *SIAM J. Math. Anal.*, 43 :1345–1368, 2011.

[33] P. Degond and S. Motch. Large scale dynamics of the persistent turning walker model of fish behavior. *J ; Stat. Phys.*, 2008.

[34] A. DeSimone. Hysteresis and imperfection sensitivity in small ferromagnetic particles. *Meccanica*, 30 :591–603, 1995.

[35] A. DeSimone and L. Teresi. Elastic energies for nematic elastomers. *Eur. Phys. J. E*, 29 :191–204, 2009.

[36] R. Dreyfus, J. Baudry, M. L. Roper, M. Fermigier, H. A. Stone, and J. Bibette. Microscopic artificial swimmers. *Nature*, 437 :862–865, 2005.

[37] B. M. Friedrich, I. H. Riedel-Kruse, J. Howard, and F. Jülicher. High-precision tracking of sperm swimming fine structure provides strong test of resistive force theory. *The Journal of Experiment Biology*, 2010.

[38] E. A. Gaffney, H. Gadêlha, D. J. Smith, J. R. Blake, and J. C. Kirkman-Brown. Mammalian sperm motility : observation and theory. *Annual Review of Fluid Mechanics*, 43 :501–528, 2011.

[39] G. P. Galdi. *An Introduction to the Mathematical Theory of the Navier-Stockes Equations*. Springer, 2011.

[40] G. P. Galdi and M. Kyied. Steady flow of a Navier-Stokes liquid past an elastic body. *Arch. Rational Mech. Anal.*, 2011.

[41] G. P. Galdi and A. L. Sylvestre. On the motion of a rigid body in a Navier-Stokes liquid under the action of a time-periodic force. *Indiana Univ. Math. J.*, 2009.

[42] A. Gebremedhin, A. Pothen, and A. Walther. Exploiting sparsity in Jacobian computation via coloring and automatic differentiation : a case study in a simulated moving bed process. In C. Bischof et al, editor, *Lecture Notes in Computational Science and Engineering 64*, pages 339–349. Springer, 2008. Proceedings of the Fifth International Conference on Automatic Differentiation (AD2008).

[43] D. Gérard Varet and M. Hillairet. Computation of the drag force on a rough sphere close to a wall. *M2AN*, 46 :1201–1224, 2012.

[44] L. Giraldi, P. Martinon, and M. Zoppello. Controllability and optimal strokes for N-link micro-swimmer. submitted to CDC, 2013.

[45] O. Glass and T. Horsin. Approximate Lagrangian controllability for the 2D Euler equation. Application to the control of the shape of vortex patches. *Journal de Mathématiques Pures et Appliquées*, 2010.

[46] O. Glass and T. Horsin. Prescribing the motion of a set of particles in a 3D perfect fluid. *SIAM Journal on Control and Optimization*, 2012.

[47] R. Golestanian and A. Ajdari. Analytic results for the three-sphere swimmer at low Reynolds. *Physical Review E*, 77 :036308, 2008.

[48] R. Golestanian and A. Ajdari. Stochastic low Reynolds number swimmers. *J. Phys. : Condens. J. Phys. : Condens. Matter*, 21(204104), 2009.

[49] J. Gray and J. Hancock. The propulsion of sea-urchin spermatozoa. *Journal of Experimental Biology*, 1955.

[50] R. E. Johnson and C. J. Brokaw. Flagellar hydrodynamics. *Biophys. J.*, 25 :113–127, 1979.

[51] V. Jurdjevic. *Geometric control theory*. Cambridge University Press., 1997.

[52] J. B. Keller and S. I. Rubinow. Swimming of flagellated microorganisms. *Biophys. J.*, 16 :151–170, 1976.

[53] E. Lauga and T. Powers. The hydrodynamics of swimming micro-organisms. *Rep. Prog. Phys.*, 72(09660), 2009.

[54] J. Lighthill. Mathematical biofluiddynamic. *Society for Industrial and Applied Mathematics, Philadelphia, Pa.*, 1975.

[55] J. L. Lighthill. Flagellar hydrodynamics. *SIAM Rev.*, 18 :161–230, 1976.

[56] M. J. Lighthill. On the squirming motion of nearly spherical deformable bodies through liquids at very small Reynolds numbers. *Comm. Pure Appl. Math.*, 5 :109–118, 1952.

[57] A. M. Lishansky and O. Kenneth. Surface tank treading : Propulsion of Purcell's toroidal swimmer. *Physics of fluids*, 20(063104), 2008.

[58] J. Lohéac. *Contrôle en temps optimal et nage à bas nombre de Reynolds.* PhD thesis, Université de Lorraine, 2012.

[59] J. Lohéac and A. Munnier. Controllability of 3D low Reynolds swimmers. *To appear in COCV*, 2013.

[60] J. Lohéac, J. F. Scheid, and M. Tucsnak. Controllability and time optimal control for low Reynolds numbers swimmers. *Acta Applicandae Mathematicae*, 2013.

[61] J. San Martìn, T. Takahashi, and M. Tucsnak. A control theoretic approach to the swimming of microscopic organisms. *Quart. Appl. Math.*, 65(3), 2007.

[62] S. Michelin and E. Lauga. Efficiency optimization and symmetry-breaking in a model of ciliary locomotion. *Physics of fluids.*, 2010.

[63] R. Montgomery. *A tour of subriemannian geometries, theirs geodesics and applications.* American Mathematical Society, 2002.

[64] A. Munnier. Locomotion of deformable bodies in an ideal fluid : Newtonian versus Lagrangian formalism. *J. Nonlinear Sci.*, 19(6) :665–715, 2009.

[65] A. Munnier. Passive and self-propelled locomotion of an elastic swimmer in a perfect fluid. *SIAM J. Appl. Dyn. Syst.*, 10(4) :1363–1403, 2011.

[66] A. Najafi and R. Golestanian. Simple swimmer at low Reynolds number : Three linked spheres. *Physical Review E*, 69(6) :062901, 2004.

[67] A. Najafi and R. Zargar. Two-sphere low Reynolds number propeller. *Physical Review E*, 81, 2010.

[68] Y. Or and M. Murray. Dynamics and stability of a class of low Reynolds number swimmers near a wall. *Physical Review E*, 79 :045302(R), 2009.

[69] E. Passov and Y. Or. Dynamics of Purcell's three-link microswimmer with a passive elastic tail. *Eur Phys J E*, 78(35) :1–9, 2012.

[70] E. M. Purcell. Life at low Reynolds number. *American Journel of Physics*, 45 :3–11, 1977.

[71] S. H. Rad and A. Najafi. Hydrodynamic interactions of spherical particles in a fluid confined by a rough no-slip wall. *Physical Review E*, 2010.

[72] I. H. Riedel-Kruse, A. Hilfinger, J. Howard, and F. Jülicher. How molecular motors shape the flagellar beat. *HFSP*, 1 :192–208, 2007.

[73] R. Rikmenspoel, G. van Herpen, and P. Eijkout. Cinematographic observations of the movements of bull sperm cells. *Phys. Med. Biol.*, 5 :167–181, 1960.

[74] L. Rothschild. Non-random distribution of bull spermatozoa in a drop of sperm suspension. *Nature*, 1963.

[75] J. San Martìn, J. F. Scheid, T. Takahashi, and M. Tucsnak. An initial and boundary value problem modeling of fish-like swimming. *Arch. Ration. Mech. Anal.*, 2008.

[76] J. P. Sauvage. *Molecular Machines and Motors.* Springer, 2001.

[77] Y. Sawa, K. Urayama, T. Tokigawa, A. DeSimone, and L. Teresi. Thermally driven giant bending of liquid crystal elastomer films with hybrid alignment. *Macromolecules*, 43(9) :4362–4369, 2010.

[78] W. J. Shack, C. S. Fray, and T. J. Lardner. Observations on the hydrodynamics and swimming motions of mammalian spermatozoa. *Bull. Math. Biol.*, 36 :555–565, 1974.

[79] A. Shapere and F. Wilczek. Efficiencies of self-propulsion at low Reynolds number. *J. Fluid Mech.*, 1989.

[80] H. Shum, E. A. Gaffney, and D. J. Smith. Modelling bacterial behaviour close to a no-slip plane boundary : the influence of bacterial geometry. *Proc. R. Soc.*, 466(1725-1748), 2010.

[81] D. J. Smith and J. R. Blake. Surface accumulation of spermatozoa : a fluid dynamic phenomenon. *The mathematical scientist*, 2009.

[82] D. J. Smith, E. A. Gaffney, J. R. Blake, and J. C. Kirkman-Brown. Human sperm accumulation near surfaces : a simulation study. *J. Fluid Mech.*, 621(289-320), 2009.

[83] D. Tam and A. E. Hosoi. Optimal strokes patterns for Purcell's three link swimmer. *Physical Review Letters*, 2007.

[84] G. Taylor. Analysis of the swimming of microscopic organisms. *Proc. R. Soc. Lond. A*, 209 :447–461, 1951.

[85] E. Trelat. *Contrôle optimal : théorie and applications.* Vuibert, Collection Mathématiques Concrètes, 2005.

[86] A. Wächter and L. T. Biegler. On the implementation of a primal-dual interior point filter line search algorithm for large-scale nonlinear programming. *Mathematical Programming*, 106(1) :25–57, 2006.

[87] A. Walther and A. Griewank. Getting started with adol-c. In U. Naumann and O. Schenk, editors, *Combinatorial Scientific Computing.* Chapman-Hall CRC Computational Science, 2012.

[88] B. Watson, J. Friend, and L. Yeo. Piezoelectric ultrasonic resonant motor with stator diameter less than 250 μm : the proteus motor. *J. Micromech. Microeng.*, 19, 2009.

[89] E. F. Whittlesey. Analytic functions in Banach spaces. *Proc. Amer. Math. Soc.*, 16 :1077–1083, 1965.

[90] E. F. Whittlesey. Analytic functions in Banach spaces. *Proc. Amer. Math. Soc.*, 16 :1077–1083, 1965.

[91] H. Winet, G. S. Bernstein, and J. Head. Observation on the response of human spermatozoa to gravity, boundaries and fluid shear. *Reproduction*, 70, 1984.

[92] H. Winet, G. S. Bernstein, and J. Head. Spermatozoon tendency to accumulate at walls is strongest mechanical response. *J. Androl*, 1984.

[93] T. Y. Wu. Mathematical biofluiddynamic and mechanophysiology of fish locotion. *Math. Method Applied Sci.*, 2001.

[94] C. Ybert, C. Barentin, C. Cottin-Bizonne, P. Joseph, and L. Bocquet. Achieving large slip with superhydrophobic surfaces : scaling laws for generic geometries. *Physics of Fluids*, 2007.

[95] Y. Yekutieli, R. Sagiv-Zohar, R. Aharonov, Y. Engel, B. Hochner, and T. Flash. Dynamic model of the octopus arm. I. biomechanics of the octopus reaching movement. *J Neurophysiol*, 94 :1443–1458, 2005.

[96] A. P. Yundt, W. J. Shack, and T. J. Lardner. Applicability of hydrodynamic analyses of spermatozoan motion. *J. Exp. Biol.*, 62 :27–41, 1975.

[97] R. Zargar, A. Najafi, and M. Miri. Three-sphere low Reynolds number swimmer near a wall. *Physical Review E*, 80 :026308, 2009.

[98] S. Zhang, Y. Or, and M. Murray. Experimental demonstration of the dynamics and stability of a low Reynolds number swimmer near a plane wall, 2010.

Résumé

Cette thèse de mathématiques appliquées traite de la modélisation des déplacements de nageurs microscopiques. Nous étudions principalement les problèmes de contrôlabilité et d'optimalité associés à la mobilité d'un micro-nageur.

Dans une première partie, nous présentons un modèle de nageur simplifié, appelé le "N-link swimmer". Ensuite, nous étudions sa contrôlabilité ainsi que l'existence de stratégies lui permettant d'atteindre un point donné le plus vite possible. Dans une deuxième partie, nous analysons les effets de la présence d'un bord sur la mobilité d'un micro-nageur. Nous montrons qu'un nageur qui est contrôlable lorsqu'il évolue dans l'espace non borné, reste "presque partout" localement contrôlable lorsqu'il nage dans un domaine délimité par un mur plat ou rugueux. Au contraire, nous prouvons qu'un nageur qui n'est pas capable d'atteindre toutes les directions lorsqu'il se déplace dans un domaine sans bord peut élargir ses directions accessibles en présence d'un mur (plat ou rugueux). Enfin, la dernière partie de la thèse fournit un cadre à l'étude de problèmes de contrôle optimal associés aux déplacements de nageurs ayant une dynamique sans dérive. Tout d'abord, nous étudions les propriétés mathématiques de plusieurs problèmes de contrôle optimal ayant des coûts fonctionnels différents (existence puis comportement). Ensuite, nous considérons les nageurs ayant deux degrés de liberté. Pour ces modèles particuliers de nageurs, nous présentons un cadre permettant d'en déduire des propriétés géométriques locales pour les solutions de certains problèmes de contrôle optimal. Tout au long de ce dernier chapitre, des simulations numériques, réalisées sur un exemple de nageur ayant une dynamique explicite, illustrent les résultats théoriques.

Mots-clés: Locomotion à faible nombre de Reynolds ; Interaction fluide-structure ; Contrôle optimal géométrique ; Modèles de robots microscopiques

Abstract

This thesis is devoted to the mathematical study of the swimming at low Reynolds number. The controllability and the optimal problems associated with the displacement of micro-swimmers are the main points developed in this work.

In the first part, we study the controllability and the optimal control problem in time associated with a reduced model of swimmers, called the "N-link swimmer". In the second part, we study the boundary effect on the controllability of particular micro-swimmers made by several balls linked each others by thin jacks. Firstly, we analyze the effect of a plane wall on the mobility of these swimmers. Then, we generalize these results where the wall is rough. We demonstrate that a controllable swimmer remains controllable in a half space delimited by a wall (plane or rough) whereas the reachable set of a non controllable one is increased by the presence of a wall. The last part is devoted to provide a general framework to study optimal controllability of driftless swimmers. We focus on the study of optimal strokes i.e. periodic shape changes. More precisely, we are interested in the existence of optimal strokes, minimizing or maximizing various cost functionals, qualitative properties of the optimal strokes, regularity and monotony of the value functions.

Keywords: Swimming at low Reynolds number ; Fluid-structure interaction ; Geometric optimal control theory ; Natural and artificial micro-swimmers